WILEY-VCH

Shigeo Katoh, Jun-ichi Horiuchi,
and Fumitake Yoshida

Biochemical Engineering

A Textbook for Engineers, Chemists and Biologists

Second, Completely Revised and Enlarged Edition

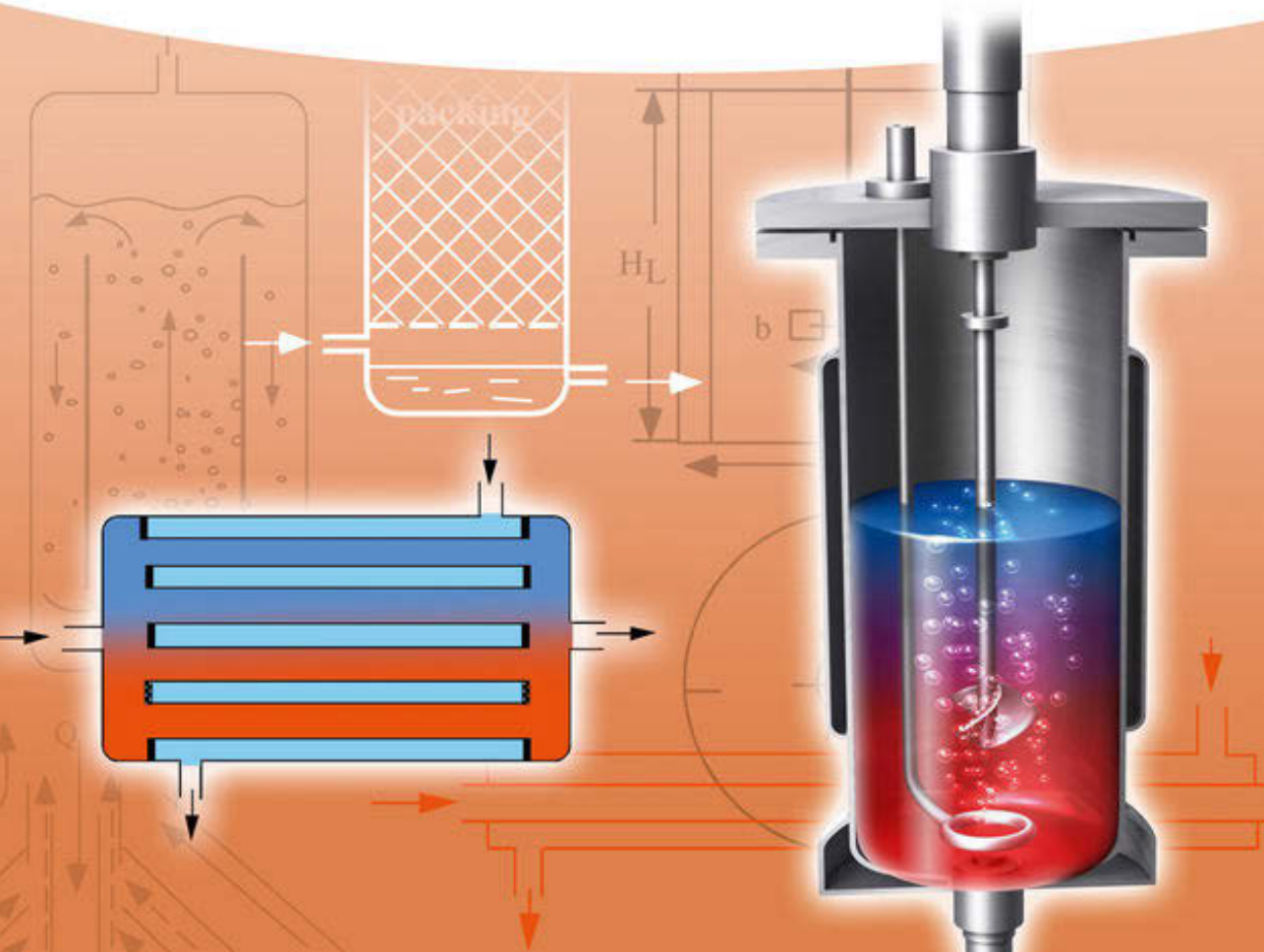

Shigeo Katoh, Jun-ichi Horiuchi, and Fumitake Yoshida

Biochemical Engineering

Related Titles

Hill, C.G., Root, T.W.

Introduction to Chemical Engineering Kinetics & Reactor Design

Second Edition

2014
Print ISBN: 978-1-118-36825-1; also available in electronic formats

Soetaert, W., Vandamme, E.J. (eds.)

Industrial Biotechnology

Sustainable Growth and Economic Success

2010
Print ISBN: 978-3-527-31442-3; also available in electronic formats

Wiley-VCH (ed.)

Ullmann's Biotechnology and Biochemical Engineering

2 Volume Set

2007
Print ISBN: 978-3-527-31603-8

Buchholz, K., Collins, J.

Concepts in Biotechnology

History, Science and Business

2010
Print ISBN: 978-3-527-31766-0

Buchholz, K., Kasche, V., Bornscheuer, U.T.

Biocatalysts and Enzyme Technology

2nd Edition

2012
Print ISBN: 978-3-527-32989-2; also available in electronic formats

Wiley-VCH (ed.)

Ullmann's Reaction Engineering

2 Volume Set

2013
Print ISBN: 978-3-527-33371-4

Buzzi-Ferraris, G./Manenti, F.

Fundamentals and Linear Algebra for the Chemical Engineer

Solving Numerical Problems

2010
Print ISBN: 978-3-527-32552-8

Interpolation and Regression Models for the Chemical Engineer

Solving Numerical Problems

2010
Print ISBN: 978-3-527-32652-5

Nonlinear Systems and Optimization for the Chemical Engineer

Solving Numerical Problems

2013
Print ISBN: 978-3-527-33274-8; also available in electronic formats

Differential and Differential-Algebraic Systems for the Chemical Engineer

Solving Numerical Problems

2014
Print ISBN: 978-3-527-33275-5; also available in electronic formats

Shigeo Katoh, Jun-ichi Horiuchi, and Fumitake Yoshida

Biochemical Engineering

A Textbook for Engineers, Chemists and Biologists

Second, Completely Revised and Enlarged Edition

WILEY-VCH
Verlag GmbH & Co. KGaA

The Authors

Dr. Shigeo Katoh
Kobe University
Graduate School of Science and Technology
Kobe 657-8501
Japan

Prof. Jun-ichi Horiuchi
Kitami Institute of Technology
Biotechnology & Environmental Chemistry
Koen-cho 165
Kitami
Hokkaido
Japan

Fumitake Yoshida
Formerly Kyoto University, Japan
Sakyo-ku Matsugasaki
Yobikaeshi-cho 2
Kyoto 606-0912
Japan

Library of Congress Card No.: applied for

British Library Cataloguing-in-Publication Data
A catalogue record for this book is available from the British Library.

Bibliographic information published by the Deutsche Nationalbibliothek
The Deutsche Nationalbibliothek lists this publication in the Deutsche Nationalbibliografie; detailed bibliographic data are available on the Internet at <http://dnb.d-nb.de>.

Print ISBN: 978-3-527-33804-7
ePDF ISBN: 978-3-527-68499-1
ePub ISBN: 978-3-527-68501-1
Mobi ISBN: 978-3-527-68500-4
oBook ISBN: 978-3-527-68498-4

Cover Design Formgeber, Mannheim, Germany
Typesetting Laserwords Private Limited, Chennai, India
Printing and Binding Markono Print Media Pte Ltd., Singapore

Printed on acid-free paper

Contents

Preface to the Second Edition

Bioengineering can be defined as the application of the various branches of engineering, including mechanical, electrical, and chemical engineering, to biological systems, including those related to medicine. Likewise, biochemical engineering refers to the application of chemical engineering to biological systems. This book is intended for use by undergraduates, and deals with the applications of chemical engineering to biological systems in general. In that respect, no preliminary knowledge of chemical engineering is assumed.

In the first edition of *Biochemical Engineering*, published in 2009, we attempted to demonstrate how a typical chemical engineer would address and solve such problems in order to facilitate an understanding by newcomers to this field of study. In Part I of the book, we outlined some very elementary concepts of chemical engineering for those new to the field, and in Part II, "Unit operations and apparatus for bio-systems" were covered. Although in Part III we described applications of biochemical engineering to bioprocesses and to other areas, this part did not include a chapter for "Bioprocess control." In bioindustry processes, the control of bioreactors is essential for the production of high-quality products under validated conditions. A fundamental understanding of process control should be very useful for all biochemical engineers, as well as for chemical engineers. Thus, we welcome a new coauthor, Prof. Jun-ichi Horiuchi, who is a leading researcher in the Department of Biotechnology and Environmental Chemistry, Kitami Institute of Technology.

Currently, many biopharmaceuticals, which are proteins in many cases, are produced in many bioindustry fields, and the measuring of the concentrations and bioactivities of these products is thus becoming essential in bioindustry. We have added a new section for "Biorecognition assay" in Chapter 11, and we explain the fundamental aspects of biorecognition and its application for the measurement of bioproducts at low concentrations. In this edition, we have included some examples and some new problems to assist in the progress with learning how to solve problem.

We would like to express great thanks to Prof. Michimasa Kishimoto and Prof. Yoichi Kumada for their useful discussion, particularly for Chapters 11–13.

We also thank the external reviewers for providing invaluable suggestions and the staffs of Wiley-VCH Verlag for planning, editing, and producing this second edition.

Shigeo Katoh

Preface to the First Edition

Bioengineering can be defined as the application of the various branches of engineering, including mechanical, electrical, and chemical engineering, to biological systems, including those related to medicine. Likewise, biochemical engineering refers to the application of chemical engineering to biological systems. This book is intended for use by undergraduates, and deals with the applications of chemical engineering to biological systems in general. In that respect, no preliminary knowledge of chemical engineering is assumed.

Since the publication of the pioneering text *Biochemical Engineering*, by Aiba, Humphrey, and Millis in 1964, several articles on the so-called "biochemical" or "bioprocess" engineering have been published. While all of these have combined the applications of chemical engineering and biochemistry, the relative space allocated to the two disciplines has varied widely among the different texts.

In this book, we describe the application of chemical engineering principles to biological systems, but in doing so assume that the reader has some practical knowledge of biotechnology, but no prior background in chemical engineering. Hence, we have attempted to demonstrate how a typical chemical engineer would address and solve such problems. Consequently, a simplified rather than rigorous approach has often been adopted in order to facilitate an understanding by newcomers to this field of study. Although in Part I of the book we have outlined some very elementary concepts of chemical engineering for those new to the field, the book can be used equally well for senior or even postgraduate level courses in chemical engineering for students of biotechnology, when the reader can simply start from Part II. Naturally, this book should prove especially useful for those biotechnologists interested in self-studying chemical bioengineering. In Part III, we provide descriptions of the applications of biochemical engineering not only to bioprocessing but also to other areas, including the design of selected medical devices. Moreover, to assist progress in learning, a number of worked examples, together with some "homework" problems, are included in each chapter.

I would like to thank the two external reviewers, Prof. Ulfert Onken (Dortmund University) and Prof. Alois Jungbauer (University of Natural Resources and Applied Life Sciences), for providing invaluable suggestions. I also thank the staff of Wiley-VCH Verlag for planning, editing, and producing this book. Finally I thank Kyoko, my wife, for her support while I was writing this book.

About the companion website

This book is accompanied by a companion website:

www.wiley.com/go//katoh/biochem_eng

The website includes detailed solutions to the problems in the book.

Nomenclature

(Some symbols and subscripts explained in the text are omitted.)

A	area (m^2)
a	specific interfacial area ($m^2\ m^{-3}$ or m^{-1})
b	width of rectangular conduit (m)
C	concentration (kg or kmol m^{-3}, g or mol cm^{-3})
C_n	cell number density (m^{-3})
C_p	heat capacity (kcal °C^{-1} or kJ K^{-1})
Cl	clearance of kidney or hemodialyzer ($cm^3\ min^{-1}$)
c_p	specific heat capacity (kJ $kg^{-1}\ K^{-1}$ or kcal kg^{-1} °C^{-1})
D	diffusivity ($m^2\ h^{-1}$ or $cm^2\ s^{-1}$)
D	tank or column diameter (m)
Dl	dialysance of hemodialyzer ($cm^3\ min^{-1}$)
d	diameter (m or cm)
d_e	equivalent diameter (m or cm)
E	enhancement factor $= k^*/k$ (–)
E	internal energy (kJ)
E_a	activation energy (kJ $kmol^{-1}$)
E_D, E_H, E_V	eddy diffusivity, eddy thermal diffusivity, and eddy kinematic viscosity, respectively ($m^2\ h^{-1}$ or $cm^2\ s^{-1}$)
E_f	effectiveness factor (–)
F	volumetric flow rate ($m^3\ h^{-1}$ or $cm^3\ s^{-1}$ or min^{-1})
f	friction factor
G_m	fluid mass velocity (kg $h^{-1}\ m^{-2}$)
G_V	volumetric gas flow rate per unit area (m h^{-1})
g	gravity acceleration (=9.807 m s^{-2})
H	henry's law constant (atm or Pa $kmol^{-1}$ (or kg^{-1}) m^3)
H	height, height per transfer unit (m)
H	enthalpy (kJ)
Hs	height equivalent to an equilibrium stage (–)
Ht	hematocrit (%)
h	individual phase film coefficient of heat transfer (W $m^{-2}\ K^{-1}$ or kcal $h^{-1}\ m^{-2}$ °C^{-1})

J	mass transfer flux (kg or kmol h^{-1} m^{-2})
J_F	filtrate flux (m s^{-1}, m h^{-1}, cm min^{-1}, or cm s^{-1})
K	consistency index (g cm^{-1} s^{n-2} or kg m^{-1} s^{n-2})
K	overall mass transfer coefficient (m h^{-1})
K	distribution coefficient, equilibrium constant (–)
K_m	michaelis constant (kmol m^{-3} or mol cm^{-3})
K_p	proportional gain (–)
K_c	ultimate gain (–)
k	individual phase mass transfer coefficient (m h^{-1} or cm s^{-1})
k	reaction rate constant (s^{-1}, m^3 $kmol^{-1}$ s^{-1}, etc.)
k_M	diffusive membrane permeability coefficient (m h^{-1} or cm s^{-1})
L	length (m or cm)
L_v	volumetric liquid flow rate per unit area (m h^{-1})
m	partition coefficient (–)
N	mass transfer rate per unit volume (kmol or kg h^{-1} m^{-3})
N	number of revolutions (s^{-1})
N	number of transfer unit (–)
N	number of theoretical plate (–)
N_i	number of moles of i component (kmol)
n	flow behavior index (–)
n	cell number (–)
O	output signal (–)
P	total pressure (Pa or bar)
P	power requirement (kJ s^{-1} or W)
p	partial pressure (Pa or bar)
Q	heat transfer rate (kcal h^{-1} or kJ s^{-1} or W)
Q	total flow rate (m^3 s^{-1})
q	heat transfer flux (W m^{-2} or kcal h^{-1} m^{-2})
q	adsorbed amount (kmol kg^{-1})
R	gas law constant, 0.08206 atm l $gmol^{-1}$ K^{-1}, (= 8.314 kJ $kmol^{-1}$ K^{-1}, etc.)
R	hydraulic resistance in filtration (m^{-1})
R, r	radius (m or cm)
r	sphere-equivalent particle radius (m or cm)
r_i	reaction rate of i component (kmol m^{-3} s^{-1})
RQ	respiratory quotient (–)
T	temperature (K)
T_I	integration time constant (s)
T_D	differential time constant (s)
T	temperature (°C or K)
t	time (s)
U	overall heat transfer coefficient (kcal h^{-1} m^{-2} $°C^{-1}$ or W m^{-2} K^{-1})
U	superficial velocity (m s^{-1} or cm s^{-1})
u	velocity (m s^{-1} or cm s^{-1})
V	volume (m^3)

V_{max}	maximum reaction rate (kmol m^{-3} s^{-1})
v	velocity averaged over conduit cross section (m s^{-1} or cm s^{-1})
v_t	terminal velocity (m s^{-1})
W	work done to system (kJ s^{-1} or W)
W	mass flow rate per tube (kg s^{-1} or g s^{-1})
W	peak width (m^3 or s)
w	weight (kg)
x	thickness of wall or membrane (m or cm)
x	mole fraction (–)
x	fractional conversion (–)
Y_{xS}	cell yield (kg dry cells/kg substrate consumed)
y	distance (m or cm)
y	oxygen saturation (% or –)
Δy	effective film thickness (m or cm)
Z	column height (m)
z	height of rectangular conduit of channel (m or cm)

Subscripts

G	gas
i	interface, inside, inlet
L	liquid
O	outside, outlet
0	initial

Superscripts

*	value in equilibrium with the other phase

Greek letters

α	thermal diffusivity (m^2 h^{-1} or cm^2 s^{-1})
α	specific cake resistance (m kg^{-1})
γ	shear rate (s^{-1})
ε	void fraction (–)
ε	gas holdup (–)
ε	deviation (–)
ϕ	thiele modulus (–)
κ	thermal conductivity (W m^{-1} K^{-1} or kcal m^{-1} h^{-1} °C^{-1})
μ	viscosity (Pa s or g cm^{-1} s^{-1})
μ	specific growth rate (h^{-1})
ν	kinematic viscosity = μ/ρ (cm^2 s^{-1} or m^2 h^{-1})

ν specific substrate consumption rate (g-substrate g-cell^{-1} h^{-1})
Π osmotic pressure (atm or Pa)
ρ density (kg m^{-3})
ρ specific product formation rate (g-product g-cell^{-1} h^{-1})
σ surface tension (kg s^{-2})
σ reflection coefficient (–)
σ standard deviation (–)
τ shear stress (Pa)
τ residence time (s)
ω angular velocity (s^{-1})

Dimensionless numbers

$(\mathrm{Bo}) = (g D^2 \rho/\sigma)$	bond number
$(\mathrm{Da}) = (-r_{\mathrm{a,max}}/k_{\mathrm{L}} A\, C_{\mathrm{ab}})$	damköhler number
$(\mathrm{Fr}) = [U_{\mathrm{G}}/(g D)^{1/2}]$	froude number
$(\mathrm{Ga}) = (g D^3/\nu^2)$	galilei number
$(\mathrm{Gz}) = (W c_{\mathrm{p}}/\kappa L)$	graetz number
$(\mathrm{Nu}) = (h d/\kappa)$	nusselt number
$(\mathrm{Nx}) = (F/D L)$	unnamed
$(\mathrm{Pe}) = (\nu L/E_{\mathrm{D}})$	peclet number
$(\mathrm{Pr}) = (c_{\mathrm{p}}\, \mu/\kappa)$	prandtl number
$(\mathrm{Re}) = (d \nu \rho/\mu)$	reynolds number
$(\mathrm{Sc}) = (\mu/\rho D)$	schmidt number
$(\mathrm{Sh}) = (k d/D)$	sherwood number
$(\mathrm{St}) = (k/\nu)$	stanton number

Part I
Basic Concepts and Principles

Biochemical Engineering: A Textbook for Engineers, Chemists and Biologists, Second Edition.
Shigeo Katoh, Jun-ichi Horiuchi, and Fumitake Yoshida.

Companion Website: www.wiley.com\go\katoh\biochem_eng_e2

1
Introduction

1.1
Background and Scope

Engineering can be defined as "the science or art of practical applications of the knowledge of pure sciences such as physics, chemistry, and biology."

Compared with civil, mechanical, and other forms of engineering, chemical engineering is a relatively young branch of the subject that has been developed since the early twentieth century. The design and operation of efficient chemical plant equipment are the main duties of chemical engineers. It should be pointed out that industrial-scale chemical plant equipment cannot be built simply by enlarging the laboratory apparatus used in basic chemical research. Consider, for example, the case of a chemical reactor – that is, the apparatus used for chemical reactions. Although neither the type nor size of the reactor will affect the rate of chemical reaction *per se*, they will affect the overall or apparent reaction rate, which involves effects of physical processes, such as heat and mass transfer and fluid mixing. Thus, in the design and operation of plant-size reactor, knowledge of such physical factors – which is often neglected by chemists – is important.

G. E. Davis, a British pioneer in chemical engineering, described in his book, *A Handbook of Chemical Engineering* (1901, 1904), a variety of physical operations commonly used in chemical plants. In the United States, such physical operations as distillation, evaporation, heat transfer, gas absorption, and filtration were termed "unit operations" in 1915 by A. D. Little of the Massachusetts Institute of Technology (MIT), where the instruction of chemical engineering was organized via unit operations. The first complete textbook of unit operations entitled *Principles of Chemical Engineering* by Walker, Lewis, and McAdams of the MIT was published in 1923. Since then, the scope of chemical engineering has been broadened to include not only unit operations but also chemical reaction engineering, chemical engineering thermodynamics, process control, transport phenomena, and other areas.

Bioprocess plants using microorganisms and/or enzymes, such as fermentation plants, have many characteristics similar to those of chemical plants. Thus, a chemical engineering approach should be useful in the design and operation of

Biochemical Engineering: A Textbook for Engineers, Chemists and Biologists, Second Edition.
Shigeo Katoh, Jun-ichi Horiuchi, and Fumitake Yoshida.

Companion Website: www.wiley.com\go\katoh\biochem_eng_e2

various plants that involve biological systems, if differences in the physical properties of some materials are taken into account. Furthermore, chemical engineers are required to have some knowledge of biology when tackling problems that involve biological systems.

Since the publication of a pioneering textbook [1] in 1964, some excellent books [2, 3] have been produced in the area of the so-called biochemical or bioprocess engineering. Today, the applications of chemical engineering are becoming broader to include not only bioprocesses but also various biological systems involving environmental technology and even some medical devices, such as artificial organs.

1.2 Dimensions and Units

A quantitative approach is important in any branch of engineering. However, this does not necessarily mean that engineers can solve everything theoretically, and quite often they use empirical rather than theoretical equations. Any equation – whether theoretical or empirical – that expresses some quantitative relationship must be dimensionally sound, as stated below.

In engineering calculations, a clear understanding of dimensions and units is very important. *Dimensions* are the basic concepts in expressing physical quantities. Dimensions used in chemical engineering are length (L), mass (M), time (T), the amount of substance (n), and temperature (θ). Some physical quantities have combined dimensions; for example, the dimensions of velocity and acceleration are $L\,T^{-1}$ and $L\,T^{-2}$, respectively. Sometimes, force (F) is also regarded as a dimension; however, as the force acting on a body is equal to the product of the mass of that body and the acceleration working on the body in the direction of force, F can be expressed as $M\,L\,T^{-2}$.

Units are measures for dimensions. Scientists normally use the centimeter (cm), gram (g), second (s), mole (mol), and degree centigrade (°C) as the units for the length, mass, time, amount of substance, and temperature, respectively (the CGS (centimeter–gram–second) system), whereas the units often used by engineers are m, kg, h, kmol, and °C. Traditionally, engineers have used the kilogram as the unit for both mass and force. However, this practice sometimes causes confusion, and to avoid this, a designation of kilogram-force (kg_f) is recommended. The unit for pressure, $kg\,cm^{-2}$, often used by plant engineers should read $kg_f\,cm^{-2}$. Mass and weight are different entities; the *weight* of a body is the gravitational force acting on the body, that is, (mass) (gravitational acceleration g). Strictly speaking, g – and hence weight – will vary slightly with locations and altitudes on the Earth. It would be much smaller in a space ship.

In recent engineering research papers, units with the International System of Units (SI) are generally used. The SI system is different from the CGS system often used by scientists or from the conventional metric system used by engineers [4]. In the SI system, kilogram is used for mass only, and newton (N), which is the

unit for force or weight, is defined as $\mathrm{kg\,m\,s^{-2}}$. The unit for pressure, Pa (pascal), is defined as $\mathrm{N\,m^{-2}}$. It is roughly the weight of an apple distributed over the area of $1\ \mathrm{m^2}$. As it is generally too small as a unit for pressure, kPa (kilopascal) (i.e., 1000 Pa), and MPa (megapascal) (i.e., 10^6 Pa) are more often used. One bar, which is equal to 0.987 atm, is 100 kPa = 0.1 MPa = 1000 hPa (hectopascal).

The SI unit for energy or heat is the joule (J), which is defined as $\mathrm{J = N\,m = kg\,m^2\,s^{-2} = Pa\,m^3}$. In the SI system, calorie is not used as a unit for heat, and hence no conversion between heat and work, such as 1 cal = 4.184 J, is needed. Power is defined as energy per unit time, and the SI unit for power is $\mathrm{W\ (watt) = J\,s^{-1}}$. Since W is usually too small for engineering calculations, kilowatt (=1000 W) is more often used. Although use of the SI units is preferred, we shall also use in this book the conventional metric units that are still widely used in engineering practice. The English engineering unit system is also used in engineering practice, but we do not use it in this text book. Values of the conversion factors between various units that are used in practice are listed in Appendix A, at the back of this book.

Empirical equations are often used in engineering calculations. For example, the following type of equation can relate the specific heat capacity c_p ($\mathrm{J\,kg^{-1}\,K^{-1}}$) of a substance with its absolute temperature T (K).

$$c_p = a + bT \tag{1.1}$$

where a ($\mathrm{kJ\,kg^{-1}\,K^{-1}}$) and b ($\mathrm{kJ\,kg^{-1}\,K^{-2}}$) are empirical constants. Their values in the kcal, kg, and °C units are different from those in the kJ, kg, and K units. Equations such as Equation 1.1 are called *dimensional equations*. The use of dimensional equations should preferably be avoided; hence, Equation 1.1 can be transformed to a nondimensional equation such as

$$\left(\frac{c_p}{R}\right) = a' + b'\left(\frac{T}{T_c}\right) \tag{1.2}$$

where R is the gas law constant with the same dimension as c_p and T_c is the critical temperature of the substance in question. Thus, as long as the same units are used for c_p and R and for T and T_c, respectively, the values of the ratios in the parentheses as well as the values of coefficients a' and b' do not vary with the units used. Ratios such as those in the above parentheses are called *dimensionless numbers* (groups), and equations involving only dimensionless numbers are called *dimensionless equations*.

Dimensionless equations – some empirical and some with theoretical bases – are often used in chemical engineering calculations. Most dimensionless numbers are usually called by the names of person(s) who first proposed or used such numbers. They are also often expressed by the first two letters of a name, beginning with a capital letter; for example, the well-known Reynolds number, the values of which determine conditions of flow (laminar or turbulent) is usually designated as Re, or sometimes as N_{Re}. The Reynolds number for flow inside a round straight tube is defined as $dv\rho/\mu$, in which d is the inside tube diameter (L), v is the fluid velocity averaged over the tube cross section ($\mathrm{L\,T^{-1}}$), ρ is the fluid density ($\mathrm{M\,L^{-3}}$), and μ is the fluid viscosity ($\mathrm{M\,L^{-1}\,T^{-1}}$) (this is defined

in Chapter 2). Most dimensionless numbers have some significance, usually ratios of two physical quantities. How known variables could be arranged in a dimensionless number in an empirical dimensionless equation can be determined by a mathematical procedure known as *dimensional analysis* [5], which is not described in this text. Examples of some useful dimensionless equations or correlations appear in the following chapters of the book.

Example 1.1

A pressure gauge reads 5.80 $kg_f\,cm^{-2}$. What is the pressure in SI units?

Solution

Let $g = 9.807\ m\ s^{-2}$.

$$p = \frac{(5.80)(9.807)}{(0.01^{-2})} = 569\,000\ Pa = 569\ kPa = 0.569\ MPa$$

1.3 Intensive and Extensive Properties

It is important to distinguish between the intensive (state) properties (functions) and the extensive properties (functions).

Properties that do not vary with the amount of mass of a substance – for example, temperature, pressure, surface tension, mole fraction – are termed *intensive properties*. On the other hand, those properties that vary in proportion to the total mass of substances – for example, total volume, total mass, and heat capacity – are termed *extensive properties*.

It should be noted, however, that some extensive properties become intensive properties, in case their specific values – that is, their values for unit mass or unit volume – are considered. For example, specific heat (i.e., heat capacity per unit mass) and density (i.e., mass per unit volume) are intensive properties.

Sometimes, capital letters and small letters are used for extensive and intensive properties, respectively. For example, C_p indicates heat capacity ($kJ\,°C^{-1}$) and c_p specific heat capacity ($kJ\,kg^{-1}\,°C^{-1}$). Measured values of intensive properties for common substances are available in various reference books [6].

1.4 Equilibria and Rates

Equilibria and rates should be clearly distinguished. *Equilibrium* is the end point of any spontaneous process, whether chemical or physical, in which the driving forces (potentials) for changes are balanced and there is no further tendency to

change. *Chemical equilibrium* is the final state of a reaction at which no further changes in compositions occur at a given temperature and pressure. As an example of a physical process, let us consider the absorption of a gas into a liquid. When the equilibrium at a given temperature and pressure is reached after a sufficiently long time, the compositions of the gas and liquid phases cease to change. How much of a gas can be absorbed in the unit volume of a liquid at equilibrium – that is, the solubility of a gas in a liquid – is usually given by Henry's law:

$$p = HC \tag{1.3}$$

where p is the partial pressure (Pa) of a gas, C is its equilibrium concentration ($\mathrm{kg\,m^{-3}}$) in a liquid, and H ($\mathrm{Pa\,kg^{-1}\,m^3}$) is the Henry's law constant, which varies with temperature. Equilibrium values do not vary with the experimental apparatus and procedure.

The *rate* of a chemical or physical process is its rapidity – that is, the speed of spontaneous changes toward the equilibrium. The rate of absorption of a gas into a liquid is the amount of the gas absorbed into the liquid per unit time. Such rates vary with the type and size of the apparatus, as well as its operating conditions. The rates of chemical or biochemical reactions in a homogeneous liquid phase depend on the concentrations of reactants, the temperature, the pressure, and the type and concentration of dissolved catalysts or enzymes. However, in the cases of heterogeneous chemical or biochemical reactions using particles of catalyst, immobilized enzymes or microorganisms, or microorganisms suspended in a liquid medium, and with an oxygen supply from the gas phase in case of an aerobic fermentation, the overall or apparent reaction rate(s) or growth rate(s) of the microorganism depend not only on chemical or biochemical factors but also on physical factors such as rates of transport of reactants outside or within the particles of catalyst or of immobilized enzymes or microorganisms. Such physical factors vary with the size and shape of the suspended particles, and with the size and geometry of the reaction vessel, as well as with operating conditions such as the degree of mixing or the rate(s) of gas supply. The physical conditions in industrial plant equipment are often quite different from those in the laboratory apparatus used in basic research.

Let us consider, as an example, a case of aerobic fermentation. The maximum amount of oxygen that can be absorbed into the unit volume of a fermentation medium at given temperature and pressure (i.e., the equilibrium relationship) is independent of the type and size of vessels used. On the other hand, the rates of oxygen absorption into the medium vary with the type and size of the fermentor and also with its operating conditions, such as the agitator speeds and rates of oxygen supply.

To summarize, chemical and physical equilibria are independent of the configuration of apparatus, whereas overall or apparent rates of chemical, biochemical, or microbial processes in industrial plants are substantially dependent on the configurations and operating conditions of the apparatus used. Thus, it is not appropriate to perform the so-called scaling-up using only those data obtained with a small laboratory apparatus.

1.5 Batch Versus Continuous Operation

Most chemical, biochemical, and physical operations in chemical and bioprocess plants can be performed batchwise or continuously.

A simple example is the heating of a liquid. If the amount of the fluid is rather small (e.g., 1 kl day^{-1}), then batch heating is more economical and practical, with the use of a tank that can hold the entire liquid volume and is equipped with a built-in heater. However, when the amount of the liquid is fairly large (e.g., 1000 kl day^{-1}), then continuous heating is more practical, using a heater in which the liquid flows at a constant rate and is heated to a required constant temperature. Most unit operations can be carried out either batchwise or continuously, depending on the scale of operation.

Most liquid phase chemical and biochemical reactions, with or without catalysts or enzymes, can be carried out either batchwise or continuously. For example, if the production scale is not large, then a reaction to produce C from A and B, all of which are soluble in water, can be carried out batchwise in a stirred tank reactor; that is, a tank equipped with a mechanical stirrer. The reactants A and B are charged into the reactor at the start of the operation. The product C is subsequently produced from A and B as time goes on, and can be separated from the aqueous solution when its concentration has reached a predetermined value.

When the production scale is large, the same reaction can be carried out continuously in the same type of reactor, or even with another type of reactor (Chapter 7). In this case, the supplies of the reactants A and B and the withdrawal of the solution containing product C are performed continuously, all at constant rates. The washout of the catalyst or enzyme particles can be prevented by installing a filter mesh at the exit of the product solution. Except for the transient start-up and finish-up periods, all the operating conditions such as temperature, stirrer speed, flow rates, and the concentrations of incoming and outgoing solutions remain constant – that is, in the steady state.

1.6 Material Balance

Material (mass) balance, the natural outcome from the law of conservation of mass, is a very important and useful concept in chemical engineering calculations. With usual chemical and/or biological systems, we need not consider nuclear reactions that convert mass into energy.

Let us consider a system that is separated from its surroundings by an imaginary boundary. The simplest expression for the total mass balance for the system is as follows:

$$\text{input} - \text{output} = \text{accumulation} \tag{1.4}$$

The accumulation can be either positive or negative, depending on the relative magnitudes of the input and output. It should be zero with a continuously operated reactor mentioned in the previous section.

We can also consider the mass balance for a particular component in the total mass. Thus, for a component in a chemical reactor,

$$\text{input} - \text{output} + \text{formation} - \text{disappearance} = \text{accumulation} \tag{1.5}$$

In mass balance calculations involving chemical and biochemical systems, it is sometimes more convenient to use the molar units, such as kilomoles, rather than simple mass units, such as the kilograms.

Example 1.2

A flow of 2000 kg h^{-1} of aqueous solution of ethanol (10 wt% ethanol) from a fermentor is to be separated by continuous distillation into the distillate (90 wt% ethanol) and waste solution (0.5 wt% ethanol). Calculate the amounts of the distillate D (kg h^{-1}) and the waste solution W (kg h^{-1}).

Solution

Total mass balance:

$$2000 = D + W$$

Mass balance for ethanol:

$$2000 \times 0.10 = D \times 0.90 + (2000 - D) \times 0.005$$

From these relations, we obtain $D = 212$ kg h^{-1} and $W = 1788$ kg h^{-1}.

1.7 Energy Balance

Energy balance is an expression of the first law of thermodynamics – that is, the law of conservation of energy.

For a nonflow system separated from the surroundings by a boundary, the increase in the total energy of the system is given by

$$\Delta(\text{total energy of the system}) = Q - W \tag{1.6}$$

in which Q is the net heat supplied to the system and W is the work done by the system. Q and W are both energy in transit and hence have the same dimension as energy. The total energy of the system includes the total internal energy E, potential energy (PE), and kinetic energy (KE). In normal chemical engineering calculations, changes in (PE) and (KE) can be neglected. The internal energy E is the intrinsic energy of a substance including chemical and thermal energy of molecules. Although absolute values of E are unknown, ΔE, the difference from

its base values, for example, from those at 0 °C and 1 atm, is often available or can be calculated.

Neglecting Δ(PE) and Δ(KE) we obtain from Equation 1.6

$$\Delta E = Q - W \tag{1.7}$$

The internal energy per unit mass e is an intensive (state) function. Enthalpy h, a compound thermodynamic function defined by Equation 1.8, is also an intensive function.

$$h = e + pv \tag{1.8}$$

in which p is the pressure and v is the specific volume. For a constant pressure process, it can be shown that

$$\mathrm{d}h = c_\mathrm{p}\mathrm{d}t \tag{1.9}$$

where c_p is the specific heat at constant pressure.

For a steady-state flow system, again neglecting changes in the PEs and KEs, the energy balance per unit time is given by Equation 1.10.

$$\Delta H = Q - W_\mathrm{s} \tag{1.10}$$

where ΔH is the total enthalpy change, Q is the heat supplied to the system, and W_s is the so-called shaft work done by moving fluid to the surroundings, for example, work done by a turbine driven by a moving fluid.

Example 1.3

In the second milk heater of a milk pasteurization plant 1000 l h^{-1} of raw milk is to be heated continuously from 75 to 135 °C by saturated steam at 500 kPa (152 °C). Calculate the steam consumption (kg h^{-1}), neglecting heat loss. The density and specific heat of milk are 1.02 kg l^{-1} and 0.950 (kcal kg^{-1} °C^{-1}), respectively.

Solution

Applying Equation 1.10 to this case, W_s is zero.

$$\Delta H = Q = (0.950)(1.02)(1000)(135 - 75) = 58\,140 \text{ kcal h}^{-1}$$

The heat of condensation (latent heat) of saturated steam at 500 kPa is given in the steam table as 503.6 kcal kg^{-1}. Hence, steam consumption is 58 140/503.6 = 115.4 kg h^{-1}.

Problems

1.1 What are the dimensions and SI units for the following physical quantities?

a. Pressure
b. Power
c. Heat capacity

1.2 Is the following equation dimensionally sound?

$$\frac{dp}{dz} = -\rho g$$

where p is the atmospheric pressure, z is the height above the sea level, ρ is the specific density of air, and g is the gravity acceleration.

1.3 Convert the following units.

a. energy of 1 cm^3 bar into J
b. a pressure of 25.3 $lb_f\,in^{-2}$ into SI units.

1.4 Explain the difference between mass and weight.

1.5 The Henry constant $H' = p/x$ for NH_3 in water at 20 °C is 2.70 atm. Calculate the value of $H = p/C$, where C is kmol m^{-3}, and $m = y/x$ where x and y are the mole fractions in the liquid and gas phases, respectively.

1.6 It is required to remove 99% of CH_4 from 200 $m^3\,h^{-1}$ of air (1 atm, 20 °C) containing 20 mol% of CH_4 by absorption into water. Calculate the minimum amount of water required ($m^3\,h^{-1}$). The solubility of CH_4 in water $H' = p/x$ at 20 °C is 3.76×10^4 atm.

1.7 A weight with a mass of 1 kg rests at 10 m above ground. It then falls freely to the ground. The acceleration of gravity is 9.8 m s^{-2}. Calculate

a. the PE of the weight relative to the ground
b. the velocity and KE of the weight just before it strikes the ground.

1.8 100 kg h^{-1} of ethanol vapor at 1 atm, 78.3 °C is to be condensed by cooling with water at 20 °C. How much water will be required in the case where the exit water temperature is 30 °C? The heat of vaporization of ethanol at 1 atm, 78.3 °C is 204.3 kcal kg^{-1}.

1.9 In the milk pasteurization plant of Example 1.3, what percentage of the heating steam can be saved, if a heat exchanger is installed to heat fresh milk at 75–95 °C by pasteurized milk at 132 °C?

References

1. Aiba, S., Humphrey, A.E., and Millis, N.F. (1964, 1973) *Biochemical Engineering*, University of Tokyo Press.
2. Lee, J.M. (1992) *Biochemical Engineering*, Prentice Hall.
3. Doran, P.M. (1995) *Bioprocess Engineering Principles*, Academic Press.
4. Oldeshue, J.Y. (1977) *Chem. Eng. Prog.*, **73** (8), 135.

5. McAdams, W.H. (1954) *Heat Transmission*, McGraw-Hill.
6. Perry, R.H., Green, D.W., and Malony, J.O. (eds) (1984, 1997) *Chemical Engineers' Handbook*, 6th and 7th edn, McGraw-Hill.

Further Reading

Hougen, O.A., Watson, K.M., and Ragatz, R.A. (1943, 1947, 1947) *Chemical Process Principles, Parts I, II, III*, John Wiley & Sons.

2
Elements of Physical Transfer Processes

2.1
Introduction

The role of physical transfer processes in bioprocess plants is as important as that of biochemical and microbial processes. Thus, knowledge of the engineering principles of such physical processes is important in the design and operation of bioprocess plants. Although this chapter is intended mainly for nonchemical engineers who are unfamiliar with such engineering principles, it might also be useful to chemical engineering students at the start of their careers.

In chemical engineering, the terms transfer of heat, mass, and momentum are referred to as the "transport phenomena." The heating or cooling of fluids is a case of heat transfer, a good example of mass transfer being the transfer of oxygen from air into the culture media in an aerobic fermentor. When a fluid flows through a conduit, its pressure drops because of friction due to transfer of momentum, as shown later.

The driving forces, or driving potentials, for transport phenomena are (i) the temperature difference for heat transfer; (ii) the concentration or partial pressure difference for mass transfer; and (iii) the difference in momentum for momentum transfer. When the driving force becomes negligible, then the transport phenomenon will cease to occur, and the system will reach equilibrium.

It should be mentioned here that, in living systems the transport of mass sometimes takes place apparently against the concentration gradient. Such "uphill" mass transport, which usually occurs in biological membranes with the consumption of biochemical energy, is called "active transport," and should be distinguished from "passive transport," which is the ordinary "downhill" mass transport as discussed in this chapter. Active transport in biological systems is beyond the scope of this book.

Transport phenomena can take place between phases, as well as within one phase. Let us begin with the simpler case of transport phenomena within one phase, in connection with the definitions of transport properties.

Biochemical Engineering: A Textbook for Engineers, Chemists and Biologists, Second Edition.
Shigeo Katoh, Jun-ichi Horiuchi, and Fumitake Yoshida.

Companion Website: www.wiley.com\go\katoh\biochem_eng_e2

2.2
Heat Conduction and Molecular Diffusion

Heat can be transferred by conduction, convection, or radiation and/or combinations thereof. Heat transfer within a homogeneous solid or a perfectly stagnant fluid in the absence of convection and radiation takes place solely by conduction. According to *Fourier's law*, the rate of heat conduction along the y-axis per unit area perpendicular to the y-axis (i.e., the heat flux q, expressed as $\mathrm{W\,m^{-2}}$ or $\mathrm{kcal\,m^{-2}\,h^{-1}}$) will vary in proportion to the temperature gradient in the y direction, $\mathrm{d}t/\mathrm{d}y$ ($^\circ\mathrm{C\,m^{-1}}$ or $\mathrm{K\,m^{-1}}$), and also to an intensive material property called *heat or thermal conductivity* κ ($\mathrm{W\,m^{-1}\,K^{-1}}$ or $\mathrm{kcal\,h^{-1}\,m^{-1}\,^\circ C^{-1}}$). Thus,

$$q = -\kappa \frac{\mathrm{d}t}{\mathrm{d}y} \tag{2.1}$$

The negative sign indicates that heat flows in the direction of negative temperature gradient, namely, from warmer to colder points. Some examples of the approximate values of thermal conductivity ($\mathrm{kcal\,h^{-1}\,m^{-1}\,^\circ C^{-1}}$) at 20 °C are 330 for copper, 0.513 for liquid water, and 0.022 for oxygen gas at atmospheric pressure. Values of thermal conductivity generally increase with increasing temperature.

According to *Fick's law*, the flux of the transport of component A in a mixture of A and B along the y axis by pure molecular diffusion, that is, in the absence of convection, J_A ($\mathrm{kg\,h^{-1}\,m^{-2}}$) is proportional to the concentration gradient of the diffusing component in the y direction, $\mathrm{d}C_\mathrm{A}/\mathrm{d}y$ ($\mathrm{kg\,m^{-4}}$) and a system property called *diffusivity* or the *diffusion coefficient* of A in a mixture of A and B, D_AB ($\mathrm{m^2\,h^{-1}}$ or $\mathrm{cm^2\,s^{-1}}$). Thus,

$$J_\mathrm{A} = -D_\mathrm{AB} \frac{\mathrm{d}C_\mathrm{A}}{\mathrm{d}y} \tag{2.2}$$

It should be noted that D_AB is a property of the mixture of A and B, and is defined with reference to the mixture and not to the fixed coordinates. Except in the case of equimolar counter-diffusion of A and B, the diffusion of A would result in the movement of the mixture as a whole. However, in the usual case where the concentration of A is small, the value of D_AB is practically equal to the value defined with reference to the fixed coordinates.

Values of diffusivity in gas mixtures at normal temperature and atmospheric pressure are in the approximate range of $0.03-0.3\,\mathrm{m^2\,h^{-1}}$ and usually increase with temperature and decrease with increasing pressure. Values of the liquid phase diffusivity in dilute solutions are in the approximate range of $0.2-1.2\times10^{-5}\,\mathrm{m^2\,h^{-1}}$, and increase with temperature. Both gas-phase and liquid-phase diffusivities can be estimated by various empirical correlations available in reference books.

There exists a conspicuous analogy between heat transfer and mass transfer. Hence, Equation 2.1 can be rewritten as

$$q = -(\kappa/c_p\rho)\ \frac{d(c_p\rho t)}{dy}$$
$$= -\alpha\ \frac{d(c_p\rho t)}{dy} \tag{2.3}$$

where c_p is specific heat (kcal kg^{-1} °C^{-1}), ρ is density (kg m^{-3}), and α $\{=\kappa/(c_p\ \rho)\}$ is the thermal diffusivity (m^2 h^{-1}), which has the same dimension as diffusivity.

2.3 Fluid Flow and Momentum Transfer

The flow of fluid – whether gas or liquid – through pipes takes place in most chemical or bioprocess plants. There are two distinct regimes or modes of fluid flow. In the first regime, when all fluid elements flow only in one direction, and with no velocity components in any other direction, the flow is called *laminar*, *streamline*, or *viscous flow*. In the second regime, the fluid flow is *turbulent*, with random movements of the fluid elements or clusters of molecules occurring, but the flow as a whole is in one general direction. Incidentally, such random movements of fluid elements or clusters of molecules should not be confused with the random motion of individual molecules that causes molecular diffusion and heat conduction discussed in the previous sections, and also the momentum transport in laminar flow discussed below. Figure 2.1 shows, in a conceptual manner, the velocity profile in the laminar flow of a fluid between two large parallel plates moving at different velocities. If both plates move at constant but different velocities, with the top plate A at a faster velocity than the bottom plate B, a straight velocity profile such as shown in the figure will be established when steady conditions have been reached. This is due to the friction between the fluid layers parallel to the plates, and also between the plates and the adjacent fluid layers. In other words, a faster moving fluid layer tends to pull the adjacent slower moving fluid layer, and the latter tends to resist it. Thus, momentum is transferred from the faster moving fluid layer to the adjacent slower moving fluid

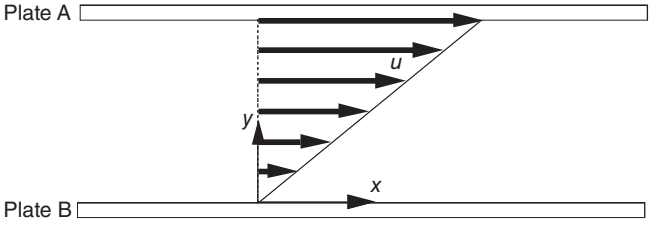

Figure 2.1 Velocity profile of laminar flow between parallel plates moving at different velocities.

layer. Therefore, a force must be applied to maintain the velocity gradient; such force per unit area parallel to the fluid layers τ (Pa) is called the *shear stress*. This varies in proportion to the velocity gradient du/dy (s^{-1}), which is called the *shear rate* and is denoted by γ (s^{-1}). Thus,

$$\tau = -\mu \left(\frac{du}{dy} \right) = -\mu\gamma \tag{2.4}$$

The negative sign indicates that momentum is transferred down the velocity gradient. The proportionality constant μ (Pa s) is called *molecular viscosity* or simply *viscosity*, which is an intensive property. The unit of viscosity in CGS (centimeter–gram–second) units is called poise ($g\,cm^{-1}\,s^{-1}$). From Equation 2.4 we obtain

$$\tau = -(\mu/\rho)\,\frac{d(u\rho)}{dy} = -\nu\,\frac{d(u\rho)}{dy} \tag{2.5}$$

which indicates that the shear stress; that is, the flux of momentum transfer varies in proportion to the momentum gradient and kinematic viscosity ν ($= \mu/\rho$) ($cm^2\,s^{-1}$ or $m^2\,h^{-1}$). The unit ($cm^2\,s^{-1}$) is sometimes called Stokes and denoted as St. This is Newton's law of viscosity. A comparison of Equations 2.2, 2.3, and 2.5 indicates evident analogies among the transfer of mass, heat, and momentum. If the gradients of concentration, heat content, and momentum are taken as the driving forces in the three respective cases, the proportionality constants in the three rate equations are diffusivity, thermal diffusivity, and kinematic viscosity, respectively, all having the same dimension ($L^2\,T^{-1}$) and the same units ($cm^2\,s^{-1}$ or $m^2\,h^{-1}$).

A fluid with viscosity that is independent of shear rates is called a *Newtonian fluid*. On a shear stress–shear rate diagram, such as Figure 2.2, it is represented by a straight line passing through the origin, the slope of which is the viscosity. All gases, and most common liquids of low molecular weights (e.g., water and

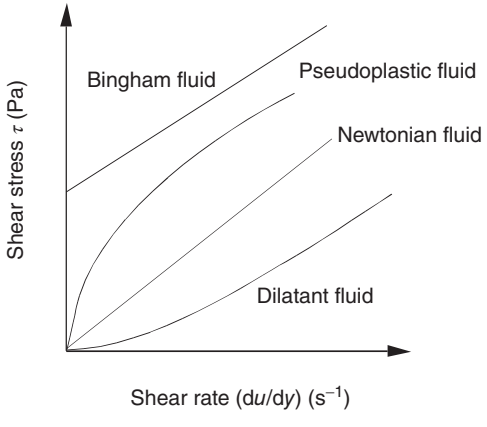

Figure 2.2 Relationships between shear rate and shear stress for Newtonian and non-Newtonian fluids.

ethanol) are Newtonian fluids. It is worth remembering that the viscosity of water at 20 °C is 0.01 poise (1 cp) in the CGS units and 0.001 Pa s in SI units. Liquid viscosity decreases with increasing temperature, whereas gas viscosity increases with increasing temperature. The viscosities of liquids and gases generally increase with pressure. Gas and liquid viscosities can be estimated by various equations and correlations available in reference books.

Fluids that show viscosity variations with shear rates are called *non-Newtonian fluids*. Depending on how the shear stress varies with the shear rate, they are categorized into pseudoplastic, dilatant, and Bingham plastic fluids (Figure 2.2). The viscosity of pseudoplastic fluids decreases with increasing shear rate, whereas dilatant fluids show an increase in viscosity with shear rate. Bingham plastic fluids do not flow until a threshold stress called the *yield stress* is applied, after which the shear stress increases linearly with the shear rate. In general, the shear stress τ can be represented by Equation 2.6:

$$\tau = K\left(\frac{\mathrm{d}u}{\mathrm{d}y}\right)^n = \mu_a\left(\frac{\mathrm{d}u}{\mathrm{d}y}\right) \tag{2.6}$$

where K is called the *consistency index* and n is the *flow behavior index*. Values of n are smaller than 1 for pseudoplastic fluids, and >1 for dilatant fluids. The apparent viscosity μ_a (Pa s), which is defined by Equation 2.6, varies with shear rates ($\mathrm{d}u/\mathrm{d}y$) (s^{-1}); for a given shear rate, μ_a is given as the slope of the straight line joining the origin and the point for the shear rate on the shear rate – shear stress curve.

Fermentation broths – that is, fermentation medium containing microorganisms – often behave as non-Newtonian liquids, and in many cases their apparent viscosities vary with time, notably during the course of fermentation.

Fluids that show elasticity to some extent are termed *viscoelastic fluids*, and some polymer solutions demonstrate such behavior. *Elasticity* is the tendency of a substance or body to return to its original form, after the applied stress that caused strain (i.e., a relative volumetric change in the case of a polymer solution) has been removed. The *elastic modulus* (Pa) is the ratio of the applied stress (Pa) to strain (–). The relaxation time (s) of a viscoelastic fluid is defined as the ratio of its viscosity (Pa s) to its elastic modulus.

Example 2.1

The following experimental data were obtained with use of a rotational viscometer for an aqueous solution of carboxylmethyl cellulose (CMC) containing 1.3 g CMC per 100 cm^3 solution.

Shear rate $\mathrm{d}u/\mathrm{d}y$ (s^{-1})	0.80	3.0	12	50	200
Shear stress τ (Pa)	0.329	0.870	2.44	6.99	19.6

Determine the values of the consistency index K, the flow behavior index n, and also the apparent viscosity μ_a at the shear rate of 50 s^{-1}.

Solution

Taking the logarithms of Equation 2.6 we get

$$\log \tau = \log K + n \log \left(\frac{du}{dy} \right)$$

Thus, plotting the shear stress τ on the ordinate and the shear rate du/dy on the abscissa of a log–log paper gives a straight line (Figure 2.3), the slope of which is $n = 0.74$. The value of the ordinate for the abscissa $du/dy = 1.0$ gives $K = 0.387$. Thus, this CMC solution is pseudoplastic. Also, the average viscosity at μ_a at the shear rate of 50 s^{-1} is 6.99/50 = 0.140 Pa s = 140 cp.

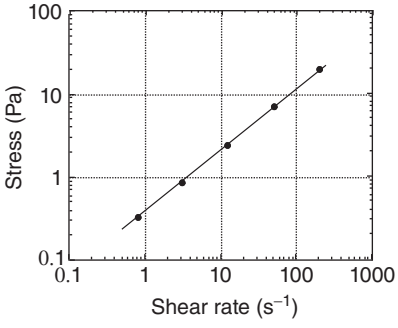

Figure 2.3 Relationships between shear rate and shear stress.

Incidentally, plotting data on a log–log paper (i.e., log–log plot) is often used for determining the value of an exponent, if the data can be represented by an empirical power function, such as Equation 2.6.

2.4 Laminar Versus Turbulent Flow

As mentioned above, two distinct patterns of fluid flow can be identified, namely laminar flow and turbulent flow. Whether a fluid flow becomes laminar or turbulent depends on the value of a dimensionless number called the Reynolds number, (Re). For a flow through a conduit with a circular cross section (i.e., a round tube), (Re) is defined as:

$$\mathrm{Re} = \frac{dv\rho}{\mu} \tag{2.7}$$

where d is the inside diameter of the tube (L), v is the linear flow velocity averaged over the tube cross section (L T^{-1}) (i.e., volumetric flow rate divided by the inside cross-sectional area of the tube), ρ is the fluid density (M L^{-3}), and μ is the fluid viscosity (M L^{-1} T^{-1}). Under steady conditions, the flow of fluid through a

straight round tube is laminar, when (Re) is less than approximately 2300. However, when (Re) is higher than 3000, the flow becomes turbulent. In the transition range between these two (Re) values the flow is unstable; that is, a laminar flow exists in a very smooth tube, but only small disturbances will cause a transition to turbulent flow. This holds true also for the fluid flow through a conduit with noncircular cross section, if the equivalent diameter defined later is used in place of d in Equation 2.7. However, fluid flow outside a tube bundle, whether perpendicular or oblique to the tubes, becomes turbulent at much smaller (Re), in which case the outer diameter of tubes and fluid velocity, whether perpendicular or oblique to the tubes, are substituted for d and v in Equation 2.7, respectively.

Figure 2.4a shows the velocity distribution in a steady isothermal laminar flow of an incompressible Newtonian fluid through a straight, round tube. The velocity distribution in laminar flow is parabolic and can be represented by

$$\frac{u}{v} = 2\left[1 - \left(\frac{r^2}{r_i{}^2}\right)\right] \tag{2.8}$$

where u is the local velocity (m s^{-1}) at a distance r (m) from the tube axis, v is the average velocity over the entire cross section (m s^{-1}) (i.e., volumetric flow rate

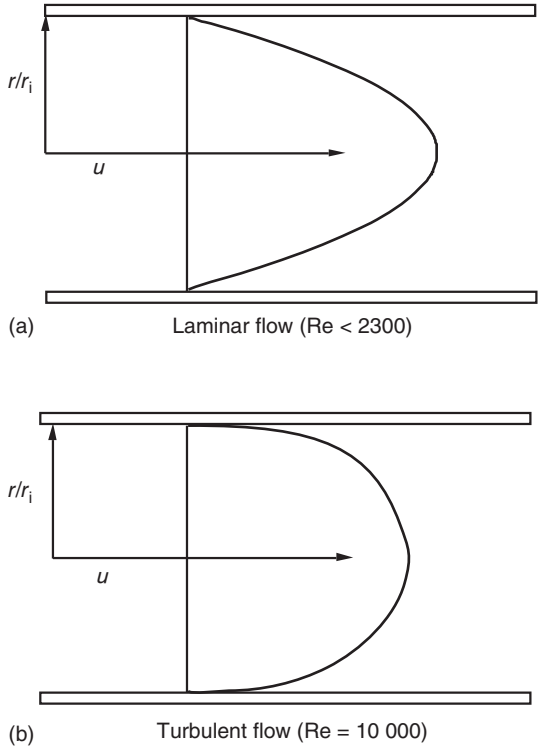

Figure 2.4 Velocity profiles of laminar and turbulent flows through a tube: (a) laminar flow (Re < 2300) and (b) turbulent flow (Re = 10 000).

divided by the cross section), and r_i is the inner radius of the tube (m). Equation 2.8 indicates that the maximum velocity at the tube axis, where $r = 0$, is twice the average velocity.

Equation 2.8 can be derived theoretically if one considers in the stream an imaginary coaxial fluid cylinder of radius r and length L; equates (i) the force $\pi r^2 \Delta P$ due to the pressure drop (i.e., the pressure difference ΔP between the upstream and down stream ends of the imaginary cylinder) to (ii) the force due to inner friction (i.e., the shear stress on the cylindrical surface of the imaginary cylinder, $2\pi rL\tau = -2\pi rL\mu\ (\mathrm{d}u/\mathrm{d}r)$); and integrates the resulting equation for the range from the tube axis, where $r = 0$ and $u = u_{max}$ to the tube surface, where $r = r_i$ and $u = 0$.

From the above relationships it can also be shown that the pressure drop ΔP (Pa) in the laminar flow of a Newtonian fluid of viscosity μ (Pa s) through a straight round tube of diameter d (m) and length L (m) at an average velocity of v (m s^{-1}) is given by Equation 2.9, which expresses the Hagen–Poiseuille law:

$$\Delta P = \frac{32\,\mu\, v L}{d^2} \tag{2.9}$$

Thus, the pressure drop ΔP for laminar flow through a tube varies in proportion to the viscosity μ, the average flow velocity v, and the tube length L, and in inverse proportion to the square of the tube diameter d. Since v is proportional to the total flow rate Q (m^3 s^{-1}) and to d^{-2}, ΔP should vary in proportion to μ, Q, L, and d^{-4}. The principle of the capillary tube viscometer is based on this relationship.

Example 2.2

Derive an equation for the shear rate at the tube surface γ_w for laminar flow of Newtonian fluids through a tube of radius r_i.

Solution

Differentiation of Equation 2.8 gives

$$\gamma_w = -\left(\frac{\mathrm{d}u}{\mathrm{d}r}\right)_{r=r_i} = \frac{4v}{r_i}$$

Figure 2.4b shows, conceptually, the velocity distribution in steady turbulent flow through a straight round tube. The velocity at the tube wall is zero, and the fluid near the wall moves in laminar flow, even though the flow of the main body of fluid is turbulent. The thin layer near the wall in which the flow is laminar is called the *laminar sublayer* or *laminar film*, while the main body of fluid where turbulence always prevails is called the *turbulent core*. The intermediate zone between the laminar sublayer and the turbulent core is called the *buffer layer*, where the motion of fluid may be either laminar or turbulent at a given instant. With a relatively long tube, the above statement holds for most of the tube length, except for

the entrance region. A certain length of tube is required for the laminar sublayer to develop fully.

Velocity distributions in turbulent flow through a straight, round tube vary with the flow rate or the Reynolds number. With increasing flow rates the velocity distribution becomes flatter and the laminar sublayer thinner. Dimensionless empirical equations involving viscosity and density are available that correlate the local fluid velocities in the turbulent core, buffer layer, and the laminar sublayer as functions of the distance from the tube axis. The ratio of the average velocity over the entire tube cross section to the maximum local velocity at the tube axis is approximately 0.7–0.85, and increases with the Reynolds number.

The pressure drop ΔP (Pa) in turbulent flow of an incompressible fluid with density ρ (kg m^{-3}) through a tube of length L (m) and diameter d (m) at an average velocity of v (m s^{-1}) is given by Equation 2.10, namely, the Fanning equation:

$$\Delta P = 2f\rho v^2 \left(\frac{L}{d}\right) \tag{2.10}$$

where f is the dimensionless friction factor, which can be correlated with the Reynolds number by various empirical equations; for example,

$$f = \frac{0.079}{(\mathrm{Re})^{0.25}} \tag{2.11}$$

for the range of (Re) from 3000 to 100 000. It can be seen from comparison of Equations 2.9 and 2.10 that Equation 2.10 also holds for laminar flow, if f is given as

$$f = \frac{16}{(\mathrm{Re})} \tag{2.12}$$

Correlations are available for pressure drops in flow through pipe fittings, such as elbows, bends, and valves, and for sudden contractions and enlargements of the pipe diameter as the ratio of equivalent length of straight pipe to its diameter.

2.5
Transfer Phenomena in Turbulent Flow

The transfer of heat and/or mass in turbulent flow occurs mainly by eddy activity, namely the motion of gross fluid elements that carry heat and/or mass. Transfer by heat conduction and/or molecular diffusion is much smaller compared to that by eddy activity. In contrast, heat and/or mass transfer across the laminar sublayer near a wall, in which no velocity component normal to the wall exists, occurs solely by conduction and/or molecular diffusion. A similar statement holds for momentum transfer. Figure 2.5 shows the temperature profile for the case of heat transfer from a metal wall to a fluid flowing along the wall in turbulent flow. The temperature gradient in the laminar sublayer is linear and steep, because heat transfer across the laminar sublayer is solely by conduction and the thermal conductivities of fluids are much smaller those of metals. The temperature gradient in the turbulent core is much smaller, as heat transfer occurs mainly by convection – that is, by

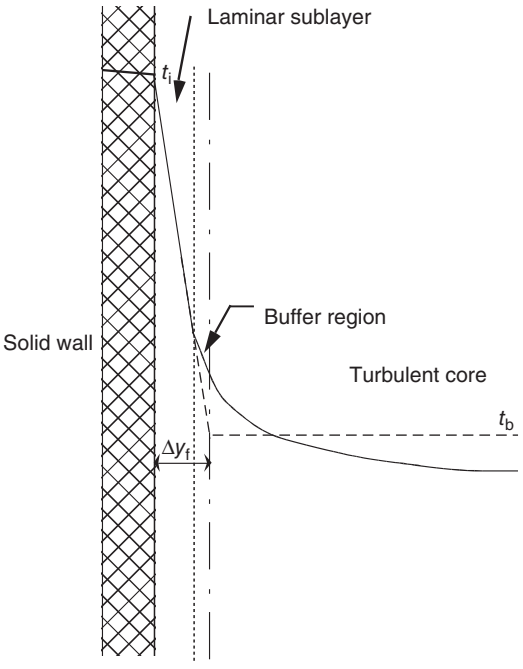

Figure 2.5 Temperature gradient in turbulent heat transfer from solid to fluid.

mixing of the gross fluid elements. The gradient becomes smaller with increasing distance from the wall due to increasing turbulence. The temperature gradient in the buffer region between the laminar sublayer and the turbulent core is smaller than in the laminar sublayer, but greater than in the turbulent core, and becomes smaller with increasing distance from the wall. Conduction and convection are comparable in the buffer region. It should be noted that no distinct demarcations exist between the laminar sublayer and the buffer region, or between the turbulent core and the buffer region.

What has been said above also holds for solid-fluid mass transfer. The concentration gradients for mass transfer from a solid phase to a fluid in turbulent flow should be analogous to the temperature gradients, such as shown in Figure 2.5.

When representing rates of transfer of heat, mass, and momentum by eddy activity, the concepts of eddy thermal conductivity, eddy diffusivity, and eddy viscosity are sometimes useful. Extending the concepts of heat conduction, molecular diffusion, and molecular viscosity to include the transfer mechanisms by eddy activity, one can use Equations 2.13 – 2.15, which correspond to Equations 2.2, 2.3, and 2.5, respectively.

For heat transfer,

$$q = -(\alpha + E_H)\frac{d(c_p \rho t)}{dy} \tag{2.13}$$

For mass transfer

$$J_A = -(D_{AB} + E_D)\left(\frac{dC_A}{dy}\right) \tag{2.14}$$

For momentum transfer,

$$\tau = -(\nu + E_V)\frac{d(u\rho)}{dy} \tag{2.15}$$

In the above equations, E_H, E_D, and E_V are eddy thermal diffusivity, eddy diffusivity, and eddy kinematic viscosity, respectively, all having the same dimensions ($L^2\,T^{-1}$). It should be noted that these are not properties of fluid or system, because their values vary with the intensity of turbulence which depends on flow velocity, geometry of flow channel, and other factors.

2.6 Film Coefficients of Heat and Mass Transfer

If the temperature gradient across the laminar sublayer and the value of thermal conductivity were known, it would be possible to calculate the rate of heat transfer by Equation 2.1. This is usually impossible, however, because the thickness of the laminar sublayer and the temperature distribution, such as shown in Figure 2.5, are usually immeasurable and vary with fluid velocity and other factors. Thus, a common engineering practice is the use of the film (or individual) coefficient of heat transfer, h, which is defined by Equation 2.16 and based on the difference between the temperature at the interface, t_i and the temperature of the bulk of fluid, t_b:

$$q = h(t_i - t_b) \tag{2.16}$$

where q is the heat flux ($W\,m^{-2}$ or $kcal\,h^{-1}\,m^{-2}$) and h is the film coefficient of heat transfer ($W\,m^{-2}\,K^{-1}$ or $kcal\,h^{-1}\,m^{-2}\,°C^{-1}$). It is worth remembering that $1\,kcal\,m^{-2}\,h^{-1}\,°C^{-1} = 1.162\,W\,m^{-2}\,K^{-1}$. The bulk (mixing-cup) temperature t_b, which is shown in Figure 2.5 by a broken line, is the temperature that a stream would have, if the whole fluid flowing at a cross section of the conduit were to be thoroughly mixed. The temperature of a fluid emerging from a heat transfer device is the bulk temperature at the exit of the device. If the temperature profile were known, as in Figure 2.5, then the thickness of the effective (or fictive) laminar film shown by the chain line could be determined from the intersection of the extension of the temperature gradient in the laminar film with the line for the bulk temperature. It should be noted that the effective film thickness Δy_f is a fictive concept for convenience. This is thicker than the true thickness of the laminar sublayer. From Equations 2.1 and 2.16, it is seen that

$$h = \frac{\kappa}{\Delta y_f} \tag{2.17}$$

Thus, values of h for heating or cooling increase with thermal conductivity κ. Also, h values can be increased by decreasing the effective thickness of the laminar film

Δy_f by increasing fluid velocity along the interface. Various correlations for predicting film coefficients of heat transfer are provided in Chapter 5.

The film (individual) coefficients of mass transfer can be defined similarly to the film coefficient of heat transfer. A few different driving potentials are used today to define the film coefficients of mass transfer. Some investigators use the mole fraction or molar ratio, but often the concentration difference ΔC (kg or kmol m^{-3}) is used to define the liquid phase coefficient k_L (m h^{-1}), while the partial pressure difference Δp (atm) is used to define the gas film coefficient k_{Gp} (kmol h^{-1} m^{-2} atm^{-1}). However, using k_L and k_{Gp} of different dimensions is not very convenient. In this book, except for Chapter 15, we shall use the gas phase coefficient k_{Gc} (m h^{-1}) and the liquid phase coefficient k_L (m h^{-1}), both of which are based on the molar concentration difference ΔC (kmol m^{-3}). With such practice, the mass transfer coefficients for both phases have the same simple dimension (L T^{-1}). Conversion between k_{Gp} and k_{Gc} is easy, as can be seen from Example 2.4.

By applying the effective film thickness concept, we obtain Equation 2.18 for the individual phase mass transfer coefficient k_C (L T^{-1}), which is analogous to Equation 2.17 for heat transfer.

$$k_C = \frac{D}{\Delta y_f} \tag{2.18}$$

where D is diffusivity (L^2 T^{-1}) and Δy_f is the effective film thickness (L).

Example 2.3

Air is heated from 20 to 80 °C with use of an air heater. From operating data, the air-side film coefficient of heat transfer was determined as 44.2 kcal h^{-1} m^{-2} $°C^{-1}$. Estimate the effective thickness of the air film. The heat conductivity of air at 50 °C is 0.0481 kcal h^{-1} m^{-1} $°C^{-1}$.

Solution

From Equation 2.17 the effective thickness of the air film is

$$\Delta y_f = \frac{\kappa}{h} = \frac{0.0481}{44.2} = 0.00109 \text{ m} = 0.109 \text{ cm}$$

Example 2.4

Show the relationship between k_{Gp} and k_{Gc}.

Solution

Applying the ideal gas law to the diffusing component A in the gas phase, p_A, the partial pressure of A, is given as

$$p_A(\text{atm}) = \frac{RT}{V} = R\,(\text{K})(\text{kmol m}^{-3}) = 0.0821\,(\text{K})C_A$$

where R is the gas constant (atm m^3 $kmol^{-1}$ K^{-1}), T is the absolute temperature (K), and C_A is the molar concentration of A in the gas phase (kmol m^{-3}). Thus, the driving potential

$$\Delta p_A(\text{atm}) = RT\Delta C_A = 0.0821 \text{ K kmol m}^{-3}$$

$$\begin{aligned} 1k_{Gp} &= 1 \text{ kmol m}^{-2}\text{ h}^{-1}\text{ atm}^{-1} \\ &= 1 \text{ kmol m}^{-2}\text{ h}^{-1}(0.0821 \text{ K kmol m}^{-3})^{-1} \\ &= 12.18 \text{ m h}^{-1}/(\text{K}) = 12.18k_{Gc}(\text{K})^{-1} \end{aligned}$$

or

$$1k_{Gc} = 0.0821 \text{ (K)}k_{Gp} \quad \text{i.e., } 1k_{Gc} = RTk_{Gp}$$

Problems

2.1 Consider a straight, round tube of L (m) length, having inside and outside radii of r_i (m) and r_o (m) with the inside surface temperature T_i (°C) and outside temperature T_o (°C). The heat conductivity of the tube material is κ (kcal h^{-1} m^{-1} °C^{-1}).
Show that the steady state heat transfer rate is given by the following equation.

$$Q = \frac{2\pi\kappa L(T_i - T_o)}{\ln(r_o/r_i)}$$

2.2 According to the Wilke and Chang equation, the variation of the diffusivity in liquids with temperature can be estimated by the following equation.

$$\frac{(D_{AB}\mu_B)}{T} = \text{constant}$$

where μ_B is the viscosity of the solvent and T is the absolute temperature.
The diffusivity of oxygen in water at 20 °C is 2.1×10^{-9} m^2 s^{-1}.
Estimate the diffusivity of oxygen in water at 37 °C. The viscosity of water is given in Table P2.2.

Table P2.2 Viscosity of water

Temperature (°C)	10	20	30	40
Viscosity (Pa s)	1.31×10^{-3}	1.00×10^{-3}	0.80×10^{-3}	0.65×10^{-3}

2.3 Derive Equations 2.8 and 2.9.

2.4 Estimate the pressure drop when $5\,m^3\,h^{-1}$ of oil flows through a horizontal pipe of 3 cm i.d. and 50 m length. Properties of the oil: density $\rho = 0.800\,g\,cm^{-3}$; viscosity $\mu = 20$ poise.

2.5 From a flat surface of water at 20 °C water is vaporizing into air (25 °C, water pressure 15.0 mmHg) at a rate of $0.0041\,g\,cm^{-2}\,h^{-1}$. The vapor pressure of water at 20 °C is 17.5 mmHg. The diffusivity of water vapor in air at the air film temperature is $0.25\,cm^2\,s^{-1}$. Estimate the effective thickness of the air film above the water surface.

2.6 The film coefficient of heat transfer in a water heater to heat water from 20 to 80 °C is $2300\,kcal\,h^{-1}\,m^{-2}\,°C^{-1}$. Estimate the effective thickness of the water film. The thermal conductivity of water at 50 °C is $0.55\,kcal\,h^{-1}\,m^{-1}\,°C^{-1}$.

2.7 The values of the consistency index K and the flow behavior index n of a dilatant fluid are 0.415 and 1.23, respectively. Estimate the value of the apparent viscosity of this fluid at a shear rate of $60\,s^{-1}$.

Further Reading

Bennett, C.O. and Myers, J.E. (1962) *Momentum, Heat, and Mass Transfer*, McGraw-Hill.

Bird, R.B., Stewart, W.E., and Lightfoot, E.N. (2001) *Transport Phenomena*, 2nd edn, John Wiley & Sons, Inc.

3
Chemical and Biochemical Kinetics

3.1
Introduction

Bioprocesses involve many chemical and/or biochemical reactions. Knowledge concerning changes in the compositions of reactants and products, as well as their rates of utilization and production under given conditions, is essential when determining the size of a reactor. With a bioprocess involving biochemical reactions, for example, the formation and disappearance terms in Equation 1.5, as well as the mass balance of a specific component, must be calculated. It is important, therefore, that we have some knowledge of the rates of those enzyme-catalyzed biochemical reactions that are involved in the growth of microorganisms and are utilized for various bioprocesses.

In general, bioreactions can occur in either a homogeneous liquid phase or in heterogeneous phases including gas, liquid, and/or solid. Reactions with particles of catalysts, or of immobilized enzymes and aerobic fermentation with oxygen supply, represent examples of reactions in heterogeneous phases.

In this chapter we provide the fundamental concepts of chemical and biochemical kinetics that are important for understanding the mechanisms of bioreactions and also for the design and operation of bioreactors. First, we shall discuss general chemical kinetics in a homogeneous phase and then apply its principles to enzymatic reactions in homogeneous and heterogeneous systems.

3.2
Fundamental Reaction Kinetics

3.2.1
Rates of Chemical Reaction

The rate of reaction r_i (kmol m^{-3} s^{-1}) is usually defined per unit volume of the fluid in which the reaction takes place, that is,

$$r_i = \frac{1}{V}\left(\frac{dN_i}{dt}\right) \tag{3.1}$$

Biochemical Engineering: A Textbook for Engineers, Chemists and Biologists, Second Edition.
Shigeo Katoh, Jun-ichi Horiuchi, and Fumitake Yoshida.

Companion Website: www.wiley.com\go\katoh\biochem_eng_e2

where V is the fluid volume (m^3) in a reactor, N_i the number of moles of i formed (kmol), and t is the time (s).

In Equation 3.1, the suffix i usually designates a reaction product. The rate r_i is negative, in case i is a reactant. Several factors, such as temperature, pressure, the concentrations of the reactants, and also the existence of a catalyst affect the rate of a chemical reaction. In some cases, what appears to be one reaction may in fact involve several reaction steps in series or in parallel, one of which may be rate limiting.

3.2.1.1 Elementary Reaction and Equilibrium

If the rate-limiting step in an irreversible second-order reaction to produce P from reactants A and B is the collision of single molecules of A and B, then the reaction rate should be proportional to the concentrations (C) of A and B; that is, C_A (kmol m^{-3}) and C_B (kmol m^{-3}). The rate of reaction can be given as

$$-r_A = kC_AC_B \tag{3.2}$$

where k is the rate constant for the second-order reaction (m^3 $kmol^{-1}$ s^{-1}). Its value for a given reaction varies with temperature and the properties of the fluid in which the reaction occurs, but is independent of the concentrations of A and B. The dimension of the rate constant varies with the order of the reaction.

Equation 3.2 corresponds to the simple stoichiometric relationship:

$$A + B \rightarrow P$$

This type of reaction for which the rate equation can be written according to the stoichiometry is called an elementary reaction. Rate equations for such cases can easily be derived. Many reactions, however, are non-elementary, and consist of a series of elementary reactions. In such cases, we must assume all possible combinations of elementary reactions in order to determine one mechanism that is consistent with the experimental kinetic data. Usually, we can measure only the concentrations of the initial reactants and final products, since measurements of the concentrations of intermediate reactions in series are difficult. Thus, rate equations can be derived under assumptions that rates of change in the concentrations of those intermediates are approximately zero (steady-state approximation). An example of such treatment applied to an enzymatic reaction is shown in Section 3.2.2.

In a reversible elementary reaction such as

$$A + B \leftrightarrow R + S$$

the rates of the forward and reverse reactions are given by Equations 3.3 and 3.4, respectively:

$$r_{R,forward} = k_fC_AC_B \tag{3.3}$$

$$-r_{R,reverse} = k_bC_RC_S \tag{3.4}$$

The rates of the forward and reverse reactions should balance at the reaction equilibrium. Hence

$$\frac{C_R C_S}{C_A C_B} = \frac{k_f}{k_b} = K_c \tag{3.5}$$

where K_c is the reaction equilibrium constant.

3.2.1.2 Temperature Dependence of Reaction Rate Constant k

The rates of chemical and biochemical reactions usually increase with temperature. The dependence of the reaction rate on temperature can usually be represented by the following Arrhenius-type equation over a wide temperature range:

$$k = k_0 e^{-\frac{E_a}{RT}} \tag{3.6}$$

where k_0 and E_a are the frequency factor and the activation energy (kJ kmol^{-1}), R is the gas law constant (8.31 kJ kmol^{-1} K^{-1}), and T is the absolute temperature (K). The frequency factor and the rate constant k should be of the same unit. The frequency factor is related to the number of collisions of reactant molecules, and is slightly affected by temperature in actual reactions. The activation energy is the minimum excess energy that the reactant molecules should possess for a reaction to occur. From Equation 3.6,

$$\ln k - \ln k_0 = -\frac{E_a}{RT} \tag{3.7}$$

Hence, as shown in Figure 3.1, a plot of the natural logarithm of k against $1/T$ gives a straight line with a slope of $-E_a/R$, from which the value of E_a can be calculated.

Example 3.1

Calculate the activation energy of a reaction from the plot of the experimental data, ln k versus $1/T$, as shown in Figure 3.1.

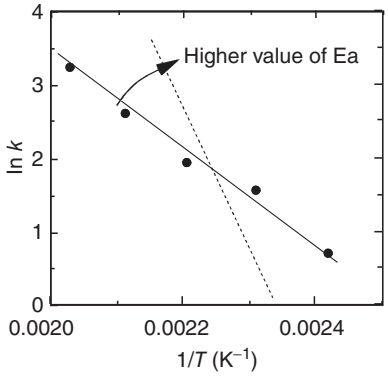

Figure 3.1 Arrhenius plot.

Solution

The slope of the straight line through the data points $(-E_a/R)$ is −6740 K. Thus, the activation energy is given as:

$$E_a = 6740 \times 8.31 = 56\,000 \text{ kJ kmol}^{-1}$$

Rates of reactions with larger values of activation energy are more sensitive to temperature changes. If the activation energy of a reaction is approximately 50 000 kJ kmol^{-1}, the reaction rate will be doubled with a 10 °C increase in reaction temperature at room temperature. Strictly, the Arrhenius equation is valid only for elementary reactions. Apparent activation energies can be obtained for non-elementary reactions.

3.2.1.3 Rate Equations for First- and Second-Order Reactions

The rates of liquid-phase reactions can generally be obtained by measuring the time-dependent concentrations of reactants and/or products in a constant-volume batch reactor. From experimental data, the reaction kinetics can be analyzed either by the integration method or by the differential method:

- In the *integration method*, an assumed rate equation is integrated and mathematically manipulated to obtain the best straight line plot to fit the experimental data of concentrations against time.
- In the *differentiation method,* values of the instantaneous reaction rate per unit volume $(1/V)(\mathrm{d}N_i/\mathrm{d}t)$ are obtained directly from experimental data points by differentiation and fitted to an assumed rate equation.

Each of these methods has both merits and demerits. For example, the integration method can easily be used to test several well-known specific mechanisms. In more complicated cases the differential method may be useful, but this requires more data points. Analysis by the integration method can generally be summarized as follows.

The rate equation for a reactant A is usually given as a function of the concentrations of reactants. Thus,

$$-r_A = -\left(\frac{\mathrm{d}C_A}{\mathrm{d}t}\right) = kf(C_i) \tag{3.8}$$

where $f(C_i)$ is an assumed function of the concentrations C_i.

If $f(C_i)$ is expressed in terms of C_A and k is independent of C_A, the above equation can be integrated to give

$$-\int_{C_{A0}}^{C_A} \frac{\mathrm{d}C_A}{f(C_A)} = k\int_0^t \mathrm{d}t = kt \tag{3.9}$$

where C_{A0} is the initial concentration of A. Plotting the left-hand side of Equation 3.9 against t should give a straight line of slope k. If experimental data points fit this straight line well, then the assumed specific mechanism can be

considered valid for the system examined. If not, another mechanism could be assumed.

Irreversible First-Order Reaction If a reactant A is converted to a product P by an irreversible unimolecular elementary reaction

$$A \rightarrow P$$

then the reaction rate is given as

$$-r_A = -\frac{dC_A}{dt} = kC_A \tag{3.10}$$

Rearrangement and integration of Equation 3.10 give

$$\ln \frac{C_{A0}}{C_A} = kt \tag{3.11}$$

The fractional conversion of a reactant A is defined as

$$x_A = \frac{N_{A0} - N_A}{N_{A0}} \tag{3.12}$$

where N_{A0} (kmol) is the initial amount of A at $t = 0$ and N_A (kmol) is the amount of A at $t = t$. The fractional conversion can be expressed also in terms of the concentrations (kmol m^{-3}),

$$x_A = \frac{C_{A0} - C_A}{C_{A0}} \tag{3.13}$$

Thus,

$$C_{A0} = \frac{C_A}{(1 - x_A)} \tag{3.14}$$

Substitution of Equation 3.14 into Equation 3.11 gives

$$-\ln(1 - x_A) = kt \tag{3.15}$$

If the reaction is of the first order, then plotting $-\ln(1 - x_A)$ or $\ln(C_{A0}/C_A)$ against time t should give a straight line through the origin, as shown in Figure 3.2. The slope gives the value of the rate constant k (s^{-1}).

The heat sterilization of microorganisms and heat inactivation of enzymes are examples of first-order reactions. In the case of an enzyme being irreversibly heat-inactivated as follows:

$$\text{N (active form)} \xrightarrow{k_d} \text{D (inactivated form)}$$

where k_d is the inactivation rate constant, and the rate of decrease in the concentration C_N of the active form is given by

$$-\frac{dC_N}{dt} = k_d C_N \tag{3.16}$$

Upon integration

$$\ln \frac{C_N}{C_{N_0}} = -k_d t \tag{3.17}$$

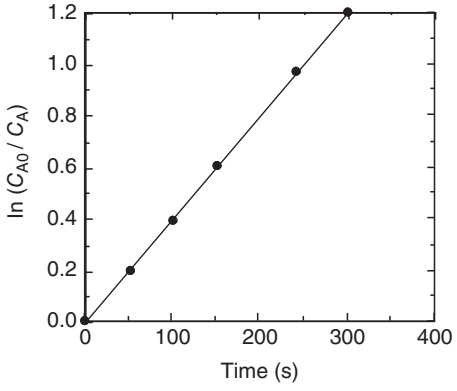

Figure 3.2 Analysis of a first-order reaction by integration method.

Plots of the natural logarithm of the fractional remaining activity $\ln(C_N/C_{N0})$ against incubation time at several temperatures should give straight lines. The time at which the activity becomes one-half of the initial value is called the half-life, $t_{1/2}$. The relationship between k_d and $t_{1/2}$ is given by

$$k_d = \frac{\ln 2}{t_{1/2}} \tag{3.18}$$

An enzyme with a higher inactivation constant loses its activity in a shorter time.

Example 3.2

The percentage decreases in the activities of α-amylase incubated at 70, 80, and 85 °C are given in Table 3.1. Calculate the inactivation constants of α-amylase at each temperature.

Table 3.1 Heat inactivation of α-amylase.

Incubation time (min)	Remaining activity (%)		
	70 °C	80 °C	85 °C
0	100	100	100
5	100	75	25
10	100	63	10
15	100	57	—
20	100	47	—

Solution

Plots of the fractional remaining activity C_N/C_{N0} against incubation time on semi-logarithmic coordinates give straight lines, as shown in Figure 3.3. The values of the inactivation constant k_d calculated from the slopes of these straight lines are as follows:

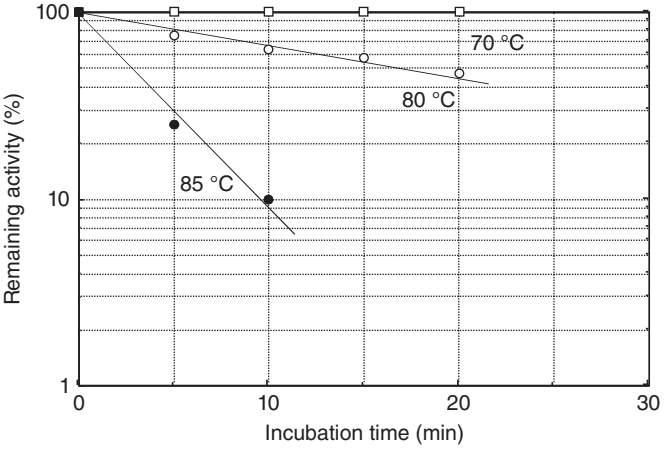

Figure 3.3 Heat inactivation of α-amylase.

Temperature (°C)	k_d (s^{-1})
70	Almost zero
80	0.00066
85	0.004

At higher temperatures, the enzyme activity decreases more rapidly with incubation time. The heat inactivation of many enzymes follows such patterns.

Irreversible Second-Order Reaction In the case where the reactants A and B are converted to a product P by a bimolecular elementary reaction:

$$A + B \rightarrow P$$

the rate equation is given as

$$-r_A = -\frac{dC_A}{dt} = -\frac{dC_B}{dt} = kC_AC_B \tag{3.19}$$

As this reaction is equimolar, the amount of reacted A should be equal to that of B; that is,

$$C_{A0}x_A = C_{B0}x_B \tag{3.20}$$

Thus, the rate equation can be rewritten as

$$\begin{aligned} -r_A &= C_{A0}\frac{dx_A}{dt} = k(C_{A0} - C_{A0}x_A)(C_{B0} - C_{A0}x_A) \\ &= kC_{A0}{}^2(1 - x_A)\left(\frac{C_{B0}}{C_{A0}} - x_A\right) \end{aligned} \tag{3.21}$$

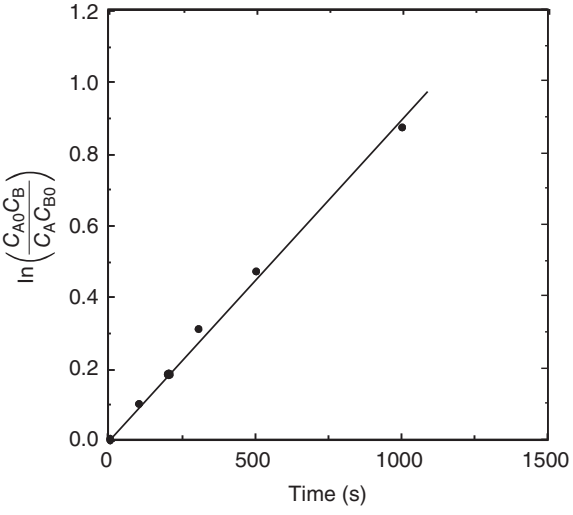

Figure 3.4 Analysis of a second-order reaction by integration method.

Integration and rearrangement give

$$\ln \frac{(1-x_B)}{(1-x_A)} = \ln \frac{C_B C_{A0}}{C_{B0} C_A} = (C_{B0} - C_{A0})kt \tag{3.22}$$

As shown in Figure 3.4, a plot of $\ln [(C_B C_{A0})/(C_{B0} C_A)]$ or $\ln [(1-x_B)/(1-x_A)]$ against t gives a straight line, from the slope of which k can be evaluated.

3.2.2 Rates of Enzyme Reactions

Most biochemical reactions in living systems are catalyzed by enzymes – that is, biocatalysts – which includes proteins and, in some cases, cofactors and coenzymes such as vitamins, nucleotides, and metal cations. Enzyme-catalyzed reactions generally proceed via intermediates, for example,

$$\begin{aligned} A + B + - - - - - - - + E\ (\text{Enzyme}) &\rightleftarrows EAB - - -\ (\text{intermediate}) \\ &\rightleftarrows P + Q + - - - - - - - + E \end{aligned}$$

The reactants in enzyme reactions are known as substrates. Enzyme reactions may involve uni-, bi-, or trimolecule reactants and products. An analysis of the reaction kinetics of such complicated enzyme reactions, however, is beyond the scope of this chapter, and the reader is referred elsewhere [1] or to other reference books. Here, we shall treat only the simplest enzyme-catalyzed reaction – that is, an irreversible, unimolecular reaction.

We consider that the reaction proceeds in two steps, namely,

$$\begin{matrix} & \text{(first reaction)} & & \text{(second reaction)} & \\ A + E & \rightleftarrows & EA & \rightarrow & P + E \end{matrix}$$

where A is a substrate, E an enzyme and EA is an intermediate (i.e., an enzyme-substrate complex), and P is a product. Enzyme-catalyzed hydrolysis and isomerization reactions are examples of this type of reaction mechanism. In this case, the kinetics can be analyzed by the following two different approaches, which lead to similar expressions.

3.2.2.1 Kinetics of Enzyme Reaction

Michaelis–Menten Approach In enzyme reactions, the total molar concentration of the free and combined enzyme, C_{E0} (kmol m^{-3}) should be constant; that is,

$$C_{E0} = C_E + C_{EA} \tag{3.23}$$

where C_E (kmol m^{-3}) and C_{EA} (kmol m^{-3}) are the concentrations of the free enzyme and the enzyme–substrate complex, respectively. It is assumed that the aforementioned first reaction is reversible and very fast, reaches equilibrium instantly, and that the rate of the product formation is determined by the rate of the second reaction, which is slower and proportional to the concentration of the intermediate [2].

For the first reaction at equilibrium the rate of the forward reaction should be equal to that of the reverse reaction, as stated in Section 3.2.1.1.

$$k_1 C_A C_E = k_{-1} C_{EA} \tag{3.24}$$

Thus, the equilibrium constant K of the first reaction is

$$K = \frac{k_1}{k_{-1}} \tag{3.25}$$

The rate of the second reaction for product formation is given as

$$r_P = \frac{dC_P}{dt} = k_2 C_{EA} \tag{3.26}$$

Substitution of Equation 3.23 into Equation 3.24 gives the concentration of the intermediate, C_{EA}.

$$C_{EA} = \frac{C_{E0} C_A}{\frac{k_{-1}}{k_1} + C_A} \tag{3.27}$$

Substitution of Equation 3.27 into Equation 3.26 gives the following Michaelis–Menten equation:

$$r_P = \frac{k_2 C_{E0} C_A}{\frac{k_{-1}}{k_1} + C_A} = \frac{V_{max} C_A}{K_m + C_A} \tag{3.28}$$

where V_{max} is the maximum rate of the reaction attained at very high substrate concentrations (kmol m^{-3} s^{-1}); K_m is the Michaelis constant (kmol m^{-3}), which is equal to the reciprocal of the equilibrium constant of the first reaction. Thus, a small value of K_m means a strong interaction between the substrate and the enzyme. An example of the relationship between the reaction rate and the

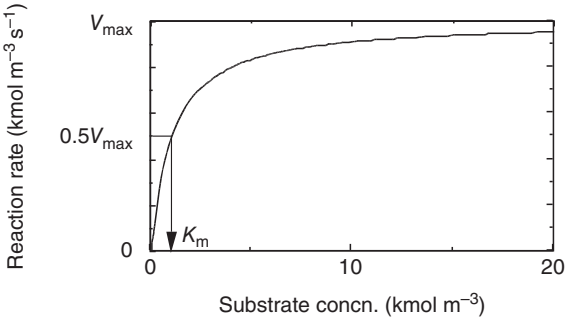

Figure 3.5 Relation between reaction rate and substrate concentration.

substrate concentration given by the Equation 3.28 is shown in Figure 3.5. Here, the reaction rate is roughly proportional to the substrate concentration at low substrate concentrations, and is asymptotic to the maximum rate V_{max} at high substrate concentrations. The reaction rate is one half of V_{max} at the substrate concentration equal to K_m.

It is usually difficult to express the enzyme concentration in molar unit because of difficulties in determining enzyme purity. Thus, the concentration is sometimes expressed as a "unit," which is proportional to the catalytic activity of an enzyme. The definition of an enzyme unit is arbitrary, but one unit is generally defined as the amount of enzyme that produces 1 μmol of the product in 1 min at the optimal temperature, pH and substrate concentration.

Briggs–Haldane Approach In this approach, the concentration of the intermediate is assumed to attain a steady-state value shortly after the start of a reaction (steady state approximation); that is, the change of C_{EA} with time becomes nearly zero [3]. Thus,

$$\frac{dC_{EA}}{dt} = k_1 C_A C_E - k_{-1} C_{EA} - k_2 C_{EA} \cong 0 \tag{3.29}$$

Substitution of Equation 3.23 into Equation 3.29 and rearrangement give the following equation.

$$C_{ES} = \frac{k_1 C_{E0} C_A}{k_{-1} + k_2 + k_1 C_A} \tag{3.30}$$

Then, the rate of product formation is given by

$$r_P = \frac{dC_P}{dt} = \frac{k_2 C_{E0} C_A}{\frac{k_{-1}+k_2}{k_1} + C_A} = \frac{V_{max} C_A}{K_m + C_A} \tag{3.31}$$

This expression by Briggs–Haldane is similar to Equation 3.28, obtained by the Michaelis–Menten approach, except that K_m is equal to $(k_{-1} + k_2)/k_1$. These two approaches become identical if $k_{-1} >> k_2$, which is the case of most enzyme reactions.

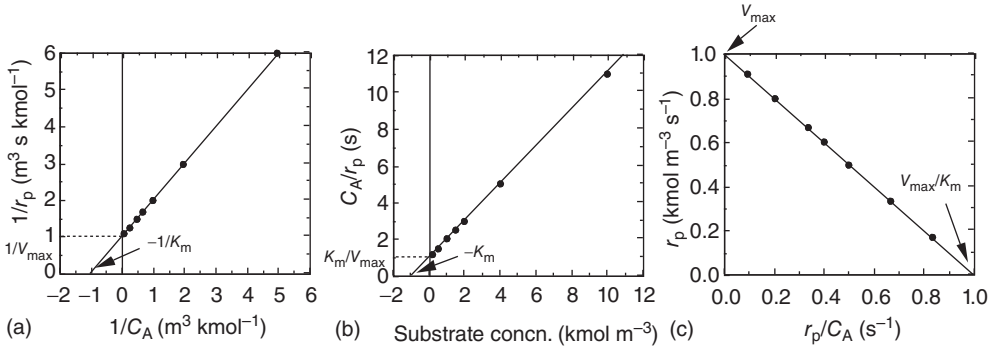

Figure 3.6 Evaluation of kinetic parameters in Michaelis–Menten equation: (a) Lineweaver–Burk plot, (b) C_A/r_p versus C_A plot, and (c) Eadie–Hofstee plot.

3.2.2.2 Evaluation of Kinetic Parameters in Enzyme Reactions

In order to test the validity of the kinetic models expressed by Equations 3.28 and 3.31, and to evaluate the kinetic parameters K_m and V_{max}, experimental data with different concentrations of substrate are required. Several types of plots for this purpose have been proposed.

Lineweaver–Burk Plot Rearrangement of the Michaelis–Menten equation (Equation 3.28) gives [4]

$$\frac{1}{r_P} = \frac{1}{V_{max}} + \frac{K_m}{V_{max}}\frac{1}{C_A} \tag{3.32}$$

A plot of $1/r_p$ against $1/C_A$ would give a straight line with an intercept of $1/V_{max}$. The line crosses the x-axis at $-1/K_m$, as shown in Figure 3.6a. Although the Lineweaver–Burk plot is widely used to evaluate the kinetic parameters of enzyme reactions, its accuracy is affected greatly by the accuracy of data at low substrate concentrations.

C_A/r_p Versus C_A Plot Multiplication of both sides of Equation 3.32 by C_A gives

$$\frac{C_A}{r_P} = \frac{K_m}{V_{max}} + \frac{C_A}{V_{max}} \tag{3.33}$$

A plot of C_A/r_p against C_A would give a straight line, from which the kinetic parameters can be determined, as shown in Figure 3.6b. This plot is suitable for regression by the method of least squares.

Eadie–Hofstee Plot Another rearrangement of the Michaelis–Menten equation gives

$$r_P = V_{max} - K_m\frac{r_P}{C_A} \tag{3.34}$$

A plot of r_p against r_p/C_A would give a straight line with a slope of $-K_m$ and an intercept of V_{max}, as shown in Figure 3.6c. Results with a wide range of substrate

concentrations can be compactly plotted when using this method, although the measured values of r_p appear in both coordinates.

All of the above treatments are applicable only to unimolecular irreversible enzyme reactions. In case of more complicated reactions, additional kinetic parameters must be evaluated, but plots similar to that for Equation 3.32, giving straight lines, are often used to evaluate kinetic parameters.

Example 3.3

Rates of hydrolysis of *p*-nitrophenyl-β-D-glucopyranoside by β-glucosidase, an irreversible unimolecular reaction, were measured at several concentrations of the substrate. The initial reaction rates were obtained as given in Table 3.2. Determine the kinetic parameters of this enzyme reaction.

Table 3.2 Hydrolysis rate of *p*-nitrophenyl-β-D-glucopyranoside by β-glucosidase.

Substrate concentration (gmol m^{-3})	Reaction rate (gmol m^{-3} s^{-1})
5.00	4.84×10^{-4}
2.50	3.88×10^{-4}
1.67	3.18×10^{-4}
1.25	2.66×10^{-4}
1.00	2.14×10^{-4}

Solution

The Lineweaver–Burk plot of the experimental data is shown in Figure 3.7. The straight line was obtained by the method of least squares. From the figure, the values of K_m and V_{max} were determined as 2.4 gmol m^{-3} and 7.7×10^{-4} gmol m^{-3} s^{-1}, respectively.

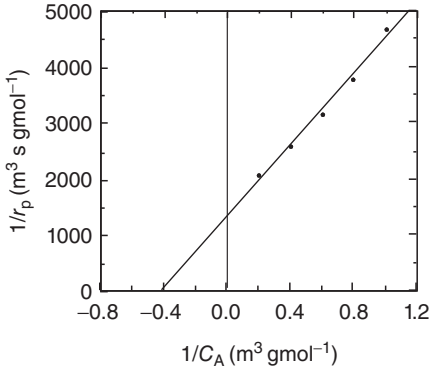

Figure 3.7 Linewever–Burk plot for hydrolysis of substrate by β-glucosidase.

3.2.2.3 Inhibition and Regulation of Enzyme Reactions

Rates of enzyme reactions are often affected by the presence of various chemicals and ions. Enzyme inhibitors combine, either reversibly or irreversibly, with enzymes and cause a decrease in enzyme activity. Effectors control enzyme reactions by combining with the regulatory site(s) of enzymes. There are several mechanisms of reversible inhibition and for the control of enzyme reactions.

Competitive Inhibition An inhibitor competes with a substrate for the binding site of an enzyme. As an enzyme–inhibitor complex does not contribute to product formation, it decreases the rate of product formation. Many competitive inhibitors have steric structures similar to substrates, and are referred to as substrate analogs.

Product inhibition is another example of such an inhibition mechanism of enzyme reactions, and is due to a structural similarity between the substrate and the product. The mechanism of competitive inhibition in a unimolecular irreversible reaction is considered as follows:

$$\begin{aligned} \mathrm{A} + \mathrm{E} &\rightleftarrows \mathrm{EA} \\ \mathrm{I} + \mathrm{E} &\rightleftarrows \mathrm{EI} \\ \mathrm{EA} &\rightarrow \mathrm{P} + \mathrm{E} \end{aligned}$$

where A, E, I, and P designate the substrate, enzyme, inhibitor, and product, respectively.

The sum of the concentrations of the remaining enzyme C_E and its complexes, C_{EA} and C_{EI}, should be equal to its initial concentration C_{E0}.

$$C_{E0} = C_{EA} + C_{EI} + C_E \tag{3.35}$$

If the rates of formation of the complexes EA and EI are very fast, then the following two equilibrium relationships should hold:

$$\frac{C_E C_A}{C_{EA}} = \frac{k_{-1}}{k_1} = K_m \tag{3.36}$$

$$\frac{C_E C_I}{C_{EI}} = \frac{k_{-i}}{k_i} = K_I \tag{3.37}$$

where K_I is the equilibrium constant of the inhibition reaction and is called the *inhibitor constant*.

From Equations 3.35 to 3.37, the concentration of the enzyme–substrate complex is given as

$$C_{EA} = \frac{C_{E0} C_A}{C_A + K_m \left(1 + \frac{C_I}{K_I}\right)} \tag{3.38}$$

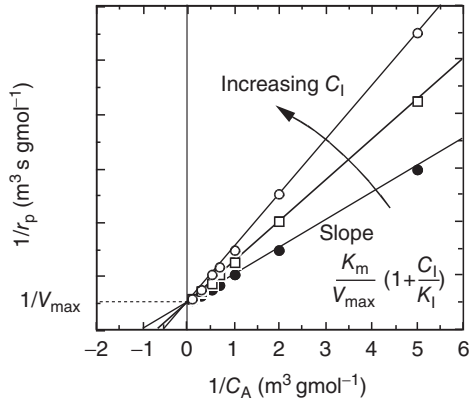

Figure 3.8 Evaluation of kinetic parameters of competitive inhibition.

Thus, the rate of product formation is given as

$$r_p = \frac{V_{max} C_A}{C_A + K_m \left(1 + \frac{C_I}{K_I}\right)} \tag{3.39}$$

In comparison with Equation 3.28 for the reaction without inhibition, the apparent value of the Michaelis constant increases by $(K_m C_I)/K_I$, and hence the reaction rate decreases. At high substrate concentrations, the reaction rates approach the maximum value because large amounts of the substrate decrease the effect of the inhibitor.

Rearrangement of Equation 3.39 gives

$$\frac{1}{r_p} = \frac{1}{V_{max}} + \frac{K_m}{V_{max}} \left(1 + \frac{C_I}{K_I}\right) \frac{1}{C_A} \tag{3.40}$$

Thus, by the Lineweaver–Burk plot the kinetic parameters K_m, K_I, and V_{max} can be graphically evaluated, as shown in Figure 3.8.

Other Reversible Inhibition Mechanisms In noncompetitive inhibition, an inhibitor is considered to combine with both an enzyme and the enzyme–substrate complex. Thus, the following reaction is added to the competitive inhibition mechanism:

$$I + EA \rightleftarrows EAI$$

We can assume that the equilibrium constants of the two inhibition reactions are equal in many cases. Then, the following rate equation can be obtained by the

Michaelis–Menten approach:

$$r_p = \frac{V_{max}}{\left(1 + \frac{K_m}{C_A}\right)\left(1 + \frac{C_I}{K_I}\right)} = \frac{V_{max} C_A}{(C_A + K_m)\left(1 + \frac{C_I}{K_I}\right)} \tag{3.41}$$

For the case of uncompetitive inhibition, where an inhibitor can combine only with the enzyme–substrate complex, the rate equation is given as

$$r_p = k_2 C_{EA} = \frac{V_{max} C_A}{C_A\left(1 + \frac{C_I}{K_I}\right) + K_m} \tag{3.42}$$

The substrate inhibition, in which the reaction rate decreases at high concentrations of substrate, follows this mechanism.

Example 3.4

A substrate L-benzoyl arginine *p*-nitroanilide hydrochloride was hydrolyzed by trypsin, with inhibitor concentrations of 0, 0.3, and 0.6 mmol l^{-1}. The hydrolysis rates obtained are listed in Table 3.3 [5]. Determine the inhibition mechanism and the kinetic parameters (K_m, V_{max}, and K_I) of this enzyme reaction.

Table 3.3 Hydrolysis rate of L-benzoyl arginine *p*-nitroanilide hydrochloride by trypsin with and without an inhibitor.

Substrate concentration (mmol l^{-1})	Inhibitor concentration (mmol l^{-1})		
	0	0.3	0.6
0.1	0.79	0.57	0.45
0.15	1.11	0.84	0.66
0.2	1.45	1.06	0.86
0.3	2.00	1.52	1.22

Hydrolysis rate, μmol l^{-1} s^{-1}.

Solution

The results given in Table 3.3 are plotted as shown in Figure 3.9. This Lineweaver–Burk plot shows that the inhibition mechanism is *competitive* inhibition. From the line for the data without the inhibitor, K_m and V_{max} are obtained as 0.98 gmol m^{-3} and 9.1 mmol m^{-3} s^{-1}, respectively. From the slopes of the lines, K_I is evaluated as 0.6 gmol m^{-3}.

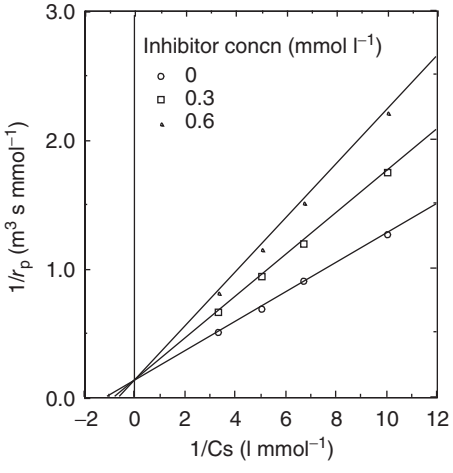

Figure 3.9 Lineweaver–Burk plot of hydrolysis reaction by trypsin.

▶ Problems

3.1 The rate constants of a first-order reaction

$$A \xrightarrow{k} P$$

are obtained at different temperature, as listed in Table P3.1.

Table P3.1 Reaction rate

Temperature (K)	Reaction rate constant (s^{-1})
293	0.011
303	0.029
313	0.066
323	0.140

Calculate the frequency factor and the activation energy for this reaction.

3.2 In a constant batch reactor, an aqueous reaction of a reactant A proceeds as given in Table P3.2. Find the rate equation and calculate the rate constant for the reaction, using the integration method.

Table P3.2 Time course of reaction

Time (min)	0	10	20	50	100
C_A (kmol m^{-3})	1.0	0.85	0.73	0.45	0.20

3.3 Derive an integrated rate equation similar to Equation 3.22 for the irreversible second-order reaction, when reactants A and B are introduced in the stoichiometric ratio:

$$\frac{1}{C_A} - \frac{1}{C_{A0}} = \frac{[x_A/(1 - x_A)]}{C_{A0}} = kt$$

3.4 An irreversible second-order reaction in the liquid phase

$$2A \rightarrow P$$

proceeds as shown in Table P3.4. Calculate the second-order rate constant for this reaction, using the integration method.

Table P3.4 Time course of reaction

Time (min)	0	50	100	200	300
C_A (kmol m^{-3})	1.00	0.600	0.450	0.295	0.212

3.5 An enzyme is irreversibly heat inactivated with an inactivation rate of $k_d = 0.001\ s^{-1}$ at 80 °C. Estimate the half-life $t_{1/2}$ of this enzyme at 80 °C.

3.6 An enzyme β-galactosidase catalyzes the hydrolysis of a substrate *p*-nitorophenyl-β-D-glucopyranoside to *p*-nitrophenol, the concentrations of which are given at 10, 20, and 40 min in the reaction mixture, as shown in Table P3.6.

Table P3.6 Time course of enzyme reaction

Time (min)	10	20	40
p-Nitrophenol concentration (gmol m^{-3})	0.45	0.92	1.83

1. Calculate the initial rate of the enzyme reaction.
2. What is the activity (units cm^{-3}) of β-glucosidase in the enzyme solution?

3.7 Rates of hydrolysis of *p*-nitrophenyl-β-D-glucopyranoside by β-glucosidase, an irreversible unimolecular reaction, were measured at several concentrations of the substrate, and the results shown in Table P3.7 were obtained. Determine K_m and V_{max} for this reaction.

Table P3.7 Initial rate of hydrolysis

Substrate concentration (gmol m^{-3})	Initial reaction rate (gmol m^{-3} s^{-1})
5.00	5.61×10^{-6}
2.50	3.85×10^{-6}
1.25	2.75×10^{-6}
1.00	2.22×10^{-6}
0.50	1.38×10^{-6}

3.8 Angiotensin-I converting enzyme (ACE) controls blood pressure by catalyzing the hydrolysis of two amino acids (His-Leu) at the C-terminus of angiotensin-I to produce a vasoconstrictor, angiotensin-II. The enzyme can also hydrolyze a synthetic substrate, hippuryl-L-histidyl-L-leucine (HHL), to hippuric acid (HA). At four different concentrations of HHL solutions (pH 8.3), the initial rates of HA formation ($\mu mol\, min^{-1}$) are obtained as shown in Table P3.8. Several small peptides (e.g., Ile-Lys-Tyr) can reversibly inhibit the ACE activity. The reaction rates of HA formation in the presence of 1.5 and 2.5 $\mu mol\, l^{-1}$ of an inhibitory peptide (Ile-Lys-Tyr) are also given in the table.

Table P3.8 Hydrolysis rate of HHL with and without inhibition

HHL concentration ($gmol\, m^{-3}$)	20	8.0	4.0	2.0
Reaction rate ($mmol\, m^{-3}\, min^{-1}$)				
Without peptide	1.83	1.37	1.00	0.647
1.5 $\mu mol\, l^{-1}$ peptide	1.37	0.867	0.550	0.313
2.5 $\mu mol\, l^{-1}$ peptide	1.05	0.647	0.400	0.207

1. Determine the kinetic parameters of the Michaelis–Menten reaction for the ACE reaction without the inhibitor.
2. Determine the inhibition mechanism and the value of K_I.

3.9 The enzyme invertase catalyzes the hydrolysis of sucrose to glucose and fructose. The rate of this enzymatic reaction decreases at higher substrate concentrations. Using the same amount of invertase, the initial rates at different sucrose concentrations are given in Table P3.9.

Table P3.9 Initial rate of hydrolysis

Sucrose concentration ($gmol\, m^{-3}$)	Reaction rate ($gmol\, m^{-3}\, min^{-1}$)
10	0.140
25	0.262
50	0.330
100	0.306
200	0.216

1. Assuming the following reaction mechanism of substrate inhibition, derive Equation 3.42.

$$E + S \rightleftarrows ES \qquad k_{-1}/k_1 = K_m$$
$$ES + S \rightleftarrows ES_2 \qquad k_{-i}/k_i = K_I$$
$$ES \rightarrow E + P$$

2. Assuming that the values of K_m and K_I are equal, determine their value.

References

1. King, E.L. and Altman, C. (1963) *J. Phys. Chem.*, **60**, 1375.
2. Michaelis, L. and Menten, M.L. (1913) *Biochem. Z.*, **49**, 333.
3. Briggs, G.E. and Halden, J.B.S. (1925) *Biochem. J.*, **19**, 338.
4. Lineweaver, H. and Burk, D. (1934) *J. Am. Chem. Soc.*, **56**, 658.
5. Erlanger, B.F., Kokowsky, N., and Cohen, W. (1961) *Arch. Biochem. Biophys.*, **95**, 271.

Further Reading

Hougen, O.A., Watson, K.M., and Ragatz, R.A. (1947) *Chemical Process Principles, Parts III*, John Wiley & Sons, Ltd.

Levenspiel, O. (1962) *Chemical Reaction Engineering*, 2nd edn, John Wiley & Sons, Ltd.

Smith, J.M. (1956) *Chemical Engineering Kinetics*, McGraw-Hill.

4
Cell Kinetics

4.1
Introduction

A number of foods, alcohols, amino acids, and others have long been produced via fermentation employing microorganisms. Recent developments in biotechnology – and especially gene technology – have made it possible to use genetically engineered microorganisms and cells for production of new pharmaceuticals and agricultural chemicals. These materials are generally produced via complicated metabolic pathways of the microorganisms and cells, and achieved by complicated parallel and serial enzyme reactions that are accompanied by physical processes, such as those described in Chapter 2. At this point, it is not appropriate to follow such mechanisms of cell growth only from the viewpoints of individual enzyme kinetics, such as discussed in Chapter 3. Rather, in practice, we can assume some simplified mechanisms, and consequently a variety of models of kinetics of cell growth have been developed on the basis of such assumptions. In this chapter, we discuss the characteristics and kinetics of cell growth.

4.2
Cell Growth

If microorganisms are placed under suitable physical conditions in an aqueous medium containing suitable nutrients, they are able to increase their number and mass by processes of fission, budding, and/or elongation. As the microorganisms contain 80–90% water, some elements – such as carbon, nitrogen, phosphorus, sulfur, as well as several other metallic elements – must be supplied from the culture medium. Typical compositions of culture media for bacteria and yeast are listed in Table 4.1. For animal cell culture, the media normally consist of a basal medium containing amino acids, salts, vitamins, glucose, and so on, in addition to 5–20% blood serum. Aerobic cells need oxygen for their growth, whereas anaerobic cells are able to grow without oxygen.

The cell concentration is usually expressed by the cell number density C_n (the number of cells per unit volume of medium), or by the cell mass concentration

Biochemical Engineering: A Textbook for Engineers, Chemists and Biologists, Second Edition.
Shigeo Katoh, Jun-ichi Horiuchi, and Fumitake Yoshida.

Companion Website: www.wiley.com\go\katoh\biochem_eng_e2

Table 4.1 Typical compositions of fermentation media.

For bacteria (LMB medium)		For yeast (YEPD medium)	
Yeast extract	5 g	Yeast extract	10 g
Tryptone	10 g	Peptone	20 g
NaCl	5 g	Glucose (20%)	100 ml
$MgCl_2$ (2 M)	5 ml	Water to make	1 l
Tris-HCl buffer (2 M, pH 7.4)	4 ml		
Water to make	1 l		

C_x (the dry weight, in kg or g, of cells per unit volume of medium). For a given size and composition of a cell, the cell mass and the cell number per unit volume of medium should be proportional. Such is the case of balanced growth, which is generally attained under suitable conditions. The growth rate of cells on a dry mass basis r_x (expressed as (kg dry cell) $m^{-3}\,h^{-1}$) is defined by

$$r_x = \frac{dC_x}{dt} \tag{4.1}$$

In balanced growth,

$$r_x = \frac{dC_x}{dt} = \mu C_x \tag{4.2}$$

where the constant μ (h^{-1}) is the *specific growth rate*, a measure of the rapidity of growth. The time required for the cell concentration (mass or number) to double – the *doubling time* t_d (h) – is given by Equation 4.3, upon integration of Equation 4.2.

$$t_d = \frac{(\ln 2)}{\mu} \tag{4.3}$$

The time from one fission to the next fission, or from budding to budding, is the generation time t_g (h), and is approximately equal to the doubling time. Several examples of specific growth rates are given in Table 4.2.

As cells grow, they consume the nutrients (i.e., substrates) from the medium. A portion of a substrate is used for the growth of cells and constitutes the cell

Table 4.2 Examples of specific growth rates.

Bacteria or cells	Temperature (°C)	Specific growth rate (h^{-1})
Escherichia coli	40	2.0
Aspergillus niger	30	0.35
Saccharomyces cerevisiae	30	0.17 – 0.35
HeLa cell	37	0.015 – 0.023

Table 4.3 Cell yields of several microorganisms.

Microorganisms	Substrate	Y_{xS} (kg dry cell (kg substrate)$^{-1}$)
Aerobacter aerogenes	Glucose	0.40
Saccharomyces cerevisiae	Glucose (aerobic)	0.50
Candida utilis	Glucose	0.51
Candida utilis	Acetic acid	0.36
Candida utilis	Ethanol	0.68
Pseudomonas fluorescens	Glucose	0.38

components. The cell yield with respect to a substrate S in the medium Y_{xS} ((kg dry cells formed)/(kg substrate consumed)) is defined by

$$Y_{xS} = \frac{C_x - C_{x0}}{C_{S0} - C_S} \tag{4.4}$$

where C_S is the mass concentration of the substrate and C_{S0} and C_{x0} are the initial values of C_S and C_x, respectively. Examples of the cell yields for various cells with some substrates are given in Table 4.3 [1].

4.3 Growth Phases in Batch Culture

When a small number of cells are added (inoculated) to a fresh medium of a constant volume, the cells will first self-adjust to their new environment and then begin to grow. At the laboratory scale, oxygen needed for aerobic cell growth is supplied by (i) shaking the culture vessel (shaker flask), which contains the culture medium and is equipped with a closure that is permeable only to air and water vapor; or (ii) bubbling sterile air through the medium contained in a static culture vessel. The cell concentration increases following a distinct time course; an example is shown in Figure 4.1, where logarithms of the cell concentrations are plotted against the cultivation time. A semi-logarithmic paper can conveniently be used for such a plot.

The time course curve, or *growth curve*, for a batch culture usually consists of six phases, namely the lag, accelerating, exponential growth, decelerating, stationary, and declining phases. During the *lag phase*, cells inoculated into a new medium self-adjust to the new environment and begin to synthesize the enzymes and components necessary for growth. The number of cells does not increase during this period. The duration of the lag phase depends on the type of cells, the age and number of inoculated cells, adaptability to the new culture conditions, and other factors. For example, if cells already growing in the exponential growth phase are inoculated into a medium of the same composition, the lag phase may be very

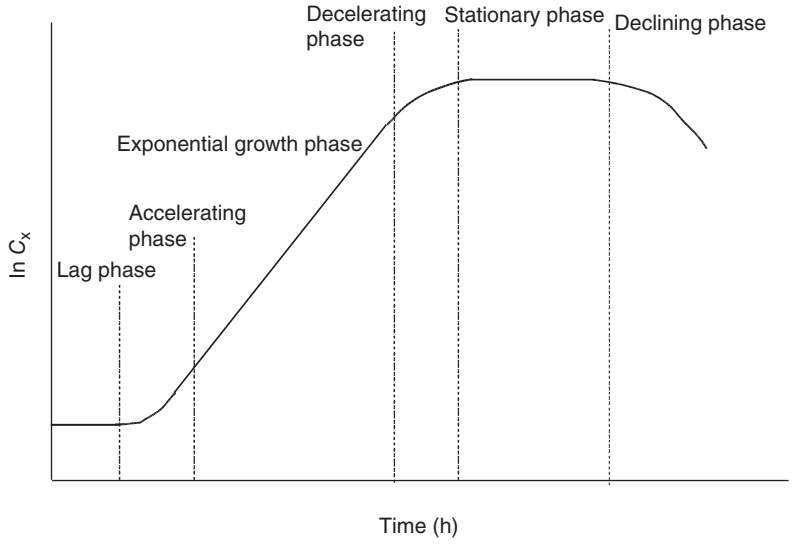

Figure 4.1 Typical growth curve in batch cell culture.

short. On the other hand, if cells in the stationary phase are inoculated, they may show a longer lag phase.

Cells that have adapted to the new culture conditions begin to grow after the lag phase; this period is called the *accelerating phase*. The growth rate of the cells gradually increases and reaches a maximum value in the *exponential growth phase*, where cells grow with a constant specific growth rate, μ_{max} (balanced growth). For the exponential growth phase Equation 4.2 can be integrated from time zero to t to give

$$C_x = C_{x0} \exp(\mu_{max} t) \tag{4.5}$$

where C_{x0} (kg dry cell m^{-3} medium) is the cell mass concentration at the start of the exponential growth phase. It is clear from Equation 4.5 why this phase is called the exponential growth phase; the cell concentration–time relationship for this phase can be represented by a straight line on a log C_x versus t plot, as shown in Figure 4.1.

After the exponential growth phase, the cell growth is limited by the availability of nutrients and the accumulation of waste products of metabolism. Consequently, the growth rate gradually decreases, and this phase is called the *decelerating phase*. Finally, growth stops in the *stationary phase*. In some cases, the rate of cell growth is limited by the supply of oxygen to the medium. After the stationary phase, cells begin to die and destroy themselves (lysis) in the *declining phase*; the result is a decrease in the cell concentration.

Example 4.1

Yeast cells grow in the exponential phase. The cell mass concentrations are given in Table 4.4. Calculate the specific growth rate, μ_{max}.

Table 4.4 Time course of cell growth

Time (h)	0	5	10	15	20	25
Cell concentration, C_x	0.5	1.3	4.0	10.2	24.0	52.5

kg dry cell m^{-3} medium.

Solution

A plot of a C_x/C_{x0} against cultivation time (Figure 4.2) gives a straight line, the slope of which can be used to evaluate μ_{max}.

$$\mu_{max} = 0.20\,h^{-1}$$

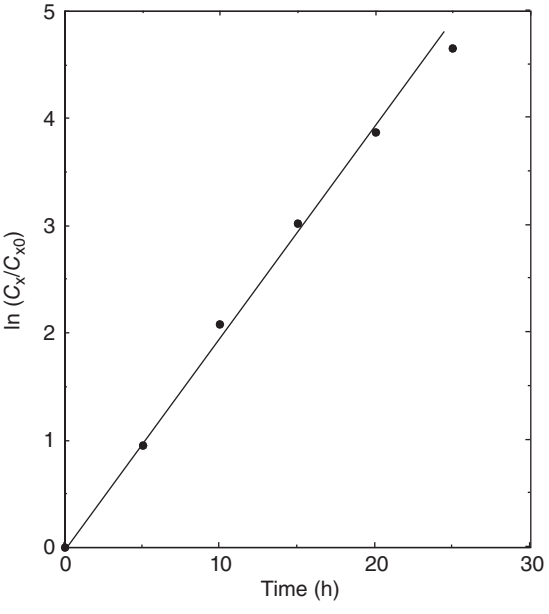

Figure 4.2 Determination of a specific growth rate in the exponential growth phase.

4.4
Factors Affecting Rates of Cell Growth

The rate of cell growth is influenced by temperature, pH, composition of medium, rate of air supply, and other factors. In the case that all other conditions are kept constant, the specific growth rate may be affected by the concentration of a certain specific substrate (the limiting substrate). The simplest empirical expression for the effect of the substrate concentration on the specific growth rate is the following Monod equation, which is similar in form to the Michaelis–Menten equation for enzyme reactions:

$$\mu = \frac{\mu_{\max} C_S}{K_S + C_S} \tag{4.6}$$

where C_S is the concentration of the limiting substrate (kmol m^{-3}) and the constant K_S is equal to the substrate concentration at which the specific growth rate is one half of μ_{max} (h^{-1}). It is assumed that cells grow with a constant cell composition and a constant cell yield. Examples of the relationships between the concentrations of the limiting substrate and the specific growth rates are shown in Figure 4.3.

Several improved expressions for cell growth have been proposed. In the case that cells do not grow below a certain concentration of the limiting substrate, because of the maintenance metabolism, a term μ_s (h^{-1}) corresponding to the substrate concentration required for maintenance is subtracted from the right-hand side of Equation 4.6. Thus,

$$\mu = \frac{\mu_{\max} C_S}{K_S + C_S} - \mu_s \tag{4.7}$$

$$\mu = 0 \quad \text{when} \quad \frac{\mu_{\max} C_S}{K_S + C_S} \leq \mu_s \tag{4.8}$$

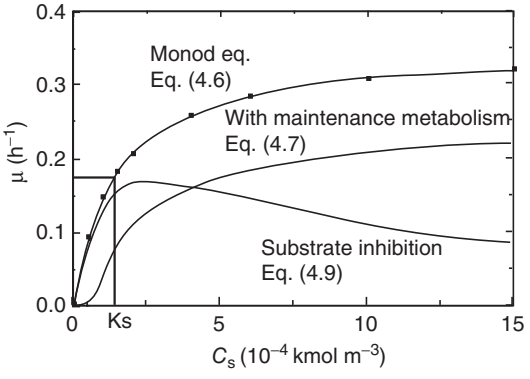

Figure 4.3 Specific growth rates by several models $\mu_{max} = 0.35\,h^{-1}$, $K_s = 1.4 \times 10^{-4}$ kmol m^{-3}, $\mu_s = 0.1\,h^{-1}$, and $K_I = 5 \times 10^{-4}$ kmol m^{-3}.

Some substrates inhibit cell growth at high concentrations. Equation 4.9, one of the expressions for such cases, can be obtained on the assumption that excess substrate will inhibit cell growth, in analogy to the uncompetitive inhibition in enzyme reactions, for which Equation 3.42 holds:

$$\mu = \frac{\mu_{max} C_S}{K_S + C_S + \frac{C_S^2}{K_I}} \tag{4.9}$$

K_I can be defined similarly to Equation 3.42.

The products by cell growth, such as ethyl alcohol and lactic acid, occasionally inhibit cell growth. In such cases, the product is considered to inhibit cell growth in the same way as inhibitors do in enzyme reactions, and the following equation (which is similar to Equation 3.41, for noncompetitive inhibition in enzyme reactions) can be applied:

$$\mu = \frac{\mu_{max} C_S}{K_S + C_S} \frac{K_I}{K_I + C_p} \tag{4.10}$$

where C_p is the concentration of the product.

4.5 Cell Growth in Batch Fermentors and Continuous Stirred-Tank Fermentors (CSTF)

4.5.1 Batch Fermentor

In case the Monod equation holds for the rates of cell growth in the exponential growth, with decelerating and stationary phases in a uniformly mixed fermentor operated batchwise, a combination of Equations 4.2 and 4.6 gives

$$\frac{dC_x}{dt} = \frac{\mu_{max} C_S}{K_S + C_S} C_x \tag{4.11}$$

As the cell yield is considered to be constant during these phases,

$$-\frac{dC_S}{dt} = \frac{1}{Y_{xS}} \frac{dC_x}{dt} \tag{4.12}$$

Thus, plotting C_x against C_S should give a straight line with a slope of $-Y_{xS}$, and the following relationship should hold:

$$C_{x0} + Y_{xS} C_{S0} = C_x + Y_{xS} C_S = \text{constant} \tag{4.13}$$

where C_{x0} and C_{S0} are the concentrations of cell and the limiting substrate at $t = 0$, respectively. Substitution of Equation 4.13 into Equation 4.11 and integration give the following equation:

$$\mu_{max} t = \left(\frac{K_S Y_{xS}}{C_{x0} + Y_{xS} C_{S0}} + 1 \right) \ln \frac{X}{X_0} + \frac{K_S Y_{xS}}{C_{x0} + Y_{xS} C_{S0}} \ln \frac{1 - X_0}{1 - X} \tag{4.14}$$

where

$$X = \frac{C_x}{C_{x0} + Y_{xS} C_{S0}} \tag{4.15}$$

Note that X is the dimensionless cell concentration.

Example 4.2

Draw dimensionless growth curves (X against $\mu_{max} t$) for $\frac{K_S Y_{xS}}{C_{x0} + Y_{xS} C_{S0}} = 0, 0.2,$ and 0.5, when $X_0 = 0.05$.

Solution

In Figure 4.4 the dimensionless cell concentrations X are plotted on semi-logarithmic coordinates against the dimensionless cultivation time $\mu_{max} t$ for the different values of $\frac{K_S Y_{xS}}{C_{x0} + Y_{xS} C_{S0}}$. With an increase in these values, the growth rate decreases and reaches the decelerating phase at an earlier time. Other models can be used for estimation of the cell growth in batch fermentors.

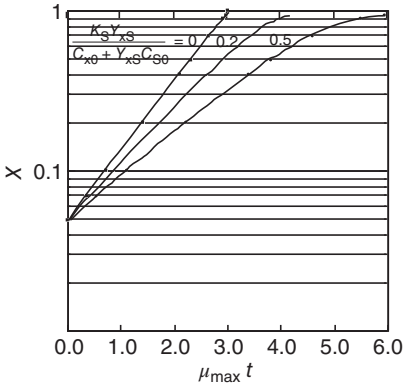

Figure 4.4 Dimensionless growth curves in batch fermenter.

4.5.2 Continuous Stirred-Tank Fermentor

Stirred-tank reactors can be used for continuous fermentation, because cells can grow in this type of fermentors without their being added to the feed medium. In contrast, if a plug flow reactor is used for continuous fermentation, then it is necessary to add the cells continuously in the feed medium, but this makes the operation more difficult.

There are two different ways of operating continuous stirred-tank fermentors (CSTFs), namely *chemostat* and *turbidostat*. In the chemostat, the flow rate of the

feed medium and the liquid volume in the fermentor are kept constant. The rate of cell growth will then adjust itself to the substrate concentration, which depends on the feed rate and substrate consumption by the growing cells. In the turbidostat the liquid volume in the fermentor and the liquid turbidity, which vary with the cell concentration, are kept constant by adjusting the liquid flow rate. While turbidostat operation requires a device to monitor the cell concentration (e.g., an optical sensor) and a control system for the flow rate, chemostat is much simpler to operate and hence is far more commonly used for continuous fermentation. The characteristics of the CSTF, when operated as a chemostat, are discussed in Chapter 12.

Problems

4.1 *Escherichia coli* grows with a doubling time of 0.5 h in the exponential growth phase.

1. What is the value of the specific growth rate?
2. How much time would be required to grow the cell culture from 0.1 to 10 kg-dry cell m^{-3}?

4.2 *E. coli* grows from 0.10 to 0.50 kg dry cell m^{-3} in 1 h.

1. Assuming exponential growth during this period, evaluate the specific growth rate.
2. Evaluate the doubling time during the exponential growth phase.
3. How much time would be required to grow from 0.10 to 1.0 kg dry cell m^{-3}? You may assume exponential growth during this period.

4.3 *Pichia pastoris* (a yeast) was inoculated at 1.0 kg dry cells m^{-3} and cultured in a medium containing 15 wt% glycerol (batch culture). The time-dependent concentrations of cells are shown in Table P4.3.

Table P4.3 Time course of cell growth

Time (h)	0	1	2	3	5	10	15	20	25	30	40	50
Cell concentration	1.0	1.0	1.0	1.1	1.7	4.1	8.3	18.2	36.2	64.3	86.1	98.4

kg dry cell m^{-3}.

1. Draw a growth curve of the cells by plotting the logarithm of the cell concentrations against the cultivation time.
2. Assign the accelerating, exponential growth, and decelerating phases of the growth curve in part 1.
3. Evaluate the specific growth rate during the exponential growth phase.

4.4 Photosynthetic microalga (*Haematococcus pluvialis*) was inoculated at 2.0 kg dry cell m^{-3} and cultured in a basal medium (containing yeast extract, acetate, asparagine, and some metals) under illumination by fluorescent lamps. The cell concentrations are shown in Table P4.4.

Table P4.4 Time course of cell growth

Time (h)	0	20	25	50	75	100	125
Cell concentration	2.0	2.0	2.3	7.0	24.5	58.5	77.0

kg dry cell m^{-3}.

Assign the exponential growth phase, and evaluate the maximum specific growth rate. How does the specific growth rate differ from those of *E. coli* and yeast cells in Problems 4.2 and 4.3?

4.5 Yeast cells grew from 19 to 54 kg dry cell m^{-3} in 7 h. During this period 81 g of glycerol was consumed per 1 l of the fermentation broth. Determine the average specific growth rate and the cell yield with respect to glycerol.

4.6 *E. coli* was continuously cultured in a continuous stirred tank fermentor with a working volume of 1.0 l by chemostat. A medium containing 4.0 g l^{-1} of glucose as a carbon source was fed to the fermentor at a constant flow rate of 0.5 l h^{-1}, and the glucose concentration in the output stream was 0.20 g l^{-1}. The cell yield with respect to glucose Y_{xS} was 0.42 g dry cells per gram glucose.
Determine the cell concentration in the output stream and the specific growth rate.

Reference

1. Nagai, S. (1979) *Adv. Biochem. Eng.*, **11**, 53.

Further Reading

Aiba, S., Humphrey, A.E., and Millis, N.F. (1973) *Biochemical Engineering*, 2nd edn, University of Tokyo Press.

Part II
Unit Operations and Apparatus for Biosystems

Biochemical Engineering: A Textbook for Engineers, Chemists and Biologists, Second Edition.
Shigeo Katoh, Jun-ichi Horiuchi, and Fumitake Yoshida.

Companion Website: www.wiley.com\go\katoh\biochem_eng_e2

5
Heat Transfer

5.1
Introduction

Heat transfer (heat transmission) is an important unit operation in chemical and bioprocess plants. In general, heat is transferred by one of the three mechanisms, namely, conduction, convection, and radiation, or by their combinations. However, we need not consider radiation in bioprocess plants, which usually operate at relatively low temperatures. The heating and cooling of solids rarely become problematic in bioprocess plants.

The term "heat exchanger" in the broader sense means heat transfer equipment in general. In the narrower sense, however, it means an equipment in which colder fluid is heated through use of the waste heat of a hotter fluid. For example, in milk pasteurization plants the raw milk is usually heated in a heat exchanger by pasteurized hot milk, before the raw milk is heated by steam in the main heater.

Figure 5.1 shows, conceptually, four commonly used types of heat transfer equipment, although many more refined designs of such equipment exist. On a smaller scale, a double-tube type is used, whereas on an industrial scale a shell-and-tube type heat exchanger is frequently used.

5.2
Overall Coefficients *U* and Film Coefficients *h*

Figure 5.2 shows the temperature gradients in the case of heat transfer from fluid 1 to fluid 2 through a flat metal wall. As the thermal conductivities of metals are greater than those of fluids, the temperature gradient across the metal wall is less steep than those in the fluid laminar sublayers, through which heat must be transferred also by conduction. Under steady-state conditions, the heat flux q (kcal h^{-1} m^{-2} or W m^{-2}) through the two laminar sublayers and the metal wall should be equal. Thus,

$$q = h_1(t_1 - t_{w1}) = \left(\frac{\kappa}{x}\right)(t_{w1} - t_{w2}) = h_2(t_{w2} - t_2) \tag{5.1}$$

where h_1 and h_2 are the film coefficients of heat transfer (kcal h^{-1} m^{-2} °C^{-1}) (cf. Section 2.6) for fluids 1 and 2, respectively, κ is the thermal conductivity of

Biochemical Engineering: A Textbook for Engineers, Chemists and Biologists, Second Edition.
Shigeo Katoh, Jun-ichi Horiuchi, and Fumitake Yoshida.

Companion Website: www.wiley.com\go\katoh\biochem_eng_e2

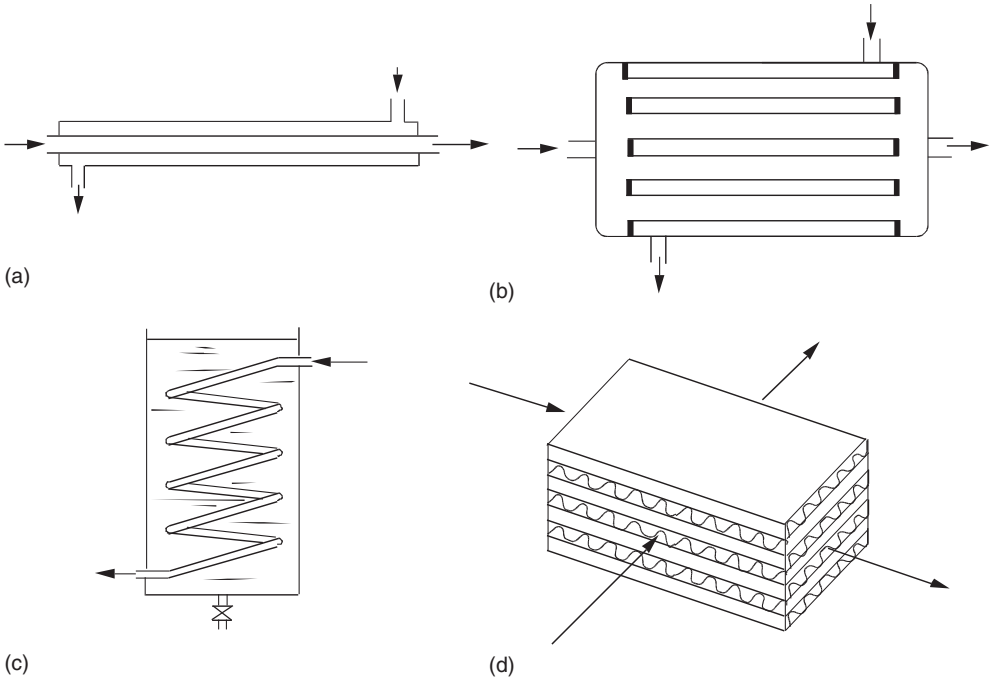

Figure 5.1 Few common types of heat exchangers. (a) Double-tube type; (b) shell-and-tube type; (c) coil-type; and (d) plate-type.

the metal wall (kcal h^{-1} m^{-1} °C^{-1} or W m^{-1} K^{-1}), and x is the metal wall thickness (m). Evidently,

$$t_1 - t_2 = (t_1 - t_{w1}) + (t_{w1} - t_{w2}) + (t_{w2} - t_2) \tag{5.2}$$

In designing and evaluating heat exchangers, Equation 5.1 cannot be used directly, as the temperatures of the wall surface t_{w1} and t_{w2} are usually unknown. Thus, the usual practice is to use the overall heat transfer coefficient U (kcal h^{-1} m^{-2} °C^{-1} or W m^{-2} K^{-1}), which is based on the overall temperature difference $(t_1 - t_2)$ – that is, the difference between the bulk temperatures of two fluids. Thus,

$$q = U(t_1 - t_2) \tag{5.3}$$

From Equations 5.1–5.3, we obtain

$$\frac{1}{U} = \frac{1}{h_1} + \frac{x}{\kappa} + \frac{1}{h_2} \tag{5.4}$$

This equation indicates that the overall heat transfer resistance, $1/U$, is the sum of the heat transfer resistances of fluid 1, metal wall, and fluid 2.

The values of κ and x are usually known, while the values of h_1 and h_2 can be estimated, as stated later. It should be noted that, as in the case of electrical resistances in series, the overall resistance for heat transfer is often

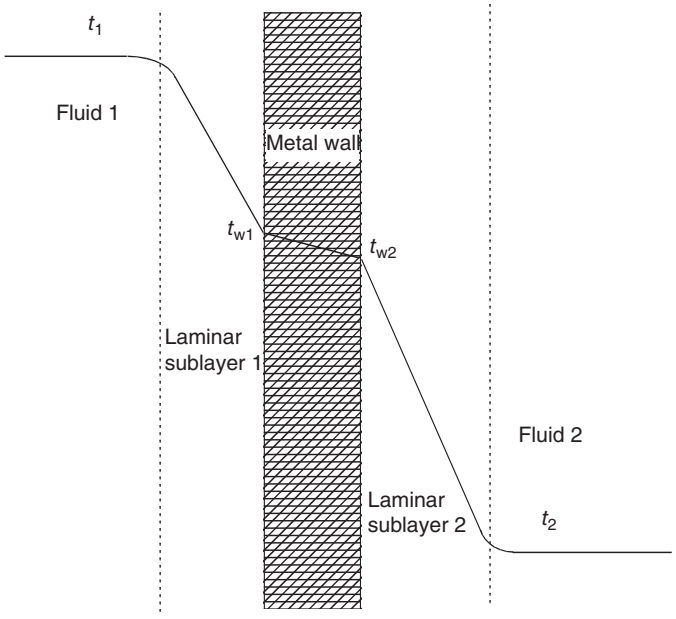

Figure 5.2 Temperature gradients in heat transfer from one fluid to another through a metal wall.

controlled by the largest individual resistance. Suppose, for instance, a gas (fluid 2) is heated by condensing steam (fluid 1) in a heat exchanger with a stainless steel wall ($\kappa = 20\,\text{kcal}\,\text{h}^{-1}\,\text{m}^{-1}\,°\text{C}^{-1}$), 1 mm thick. In case it is known that $h_1 = 7000\,\text{kcal}\,\text{h}^{-1}\,\text{m}^{-2}\,°\text{C}^{-1}$ and $h_2 = 35.0\,\text{kcal}\,\text{h}^{-1}\,\text{m}^{-2}\,°\text{C}^{-1}$, calculation by Equation 5.4 gives $U = 34.8\,\text{kcal}\,\text{h}^{-1}\,\text{m}^{-2}\,°\text{C}^{-1}$, which is almost equal to h_2. In such cases, the resistances of the metal wall and condensing steam can be neglected.

In the case of heat transfer equipment using metal tubes, one problem is which surface area – the inner surface area A_i or the outer surface area A_o – should be taken in defining U. Although this is arbitrary, the values of U will depend on which surface area is taken. Clearly, the following relationship holds:

$$U_\text{i} A_\text{i} = U_\text{o} A_\text{o} \tag{5.5}$$

where U_i is the overall coefficient based on the inner surface area A_i and U_o is based on the outer surface area A_o. In a case such as mentioned above, where h on one of the surface is much smaller than h on the other side, it is suggested that U should be defined on the basis of the surface for the smaller h. Then, U would become practically equal to the smaller h. For the general case, see Example 5.1.

In practical design calculations, we usually must consider the heat transfer resistance of the dirty deposits that accumulate on the heat transfer surface after a period of use. This problem of resistance cannot be neglected, in case the values of heat transfer coefficients h are relatively high. The reciprocal of

this resistance is termed the *fouling factor*, and this has the same dimension as h. Values of the fouling factor based on experience are available in a variety of reference books. As an example, the fouling factor with cooling water and that with organic liquids are in the (very approximate) ranges of 1000–10 000 and 1000–5000 kcal h^{-1} m^{-2} °C^{-1}, respectively.

Example 5.1

A liquid–liquid heat exchanger uses metal tubes that are of 30 mm inside diameter and 34 mm outside diameter. The values of h for the liquid 1 flowing inside the tubes $(h_1)_i = 1230$ kcal h^{-1} m^{-2} °C^{-1} and h for the liquid 2 flowing outside the tubes $(h_2)_o = 987$ kcal h^{-1} m^{-2} °C^{-1}. Estimate U_o based on the outside tube surface and U_i for the inside tube surface, neglecting the heat transfer resistance of the tube wall and the dirty deposit.

Solution

First, $(h_1)_i$ is converted to $(h_1)_o$ based on the outside tube surface.

$$(h_1)_o = (h_1)_i \times \frac{30}{34} = 1230 \times \frac{30}{34} = 1085 \text{ kcal h}^{-1} \text{ m}^{-2} \text{ °C}^{-1}$$

Then, neglecting the heat transfer resistance of the tube wall

$$\frac{1}{U_o} = \frac{1}{(h_1)_o} + \frac{1}{(h_2)_o} = \frac{1}{1085} + \frac{1}{987}$$

$$U_o = 517 \text{ kcal h}^{-1} \text{ m}^{-2} \text{ °C}^{-1}$$

By Equation 5.5

$$U_i = 517 \times \frac{34}{30} = 586 \text{ kcal h}^{-1} \text{ m}^{-2} \text{ °C}^{-1}$$

5.3 Mean Temperature Difference

The points discussed so far apply only to the local rate of heat transfer at one point on the heat transfer surface. As shown in Figure 5.3, the distribution of the overall temperature difference in practical heat transfer equipment is not uniform over the entire heat transfer surface in most cases. Figure 5.3 shows the temperature difference distributions in (a) a countercurrent heat exchanger, in which both fluids flow in opposite directions without phase change; (b) a cocurrent heat exchanger, in which both fluids flow in the same directions without phase change; (c) a fluid heater by condensing vapor, such as steam, or a vapor condenser cooled by a fluid, such as water; and (d) a fluid cooler by a boiling liquid, for example, a boiling refrigerant. In all of these cases, a mean temperature difference should be

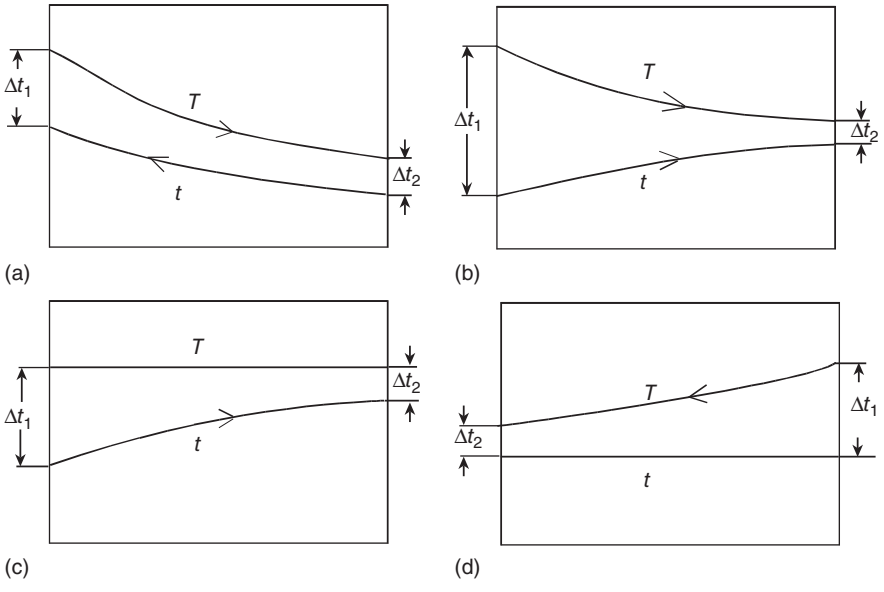

Figure 5.3 (a–d) Typical temperature differences in heat transfer equipment.

used in the design or evaluation of the heat transfer equipment. It can be shown that in the overall rate equation (Equation 5.6) the logarithmic mean temperature difference $(\Delta t)_{lm}$ as defined by Equation 5.7 should be used, provided that at least one of the two fluids, which flow in parallel or countercurrent to each other, undergoes no phase change and that the variation of U and the specific heats are negligible.

$$Q = UA(\Delta t)_{lm} \tag{5.6}$$

where

$$(\Delta t)_{lm} = \frac{(\Delta t_1 - \Delta t_2)}{\ln(\Delta t_1/\Delta t_2)} \tag{5.7}$$

where Q is the total heat transfer rate (kcal h^{-1} or W), A is the total heat transfer area (m^2), and Δt_1 and Δt_2 are the larger and smaller temperature differences (°C) at both ends of the heat transfer area, respectively. The logarithmic mean is always smaller than the arithmetic mean. When the ratio of Δt_2 and Δt_1 is <2, the arithmetic mean could be used in place of the logarithmic mean because the two mean values differ by only several percentage points. In those cases where the two fluids do not flow in countercurrent or parallel current without phase change, for example, in cross-current to each other, then the logarithmic mean temperature difference $(\Delta t)_{lm}$ must be multiplied by certain correction factors, the values of which for various cases are provided in reference books [1].

It can be shown that the logarithmic mean temperature difference may also be used for the batchwise heating or cooling of fluids. In such cases, the logarithmic

mean of the temperature differences at the beginning and the end of the operation should be used as the mean temperature difference.

Example 5.2

Derive Equation 5.6 for the logarithmic mean temperature difference.

Solution

If variations of U and the specific heat(s) and flow rate(s) of the fluid(s) flowing without phase change are negligible, then the relationship between Q and Δt should be linear. Thus,

$$\frac{\mathrm{d}(\Delta t)}{\mathrm{d}Q} = \frac{(\Delta t_1 - \Delta t_2)}{Q} \tag{a}$$

and

$$\mathrm{d}Q = U\Delta t \cdot \mathrm{d}A \tag{b}$$

Combining Equations a and b

$$\frac{\mathrm{d}(\Delta t)}{\Delta t} = \frac{(\Delta t_1 - \Delta t_2)U\mathrm{d}A}{Q} \tag{c}$$

Integration of Equation c gives

$\ln(\Delta t_1/\Delta t_2) = (\Delta t_1 - \Delta t_2)UA/Q$, that is, Equation 5.6.

5.4 Estimation of Film Coefficients *h*

Extensive experimental data and many correlations are available in the literature for individual heat transfer coefficients in various cases, such as the heating and cooling of fluids without phase change, and for cases with phase change, namely, the boiling of liquids and condensation of vapors. Individual heat transfer coefficients can be predicted by a variety of correlations, most of which are either empirical or semi-empirical, although it is possible to predict h-values from a theoretical standpoint for pure laminar flow. Correlations for h are available for heating or cooling of fluids in forced flow in various heat transfer devices, natural convection without phase change, condensation of vapors, boiling of liquids, and other cases, as functions of fluid physical properties, geometry of devices, and operating conditions such as fluid velocity. Only a few examples of correlations for h in simple cases are outlined below; for other examples the reader should refer to various reference books, if necessary [1].

5.4.1

Forced Flow of Fluids through Tubes (Conduits)

For the individual (film) coefficient h for heating or cooling of fluids, without phase change, in turbulent flow through circular tubes, the following dimensionless equation [2] is well established. In the following equations all fluid properties are evaluated at the arithmetic-mean bulk temperature.

$$\left(\frac{hd_i}{\kappa}\right) = 0.023\left(\frac{d_i v\rho}{\mu}\right)^{0.8}\left(\frac{c_p\mu}{\kappa}\right)^{1/3} \tag{5.8a}$$

or

$$(\mathrm{Nu}) = 0.023\,(\mathrm{Re})^{0.8}(\mathrm{Pr})^{1/3} \tag{5.8b}$$

in which d_i is the inner diameter of tube (m), κ is the thermal conductivity of fluid (kcal h^{-1} m^{-1} °C^{-1}), v is the average velocity of fluid through tube (m h^{-1}), ρ is the liquid density (kg m^{-3}), c_p is the specific heat at constant pressure (kcal kg^{-1} °C^{-1}), μ is the liquid viscosity (kg m^{-1} h^{-1}), (Nu) is the dimensionless Nusselt number, (Re) is the dimensionless Reynolds number (based on inner tube diameter), and (Pr) is the dimensionless Prandtl number.

The film coefficient h for turbulent flow of water through a tube can be estimated by the following dimensional equation [1]:

$$h = \frac{(3210 + 43t)v^{0.8}}{d_i^{0.2}} \tag{5.8c}$$

in which h is the film coefficient (kcal h^{-1} m^{-2} °C^{-1}), t is the average water temperature (°C), v is the average water velocity (m s^{-1}), and d_i is the inside diameter of the tube (cm).

Flow through tubes is sometimes laminar, when fluid viscosity is very high or the conduit diameter is very small, as in the case of hollow fibers. The values of h for laminar flow through tubes can be predicted by the following dimensionless equation [1, 3]:

$$(\mathrm{Nu}) = \left(\frac{hd_i}{\kappa}\right) = 1.62(\mathrm{Re})^{1/3}(\mathrm{Pr})^{1/3}\left(\frac{d_i}{L}\right)^{1/3} \tag{5.9a}$$

$$\text{or} \quad (\mathrm{Nu}) = 1.75\left(\frac{Wc_p}{\kappa L}\right)^{1/3} = 1.75(\mathrm{Gz})^{1/3} \tag{5.9b}$$

in which (Gz) is the dimensionless Graetz number, W is the mass flow rate of fluid per tube (kg h^{-1}), and L is the tube length (m), which affects h in laminar flow because of the end effect. Equation 5.9a, b holds for the range of (Gz) larger than 40. Values of (Nu) for (Gz) below 10 approach an asymptotic value of 3.66. (Nu) for the intermediate range of (Gz) can be estimated by interpolation on log–log coordinates.

Equations 5.8a and 5.9a give h for straight tubes. It is known that the values of h for fluids flowing through coils increase somewhat with decreasing radius of helix. However, in practice the values of h for straight tubes can be used in this situation.

In general, values of h for the heating or cooling of a gas (e.g., 5–50 kcal h^{-1} m^{-2} °C^{-1} for air) are much smaller than those for liquids (e.g., 1000–5000 kcal h^{-1} m^{-2} °C^{-1} for water) because the thermal conductivities of gases are much lower than those of liquids.

Values of h for turbulent or laminar flow through a conduit with a noncircular cross section can also be predicted by either Equation 5.8a or 5.9a, respectively, by using the equivalent diameter d_e, as defined by the following equation, in place of d_i.

$$d_e = 4 \times \frac{\text{(cross-sectional area)}}{\text{(wetted perimeter)}} \tag{5.10}$$

For example, d_e for a conduit with a rectangular cross section with the width b and height z is given as:

$$d_e = \frac{4bz}{[2(b+z)]} \tag{5.11}$$

Thus, d_e for a narrow space between two parallel plates, of which b is sufficiently large compared with z, is almost equal to $2z$. Values of d_e for such cases as fluid flow through the annular space between the outer and inner tubes of the double tube-type heat exchanger or fluid flow outside and parallel to the tubes of multitubular heat exchanger can be calculated using Equation 5.11.

Example 5.3

Calculate the equivalent diameter of the annular space of a double tube-type heat exchanger. The outside diameter of the inner tube d_1 is 4.0 cm and the inside diameter of the outer tube d_2 is 6.0 cm.

Solution

By Equation 5.10,

$$d_e = \frac{4(\pi/4)({d_2}^2 - {d_1}^2)}{\pi(d_1 + d_2)} = d_2 - d_1$$
$$= 6.0 \text{ cm} - 4.0 \text{ cm} = 2.0 \text{ cm}$$

In the above example, the total wetted perimeter is used in calculating d_e. In certain practices, however, the wetted perimeter for heat transfer – which would be $\pi\, d_1$ in the above example – is used in the calculation of d_e.

In the case where the fluid flow is parallel to the tubes, as in a shell-and-tube heat exchanger without transverse baffles, the equivalent diameter d_e of the shell side space is calculated as mentioned above, and h at the outside surface of tubes can be estimated by Equation 5.8a with the use of d_e.

5.4.2
Forced Flow of Fluids across a Tube Bank

In the case where a fluid flows across a bank of tubes, the film coefficient of heat transfer at the tube outside surface can be estimated using the following equation [1]:

$$\left(\frac{hd_o}{\kappa}\right) = 0.3\left(\frac{d_o G_m}{\mu}\right)^{0.6}\left(\frac{c_p\mu}{\kappa}\right)^{1/3} \tag{5.12a}$$

that is,

$$(\mathrm{Nu}) = 0.3(\mathrm{Re})^{0.6}(\mathrm{Pr})^{1/3} \tag{5.12b}$$

where d_o is the outer diameter of tubes (m) and G_m is the fluid mass velocity ($\mathrm{kg\,h^{-1}\,m^{-2}}$) in the transverse direction based on the minimum free area available for fluid flow; the other symbols are the same as in Equation 5.8a.

In the case where fluid flows in the shell side space of a shell-and-tube-type heat exchanger, with transverse baffles, in directions that are transverse, diagonal, and partly parallel to the tubes, very approximate values of the heat transfer coefficients at the tube outside surfaces can be estimated using Equation 5.12a, if G_m is calculated as the transverse velocity across the plane, including the shell axis [1].

5.4.3
Liquids in Jacketed or Coiled Vessels

Many correlations are available for heat transfer between liquids and the walls of stirred vessels or the surface of coiled tubes installed in the stirred vessels. For details of the different types of stirrer available, see Section 7.4.1.

Case 1: Data on heat transfer between liquid and the vessel wall and between liquid and the surface of helical coil in the vessels stirred with flat-blade paddle stirrers were correlated as [4]:

$$\left(\frac{hD}{\kappa}\right) = a\left(\frac{L^2N\rho}{\mu}\right)^{2/3}\left(\frac{c_p\mu}{\kappa}\right)^{1/3} \tag{5.13}$$

where h is the film coefficient of heat transfer, D is the vessel diameter, κ is the liquid thermal conductivity, L is the impeller diameter, N is the number of revolutions, ρ is the liquid density, μ is the liquid viscosity, and c_p is the liquid specific heat (all in consistent units). The values of a are 0.36 for the liquid-vessel wall heat transfer and 0.87 for the liquid-coil surface heat transfer. Any slight difference between h for heating and cooling can be neglected in practice.

Case 2: Data on heat transfer between a liquid and the wall of vessel of diameter D, stirred by a vaned-disk turbine, were correlated [5] by Equation 5.13. The values of a were 0.54 without baffles and 0.74 with baffles.

Case 3: Data on heat transfer between liquid and the surface of helical coil in the vessel stirred by flat-blade turbine were correlated [6] by Equation 5.14.

$$\left(\frac{hd_o}{\kappa}\right) = 0.17\left(\frac{L^2N\rho}{\mu}\right)^{0.67}\left(\frac{c_p\mu}{\kappa}\right)^{0.37} \tag{5.14}$$

where d_o is the outside diameter of the coil tube, and all other symbols are the same as in Equation 5.13.

5.4.4
Condensing Vapors and Boiling Liquids

Heating by condensing vapors, usually by saturated steam, is a very common practice in chemical and bioprocess plants. Liquid boiling and vapor condensation also occur in distillation or evaporation equipment.

Correlations are available for the film coefficients of heat transfer for condensing vapors and boiling liquids, usually as functions of fluid physical properties, temperature difference, and other factors such as the conditions of metal surface. Although of academic interest, the use of some assumed values of h is usually sufficient in practice, because for condensing vapors or boiling liquids these are much larger than those for the values of film coefficients of heat transfer h, for fluids without phase change, in which case the overall coefficient U is controlled by the latter. In addition, as is mentioned later, the heat transfer resistance of any dirt deposit is often larger than that of the condensing vapor and boiling liquid.

To give a few examples, h-values for film-type condensation of water vapor (when a film of condensed water would cover the entire cooling surface) will range from 4000 to 15 000 kcal h^{-1} m^{-2} °C^{-1}, and those for boiling water would be in the range of 1500 – 30 000 kcal h^{-1} m^{-2} °C^{-1}.

5.5
Estimation of Overall Coefficients *U*

The values of the film coefficients of heat transfer h, and accordingly those of the overall coefficient U, vary by orders of magnitudes, depending on the fluid properties and on whether they undergo phase change, that is, condensation or boiling. Thus, the correct estimation of U is very important in the design of heat transfer equipment.

The first consideration when designing or evaluating heat transfer equipment is as to which side of the heat transfer wall the controlling heat transfer resistance will exist on. For example, when air is heated by condensing saturated steam, the air-side film coefficient may be 30 kcal h^{-1} m^{-2} °C^{-1}, while the steam-side film coefficient might be on the order of 10 000 kcal h^{-1} m^{-2} °C^{-1}. In such a case, we need not consider the steam-side resistance. The overall coefficient would be almost equal to the air-side film coefficient, which can be predicted by

Table 5.1 Fouling factors (kcal h^{-1} m^{-2} °C^{-1}).

Condensing steam	15 000
Clean water	2 500 – 10 000
Dirty water	1 000 – 2 500
Oils (vegetable and fuel oils)	1 000 – 1 500

correlations such as those in Equation 5.8a or 5.12a. The resistance of the metal wall is negligible in most cases, except when values of U are very large.

The values of the film coefficient for liquids without phase change are usually larger than those for gases, by one or two orders of magnitude. Nonetheless, the liquid-side heat transfer resistance may be the major resistance in an equipment heated by saturated steam. Film coefficient for liquids without phase change can be predicted by correlations such as those in Equations 5.8a, 5.12a, or 5.13.

In the case of gas – gas or liquid – liquid heat exchangers, the film coefficients for the fluids on both sides of the metal wall are of the same order of magnitude, and can be predicted by correlations, for example, with Equation 5.8a or 5.12a. Neither of the fluid film resistances can be neglected. In a gas – liquid heat exchanger, the controlling resistance is on the gas side, as mentioned before.

In practice, we must consider the heat transfer resistance of the dirt or scale which has been deposited on the metal surface, except when values of U are small, as in the case of gas heater or cooler. Usually, we use the so-called fouling factor h_f, which is the reciprocal of the dirt resistance and hence has the same dimension as the film coefficient h. The dirt resistance sometimes becomes controlling, when U without dirt is very large – as in the case of liquid boiler heated by saturated steam. Thus, in case the dirt resistance is not negligible, the overall resistance for heat transfer $1/U$ is given by the following equation:

$$\frac{1}{U} = \frac{1}{h_1} + \frac{x}{\kappa} + \frac{1}{h_f} + \frac{1}{h_2} \tag{5.15}$$

The first, second, third, and fourth terms on the right-hand side of Equation 5.15 represent the resistances of the fluid 1, metal wall, dirt deposit, and film 2, respectively. Occasionally, we must also consider the resistances of the dirt on both sides of the metal wall. Some typical values of the fouling factor h_f are listed in Table 5.1.

Example 5.4

Milk, flowing at 2000 l h^{-1} through the stainless steel inner tube (40 mm i.d., 2 mm thick) of a double tube-type heater, is to be heated from 10 to 85 °C by saturated steam condensing at 120 °C on the outer surface of the inner tube. Calculate the total length of the heating tube required.

Solution

The thermal conductivity of stainless steel is 20 kcal h^{-1} m^{-2} °C^{-1}. The mean values of the properties of milk for the temperature range are as follows.

Specific heat, $c_p = 0.946$ kcal kg^{-1} °C^{-1}

Density, $\rho = 1030$ kg m^{-3}

Thermal conductivity, $\kappa = 0.457$ kcal h^{-1} m^{-1} °C^{-1} = 0.00127 cal s^{-1} cm^{-1} °C^{-1}

Viscosity, $\mu = 1.12 \times 10^{-3}$ kg m^{-1} s^{-1} = 0. 0112 g cm^{-1} s^{-1}

Velocity of milk through the tube $v = 2000 \times 1000/[(\pi/4)\, 4^2 \times 3600] = 44.2$ cm s^{-1}.
Then (Re) $= dv\,\rho/\mu = 16\,260$; (Pr) $= c_p \mu/\kappa = 8.34$.
Substitution of these values of (Re) and (Pr) into Equation 5.8a gives the milk-side film coefficient of heat transfer, $h_m = 1245$ kcal h^{-1} m^{-2} °C^{-1}.

Assumed steam-side coefficient, $h_s = 10\,000$ kcal h^{-1} m^{-2} °C^{-1}
Assumed milk-side fouling factor, $h_f = 3000$ kcal h^{-1} m^{-2} °C^{-1}

Resistance of the tube wall, $r_w = \dfrac{0.002}{20} = 0.0001$ h m^2 °C $kcal^{-1}$

Overall heat transfer resistance, $1/U = 1/h_s + r_w + 1/h_m + 1/h_f$

$= 0.00133$ h m^2°C $kcal^{-1}$

Overall heat transfer coefficient, $U = 750$ kcal h^{-1} m^{-2} °C^{-1}

Temperature differences : $(\Delta t)_1 = 120 - 10 = 110$ °C; $(\Delta t)_2 = 120 - 85 = 35$ °C

By Equation 5.7 $(\Delta t)_{lm} = (110 - 35)/\ln(110/35) = 65.6$ °C
Thus, heat to be transferred $Q = 2000 \times 1030 \times 0.946\,(85 - 10) = 146\,200$ kcal h^{-1}.
In calculating the required heat transfer surface area A of a tube, it is rational to take the area of the surface where h is smaller; that is, where the heat transfer resistance is larger and controlling – which is the milk-side inner surface area in this case. Thus,

$$A = \frac{Q}{[U(\Delta t)_{lm}]} = \frac{146\,200}{(750 \times 65.6)} = 2.97 \text{ m}^2$$

Total length of the heating tube required = 2.97/(0.040 π) = 23.6 m.

Problems

5.1 When glass tubes with the same dimension, instead of stainless tubes, are used in the liquid–liquid heat exchanger of Example 5.1, estimate U_o based on the outside tube surface, neglecting again the resistance of the dirty deposit. The thermal conductivity, κ, of glass is 0.63 kcal h^{-1} m^{-1} °C^{-1}. As for the heat transfer resistance of a round tube, see Problem 2.1.

5.2 Water enters a countercurrent shell-and-tube-type heat exchanger at 10 m^3 h^{-1} on the shell side, so as to increase the water temperature from 20 to 40 °C. The hot water enters at a temperature of 80 °C and a rate of 8.0 m^3 h^{-1}. The overall heat transfer coefficient is 900 W m^{-2} K^{-1}. You may use the specific heat $c_p = 4.2$ kJ kg^{-1} K^{-1} and density $\rho = 992$ kg m^{-3} of water.
Determine: (i) the exit temperature of the shell-side water and (ii) the required heat transfer area.

5.3 Air at 260 K and 1 atm flows through a 10 mm i.d. tube at a velocity 10 m s^{-1}. The temperature is to be increased to 300 K. Estimate the film coefficient of heat transfer. The properties of air at 280 K are $\rho = 1.26$ kg m^{-3}, $c_p = 1.006$ kJ kg^{-1} K^{-1}, $\kappa = 0.0247$ W m^{-1} K^{-1}, $\mu = 1.75 \times 10^{-5}$ Pa s.

5.4 Estimate the overall heat transfer coefficient U, based on the inside tube surface area of a shell-and-tube type vapor condenser, in which cooling water at 25 °C flows through stainless steel tubes, 25 mm i.d. and 30 mm o.d. at a velocity 1.2 m s^{-1}. It can be assumed that the film coefficient of condensing vapor at the outside tube surface is 2000 kcal h^{-1} m^{-2} °C^{-1}, and that the fouling factor of the water side is 5000 kcal h^{-1} m^{-2} °C^{-1}.

5.5 A double-tube type heat exchanger consisting of an inner copper tube 50 mm o.d. and 46 mm i.d. and a steel outer tube 80 mm i.d. is used to cool methanol from 60 to 30 °C by water entering at 20 °C and leaving at 25 °C. Methanol flows through the inner tube at an average velocity of 0.25 m s^{-1}, and water flows in a countercurrently through the annular space. Estimate the total length of the double tube that would be required. The properties of methanol at 45 °C are: $\rho = 780$ kg m^{-3}, $c_p = 0.62$ kcal kg^{-1} °C^{-1}, $\kappa = 0.18$ kcal h^{-1} m^{-1} °C^{-1}, $\mu = 0.42$ cp.

5.6 Estimate the heat transfer coefficient between an oil and the wall of a baffled kettle, 100 cm in diameter, stirred by a flat-blade paddle, 30 cm in diameter, when the impeller rotational speed N is 100 r.p.m. The properties of the oil are $\rho = 900$ kg m^{-3}, $c_p = 0.468$ kcal kg^{-1} °C^{-1}, $\kappa = 0.109$ kcal h^{-1} m^{-1} °C^{-1}, $\mu = 90$ cp.

References

1. McAdams, W.H. (1954) *Heat Transmission*, 3rd edn, McGraw-Hill.
2. Colburn, A.P. (1933) *Trans. AIChE*, **29**, 174.
3. Drew, T.B., Hottel, H.C., and McAdams, W.H. (1936) *Trans. AIChE*, **32**, 271.
4. Chilton, T.H., Drew, T.B., and Jebens, R.H. (1944) *Ind. Eng. Chem.*, **36**, 510.
5. Brooks, G. and Jen, G.-J. (1959) *Chem. Eng. Prog.*, **55** (10), 54.
6. Oldshue, J.Y. and Gretton, A.T. (1954) *Chem. Eng. Prog.*, **50** (12), 615.

Further Reading

Kern, D.Q. (1950) *Process Heat Transfer*, McGraw-Hill.

Perry, R.H., Green, D.W., and Malony, J.O. (eds) (1984, 1997) *Chemical Engineers' Handbook*, 6th and 7th edn, McGraw-Hill.

6
Mass Transfer

6.1
Introduction

Rates of gas–liquid, liquid–liquid, and solid–liquid mass transfer are important and often control the overall rates in bioprocesses. For example, the rates of oxygen absorption into fermentation broth often control the overall rates of aerobic fermentation. The extraction of some products from a fermentation broth, using an immiscible solvent, represents a case of liquid–liquid mass transfer. Solid–liquid mass transfer is important in some bioreactors using immobilized enzymes.

In various membrane processes (these will be discussed in Chapter 8), the rates of mass transfer between the liquid phase and the membrane surface often control the overall rates.

6.2
Overall Coefficients *K* and Film Coefficients *k* of Mass Transfer

In the case of mass transfer between two phases – for example, the absorption of a gas component into a liquid solvent, or the extraction of a liquid component by an immiscible solvent – we need to consider the overall as well as the individual phase coefficients of mass transfer.

As stated in Section 2.6, two kinds of gas film mass transfer coefficients – k_{Gp}, based on the partial pressure driving potential, and k_{Gc}, based on the concentration driving potential – can be defined. However, hereafter in this text only the latter type is used; in other words,

$$k_G = k_{Gc} \tag{6.1}$$

Thus,

$$J_A = k_G(C_G - C_{Gi}) \tag{6.2}$$

where J_A is the mass transfer flux (kg or kmol h^{-1} m^{-2}), C_G and C_{Gi} are gas-phase concentrations (kg or kmol m^{-3}) in the bulk of the gas phase and at the interface, respectively.

Biochemical Engineering: A Textbook for Engineers, Chemists and Biologists, Second Edition.
Shigeo Katoh, Jun-ichi Horiuchi, and Fumitake Yoshida.

Companion Website: www.wiley.com\go\katoh\biochem_eng_e2

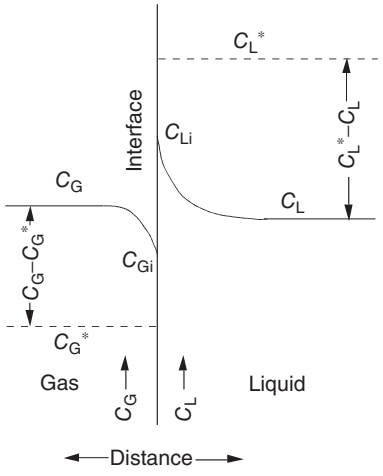

Figure 6.1 Concentration gradients near the gas-liquid interface in absorption.

The liquid phase mass transfer coefficient k_L (m h^{-1}) is defined by

$$J_A = k_L(C_{Li} - C_L) \tag{6.3}$$

where C_{Li} and C_L are liquid phase concentrations (kg or kmol m^{-3}) at the interface and the bulk of liquid phase, respectively.

The relationships between the overall mass transfer coefficient and the film mass transfer coefficients in both phases are not as simple as in the case of heat transfer, for the following reason. Unlike the temperature distribution curves in heat transfer between two phases, the concentration curves of the diffusing component in the two phases are discontinuous at the interface. The relationship between the interfacial concentrations in the two phases depends on the solubility of the diffusing component. Incidentally, it is known that there exists no resistance to mass transfer at the interface, except when a surface-active substance accumulates at the interface to give additional mass transfer resistance.

Figure 6.1 shows the gradients of the gas and liquid concentrations when a component in the gas phase is absorbed into a liquid that is in direct contact with the gas phase. As an equilibrium is known to exist at the gas–liquid interface, the gas-phase concentration at the interface C_{Gi} and the liquid phase concentration at the interface C_{Li} should be on the solubility curve that passes through the origin. In a simple case where the solubility curve is straight,

$$C_{Gi} = m C_{Li} \tag{6.4}$$

where m is the slope (−) of the curve when C_{Gi} is plotted on the ordinate against C_{Li} on the abscissa.

In general, gas solubilities in liquids are given by the Henry's law, that is,

$$p = H_m C_L \tag{6.5}$$

Table 6.1 Solubilities of common gases in water (mole fraction/atm)[a].

(°C)	NH_3	SO_2	Cl_2	CO_2	O_2	N_2
10	0.42	0.043	0.0024	9.0×10^{-4}	2.9×10^{-5}	1.5×10^{-5}
20	0.37	0.031	0.0017	6.5×10^{-4}	2.3×10^{-5}	1.3×10^{-5}
30	0.33	0.023	0.0014	5.3×10^{-4}	2.0×10^{-5}	1.2×10^{-5}
40	0.29	0.017	0.0012	4.2×10^{-4}	1.8×10^{-5}	1.1×10^{-5}

a) From Figure 6.7 in [1].

$$\text{or} \quad p = H_x x_L \tag{6.6}$$

where p is the partial pressure in the gas phase, C_L is the molar concentration in liquid, and x_L is the mole fraction in liquid. Mutual conversion of m, H_m, and H_x is not difficult, using the relationships such as given in Example 2.4; for example,

$$C_G = p(RT)^{-1} = p(0.0821T)^{-1} = 12.18\,p\ \text{K}^{-1} \tag{6.7}$$

The solubilities of gases can be defined as the reciprocals of m, H_m, or H_x. Therefore, the larger these values, the smaller the solubilities.

Table 6.1 provides approximate values of the solubilities (mole fraction atm^{-1}, i.e., $x_L/p = 1/H_x$) of some common gases in water, variations of which are negligible up to pressures of several bars. Note that the solubilities decrease with increasing temperature. It is worth remembering that values of solubility in water are high for NH_3; moderate for Cl_2, CO_2; and low for O_2, N_2.

Now, we shall define the overall coefficients. Even in the case when the concentrations at the interface are unknown (cf. Figure 6.1), we can define the overall driving potentials. Consider the case of gas absorption: the overall coefficient of gas–liquid mass transfer based on the liquid phase concentrations K_L (m h^{-1}) is defined by

$$J_A = K_L(C_L^* - C_L) \tag{6.8}$$

where C_L^* is the imaginary liquid concentration that would be in equilibrium with the gas concentration in the bulk of gas phase C_G, as shown by the broken line in Figure 6.1.

Similarly, the overall coefficient of gas–liquid mass transfer based on the gas concentrations K_G (m h^{-1}) can be defined by

$$J_A = K_G(C_G - C_G^*) \tag{6.9}$$

where C_G^* is the imaginary gas concentration that would be in equilibrium with the liquid concentration C_L in the bulk of liquid (cf. Figure 6.1).

Relationships between K_L, K_G, k_L, and k_G can be obtained easily.

As can be seen from Figure 6.1,

$$\begin{aligned}(C_G - C_G^*) &= (C_G - C_{Gi}) + (C_{Gi} - C_G^*) \\ &= (C_G - C_{Gi}) + m(C_{Li} - C_L)\end{aligned} \tag{6.10}$$

Combination of Equations 6.2–6.4, 6.9, and 6.10 gives

$$\frac{1}{K_G} = \frac{1}{k_G} + \frac{m}{k_L} \tag{6.11}$$

Similarly, we can obtain

$$\frac{1}{K_L} = \frac{1}{(mk_G)} + \frac{1}{k_L} \tag{6.12}$$

Comparison of Equations 6.11 and 6.12 gives

$$K_L = mK_G \tag{6.13}$$

Equations 6.11 and 6.12 lead to a very important concept. When the solubility of a gas into a liquid is very poor (i.e., m is very large), the second term of Equation 6.12 is negligibly small compared to the third term. In such a case, where the liquid-phase resistance is controlling,

$$K_L \cong k_L \tag{6.14}$$

It is for this reason that the gas-phase resistance can be neglected for oxygen transfer in aerobic fermentors.

On the other hand, in the case where a gas is highly soluble in a liquid (e.g., when HCl gas or NH_3 is absorbed into water), m is very small and the third term of Equation 6.11 is negligible compared to the second term. In such a case,

$$K_G \cong k_G \tag{6.15}$$

The usual practice in gas absorption calculations is to use the overall coefficient K_G in cases where the gas is highly soluble and the overall coefficient K_L in cases where the solubility of the gas is low. K_G and K_L are interconvertible by using Equation 6.13.

The overall coefficients of liquid–liquid mass transfer are important in the calculations for extraction equipment, and can be defined in the same way as the overall coefficients of gas–liquid mass transfer. In liquid–liquid mass transfer, one component dissolved in one liquid phase (phase 1) will diffuse into another liquid phase (phase 2). We can define the film coefficients k_{L1} ($m\,h^{-1}$) and k_{L2} ($m\,h^{-1}$) for phases 1 and 2, respectively, and whichever of the overall coefficients K_{L1} ($m\,h^{-1}$), defined with respect to phase 1, or K_{L2} ($m\,h^{-1}$) based on phase 2, is convenient can be used. Relationships between the two film coefficients and two overall coefficients are analogous to those for gas–liquid mass transfer; that is,

$$\frac{1}{K_{L1}} = \frac{1}{k_{L1}} + \frac{m}{k_{L2}} \tag{6.16}$$

$$\frac{1}{K_{L2}} = \frac{1}{(mk_{L1})} + \frac{1}{k_{L2}} \tag{6.17}$$

where m is the ratio of the concentrations in phase 1 and phase 2 at equilibrium, namely, the partition coefficient or its reciprocal.

Example 6.1

A gas component A in air is absorbed into water at 1 atm and 20 °C. The Henry's law constant H_m of A for this system is 1.67×10^3 Pa m^3 kmol^{-1}. The liquid film mass transfer coefficient k_L and gas film coefficient k_G are 2.50×10^{-6} and 3.00×10^{-3} m s^{-1}, respectively. (i) Determine the overall coefficient of gas–liquid mass transfer K_L (m s^{-1}). (ii) When the bulk concentrations of A in the gas phase and liquid phase are 1.013×10^4 Pa and 2.00 kmol m^{-3}, respectively, calculate the molar flux of A.

Solution

a) The Henry's constant H_m in Equation 6.5 is converted to the partition constant m in Equation 6.4.

$$m = \frac{(H_m)}{RT} = \frac{1.67 \times 10^3}{(0.0821 \times 1.0132 \times 10^5 \times 293)} = 6.85 \times 10^{-4}$$

$$\frac{1}{K_L} = \frac{1}{(mk_G)} + \frac{1}{k_L} = \frac{1}{(6.85 \times 10^{-4} \times 3.00 \times 10^{-3})} + \frac{1}{(2.50 \times 10^{-6})}$$

$$K_L = 1.13 \times 10^{-6} \text{m s}^{-1}$$

b)

$$C_L^* = \frac{1.013 \times 10^4}{H_m} = \frac{1.013 \times 10^4}{(1.67 \times 10^3)} = 6.06 \text{ kmol m}^{-3}$$

$$\begin{aligned} J_A = K_L(C_L^* - C_L) &= 1.13 \times 10^{-6} \times (6.06 - 2.00) \\ &= 4.59 \times 10^{-6} \text{ kmol s}^{-1} \text{ m}^{-2} \\ &= 1.65 \times 10^{-2} \text{ kmol h}^{-1} \text{ m}^{-2} \end{aligned}$$

6.3 Types of Mass Transfer Equipment

Numerous types of equipment are available for gas–liquid, liquid–liquid, and solid–liquid mass transfer operations. However, at this point only few representative types are described, on a conceptual basis. Some schematic illustrations of three types of mass transfer equipment are shown in Figure 6.2.

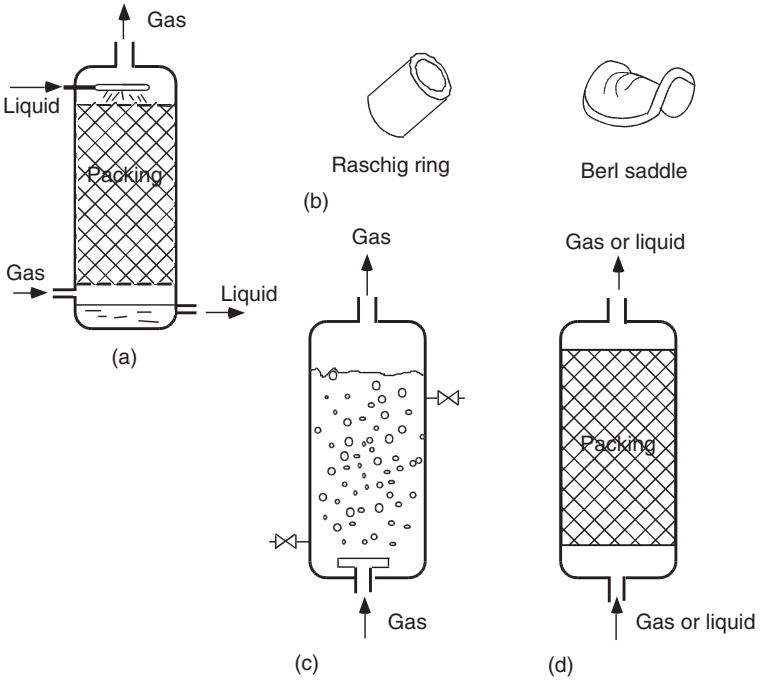

Figure 6.2 Types of mass transfer equipment (a) packed column, (b) packings, (c) bubble column, and (d) packed bed.

6.3.1 Packed Column

The packed column (packed tower) shown in Figure 6.2a is widely used for the absorption of gas into liquid (or its reverse operation), the desorption of dissolved gas from a liquid, and occasionally for distillation. Packed columns are very common equipment in chemical process plants, and are often as large as a few meters in diameter and 20–30 m high. The vessel is a vertical cylinder, the main part of which is filled with the so-called packings; these are small, regularly shaped pieces of corrosion-resistant materials (e.g., porcelain, carbon, metals, plastics) such that there is a large void space and a large surface area per unit packed volume. Figure 6.2b shows two common types of packing. The gas containing a component to be absorbed is passed through the packed column, usually in an upward direction. Liquid is supplied to the top of the column, and trickles down the surface of the packing; in this way, the liquid comes into direct contact with the gas, which flows through the void of the packing. A classical example of using packed columns can be seen in the production plant of liquefied or solid carbon dioxide. Gas containing CO_2 – for example, flue gas from a coke-burning furnace, gas obtained on burning lime stone, or gas from a fermentation plant – is passed through a packed

column, and the CO_2 in the gas is absorbed in a solution of sodium (or potassium) carbonate or bicarbonate. Pure CO_2 can be obtained by boiling the solution emerging from the bottom of the packed column. This is a case of chemical absorption – that is, gas absorption accompanied by chemical reactions. The rates of gas absorption with a chemical reaction are greater than those without reaction, as discussed in Section 6.5.

6.3.2 Plate Column

Plate columns (not shown in the figure), which can be used for the same purposes as packed columns, have many horizontal plates that are either perforated or equipped with so-called "bubble caps." The liquid supplied to the top of the column flows down the column, in a horizontal manner, over each successive plate. The upward-moving gas or vapor bubbles pass through the liquid on each plate, such that a gas–liquid mass transfer takes place at the surface of the bubbles.

6.3.3 Spray Column

The spray column or chamber (not shown in the figure) is a large, empty cylindrical column or horizontal duct through which gas is passed. Liquid is sprayed into the gas from the top, or sometimes from the side. The large number of liquid drops that are produced provide a very large gas–liquid contact surface. Owing to the high relative velocity between the liquid and the gas, the gas phase mass transfer coefficient is high, whereas the liquid phase coefficient is low because of the minimal liquid movements within the drops. Consequently, spray columns are suitable for systems in which the liquid-phase mass transfer resistance is negligible (e.g., the absorption of ammonia gas into water), or its reverse operation – that is, *desorption* – or when the resistance exists only in the gas phase; an example is the vaporization of a pure liquid or the humidification of air. This type of device is also used for the cooling of gases. Unfortunately, the spray column or chamber has certain disadvantages, primarily that a device is required to remove any liquid droplets carried over by the outgoing gas. Consequently, real gas–liquid countercurrent operation is difficult. Although the fall in gas pressure is minimal, the power requirements for liquid spraying are relatively high.

6.3.4 Bubble Column

The bubble column is shown in Figure 6.2c. In this type of equipment, gas is sparged from the bottom into a liquid contained in a large cylindrical vessel. A large number of gas bubbles provide a very large surface area for gas–liquid contact. Turbulence in the liquid phase creates a large liquid-phase mass transfer coefficient, while the gas-phase coefficient is relatively small because of the very

little gas movement within the bubbles. Thus, the bubble column is suitable for systems of low gas solubility where the liquid-phase mass transfer resistance is controlling, such as the oxygen–water system. In fact, bubble columns are widely used as aerobic fermentors, in which the main resistance for oxygen transfer exists in the liquid phase. A detailed discussion of bubble columns is provided in Chapter 7.

6.3.5
Packed- (Fixed-) Bed Column

Another type of mass transfer equipment, shown in Figure 6.2d, is normally referred to as the packed- (fixed-) bed. Unlike the packed column for gas–liquid mass transfer, the packed-bed column is used for mass transfer between the surface of packed solid particles (e.g., catalyst particles or immobilized enzyme particles) and a single-phase liquid or gas. This type of equipment, which is widely used as reactors, adsorption columns, chromatography columns, and so on, is discussed in greater detail in Chapters 7 and 11.

6.3.6
Other Separation Methods

Membrane separation processes are discussed in Chapter 8. Liquid-phase mass transfer rates at the surface of membranes – either flat or tubular – can be predicted by the correlations given in this chapter.

A variety of gas–liquid contacting equipment with mechanical moving elements (e.g., stirred (agitated) tanks with gas sparging) are discussed in Chapters 7 and 12, including rotating-disk gas–liquid contactors and others.

6.4
Models for Mass Transfer at the Interface

6.4.1
Stagnant Film Model

The film model referred to in Chapters 2 and 5 provides, in fact, an oversimplified picture of what happens in the vicinity of interface. On the basis of the film model proposed by Nernst in 1904, Whitman [2] proposed in 1923 the two-film theory of gas absorption. Although this is a very useful concept, it is impossible to predict the individual (film) coefficient of mass transfer, unless the thickness of the laminar sublayer is known. According to this theory, the mass transfer rate should be proportional to the diffusivity, and inversely proportional to the thickness of the laminar film. However, as we usually do not know the thickness of the laminar film, a convenient concept of the effective film thickness has been assumed (as

mentioned in Chapter 2). Despite this, experimental values of the film coefficient of mass transfer based on the difference between the concentrations at the interface and of the fluid bulk do not vary in proportion to diffusivity, as is required by the film theory.

6.4.2 Penetration Model

The existence of a stagnant laminar fluid film adjacent to the interface is not difficult to visualize, in the case where the interface is stationary, as when the fluid flows along a solid surface. However, this situation seems rather unrealistic with the fluid–fluid interface, as when the surface of the liquid in an agitated vessel is in contact with a gas phase above, or if gas bubbles move upward through a liquid, or when one liquid phase is in contact with another liquid phase in an extractor.

In the penetration model proposed by Higbie [3] in 1935, it is assumed that a small fluid element of uniform solute concentration is brought into contact with the interface for a certain fixed length of time t. During this time, the solute diffuses into the fluid element as a transient process, in the same manner as transient heat conduction into a solid block. Such a transient diffusion process of fixed contact time is not difficult to visualize in the situation where a liquid trickles down over the surface of a piece of packing in a packed column. Neglecting convection, Higbie derived (on a theoretical base) Equation 6.18 for the liquid-phase mass transfer coefficient k_L averaged over the contact time t.

$$k_L = 2\left(\frac{D}{\pi t}\right)^{1/2} \tag{6.18}$$

If this model is correct, k_L should vary with the diffusivity D to the 0.5 power, but this does not agree with experimental data in general. Also, t is unknown except in the case of some specially designed equipment.

6.4.3 Surface Renewal Model

In 1951, Danckwerts [4] proposed the surface renewal model as an extension of the penetration model. Instead of assuming a fixed contact time for all fluid elements, Danckwerts assumed a wide distribution of contact time, from zero to infinity, and supposed that the chance of an element of the surface being replaced with fresh liquid was independent of the length of time for which it has been exposed. Then, it was shown, theoretically, that the averaged mass transfer coefficient k_L at the interface is given as

$$k_L = (Ds)^{1/2} \tag{6.19}$$

where s is the fraction of the area of surface that is replaced with fresh liquid in unit time.

Compared to the film model or the penetration model, the surface renewal approach seems closer to reality in such a case where the surface of liquid in an

agitated tank is in contact with the gas phase above, or with the surface of a liquid flowing through an open channel. The values of s are usually unknown, although they could be estimated from the data acquired from carefully planned experiments. As with the penetration model, k_L values should vary with diffusivity $D^{0.5}$.

It can be seen that a theoretical prediction of k_L values is not possible by any of the three above-described models, because none of the three parameters – the laminar film thickness in the film model, the contact time in the penetration model, and the fractional surface renewal rate in the surface renewal model – is predictable in general. It is for this reason that the empirical correlations must normally be used for the predictions of individual coefficients of mass transfer. Experimentally obtained values of the exponent on diffusivity are usually between 0.5 and 1.0.

6.5 Liquid Phase Mass Transfer with Chemical Reactions

So far, we have considered pure physical mass transfer without any reaction. Occasionally, however, gas absorption is accompanied by chemical or biological reactions in the liquid phase. For example, when CO_2 gas is absorbed into an aqueous solution of Na_2CO_3, the following reaction takes place in the liquid phase.

$$Na_2CO_3 + CO_2 + H_2O = 2\ NaHCO_3$$

In an aerobic fermentation, the oxygen absorbed into the culture medium is consumed by microorganisms in the medium.

In general, the rates of the mass transfer increase when it is accompanied by reactions. For example, if k_L^* indicates the liquid phase coefficient, including the effects of the reaction, then the ratio E can be defined as:

$$E = \frac{k_L^*}{k_L} \tag{6.20}$$

and is referred to as the "enhancement" (reaction) factor. Values of E are always greater than unity.

Hatta [5] derived a series of theoretical equations for E, on the basis of the film model. Experimental values of E agree with the Hatta theory, and also with theoretical values of E derived later by other investigators, on the basis of the penetration model.

Figure 6.3a shows the idealized sketch of concentration profiles near the interface by the Hatta model, for the case of gas absorption with a very rapid second-order reaction. The gas component A, when absorbed at the interface, diffuses to the reaction zone where it reacts with B, which is derived from the bulk of liquid by diffusion. The reaction is so rapid that it is completed within a very thin reaction zone; this can be regarded as a plane parallel to the interface. The reaction product diffuses to the liquid main body. The absorption of CO_2 into a strong aqueous KOH solution is close to such a case. Equation 6.21 provides the enhancement

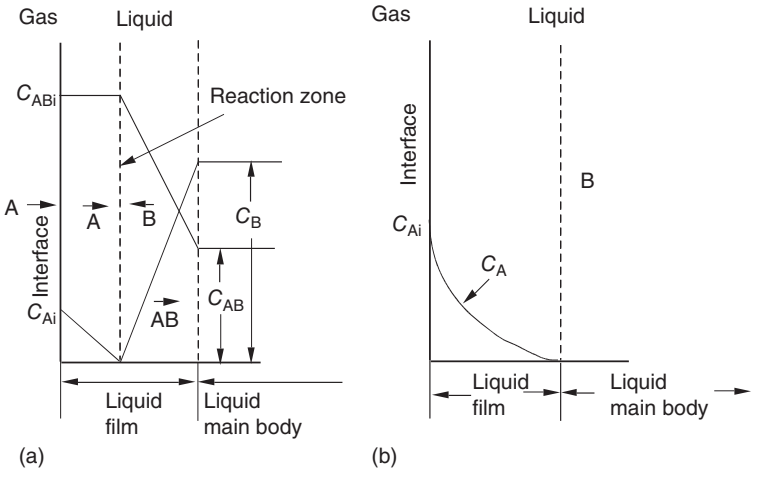

Figure 6.3 Gas absorption with chemical reaction (a) rapid second-order reaction and (b) slow pseudo first-order reaction.

factor E for such a case, as derived by the Hatta theory:

$$E = 1 + \frac{(D_B C_B)}{(D_A C_{Ai})} \tag{6.21}$$

where D_B and D_A are liquid-phase diffusivities of B and A, respectively, C_B is the concentration of B in the bulk of liquid, and C_{Ai} is the liquid-phase concentration of A at the interface.

Figure 6.3b shows the idealized concentration profile of an absorbed component A, obtained by the Hatta theory, for the case of a relatively slow reaction that is either first-order or pseudo first-order with respect to A. As A is consumed gradually while diffusing across the film, the gradient of concentration of A that is required for its diffusion gradually decreases with increasing distance from the interface. The enhancement factor for such cases is given by the Hatta theory as

$$E = \frac{\gamma}{(\tanh \gamma)} \tag{6.22}$$

where

$$\gamma = \frac{(kC_B D_A)^{1/2}}{k_L} \tag{6.23}$$

When C_B (i.e., concentration of B which reacts with A) is much larger than C_A, C_B can be considered approximately constant, and (k C_B) can be regarded as the pseudo first-order reaction rate constant (T^{-1}). The dimensionless group γ, as defined by Equation 6.23, is often designated as the Hatta number (Ha). According to Equation 6.22, if $\gamma > 5$, it becomes practically equal to E, which is sometimes also called the Hatta number. For this range,

$$k_L^* = Ek_L = (kC_B D_A)^{1/2} \tag{6.24}$$

Equation 6.24 indicates that the mass transfer rates are independent of k_L and of the hydrodynamic conditions; hence, the whole interfacial area is uniformly effective when $\gamma > 5$ [6].

As discussed in Chapter 12, any increase in the enhancement factor E due to the respiration of microorganisms can, in practical terms, be neglected as it is very close to unity.

6.6 Correlations for Film Coefficients of Mass Transfer

As mentioned in Chapter 2, close analogies exist between the film coefficients of heat transfer and those of mass transfer. Indeed, the same type of dimensionless equations can often be used to correlate the film coefficients of heat and mass transfer.

6.6.1 Single-Phase Mass Transfer Inside or Outside Tubes

Film coefficients of mass transfer inside or outside tubes are important in membrane processes using tube-type or the so-called "hollow fiber" membranes. In the case where flow inside the tubes is turbulent, the dimensionless Equation 6.25a, b (analogous to Equation 5.8a, b for heat transfer) provide the film coefficients of mass transfer k_c [7]

$$\left(\frac{k_c d_i}{D}\right) = 0.023\left(\frac{d_i v \rho}{\mu}\right)^{0.8}\left(\frac{\mu}{\rho D}\right)^{1/3} \tag{6.25a}$$

that is,

$$(\mathrm{Sh}) = 0.023\,(\mathrm{Re})^{0.8}(\mathrm{Sc})^{1/3} \tag{6.25b}$$

where d_i is the inner diameter of the tube, D is the diffusivity, v is the average linear velocity of the fluid, ρ is the fluid density, and μ is the fluid viscosity, all in consistent units. (Sh), (Re), and (Sc) are the dimensionless Sherwood, Reynolds, and Schmidt numbers, respectively.

In case the flow is laminar, Equation 6.26a (analogous to Equation 5.9a for heat transfer) can be used:

$$\left(\frac{k_c d_i}{D}\right) = 1.62\left(\frac{d_i v \rho}{\mu}\right)^{1/3}\left(\frac{\mu}{\rho D}\right)^{1/3}\left(\frac{d_i}{L}\right)^{1/3} \tag{6.26a}$$

or

$$(\mathrm{Sh}) = 1.62\,(\mathrm{Re})^{1/3}(\mathrm{Sc})^{1/3}\left(\frac{d_i}{L}\right)^{1/3}$$

where L is the tube length (this is important in laminar flow, owing to the end effects at the tube entrance). Equation 6.26a can be transformed into

$$(\mathrm{Sh}) = \left(\frac{k_c d_i}{D}\right) = 1.75\left(\frac{F}{DL}\right)^{1/3} = 1.75(\mathrm{Nx})^{1/3} \tag{6.26b}$$

where F is the volumetric flow rate ($L^3\,T^{-1}$) of a fluid through a tube. The dimensionless group $(\mathrm{Nx}) = (F/D\ L)$ affects the rate of mass transfer between a fluid in laminar flow and the tube wall. By analogy between heat and mass transfer, the relations between (Nx) and (Sh) should be the same as those between (Gz) and (Nu). (Section 5.4.1). Equation 6.26b can be used for (Nx) >40, whereas for (Nx) below 10, (Sh) approaches an asymptotic value of 3.66. Values of (Sh) for the intermediate range of (Nx) can be obtained by interpolation on log–log coordinates.

In the case that the cross section of the channel is not circular, the equivalent diameter d_e defined by Equations 5.10 and 5.11 should be used in place of d_i. As with heat transfer, taking the wetted perimeter for mass transfer rather than the total wetted perimeter provides a larger value of the equivalent diameter and hence a lower value of the mass transfer coefficient. The equivalent diameter of the channel between two parallel plates or membranes is twice the distance between the plates or membranes, as noted in relation to Equation 5.11.

In the case where the fluid flow outside the tubes is parallel to the tubes and laminar (as in some membrane devices), the film coefficient of mass transfer on the outer tube surface can be estimated using Equation 6.26a and the equivalent diameter as calculated with Equation 5.10.

In the case where the fluid flow outside tubes is normal or oblique to a tube bundle, approximate values of the film coefficient of mass transfer k_c can be estimated by using Equation 6.27a [7], which is analogous to Equation 5.12a:

$$\left(\frac{k_c d_o}{D}\right) = 0.3\left(\frac{d_o G_m}{\mu}\right)^{0.6}\left(\frac{\mu}{\rho D}\right)^{1/3} \tag{6.27a}$$

$$\text{or } (\mathrm{Sh}) = 0.3\ (\mathrm{Re})^{0.6}(\mathrm{Sc})^{1/3} \tag{6.27b}$$

where d_o is the outside diameter of tubes, G_m is the mass velocity of fluid in the direction perpendicular to tubes, ρ is the fluid density, μ is the fluid viscosity, and D is the diffusivity, all in consistent units. Equation 6.27a should hold for the range of (Re), defined as above, between 2000 and 30 000.

6.6.2
Single-Phase Mass Transfer in Packed Beds

Coefficients of single-phase mass transfer are important in a variety of processes using fixed beds. Examples include reactions using particles of catalysts or immobilized enzymes, adsorption, chromatography, and also membrane processes. Many reports have been made on the single-phase mass transfer between the surface of packings or particles and a fluid flowing through the

packed bed. In order to obtain gas-phase mass transfer data, most investigators have measured the rates of sublimation of solids or evaporation of liquids from porous packings. Liquid-phase mass transfer coefficients can be obtained, for example, by measuring rates of partial dissolution of solid particles into a liquid.

Equation 6.28 [8] can correlate well the data of many investigators for gas or liquid film mass transfer in packed beds for the ranges of (Re) from 10 to 2500, and of (Sc) from 1 to 10 000.

$$J_D = (St)_D(Sc)^{2/3} = \left(\frac{k_c}{U_G}\right)\left(\frac{\mu}{\rho D}\right)^{2/3}$$
$$= 1.17(Re)^{-0.415} = 1.17\left(\frac{d_p U_G \rho}{\mu}\right)^{-0.415} \tag{6.28}$$

where J_D is the so-called J-factor for mass transfer, as explained below, $(St)_D$ is the Stanton number for mass transfer, (Sc) the Schmidt number, k_c the mass transfer coefficient, μ the fluid viscosity, ρ the fluid density, D the diffusivity, and d_p the particle diameter or diameter of a sphere having an equal surface area or volume as the particle. U_G is not the velocity through the void space, but the superficial velocity ($L\,T^{-1}$) averaged over the entire cross section of the bed.

6.6.3 *J*-Factor

The J-factors were first used by Colburn [7] for successful empirical correlations of heat and mass transfer data. The J-factor for heat transfer, J_H, was defined as

$$J_H = (St)_H(Pr)^{2/3} = \left(\frac{h}{c_p \nu \rho}\right)\left(\frac{c_p \mu}{\kappa}\right)^{2/3} \tag{6.29}$$

where $(St)_H$ is the Stanton number for heat transfer, (Pr) is the Prandtl number, h is the film coefficient of heat transfer, c_p is the specific heat, ν the superficial fluid velocity, μ the fluid viscosity, ρ the fluid density, and κ the thermal conductivity of fluid, all in consistent units.

Data acquired by many investigators have shown a close analogy between the rates of heat and mass transfer, not only in the case of packed beds but also in other cases, such as flow through and outside tubes, and flow along flat plates. In such cases, plots of the J-factors for heat and mass transfer against the Reynolds number produce almost identical curves. Consider, for example, the case of turbulent flow through tubes. Since

$$\left(\frac{k_c d_i}{D}\right) = \left(\frac{k_c}{\nu}\right)\left(\frac{\mu}{\rho D}\right)\left(\frac{d_i \nu \rho}{\mu}\right) \tag{6.30}$$

the combination of Equations 6.25a and 6.30 gives

$$J_D = \left(\frac{k_c}{\nu}\right)\left(\frac{\mu}{\rho D}\right)^{2/3} = 0.023\left(\frac{d_i \nu \rho}{\mu}\right)^{-0.2} \tag{6.31}$$

Similar relationships are apparent for heat transfer for the case of turbulent flow through tubes. Since

$$\left(\frac{hd}{\kappa}\right) = \left(\frac{h}{c_p \nu \rho}\right)\left(\frac{c_p \mu}{\kappa}\right)\left(\frac{d_i \nu \rho}{\mu}\right) \tag{6.32}$$

the combination of Equations 5.8a and 6.32 gives

$$J_H = \left(\frac{h}{c_p \nu \rho}\right)\left(\frac{c_p \mu}{\kappa}\right)^{2/3} = 0.023\left(\frac{d_i \nu \rho}{\mu}\right)^{-0.2} \tag{6.33}$$

A comparison of Equations 6.31 and 6.33 shows that the J-factors for mass and heat transfer are exactly equal in this case. Thus, it is possible to estimate heat transfer coefficients from mass transfer coefficients, and *vice versa.*

6.7 Performance of Packed Column

So far, we have considered only mass transfer within a single phase – that is, mass transfer between fluids and solid surfaces. For gas absorption and desorption, in which mass transfer takes place between a gas and a liquid, packed columns are extensively used, while bubble columns and sparged stirred vessels are used mainly for gas–liquid reactions or aerobic fermentation. As the latter types of equipment are discussed fully in Chapter 7, we shall, at this point, describe only the performance of packed columns.

6.7.1 Limiting Gas and Liquid Velocities

The first criterion when designing a packed column is to determine the column diameter, which affects the mass transfer rates, and accordingly the column height. It is important to remember that maximum allowable gas and liquid flow rates exist, and that the higher the liquid rates the lower will be the allowable gas velocities. The gas pressure drop in a packed column increases not only with gas flow rates but also with liquid flow rates. Flooding is a phenomenon that occurs when a liquid begins to accumulate in the packing as a continuous phase; this may occur when the gas rate exceeds a limit at a given liquid rate, or when the liquid rate exceeds a limit at a given gas rate. Generalized correlations for flooding limits as functions of the liquid and gas rates, and of the gas and liquid properties, are available in many textbooks and reference books [9]. In practice, it is recommended that an optimum operating gas velocity of approximately 50% of the flooding gas velocity is used for a given liquid rate.

6.7.2 Definitions of Volumetric Coefficients and HTUs

The mass transfer coefficients considered so far – namely, k_G, k_L, K_G, and K_L – are defined with respect to known interfacial areas. However, the interfacial areas in equipment such as the packed column and bubble column are indefinite, and vary with operating conditions such as fluid velocities. It is for this reason that the volumetric coefficients defined with respect to the unit volume of the equipment are used, or more strictly, the unit packed volume in the packed column or the unit volume of liquid containing bubbles in the bubble column. Corresponding to k_G, k_L, K_G, and K_L, we define $k_G a$, $k_L a$, $K_G a$, and $K_L a$, all of which have units of $(\text{kmol h}^{-1}\,\text{m}^{-3})/(\text{kmol m}^{-3})$ – that is, (h^{-1}). Although the volumetric coefficients are often regarded as single coefficients, it is more reasonable to consider a separately from the k-terms, because the effective interfacial area per unit packed volume or unit volume of liquid–gas mixture a $(\text{m}^2\,\text{m}^{-3})$ varies not only with operating conditions such as fluid velocities but also with the types of operation, such as physical absorption, chemical absorption, and vaporization.

Corresponding to Equations 6.11–6.13, we have the following relationships:

$$\frac{1}{(K_G a)} = \frac{1}{(k_G a)} + \frac{m}{(k_L a)} \tag{6.34}$$

$$\frac{1}{(K_L a)} = \frac{1}{(m k_G a)} + \frac{1}{(k_L a)} \tag{6.35}$$

$$K_L a = m K_G a \tag{6.36}$$

where m is defined by Equation 6.4.

Now, we consider gas–liquid mass transfer rates in gas absorption and its reverse operation – that is, gas desorption in packed columns. The gas entering the column from the bottom and the liquid entering from the top exchange solute while contacting each other. In case of absorption, the amount of solute transferred from the gas to the liquid per unit sectional area of the column is

$$U_G(C_{GB} - C_{GT}) = U_L(C_{LB} - C_{LT}) \tag{6.37}$$

where U_G and U_L are the volumetric flow rates of gas and liquid, respectively, divided by the cross-sectional area of the column (m h^{-1}), that is, superficial velocities. The C-terms are solute concentrations (kg or kmol m^{-3}), with subscripts G for gas and L for liquid, B for the column bottom, and T for the column top. Although U_L and U_G will vary slightly as the absorption progresses, in practice they can be regarded as approximately constant. (Note: they can be made constant, if the concentrations are defined per unit volume of inert carrier gas and solvent.) In Figure 6.4, Equation 6.37 is represented by the straight line T–B, which is the operating line for absorption. The equilibrium curve 0–E and the operating line T′–B′ for desorption are also shown in Figure 6.4.

In the case where the equilibrium curve is straight, the logarithmic mean driving potential (which is similar to the log-mean temperature difference used in heat

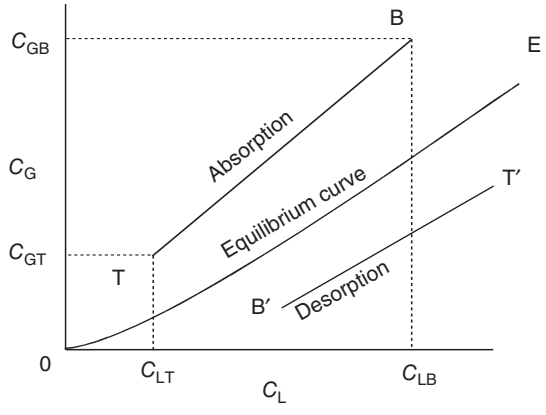

Figure 6.4 Operating lines for absorption and desorption.

transfer calculations) can be used to calculate the mass transfer rates in the column. The mass transfer rate r (kg or kmol h^{-1}) in a column of height Z per unit cross-sectional area of the column is given by

$$r = ZK_G a(\Delta C_G)_{lm} = ZK_L a(\Delta C_L)_{lm} \tag{6.38}$$

in which $(\Delta C_G)_{lm}$ and $(\Delta C_L)_{lm}$ are the logarithmic means of the driving potentials at the top and at the bottom, namely,

$$(\Delta C_G)_{lm} = \frac{[(\Delta C_G)_T - (\Delta C_G)_B]}{\ln[(\Delta C_G)_T/(\Delta C_G)_B]} \tag{6.39}$$

$$(\Delta C_L)_{lm} = \frac{[(\Delta C_L)_T - (\Delta C_L)_B]}{\ln[(\Delta C_L)_T/(\Delta C_L)_B]} \tag{6.40}$$

Thus, the required packed height Z can be calculated using Equation 6.38 with the given values of r and the volumetric coefficient $K_G\,a$ or $K_L\,a$.

In the general case where the equilibrium line is curved, the mass transfer rate for gas absorption per differential packed height dZ and unit cross-sectional area of the column is given as

$$U_G dC_G = K_G a(C_G - C_G^*)\,dZ \tag{6.41}$$

$$= U_L dC_L = K_L a(C_L^* - C_L)\,dZ \tag{6.42}$$

where C_G^* is the gas concentration in equilibrium with the liquid concentration C_L and C_L^* is the liquid concentration in equilibrium with the gas concentration C_G.

Integration of Equations 6.41 and 6.42 gives

$$Z = \frac{U_G}{K_G a}\int_{C_{GT}}^{C_{GB}} \frac{dC_G}{C_G - C_G^*} = \frac{U_G}{K_G a} N_{OG} \tag{6.43}$$

$$Z = \frac{U_L}{K_L a}\int_{C_{LT}}^{C_{LB}} \frac{dC_L}{C_L^* - C_L} = \frac{U_L}{K_L a} N_{OL} \tag{6.44}$$

The integral, that is, N_{OG} in Equation 6.43, is called the NTUs (number of transfer units) based on the overall gas concentration driving potential, and the integral in Equation 6.44, that is, N_{OL} is the NTU based on the overall liquid concentration driving potential. In general, the NTUs can be evaluated by graphical integration. In most practical cases, however, where the equilibrium curve can be regarded as straight, we can use the following relationships:

$$N_{OG} = \frac{(C_{GB} - C_{GT})}{(\Delta C_G)_{lm}} \tag{6.45}$$

$$N_{OL} = \frac{(C_{LB} - C_{LT})}{(\Delta C_L)_{lm}} \tag{6.46}$$

From Equations 6.43 and 6.44 we obtain

$$H_{OG} = \frac{U_G}{K_G a} = \frac{Z}{N_{OG}} \tag{6.47}$$

and

$$H_{OL} = \frac{U_L}{K_L a} = \frac{Z}{N_{OL}} \tag{6.48}$$

where H_{OG} is the HTU (height per transfer unit) based on the overall gas concentration driving potential, and H_{OL} is the HTU based on the overall liquid concentration driving potential. The concepts of NTU and HTU were proposed by Chilton and Colburn [10]. NTUs based on the gas film N_G and the liquid film driving potentials N_L, and corresponding H_G and H_L can also be defined. Thus,

$$H_G = \frac{U_G}{k_G a} \tag{6.49}$$

$$H_L = \frac{U_L}{k_L a} \tag{6.50}$$

From the above relationships

$$H_{OG} = H_G + \frac{H_L m U_G}{U_L} \tag{6.51}$$

$$H_{OL} = \left(\frac{U_L}{m U_G}\right) H_G + H_L \tag{6.52}$$

$$H_{OG} = H_{OL}\left(\frac{m U_G}{U_L}\right) \tag{6.53}$$

Thus, the HTUs and *Ka* terms are interconvertible, whichever is convenient for use. Since the NTUs are dimensionless, HTUs have the simple dimension of length. Variations of HTUs with fluid velocities are smaller than those of *Ka* terms; thus, the values of HTUs are easier to remember than those of *Ka*s.

6.7.3 Mass Transfer Rates and Effective Interfacial Areas

It is reasonable to separate the interfacial area a from Ka, because K and a are each affected by different factors. Also, it must be noted that a is different from the wetted area of packings, except in the case of vaporization of liquid from all-wet packings. For gas absorption or desorption, the semi-stagnant or slow-moving parts of the liquid surface are less effective than the fast-moving parts. In addition, liquids do not necessarily flow as films but more often as rivulets or as wedge-like streams. Thus, the gas–liquid interfacial areas are not proportional to the dry surface areas of packings. Usually, interfacial areas in packings of approximately 25 mm achieve maximum values compared to areas in smaller or larger packings.

One method of estimating the effective interfacial area a is to divide values of $k_G\,a$ achieved with an irrigated packed column by the k_G values achieved with an unirrigated packed bed. Values of k_G can be obtained by measuring rates of drying of all-wet porous packing [11] or rates of sublimation of packings made of naphthalene [12]. The results obtained with these two methods were in agreement, and the following dimensionless equation [11] provides such k_G values for the bed of unirrigated, all-wet Raschig rings.

$$\left(\frac{U_G}{k_G}\right) = 0.935\left(\frac{U_G \rho {A_p}^{1/2}}{\mu}\right)^{0.41}\left(\frac{\mu}{\rho D}\right)^{2/3}$$
$$= 0.935\,(\mathrm{Re})^{0.41}(\mathrm{Sc})^{2/3} \tag{6.54}$$

where A_p is the surface area of a piece of packing and U_G is the superficial gas velocity. (Note: all of the fluid properties in the above equation are for gas.)

Figure 6.5 shows values of the effective interfacial area thus obtained by comparing $k_G\,a$ values [13] for gas-phase resistance-controlled absorption and vaporization with k_G values by Equation 6.54. It is seen that the effective area for absorption is considerably smaller than that for vaporization, the latter being almost equal to the wetted area. The effect of gas rates on a is negligible.

Liquid-phase mass transfer data [13–15] were correlated by the following dimensionless equation [13].

$$\left(\frac{H_L}{d_p}\right) = 1.9\left(\frac{L}{a\mu_L}\right)^{0.5}\left(\frac{\mu_L}{\rho_L D_L}\right)^{0.5}\left(\frac{d_p g \rho_L}{{\mu_L}^2}\right)^{-1/6} \tag{6.55}$$

where d_p is the packing size (L), a is the effective interfacial area of packing (L^{-1}) given by Figure 6.5, D_L is the liquid phase diffusivity ($L^2\,T^{-1}$), g is the gravitational constant ($L\,T^{-2}$), H_L is the height per transfer unit (L), μ_L is the liquid viscosity ($M\,L^{-1}\,T^{-1}$), and ρ_L is the liquid density ($M\,L^{-3}$), all in consistent units.

The effective interfacial areas for absorption with a chemical reaction [6] in packed columns are the same as those for physical absorption, except that absorption is accompanied by rapid, second-order reactions. For absorption with a moderately fast first-order or pseudo first-order reaction, almost the entire interfacial area is effective, because the absorption rates are independent of k_L, as can be seen

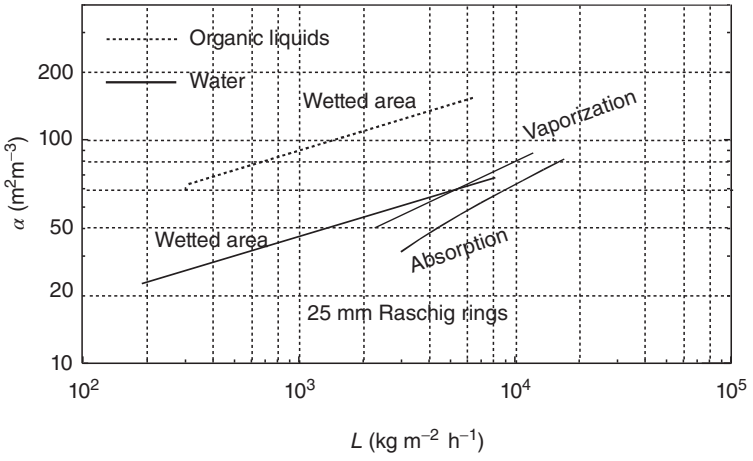

Figure 6.5 Effective and wetted areas in 25-mm Raschig rings.

from Equation 6.24 for the enhancement factor for such cases. For a new system with an unknown reaction rate constant, an experimental determination of the enhancement factor by using an experimental absorber with a known interfacial area would serve as a guide.

Ample allowance should be made in practical design calculations, since previously published correlations have been based on data obtained with carefully designed experimental apparatus.

Example 6.2

Air containing 2 vol% of ammonia is to be passed through a column at a rate of 5000 $m^3\ h^{-1}$. The column is packed with 25-mm Raschig rings, and is operating at 20 °C and 1 atm. The aim is to remove 98% of ammonia by absorption into water. Assuming a superficial air velocity of 1 $m\ s^{-1}$, and a water flow rate of approximately twice the minimum required, calculate the required column diameter and packed height. The solubility of ammonia in water at 20 °C is given by

$$m = \frac{C_G(\text{kg m}^{-3})}{C_L(\text{kg m}^{-3})} = 0.00202$$

The absorption of ammonia into water is a typical case where gas-phase resistance controls mass transfer rates.

Solution

Concentrations of NH_3 in the air at the bottom and top of the column:

$$C_{GB} = 17 \times 0.02 \times \frac{273}{(22.4 \times 293)} = 0.0141\,\text{kg m}^{-3}$$

$$C_{GT} = 0.0141(1-0.98) = 0.000282 \text{ kg m}^{-3}$$

Amount of NH_3 to be removed: $0.0141 \times 5000 \times 0.98 = 69.1 \text{ kg h}^{-1}$.
Minimum amount of water required.

$$L = G \times \left(\frac{C_G}{C_L}\right) = 5000 \times 0.00202 = 10.1 \text{ m}^3 \text{ h}^{-1}$$

If water is used at $20 \text{ m}^3 \text{ h}^{-1}$, then the NH_3 concentration in water leaving the column: $C_{LB} = 69.1/20 = 3.46 \text{ kg m}^{-3}$.
For a superficial gas velocity of 1 m s^{-1}, the required sectional area of the column is $5000/3600 = 1.388 \text{ m}^2$ and the column diameter is 1.33 m.
Then, the superficial water rate: $U_L = 20/1.39 = 14.4 \text{ m h}^{-1}$.
According to flooding limits correlations, this is well below the flooding limit.
Now, the logarithmic mean driving potential is calculated.

$$C_{GB}{}^*(\text{in equilibrium with } C_{LB}) = 3.46 \times 0.00202 = 0.00699 \text{ kg m}^{-3}$$

$$(\Delta C_G)_B = 0.0141 - 0.00699 = 0.00711 \text{ kg m}^{-3}$$

$$(\Delta C_G)_T = 0.00028 \text{ kg m}^{-3}$$

$$(\Delta C_G)_{lm} = \frac{(0.00711 - 0.00028)}{\ln(0.00711/0.00028)} = 0.00211 \text{ kg m}^{-3}$$

By Equation 6.46

$$N_{OG} = \frac{(0.0141 - 0.00028)}{0.00211} = 6.55$$

The value of k_G is estimated by Equation 6.54 with known values of $U_G = 100 \text{ cm s}^{-1}$, $A_p = 39 \text{ cm}^2$, $\rho = 0.00121 \text{ g cm}^{-3}$, $\mu = 0.00018 \text{ g cm}^{-1} \text{ s}^{-1}$, and $D = 0.22 \text{ cm}^2 \text{ s}^{-1}$.
Equation 6.54 gives

$$\frac{100}{k_G} = 0.935\,(4198)^{0.41}(0.676)^{2/3} = 22.0$$

$$k_G = 4.55 \text{ cm s}^{-1} = 164 \text{ m h}^{-1}$$

From Figure 6.5, the interfacial area a for 25-mm Raschig rings at $U_L = 14.4 \text{ m h}^{-1}$ is estimated as

$$a = 74 \text{ m}^2 \text{ m}^{-3}$$

Then, $k_G a = 164 \times 74 = 12\,100 \text{ h}^{-1}$

$$H_G = \frac{3600}{12\,100} = 0.30 \text{ m}$$

Required packed height

$$z = N_G \times H_G = 6.55 \times 0.30 = 1.97 \text{ m}$$

With an approximate 25% allowance, a packed height of 2.5 m is used.

Problems

6.1 An air–SO_2 mixture containing 10 vol% of SO_2 is flowing at 340 $m^3 h^{-1}$ (20 °C, 1 atm). If 95% of the SO_2 is to be removed by absorption into water in a countercurrent packed column operated at 20 °C, 1 atm, how much water (kg h^{-1}) is required? The absorption equilibria are given in Table P6.1.

Table P6.1 Adsorption equilibrium of SO_2 in water.

p_{SO_2} (mmHg)	26	59	123
X (kg-SO_2 per 100 kg-H_2O)	0.5	1.0	2.0

6.2 Convert the value of $k_{Gp} = 8.50$ kmol $m^{-2} h^{-1} atm^{-1}$ at 20 °C into k_{Gc} (m h^{-1}).

6.3 Ammonia in air is adsorbed into water at 20 °C. The liquid film mass transfer coefficient and the overall coefficient are 1.44×10^{-4} and 2.70×10^{-5} m s^{-1}, respectively. Use the partition coefficient given in Example 6.2. Determine

1. the gas film coefficient
2. the percentage resistance to the mass transfer in the gas phase.

6.4 The solubility of NH_3 in water at 15 °C is given as $H_m = p/C = 0.0461$ atm m^3 $kmol^{-1}$. It is known that the film coefficients of mass transfer are $k_G = 1.10$ kmol $m^{-2} h^{-1} atm^{-1}$ and $k_L = 0.34$ m h^{-1}. Estimate the value of the overall mass transfer coefficient K_{Gc} (m h^{-1}) and the percentage of the gas film resistance.

6.5 An oxygen bubble with a diameter of 0.4 cm is rising in water at 20 °C with a constant velocity of 0.2 m s^{-1}. Estimate the liquid phase mass transfer coefficient k_L using the penetration model (Equation 6.18). The diffusivity of oxygen in water at 20 °C is 2.1×10^{-9} m^2 s^{-1}.

6.6 A gas is to be absorbed into water in a countercurrent packed column. The equilibrium relation is given by $Y = 0.06X$ where Y and X are gas and liquid concentrations in molar ratio, respectively. The required conditions are $Y_B = 0.009$, $Y_T = 0.001$, $X_T = 0$, and $X_B = 0.08$ where the suffix B represents the column bottom, and T the column top. Given the values $H_L = 30$ cm, $H_G = 45$ cm, estimate the required packed height.

6.7 The value of H_L for the desorption of O_2 from water at 25 °C in a packed column is 0.30 m, when the superficial water rate is 20 000 kg m^{-2} h^{-1}. What is the value of $k_L a$?

6.8 Why is the effective interfacial area, a, for gas-phase controlled gas absorption much smaller than that for vaporization in packed columns? (Figure 6.5)

References

1. King, C.J. (1971) *Separation Processes*, McGraw-Hill.
2. Whitman, W.G. (1923) *Chem. Met. Eng.*, **29**, 146.
3. Higbie, R. (1935) *Trans. AIChE*, **31**, 365.
4. Danckwerts, P.V. (1951) *Ind. Eng. Chem.*, **43**, 1460.
5. (a) Hatta, S. (1928) *Tohoku Imp. Univ. Tech. Rept.*, **8**, 1; (b) Hatta, S. (1932) *Tohoku Imp. Univ. Tech. Rept.*, **10**, 119.
6. Yoshida, F. and Miura, Y. (1963) *AIChE J.*, **9**, 331.
7. Colburn, A.P. (1933) *Trans. AIChE*, **29**, 174.
8. Sherwood, T.K., Pigford, R.L., and Wilke, C.R. (1975) *Mass Transfer*, McGraw-Hill.
9. Perry, R.H., Green, D.W., and Malony, J.O. (eds) (1984, 1997) *Chemical Engineers' Handbook*, 6th and 7th edn, McGraw-Hill.
10. Chilton, T.H. and Colburn, A.P. (1935) *Ind. Eng. Chem.*, **27**, 255.
11. Taecker, R.G. and Hougen, O.A. (1949) *Chem. Eng. Prog.*, **45**, 188.
12. Shulman, H.L., Ullrich, C.F., and Wells, N. (1955) *AIChE J.*, **1**, 253.
13. Yoshida, F. and Koyanagi, T. (1962) *AIChE J.*, **8**, 309.
14. Sherwood, T.K. and Holloway, F.A.L. (1940) *Trans. AIChE*, **36**, 39.
15. (a) Hikita, H., Kataoka, K., and Nakanishi, K. (1959) *Chem. Eng. (Jpn.)*, **23**, 520; (b) Hikita, H., Kataoka, K., and Nakanishi, K. (1960) *Chem. Eng. (Jpn.)*, **24**, 2.

Further Reading

Danckwerts, P.V. (1970) *Gas-Liquid Reactions*, McGraw-Hill.

Treybal, R.E. (1980) *Mass Transfer Operations*, McGraw-Hill.

7
Bioreactors

7.1
Introduction

Bioreactors are the apparatus in which practical biochemical reactions are performed, often with the use of enzymes and/or living cells. Bioreactors that use living cells are usually called fermentors, and specific aspects of these are discussed in Chapter 12. The apparatus applied to waste water treatment using biochemical reactions is another example of a bioreactor. Even blood oxygenators, that is, artificial lungs as discussed in Chapter 15, can also be regarded as bioreactors.

As most biochemical reactions occur in the liquid phase, bioreactors usually handle liquids. Processes in bioreactors often also involve a gas phase, as in cases of aerobic fermentors. Some bioreactors must handle particles, such as immobilized enzymes or cells, either suspended or fixed in a liquid phase. With regard to mass transfer, microbial or biological cells may be regarded as minute particles.

Although there are many types of bioreactors, they can be categorized into the following major groups:

- Mechanically stirred (agitated) tanks (vessels)
- Bubble columns – that is, cylindrical vessels without mechanical agitation, in which gas is bubbled through a liquid, and their variations, such as airlifts
- Loop reactors with pumps or jets for forced liquid circulation
- Packed-bed reactors (tubular reactors)
- Membrane reactors, using semi-permeable membranes, usually of sheet or hollow fiber type
- Microreactors
- Miscellaneous types, for example, rotating-disk, gas–liquid contactors, and so on.

In the design and operation of various bioreactors, a practical knowledge of physical transfer processes – that is, mass and heat transfer, as described in the relevant previous chapters – are often also required in addition to knowledge of the kinetics of biochemical reactions and of cell kinetics. Some basic concepts on the effects of diffusion inside the particles of catalysts, or of immobilized enzymes or cells, is provided in the following section.

Biochemical Engineering: A Textbook for Engineers, Chemists and Biologists, Second Edition.
Shigeo Katoh, Jun-ichi Horiuchi, and Fumitake Yoshida.

Companion Website: www.wiley.com\go\katoh\biochem_eng_e2

7.2
Some Fundamental Concepts

7.2.1
Batch and Continuous Reactors

Biochemical reactors can be operated either batchwise or continuously, as noted in Section 1.5. Figure 7.1 shows, in schematic form, four modes of operation with two types of reactors for chemical and/or biochemical reactions in liquid phases, with or without suspended solid particles, such as catalyst particles or microbial cells. The modes of operation include stirred batch; stirred semi-batch; continuous stirred; and continuous plug flow reactors (PFRs). In the first three types, the contents of the tanks are completely stirred and uniform in composition.

In a batch reactor, the reactants are initially charged and, after a certain reaction time, the product(s) are recovered batchwise. In the semi-batch (or fed-batch) reactor, the reactants are fed continuously, and the product(s) are recovered batchwise. In these batch and semi-batch reactors, the concentrations of reactants and products change with time.

Figure 7.1c,d shows two types of the steady-state flow reactors with a continuous supply of reactants and continuous removal of product(s). Figure 7.1c shows the continuous stirred-tank reactor (CSTR) in which the reactor contents are perfectly mixed and uniform throughout the reactor. Thus, the composition of the outlet flow is constant, and the same as that in the reactor. Figure 7.1d shows the PFR. Plug flow is the idealized flow, with a uniform fluid velocity across the entire flow channel, and with no mixing in the axial and radial directions. The concentrations of both reactants and products in the PFR change along the flow direction, but are uniform in the direction perpendicular to flow. Usually, mixing conditions in real continuous flow reactors are intermediate between these two extreme cases, *viz*. the CSTR with perfect mixing and the PFR with no mixing in the flow direction.

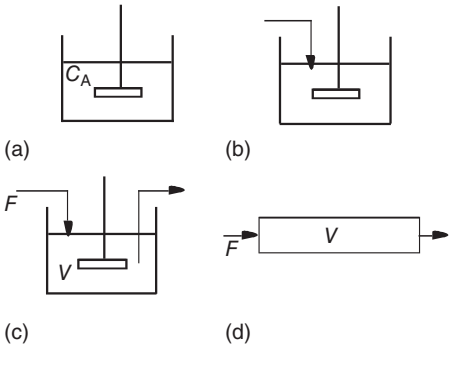

Figure 7.1 Modes of reactor operation: (a) batch reactor, (b) semi-batch reactor, (c) continuous stirred-tank reactor, and (d) continuous plug flow reactor.

The material balance relationship (i.e., Equation 1.5) holds for any reactant. If the liquid in a reactor is completely stirred and its concentration is uniform, we can apply this equation to the whole reactor. In general, it is applicable to a differential volume element and must be integrated over the whole reactor.

7.2.2 Effects of Mixing on Reactor Performance

7.2.2.1 Uniformly Mixed Batch Reactor

As there is no entering or leaving flow in the batch reactor, the material balance equation for a reactant A in a liquid of constant density is given as

$$-r_A V = -V\frac{dC_A}{dt} = VC_{A0}\frac{dx_A}{dt} \tag{7.1}$$

where r_A is the reaction rate (kmol m^{-3} s^{-1}), V is the liquid volume (m^3), and C_A is the reactant concentration (kmol m^{-3}). The fractional conversion $x_A(-)$ of A is defined as $(C_{A0} - C_A)/C_{A0}$, where C_{A0} is the initial reactant concentration in the liquid in the reactor. Integration of Equation 7.1 gives

$$t = -\int_{C_{A0}}^{C_A}\frac{dC_A}{-r_A} = C_{A0}\int_0^{\chi_A}\frac{dx_A}{-r_A} \tag{7.2}$$

Integration of Equation 7.2 for the irreversible first-order and second-order reactions leads to the previously given Equations 3.15 and 3.22, respectively.

Similarly, for enzyme-catalyzed reactions of the Michaelis–Menten type, we can derive Equation 7.3 from Equation 3.31.

$$C_{A0}x_A - K_m \ln(1 - x_A) = V_{max}t \tag{7.3}$$

7.2.2.2 Continuous Stirred-Tank Reactor (CSTR)

The liquid composition in the CSTR is uniform and equal to that of the exit stream, and the accumulation term is zero at steady state. Thus, the material balance for a reactant A is given as

$$FC_{A0} - FC_{A0}(1 - x_A) = -r_A V \tag{7.4}$$

where F is the volumetric feed rate (m^3 s^{-1}), and V is the volume of the reactor (m^3), with other symbols being the same as in Equation 7.1. The residence time τ (s) is given as

$$\tau = \frac{V}{F} = \frac{C_{A0}x_A}{-r_A} \tag{7.5}$$

The reciprocal of τ, that is, F/V, is called the dilution rate.

For the irreversible first-order reaction and the Michaelis–Menten type reaction, the following Equations 7.6 and 7.7 hold, respectively.

$$k\tau = \frac{x_A}{1 - x_A} \tag{7.6}$$

$$V_{max}\tau = C_{A0}x_A + K_m\frac{x_A}{1-x_A} \tag{7.7}$$

where K_m is the Michaelis–Menten constant.

7.2.2.3 Plug Flow Reactor (PFR)

The material balance for a reactant A for a differential volume element dV of the PFR perpendicular to the flow direction is given by

$$FC_A - F(C_A + dC_A) = -r_A dV \tag{7.8}$$

in which the symbols are the same as in Equation 7.1. Hence,

$$\tau = \frac{V}{F} = -\int_{C_{A0}}^{C_A}\frac{dC_A}{-r_A} = C_{A0}\int_0^{\chi_A}\frac{dx_A}{-r_A} \tag{7.9}$$

Substitution of the rate equations into Equation 7.9 and integration give the following performance equations.

For the first-order reaction,

$$-\ln(1-x_A) = k\tau \tag{7.10}$$

For the second-order reaction,

$$\ln\frac{(1-x_B)}{(1-x_A)} = \ln\frac{C_BC_{A0}}{C_{B0}C_A} = (C_{B0}-C_{A0})k\tau \tag{7.11}$$

For the Michaelis–Menten type reaction,

$$C_{A0}x_A - K_m\ln(1-x_A) = V_{max}\tau \tag{7.12}$$

Equations 7.10–7.12 are identical in forms with those for the uniformly mixed batch reactor, that is, Equations 3.15, 3.22, and 7.3, respectively. It is seen that the time from the start of a reaction in a batch reactor (t) corresponds to the residence time in a PFR (τ).

Example 7.1

A feed solution containing a reactant A ($C_A = 1\ \text{kmol m}^{-3}$) is fed to a CSTR or to a PFR at a volumetric flow rate of $0.001\ \text{m}^3\ \text{s}^{-1}$ and converted to product P in the reactor. The first-order reaction rate constant is $0.02\ \text{s}^{-1}$.

Determine the reactor volumes of CSTR and PFR required to attain a fractional conversion of A, $x_A = 0.95$.

Solution

a) *CSTR case*

From Equation 7.6

$$\tau = \frac{0.95}{1-0.95}\times\frac{1}{0.02} = 950\ \text{s}$$

$$V = F \times \tau = 0.001 \times 950 = 0.95 \text{ m}^3$$

b) *PFR case*
From Equation 7.10

$$\tau = \frac{-\ln(1 - 0.95)}{0.02} = 150 \text{ s}$$

$$V = F \times \tau = 0.001 \times 150 = 0.15 \text{ m}^3$$

It is seen that the required volume of the PFR is much smaller than that of the CSTR to attain an equal fractional conversion, as discussed below.

7.2.2.4 Comparison of Fractional Conversions by CSTR and PFR

Figure 7.2 shows the calculated volume ratios of CSTR to PFR plotted against the fractional conversions $(1 - x_A)$ with the same feed compositions for first-order, second-order, and Michaelis–Menten type reactions. A larger volume is always required for the CSTR than for the PFR in order to attain an equal specific conversion. The volume ratio increases rapidly with the order of reaction at higher conversions, indicating that liquid mixing strongly affects the performance of reactors in this range.

In the CSTR, the reactants in the feed are instantaneously diluted to the concentrations in the reactor, whereas in the PFR there is no mixing in the axial direction. Thus, the concentrations of the reactants in the PFR are generally higher than those in the CSTR, and reactions of a higher order proceed under favorable conditions. Naturally, the performance for zero-order reactions is not affected by the type of reactor.

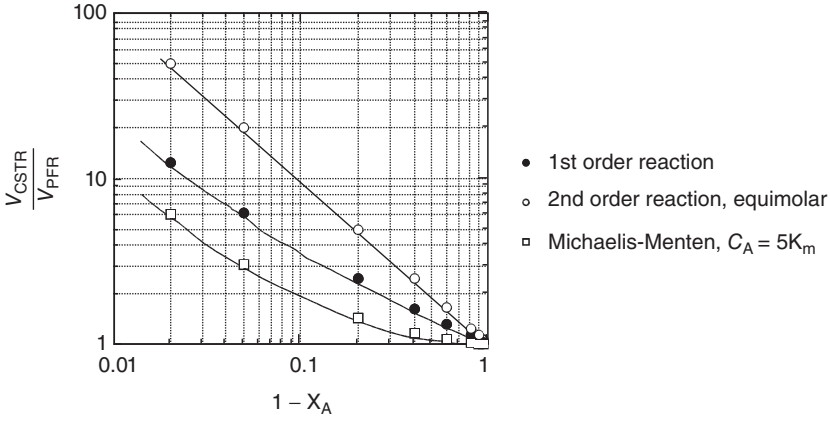

Figure 7.2 Volume ratios of CSTR to PFR for first, second order, and Michaelis–Menten type reactions.

7.2.3 Effects of Mass Transfer Around and within Catalyst or Enzymatic Particles on the Apparent Reaction Rates

For liquid-phase catalytic or enzymatic reactions, catalysts or enzymes are used as homogeneous solutes in the liquid, or as solid particles suspended in the liquid phase. In the latter case, (i) the particles *per se* may be catalysts; (ii) the catalysts or enzymes are uniformly distributed within inert particles; or (iii) the catalysts or enzymes exist at the surface of pores, inside the particles. In such heterogeneous catalytic or enzymatic systems, a variety of factors that include the mass transfer of reactants and products, heat effects accompanying the reactions, and/or some surface phenomena, may affect the apparent reaction rates. For example, in situation (iii) above, the reactants must move to the catalytic reaction sites within catalyst particles by various mechanisms of diffusion through the pores. In general, the apparent rates of reactions with catalyst or enzymatic particles are lower than the intrinsic reaction rates; this is due to the various mass transfer resistances, as is discussed below.

7.2.3.1 Liquid Film Resistance Controlling

In the case where the rate of catalytic or enzymatic reaction is controlled by the mass transfer resistance of the liquid film around the particles containing catalyst or enzyme, the rate of decrease of the reactant A per unit liquid volume (i.e., $-r_A$ (kmol m^{-3} s^{-1})) is given by Equation 7.13:

$$-r_A = k_L A(C_{Ab} - C_{Ai}) \tag{7.13}$$

where k_L is the liquid film mass transfer coefficient (m s^{-1}), A is the surface area of catalyst or enzyme particles per unit volume of liquid containing particles (m^2 m^{-3}), C_{Ab} is the concentration of reactant A in the bulk of liquid (kmol m^{-3}), and C_{Ai} is its concentration on the particle surface (kmol m^{-3}). Correlations for k_L in packed beds and other cases are given in the present chapter, as well as in Chapter 6 and in various reference books.

The apparent reaction rate depends on the magnitude of Damköhler number (Da) as defined by Equation 7.14 – that is, the ratio of the maximum reaction rate to the maximum mass transfer rate.

$$\mathrm{Da} = \frac{-r_{A,\max}}{k_L A C_{Ab}} \tag{7.14}$$

In the case where mass transfer of the reactants through the liquid film on the surface of the catalyst or enzyme particles is much slower than the reaction itself (Da $\gg$ 1), the apparent reaction rate becomes almost equal to the rate of mass transfer. This is analogous to the case of two electrical resistances of different magnitudes in series, where the overall resistance is almost equal to the higher resistance. In such a case, the apparent reaction rate is given by

$$-r_A = k_L A\, C_{Ab} \tag{7.15}$$

7.2.3.2 Effects of Diffusion within Catalyst Particles

The resistance to mass transfer of reactants within catalyst particles results in lower apparent reaction rates, due to a slower supply of reactants to the catalytic reaction sites. The long diffusional paths inside large catalyst particles, often through tortuous pores, result in a high resistance to mass transfer of the reactants and products. The overall effects of these factors involving mass transfer and reaction rates are expressed by the so-called (internal) effectiveness factor E_f, which is defined by the following equation, excluding the mass transfer resistance of the liquid film on the particle surface [1, 2]:

$$E_f = \frac{\text{apparent reaction rate involving mass transfer within catalyst particles}}{\text{intrinsic reaction rate excluding mass transfer effects within catalyst particles}} \tag{7.16}$$

If there is no mass transfer resistance within the catalyst particle, then E_f is unity. However, it will then decrease from unity with increasing mass transfer resistance within the particles. The degree of decrease in E_f is correlated with a dimensionless parameter known as the Thiele modulus [2], which involves the relative magnitudes of the reaction rate and the molecular diffusion rate within catalyst particles. The Thiele moduli for several reaction mechanisms and shapes of catalyst particles have been derived theoretically.

The Thiele modulus ϕ for the case of a spherical catalyst particle of radius R (cm), in which a first-order catalytic reaction occurs at every point within the particles, is given as

$$\phi = \frac{R}{3}\sqrt{\frac{k}{D_{\text{eff}}}} \tag{7.17}$$

where k is the first-order reaction rate constant (s^{-1}) and D_{eff} is the effective diffusion coefficient ($cm^2\ s^{-1}$) based on the overall concentration gradient inside the particle.

The radial distribution of the reactant concentrations in the spherical catalyst particle is theoretically given as:

$$C_A^* = \frac{C_A}{C_{Ab}} = \frac{\sinh(3\phi r^*)}{r^*\ \sinh(3\phi)} \tag{7.18}$$

where $\sinh x = (e^x - e^{-x})/2$, ϕ is the Thiele modulus, C_A is the reactant concentration at a distance r from the center of the sphere of radius R, C_{Ab} is C_A at the sphere's surface, and $r^* = r/R$. Figure 7.3 shows the reactant concentrations within the particle calculated by Equation 7.18 as a function of ϕ and the distance from the particle surface.

Under steady state conditions the rate of reactant transfer to the outside surface of the catalyst particles should correspond to the apparent reaction rate within catalyst particles. Thus, the effectiveness factor E_f is given by the following equation:

$$E_f = \frac{\frac{3}{R}D_{\text{eff}}\left(\frac{dC_A}{dr}\right)_{r=R}}{kC_{Ab}} = \frac{3D_{\text{eff}}\left(\frac{dC_A^*}{dr^*}\right)_{r^*=1}}{R^2k} \tag{7.19}$$

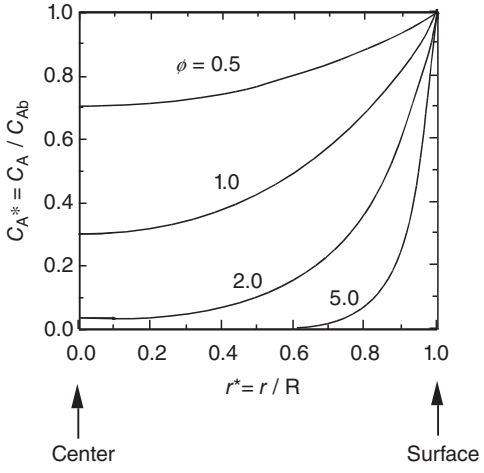

Figure 7.3 Concentration distribution of reactant within a spherical catalyst particle.

where $3/R$ is equal to the surface area divided by the volume of the catalyst particle. Combining Equations 7.18 and 7.19, the effectiveness factor for the first-order catalytic reaction in spherical particles is given as:

$$E_f = \frac{3\phi \quad \coth(3\phi) - 1}{3\phi^2} \tag{7.20}$$

In Figure 7.4 the effectiveness factor is plotted against the Thiele modulus for spherical catalyst particles. For low values of ϕ, E_f is almost equal to unity, with reactant transfer within the catalyst particles having little effect on the apparent reaction rate. On the other hand, E_f decreases in inverse proportion to ϕ for higher values of ϕ, with reactant diffusion rates limiting the apparent reaction rate. Thus, E_f decreases with increasing reaction rates and the radius of catalyst spheres, and with decreasing effective diffusion coefficients of reactants within the catalyst spheres.

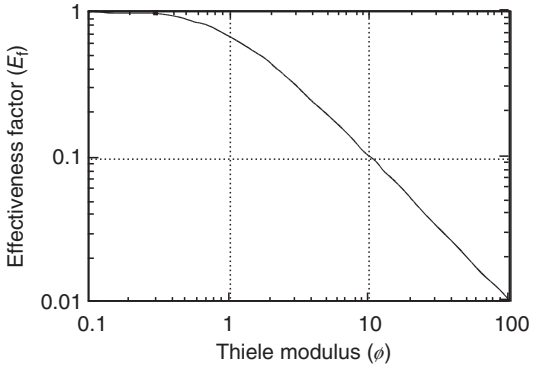

Figure 7.4 Effectiveness factor of spherical catalyst particle for first-order reaction.

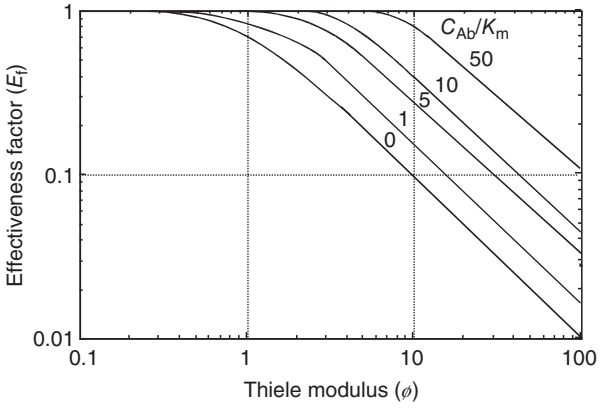

Figure 7.5 Effectiveness factor for various values of C_{Ab}/K_m (Michaelis–Menten type reaction, sphere).

7.2.3.3 Effects of Diffusion within Immobilized Enzyme Particles

Enzymes, when immobilized in spherical particles or in films made from various polymers and porous materials, are referred to as "immobilized" enzymes. Enzymes can be immobilized by covalent bonding, electrostatic interaction, cross-linking of the enzymes, and entrapment in a polymer network, among other techniques. In the case of batch reactors, the particles or films of immobilized enzymes can be reused after having been separated from the solution after reaction by physical means, such as sedimentation, centrifugation, and filtration. Immobilized enzymes can also be used in continuous fixed-bed reactors, fluidized reactors, and membrane reactors.

Apparent reaction rates with immobilized enzyme particles also decrease due to the mass transfer resistance of reactants (substrates). The Thiele modulus of spherical particles of radius R for the Michaelis–Menten type reactions is given as

$$\phi = \frac{R}{3}\sqrt{\frac{V_{max}}{D_{eff}K_m}} \tag{7.21}$$

where V_{max} is the maximum reaction rate (kmol m^{-3} s^{-1}) attained at very high substrate concentrations and K_m is the Michaelis constant (kmol m^{-3}).

Calculated values of E_f for several values of C_{Ab}/K_m are shown in Figure 7.5 where E_f is seen to increase with increasing values of C_{Ab}/K_m. When the values of C_{Ab}/K_m approach zero, the curve approaches the first-order curve shown in Figure 7.4. The values of E_f decrease with increasing reaction rate and/or immobilized enzyme concentration, and also with increasing resistance to substrate mass transfer.

Example 7.2

Immobilized enzyme beads of 0.6 cm diameter contain an enzyme that converts a substrate S to a product P by an irreversible unimolecular enzyme reaction with $K_m = 0.012\,\text{kmol m}^{-3}$ and the maximum rate $V_m = 3.6 \times 10^{-7}\,\text{kmol (kg-bead)}^{-1}\,\text{s}^{-1}$. The density of the beads and the effective diffusion coefficient of the substrate in the catalyst beads are $1000\,\text{kg m}^{-3}$ and $1.0 \times 10^{-6}\,\text{cm}^2\,\text{s}^{-1}$, respectively.

Determine the effectiveness factor and the initial reaction rate, when the substrate concentration is $0.6\,\text{kmol m}^{-3}$.

Solution

The value of the Thiele modulus is calculated from Equation 7.21.

$$\phi = \frac{0.3}{3}\sqrt{\frac{3.6 \times 10^{-7} \times 1000}{1.0 \times 10^{-6} \times 0.012}} = 17.3$$

The value of C_{Ab}/K_m is 50, and thus the value of $E_f = 0.50$ is obtained from Figure 7.5. The initial rate of the reaction is

$$r_P = E_f \frac{V_{max} C_S}{K_m + C_S} = 0.5 \times \frac{3.6 \times 10^{-4} \times 0.6}{0.012 + 0.6}$$
$$= 1.8 \times 10^{-4}\,\text{kmol m}^{-3}\,\text{s}^{-1}$$

7.3 Bubbling Gas–Liquid Reactors

In both the gassed (aerated) stirred tank and in the bubble column, the gas bubbles rise through a liquid, despite the mechanisms of bubble formation in the two types of apparatus being different. In this section, we shall consider some common aspects of the gas bubble–liquid systems in these two types of reactors.

7.3.1 Gas Holdup

Gas holdup is the volume fraction of the gas bubbles in a gassed liquid. However, it should be noted that two different bases are used for defining gas holdup: (i) the total volume of the gas bubble–liquid mixture and (ii) the clear liquid volume excluding bubbles. Thus, the gas holdup defined on basis (ii) is given as

$$\underline{\varepsilon} = \frac{V_B}{V_L} = \frac{(Z_F - Z_L)}{Z_L} \tag{7.22}$$

where V_B is the volume of bubbles (L^3), V_L is the volume of liquid (L^3), Z_F is the total height of the gas–liquid mixture (L), and Z_L is the height of liquid excluding bubbles.

The gas holdup on basis (i) is defined as

$$\varepsilon = \frac{V_B}{(V_L + V_B)} = \frac{(Z_F - Z_L)}{Z_F} \tag{7.23}$$

The gas holdups can be obtained by measuring Z_F and Z_L, or by measuring the corresponding hydrostatic heads. Evidently, the following relationship holds.

$$\frac{\underline{\varepsilon}}{\varepsilon} = \frac{(V_L + V_B)}{V_L} > 1 \tag{7.24}$$

Although use of basis (i) is more common, basis (ii) is more convenient in some cases.

7.3.2 Interfacial Area

As with the gas holdup, there are two definitions of interfacial area, namely, the interfacial area per unit volume of gas–liquid mixture a ($L^2\,L^{-3}$) and the interfacial area per unit liquid volume $\underline{a}$ ($L^2\,L^{-3}$).

There are at least three methods to measure the interfacial area in liquid–gas bubble systems.

The *light transmission technique* [3] is based on the fact that the fraction of light transmitted through a gas–liquid dispersion is related to the interfacial area and the length of the light pass, irrespective of bubble size.

In the *photographic method*, the sizes and number of bubbles are measured on photographs of bubbles, but naturally there is wide distribution among the bubble sizes.

The volume–surface mean bubble diameter d_{vs} is defined by Equation 7.25:

$$d_{vs} = \frac{\sum_{i=1}^{n} d_i^3}{\sum_{i=1}^{n} d_i^2} \tag{7.25}$$

The value of a can then be calculated by using the following relationship:

$$a = \frac{6\varepsilon}{d_{vs}} \tag{7.26}$$

Equation 7.26 also gives d_{vs}, in case the gas holdup ε and the interfacial area a are known.

The *chemical method* used to estimate the interfacial area is based on the theory of the enhancement factor for gas absorption accompanied with a chemical reaction. It is clear from Equations 6.22–6.24 that, in the range where $\gamma > 5$, the gas absorption rate per unit area of gas–liquid interface becomes independent of the liquid phase mass transfer coefficient k_L, and is given by Equation 6.24. Such criteria can be met in the case of absorption with

an approximately pseudo first-order reaction with respect to the concentration of the absorbed gas component. Reactions that could be used for the chemical method include, for example, CO_2 absorption in aqueous NaOH solution, and the air oxidation of Na_2SO_3 solution with a cupric ion or cobaltous ion catalyst (this is described in the following section).

It is a well-known fact that bubble sizes in aqueous electrolyte solutions are much smaller than in pure water with equal values of viscosity, surface tension, and so on. This can be explained by the electrostatic potential of the resultant ions at the liquid surface, which reduces the rate of bubble coalescence. This fact should be remembered when planning experiments on bubble sizes or interfacial areas.

7.3.3 Mass Transfer Coefficients

7.3.3.1 Definitions

Relationships between the gas-phase mass transfer coefficient k_G, the liquid-phase mass transfer coefficient k_L, and the overall mass transfer coefficients K_G and K_L were discussed in Section 6.2. With the definitions used in this book, all of these coefficients have a simple dimension ($L\,T^{-1}$).

With regards to handling data on industrial apparatus for gas–liquid mass transfer (such as packed columns, bubble columns, and stirred tanks), it is more practical to use volumetric mass transfer coefficients, such as K_Ga and K_La, because the interfacial area a cannot be well defined and will vary with operating conditions. As noted in Section 6.7.2, the volumetric mass transfer coefficients for packed columns are defined with respect to the packed volume – that is, the sum of the volumes of gas, liquid, and packings. In contrast, volumetric mass transfer coefficients, which involve the specific gas–liquid interfacial area a ($L^2\,L^{-3}$), for liquid–gas bubble systems (such as gassed stirred tanks and bubble columns) are defined with respect to the unit volume of gas–liquid mixture or of clear liquid volume, excluding the gas bubbles. In this book, we shall use $\underline{a}$ for the specific interfacial area with respect to the clear liquid volume, and a for the specific interfacial area with respect to the total volume of gas–liquid mixture.

The question is, why is the volumetric mass transfer coefficient K_La (T^{-1}) used so widely as a measure of performance of gassed stirred tanks and bubble columns? There is nothing wrong with using K_Ga, as did the early investigators in this field. Indeed, K_Ga and K_La are proportional and easily interconvertible by using Equation 6.13. However, as shown by Equation 6.12, if the solubility of the gas is rather low (e.g., oxygen absorption in fermentors), then K_La is practically equal to k_La, which could be directly correlated with liquid properties. On the other hand, in cases where the gas solubility is high, the use of K_Ga rather than K_La would be more convenient, as shown by Equation 6.11. In cases where the gas solubility is moderate, the mass transfer resistances of both liquid and gas phases must be considered.

7.3.3.2 Measurements of $k_L a$

Steady-State Mass Balance Method In theory, the $K_L a$ in an apparatus that is operating continuously under steady-state conditions could be evaluated from the flow rates and the concentrations of the gas and liquid streams entering and leaving, and the known rate of mass transfer (e.g., the oxygen consumption rate of microbes in the case of a fermentor). However, such a method is not practical, except when the apparatus is fairly large and highly accurate instruments such as flow meters and oxygen sensors (or gas analyzers) are available.

Unsteady-State Mass Balance Method One widely used technique for determining $K_L a$ in bubbling gas–liquid contactors is the physical absorption of oxygen or CO_2 into water or aqueous solutions, or the desorption of such a gas from a solution into a sparging inert gas such as air or nitrogen. The time-dependent concentration of dissolved gas is followed by using a sensor (e.g., for O_2 or CO_2) with a sufficiently fast response to changes in concentration.

Sulfite Oxidation Method The sulfite oxidation method is a classical, but still useful, technique for measuring $k_G a$ (or $k_L a$) [4]. The method is based on the air oxidation of an aqueous solution of sodium sulfite (Na_2SO_3) to sodium sulfate (Na_2SO_4) with a cupric ion (Cu^{2+}) or cobaltous ion (Co^{2+}) catalyst. With appropriate concentrations of sodium sulfite (about 1 N) or cupric ions ($>10^{-3}$ mol l^{-1}), the value of k_L^* for the rate of oxygen absorption into sulfite solution, which can be determined by chemical analysis, is practically equal to k_L for the physical oxygen absorption into sulfate solution; in other words, the enhancement factor E, as defined by Equation 6.20, is essentially equal to unity.

It should be noted that this method yields higher values of $k_L a$ compared to those in pure water under the same operating conditions because, due to the effects of electrolytes mentioned before, the average bubble size in sodium sulfite solutions is smaller and hence the interfacial area is larger than in pure water.

Dynamic Method This is a practical unsteady-state technique to measure $k_L a$ in fementors in operation [5] (Figure 7.6). When a fermentor is operating under steady conditions, the air supply is suddenly turned off, which causes the oxygen concentration in the liquid, C_L (kmol m^{-3}), to fall quickly. As there is no oxygen supply by aeration, the oxygen concentration falls linearly (Figure 7.6 curve a–b), due to oxygen consumption by microbes. From the slope of the curve a–b during this period, it is possible to determine the rate of oxygen consumption by microbes, q_o (kmol kg^{-1} h^{-1}), by the following relationship.

$$-\frac{dC_L}{dt} = q_o C_x \tag{7.27}$$

where C_x (kg m^{-3}) is the concentration of microbes in the liquid medium. Upon restarting the aeration, the dissolved oxygen concentration will increase as indicated by the curve b–c. The oxygen balance during this period is expressed

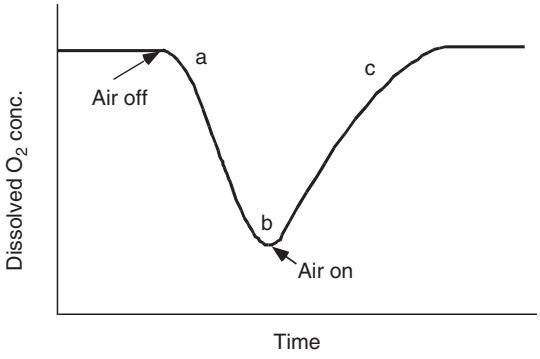

Figure 7.6 Dynamic measurement of $k_L a$ for oxygen transfer in fermentors.

by

$$\frac{dC_L}{dt} = K_L a(C_L^* - C_L) - q_o C_x \tag{7.28}$$

where C_L^* (kmol m^{-3}) is the liquid oxygen concentration in equilibrium with that in air. A rearrangement of Equation 7.28 gives

$$C_L = C_L^* - \left(\frac{1}{K_L a}\right)\left(\frac{dC_L}{dt} + q_o C_x\right) \tag{7.29}$$

Thus, plotting the experimental values of C_L after the restarting aeration against $(dC_L/dt + q_o C_x)$ would give a straight line with a slope of $-(1/K_L a)$. Possible sources of errors for this technique are bubble retention immediately after the aeration cutoff, especially with viscous liquids, and the aeration from the free liquid surface (although the latter can be prevented by passing nitrogen over the free liquid surface).

Example 7.3

In an aerated stirred tank, air is bubbled into degassed water. The oxygen concentration in water was continuously measured using an oxygen electrode such that the data shown in Table 7.1 were obtained. Evaluate the overall volumetric mass transfer coefficient of oxygen $K_L a$ (in unit of h^{-1}). The equilibrium concentration of oxygen in equilibrium with air under atmospheric pressure is 8.0 mg l^{-1}; the delay in response of the oxygen electrode may be neglected.

Solution

From the oxygen balance, the following equation is obtained:

$$\frac{dC_L}{dt} = K_L a(C_L^* - C_L)$$

Upon integration with the initial condition $C_L = 0$ at $t = 0$

$$\ln\left[\frac{C_L^*}{\left(C_L^* - C_L\right)}\right] = K_L a t$$

Table 7.1 Oxygen concentration in water.

Time (s)	O_2 concentration (mg l^{-1})
0	0
20	2.84
40	4.63
60	5.87
80	6.62
100	7.10
120	7.40

Plots of $C_L^*/C_L^* - C_L$) against time on semi-logarithmic coordinates produces a straight line, from the slope of which can be calculated the value of $K_L a = 79\,h^{-1}$.

7.4 Mechanically Stirred Tanks

7.4.1 General

Stirred (agitated) tanks, which are widely used as bioreactors (especially as fermentors), are vertical cylindrical vessels equipped with a mechanical stirrer (agitator) or stirrers that rotate around the axis of the tank.

The objectives of liquid mixing in stirred tanks are to (i) make the liquid concentration as uniform as possible; (ii) suspend the particles or cells in the liquid; (iii) disperse the liquid droplets in another immiscible liquid, as in the case of a liquid–liquid extractor; (iv) disperse gas as bubbles in a liquid in the case of aerated (gassed) stirred tanks; and (v) transfer heat from or to a liquid in the tank, through the tank wall, or to the wall of coiled tube installed in the tank.

Figure 7.7 shows three commonly used types of impellers or stirrers. The six-flat blade turbine, often called the Rushton turbine (Figure 7.7a), is widely used. The standard dimensions of this type of stirrer relative to the tank size are as follows:

$$\frac{d}{D} = \frac{1}{3} \quad D = H_L \qquad d = H_i$$
$$\frac{L}{d} = \frac{1}{4} \quad \frac{b}{d} = \frac{1}{5}$$

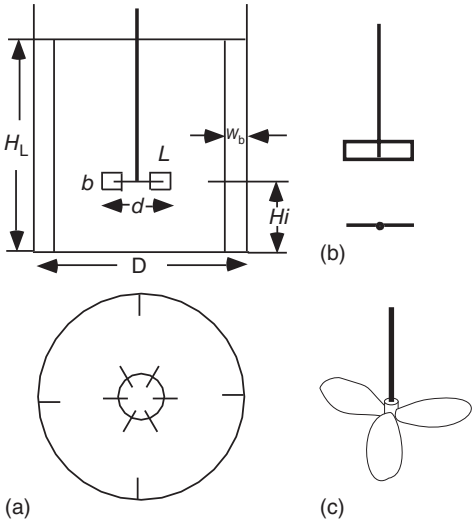

Figure 7.7 Typical impeller types: (a) a six-flat blade turbine; (b) a two-flat blade paddle; and (c) a three-blade marine propeller. See the text for details of the abbreviations.

where D is the tank diameter, H_L is the total liquid depth, d is the impeller diameter, H_i is the distance of the impeller from the tank bottom, and L and b are the length and width of the impeller blade, respectively.

When this type of impeller is used, typically four vertical baffle plates, each one-tenth of the tank diameter in width and the total liquid depth in length, are fixed perpendicular to the tank wall so as to prevent any circular flow of liquid and the formation of a concave vortex at the free liquid surface.

With this type of impeller in operation, liquid is sucked to the impeller center from below and above, and then driven radially toward the tank wall, along which it is deflected upwards and downwards. It then returns to the central region of the impeller. Consequently, this type of impeller is referred to as a *radial flow impeller*. If the ratio of the liquid depth to the tank diameter is 2 or more, then multiple impellers fixed to a common rotating shaft are often used.

When liquid mixing with this type of impeller is accompanied by aeration (gassing), the gas is supplied at the tank bottom through a single nozzle or via a circular sparging ring (which is a perforated circular tube). Gas from the sparger should rise within the radius of the impeller, so that it can be dispersed by the rotating impeller into bubbles that are usually several millimeters in diameter. The dispersion of gas into bubbles is in fact due to the high liquid shear rates produced by the rotating impeller.

Naturally, the patterns of liquid movements will vary with the type of impeller used. When marine propeller-type impellers (which often have two or three blades; see Figure 7.7c) are used, the liquid in the central part moves upwards along the tank axis and then downwards along the tank wall. Hence, this type of

impeller is categorized as an *axial flow impeller*. This type of stirrer is suitable for suspending particles in a liquid, or for mixing highly viscous liquids.

Figure 7.7b shows a two-flat blade paddle . If the flat blades are pitched, then the liquid flow pattern becomes intermediate between axial and radial flows. Many other types of impellers are used in stirred tanks, but these are not described at this point.

Details of heat transfer in stirred tanks are provided in Sections 5.4.3 and 12.3.

7.4.2
Power Requirements of Stirred Tanks

The power required to operate a stirred tank is mostly the mechanical power required to rotate the stirrer. Naturally, the stirring power varies with the stirrer type. In general, the power requirement will increase in line with the size and/or rotating speed, and will also vary according to the properties of the liquid. The stirrer power requirement for a gassed (aerated) liquid is less than that for an ungassed liquid, because the average bulk density of a gassed liquid, particularly in the vicinity of the impeller, is less than that for an ungassed liquid.

7.4.2.1 Ungassed Liquids

There are well-established empirical correlations for stirrer power requirements [6, 7]. Figure 7.8 [6] is a log–log plot of the power number N_P for ungassed liquids versus the stirrer Reynolds number (Re). These dimensionless numbers are defined as follows:

$$N_P = \frac{P}{(\rho N^3 d^5)} \tag{7.30}$$

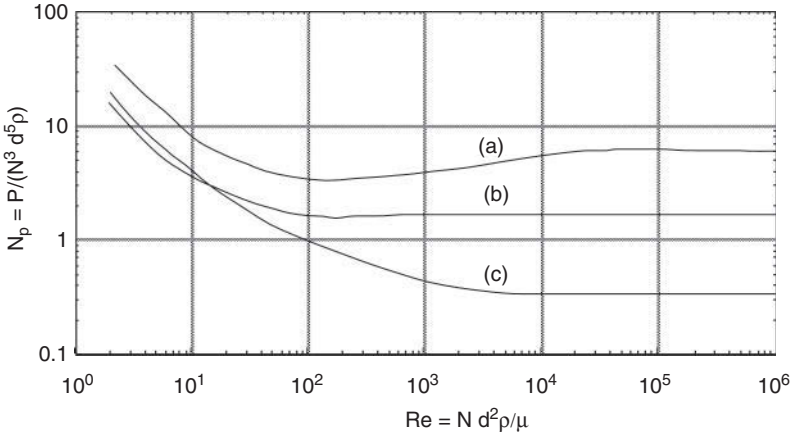

Figure 7.8 Correlation between Reynolds number (Re) and Power number (N_p). Curve (a): six-flat blade turbine, four baffles, $W_b = 0.1$ D (Figure 7.7); curve (b): two-flat blade paddle, four baffles, $W_b = 0.1$ D; and curve (c): three-blade marine propeller, four baffles, $W_b = 0.1$ D.

$$\mathrm{Re} = \frac{Nd^2\rho}{\mu} \tag{7.31}$$

where P is the power required ($\mathrm{M\,L^2\,T^{-3}}$), N is the number of revolutions of the impeller per unit time ($\mathrm{T^{-1}}$), d is the impeller diameter (L), ρ is the liquid density ($\mathrm{M\,L^{-3}}$), and μ is the liquid viscosity ($\mathrm{M\,L^{-1}\,T^{-1}}$). Since the product $N\,d$ is proportional to the peripheral speed (i.e., the tip speed of the rotating impeller), Equation 7.31 defining (Re) for the rotating impeller corresponds to Equation 2.7, the (Re) for flow through a straight tube.

In Figure 7.8, the curves a, b, and c correlate data for three types of impellers, namely, the six-flat blade turbine, two-flat blade paddle, and three-blade marine propeller, respectively. It should be noted that, for the range of (Re) $>10^4$, N_P is independent of (Re). For this turbulent regime it is clear from Equation 7.30 that

$$P = \mathrm{c}_1\,\rho N^3 d^5 \tag{7.32}$$

where c_1 is a constant that varies with the impeller types. Thus, P for a given type of impeller varies in proportion to N^3, d^5 and liquid density ρ, but is independent of liquid viscosity μ.

For the ranges of Re below approximately 10, the plots are straight lines with a slope of −1; that is, N_P is inversely proportional to (Re). Then, for this laminar regime, we can obtain Equation 7.33 from Equations 7.30 and 7.31:

$$P = \mathrm{c}_2\mu N^2 d^3 \tag{7.33}$$

Thus, P for the laminar regime varies in proportion to liquid viscosity μ, N^2, d^3 and to a constant c_2, which varies with impeller types, although P is independent of the liquid density ρ.

It is worth remembering that the power requirements of geometrically similar stirred tanks are proportional to $N^3\,d^5$ in the turbulent regime and to $N^2\,d^3$ in the laminar regime. In the case of scaling-up of geometrically similar stirred tanks, the equal power input per unit liquid volume, which should be proportional to $N^3\,d^2$ for the turbulent regime and to N^2 for the laminar regime, is sometimes used as a criterion for scale-up, because it leads to the same values of $k_\mathrm{L}a$ in a larger stirred tank with that in the smaller stirred tank (see Section 7.4.3, Equation 7.36a, and also Section 12.5).

Details of stirrer power requirement for non-Newtonian liquids are provided in Section 12.2.

7.4.2.2 Gas-Sparged Liquids

The ratio of the power requirement of gas-sparged (aerated) liquid in a stirred tank, P_G, to the power requirement of ungassed liquid in the same stirred tank, P_0, can be estimated using Equation 7.34 [7]. This is an empirical, dimensionless equation based on data for six-flat blade turbines, with a blade width that is one-fifth of the impeller diameter d, while the liquid depth H_L is equal to the tank diameter. Although these data were for tank diameters up to 0.6 m, Equation 7.34 would apply to larger tanks where the liquid depth-to-diameter ratio is typically

in the region of unity.

$$\log\left(\frac{P_G}{P_0}\right) = -192\left(\frac{d}{D}\right)^{4.38}\left(\frac{d^2N}{\nu}\right)^{0.115}\left(\frac{dN^2}{g}\right)^{1.96(d/D)}\left(\frac{Q}{Nd^3}\right) \quad (7.34)$$

where d is the impeller diameter (L), D is the tank diameter (L), N is the rotational speed of the impeller (T^{-1}), g is the gravitational constant ($L\,T^{-2}$), Q is the gas rate ($L^3\,T^{-1}$), and ν is the kinematic viscosity of the liquid ($L^2\,T^{-1}$). The dimensionless groups include ($d^2\,N/\nu$) = Reynolds number (Re); ($d\,N^2/g$) = Froude number (Fr); and ($Q/N\,d^3$) = aeration number (Na), which is proportional to the ratio of the superficial gas velocity with respect to the tank cross section to the impeller tip speed.

The ratio P_G/P_0 for flat-blade turbine impeller systems can also be estimated by Equation 7.35 [8].

$$\frac{P_G}{P_0} = 0.10\left(\frac{Q}{NV}\right)^{-1/4}\left(\frac{N^2d^4}{gbV^{2/3}}\right)^{-1/5} \quad (7.35)$$

where V is the liquid volume (L^3) and b is the impeller blade width (L). All other symbols are the same as in Equation 7.34.

Example 7.4

Calculate the power requirements, with and without aeration, of a 1.5 m-diameter stirred tank, containing water 1.5 m deep, equipped with a six-blade Rushton turbine that is 0.5 m in diameter d, with blades 0.25 d long and 0.2 d wide, operating at a rotational speed of 180 rpm. Air is supplied from the tank bottom at a rate of 0.6 $m^3\,min^{-1}$. Operation is at room temperature. Values of water viscosity $\mu = 0.001\,kg\,m^{-1}\,s^{-1}$ and water density $\rho = 1000\,kg\,m^{-3}$; hence $\mu/\rho = \nu = 10^{-6}\,m^2\,s^{-1}$ can be used.

Solution

a) The power requirement without aeration can be obtained using Figure 7.8.

$$(\mathrm{Re}) = d^2\frac{N}{\nu} = 0.5^2 \times \frac{3}{10^{-6}} = 7.5 \times 10^5$$

This is in the turbulent regime. Then, from Figure 7.8,

$$N_P = 6$$

$$P_0 = 6\rho N^3 d^5 = 6\,(1000)3^3(0.5)^5 = 5060\ \mathrm{kg\,m^2 s^{-3}} = 5060\ \mathrm{W}$$

b) Power requirement with aeration is estimated using Equation 7.34.

$$\log\left(\frac{P_G}{P_0}\right) = -192\left(\frac{1}{3}\right)^{4.38}\left(0.5^2 \times \frac{3}{10^{-6}}\right)^{0.115} \times \left(\frac{0.5 \times 3^2}{9.8}\right)^{1.96/3}\left[\frac{0.01}{(3 \times 0.5^3)}\right] = -0.119$$

$$\frac{P_G}{P_0} = 0.760$$

Hence,

$$P_G = 5060 \times 0.760 = 3850 \text{ W}$$

For comparison, calculation by Equation 7.35 gives

$$\frac{P_G}{P_0} = 0.676 \qquad P_G = 3420 \text{ W}$$

7.4.3 $k_L a$ in Gas-Sparged Stirred Tanks

Gas–liquid mass transfer in fermentors is discussed in detail in Section 12.4. In dealing with $k_L a$ in gas-sparged stirred tanks, it is more rational to separate k_L and a, because both are affected by different factors. It is possible to measure a by using either a light scattering technique [9] or a chemical method [4]. The average bubble size d_{vs} can be estimated by Equation 7.26 from measured values of a and the gas holdup ε. Correlations for k_L have been obtained in this way [10, 11], but in order to use them it is necessary that a and d_{vs} are known.

It would be more practical, if $k_L a$ in gas-sparged stirred tanks were to be directly correlated with operating variables and liquid properties. It should be noted that the definition of $k_L \underline{a}$ for a gas-sparged stirred tank (both in this text and in general) is based on the clear liquid volume, without aeration.

The empirical Equation 7.36a, b [3] can be used for very rough estimation of $k_L a$ in aerated stirred tanks with accuracy within 20–40%. It should be noted that in using Equation 7.36a, b, P_G must be estimated by the correlations given in Section 7.4.2. For an air–water system, a water volume $V < 2.6\,\text{m}^3$, and a gas-sparged power requirement P_G/V between 500 and 10 000 W m^{-3},

$$k_L \underline{a}(\text{s}^{-1}) = 0.026 \left(\frac{P_G}{V}\right)^{0.4} U_G{}^{0.5} \tag{7.36a}$$

where U_G (m s^{-1}) is the superficial gas velocity. For air–electrolyte solutions, a liquid volume $V < 4.4\,\text{m}^3$, and P_G/V between 500 and 10 000 W m^{-3},

$$k_L \underline{a}(\text{s}^{-1}) = 0.002 \left(\frac{P_G}{V}\right)^{0.7} U_G{}^{0.2} \tag{7.36b}$$

It is worth remembering that the power requirement of gas-sparged stirred tanks per unit liquid volume at a given superficial gas velocity U_G is proportional to $N^3 L^2$, where N is the rotational speed of the impeller (T^{-1}) and L is the tank size (L), such as the diameter. Usually, $k_L a$ values vary in proportion to $(P_G/V)^m$ and $U_G{}^n$, where $m = 0.4–0.7$ and $n = 0.2–0.8$, depending on operating conditions.

Thus, in some cases, such as scaling-up of geometrically similar stirred tanks, the estimation of power requirement can be simplified using the above relationship.

Correlations for $k_L a$ in gas-sparged stirred tanks such as Equation 7.36a, b apply only to water or to aqueous solutions with properties close to those of water. Values of $k_L a$ in gas-sparged stirred tanks are affected not only by the apparatus geometry and operating conditions but also by various liquid properties, such as viscosity and surface tension. The following dimensionless Equation 7.37 [12], which includes various liquid properties, is based on data on oxygen desorption from various liquids, including some viscous Newtonian liquids, in a stirred tank, with 25 cm inside diameter, of standard design with a six-blade turbine impeller:

$$\left(\frac{k_L \underline{a} d^2}{D_L}\right) = 0.060\left(\frac{d^2 N \rho}{\mu}\right)^{1.5}\left(\frac{dN^2}{g}\right)^{0.19} \times \left(\frac{\mu}{\rho D_L}\right)^{0.5}\left(\frac{\mu U_G}{\sigma}\right)^{0.6}\left(\frac{Nd}{U_G}\right)^{0.32} \tag{7.37}$$

in which d is the impeller diameter, D_L is the liquid phase diffusivity, N is the impeller rotational speed, U_G is the superficial gas velocity, ρ is the liquid density, μ is the liquid viscosity, and σ is the surface tension (all in consistent units). A modified form of the above equation for non-Newtonian fluids is given in Chapter 12.

In evaluating $k_L a$ in gas-sparged stirred tanks, it can usually be assumed that the liquid concentration is uniform throughout the tank. This is especially true with small experimental apparatus, in which the rate of gas–liquid mass transfer at the free liquid surface might be a considerable portion of total mass transfer rate. This can be prevented by passing an inert gas (e.g., nitrogen) over the free liquid.

Example 7.5

Estimate $k_L \underline{a}$ for oxygen absorption into water in the sparged stirred tank of Example 7.4. Operating conditions are the same as in Example 7.4.

Solution

Equation 7.36a is used. From Example 7.4

$$P_G = 3850 \text{ W} \quad \text{Volume of water} = 2.65 \text{ m}^3$$

$$\frac{P_G}{V} = \frac{3850}{2.65} = 1453 \text{ W m}^{-3}, \quad \left(\frac{P_G}{V}\right)^{0.4} = 18.40$$

Since the sectional area of the tank = 1.77 m^2,

$$U_G = \frac{0.6}{(1.77 \times 60)} = 0.00565 \text{ m s}^{-1}, \quad U_G{}^{0.5} = 0.0752$$

$$k_L \underline{a} = 0.026(1453)^{0.4}(0.00565)^{0.5} = 0.0360 \text{ s}^{-1} = 130 \text{ h}^{-1}$$

Although this solution appears simple, it requires an estimation of P_G, which was given in Example 7.4.

7.4.4 Liquid Mixing in Stirred Tanks

In this section, the term "liquid mixing" is used to mean the macroscopic movement of liquid, excluding "micromixing," which is a synonym of diffusion. The *mixing time* is a practical index of the degree of liquid mixing in a batch reactor. The shorter the mixing time, the more intense is mixing in the batch reactor. The mixing time is defined as the time required, from the instant a tracer is introduced into a liquid in a reactor, for the tracer concentration, measured at a fixed point, to reach an arbitrary deviation (e.g., 10%) from the final concentration. In practice, a colored substance, an acid or alkali solution, a salt solution, or a hot liquid can be used as the tracer, and fluctuations of color, pH, electrical conductivity, temperature, and so on are monitored. The mixing time is a function of size and geometry of the stirred tank and the impeller, fluid properties, and operating parameters such as impeller speed, and aeration rates. Mixing times in industrial-size stirred tanks with liquid volumes smaller than 100 kl are usually <100 s.

Correlations are available for mixing times in stirred-tank reactors with several types of stirrers. One of these, for the standard Rushton turbine with baffles [13], is shown in Figure 7.9, in which the product of the stirrer speed N (s^{-1}) and the mixing time t_m (s) is plotted against the Reynolds number on log–log coordinates. For (Re) above approximately 5000, the product $N\,t_m$ (–) approaches a constant value of about 30.

The existence of solid particles suspended in the liquid caused an increase in the liquid mixing time. In contrast, aeration caused a decrease in the liquid mixing time for water, but an increase for non-Newtonian liquids [14].

Example 7.6

A stirred-tank reactor equipped with a standard Rushton turbine of the following dimensions contains a liquid with density $\rho = 1.0\ g\,cm^{-3}$ and viscosity $\mu = 0.013\ g\,cm^{-1}\,s^{-1}$. The tank diameter $D = 2.4$ m, liquid depth $H_L = 2.4$ m, impeller diameter $d = 0.8$ m, and liquid volume = 10.85 m^3. Estimate the stirrer power required and the mixing time, when the rotational stirrer speed N is 90 rpm, that is, 1.5 s^{-1}.

Solution

The Reynolds number

$$\mathrm{Re} = \frac{Nd^2\rho}{\mu} = 1.5 \times 80^2 \times \frac{1}{0.013} = 7.38 \times 10^5$$

From Figure 7.8 the power number $N_p = 6$.

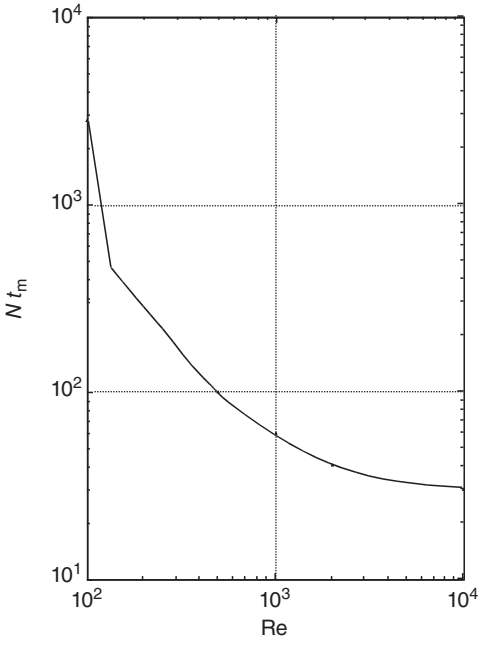

Figure 7.9 Correlations for mixing times (with standard Rushton turbine).

The power required $P = 6N^3d^5\rho = 6 \times 1.5^3 \times 0.8^5 \times 1000\,\text{kg m}^2\,\text{s}^{-3} = 6650\,\text{kg m}^2\,\text{s}^{-3} = 6650\,\text{W} = 6.65\,\text{kW}$.

From Figure 7.9 values of $N\,t_m$ for the above Reynolds number should be about 30. Then, $t_m = 30/1.5 = 20\,\text{s}$.

7.4.5
Suspending of Solid Particles in Liquid in Stirred Tanks

On occasion, solid particles – such as catalyst particles, immobilized enzymes, or even solid reactant particles – must be suspended in liquid in stirred-tank reactors. In such cases, it becomes necessary to estimate the dimension and speed of the stirrer required for suspending solid particles. The following empirical equation [15] gives the minimum critical stirrer speed N_s (s^{-1}) to suspend the particles.

$$N_s = S\nu^{0.1}x^{0.2}\left(\frac{g\Delta\rho}{\rho}\right)^{0.45}\frac{B^{0.13}}{d^{0.85}} \tag{7.38}$$

in which ν is the liquid kinematic viscosity ($m^2\,s^{-1}$), x is the size of the solid particle (m), g is the gravitational constant ($m\,s^{-2}$), ρ is the liquid density ($kg\,m^{-3}$), $\Delta\rho$ is the solid density minus liquid density ($kg\,m^{-3}$), B is the solid weight per liquid weight (%), and d is the stirrer diameter (m). S is an empirical constant that varies with the types of stirrers, the ratio of tank diameter to the stirrer diameter D/d,

and with the ratio of the tank diameter to the distance between the stirrer and the tank bottom D/H_i. Values of S for various stirrer types are given graphically as functions of D/d and D/H_i [15]. For example, S-values for the Rushton turbine ($D/H_i = 1-7$) are 4 for $D/d = 2$ and 8 for $D/d = 3$.

The critical stirrer speed for solid suspension increases slightly with increasing aeration rate, solid loading, and non-Newtonian flow behavior [14].

7.5 Gas Dispersion in Stirred Tanks

One of the functions of the impeller in an aerated stirred tank is to disperse gas into the liquid as bubbles. For a given stirrer speed there is a maximum gas flow rate, above which the gas is poorly dispersed. Likewise, for a given gas flow rate there is a minimum stirrer speed, below which the stirrer cannot disperse gas.

Under such conditions the gas passes up along the stirrer shaft, without being dispersed. This phenomenon, which is called "flooding" of the impeller, can be avoided by decreasing the gas rate for a given stirrer speed, or by increasing the stirrer speed for a given gas rate. The following dimensionless empirical equation [16] can predict the limiting maximum gas flow rate Q ($m^3\,s^{-1}$) and the limiting minimum impeller speed N (s^{-1}) for flooding with the Rushton turbine and for liquids with viscosities not much greater than water.

$$\left(\frac{Q}{Nd^3}\right) = 30\left(\frac{d}{D}\right)^{3.5}\left(\frac{dN^2}{g}\right) \tag{7.39}$$

where d is the impeller diameter (m), D is the tank diameter (m), and g is the gravitational constant ($m\,s^{-2}$).

7.6 Bubble Columns

7.6.1 General

Unlike the mechanically stirred tank, the bubble column has no mechanical stirrer (agitator). Rather, it is a relatively tall cylindrical vessel that contains a liquid through which gas is bubbled, usually from the bottom to the top. A single-nozzle gas sparger or a gas sparger with perforations is normally used. The power required to operate a bubble column is mainly the power to feed a gas against the static head of the liquid in the tank. The gas pressure drop through the gas sparger is relatively small. In general, the power requirements of bubble columns are less than those of mechanically stirred tanks of comparative capacities. The other advantages of a bubble column over a mechanically stirred tank are a simpler construction, with no moving parts and an easier scaling-up. Thus, bubble

columns are increasingly used for large gas–liquid reactors, such as large-scale aerobic fermentors.

Two different regimes have been developed for bubble column operation, in addition to the intermediate transition regime. When the superficial gas velocity (i.e., the total gas rate divided by the cross-sectional area of the column) is relatively low (e.g., $3-5\,\mathrm{cm\,s^{-1}}$), known as the "homogeneous" or "quiet flow" regime, the bubbles rise without interfering with one another. However, at the higher superficial gas velocities that are common in industrial practice, the rising bubbles interfere with each other and repeat coalescence and breakup. In this "heterogeneous" or "turbulent flow" regime, the mean bubble size depends on the dynamic balance between the surface tension force and the turbulence force, and is almost independent of the sparger design, except in the relatively small region near the column bottom. In ordinary bubble columns without any internals, the liquid–gas mixtures move upwards in the central region and downwards in the annular region near the column wall. This is caused by differences in the bulk densities of the liquid–gas mixtures in the central region and the region near the wall. Usually, a uniform liquid composition can be assumed in evaluating $k_L a$, except when the aspect ratio (the column height/diameter ratio) is very large, or the operation is conducted in the quiet regime.

Bubble columns in which gas is bubbled through suspensions of solid particles in liquids are known as "slurry bubble columns". These are widely used as reactors for a variety of chemical reactions, and also as bioreactors with suspensions of microbial cells or particles of immobilized enzymes.

7.6.2
Performance of Bubble Columns

The correlations detailed in Sections 7.6.2.1–7.6.2.5 [17, 18] are based on data for the turbulent regime with 4 bubble columns, up to 60 cm in diameter, and for 11 liquid–gas systems with varying physical properties. Unless otherwise stated, the gas holdup, interfacial area, and volumetric mass transfer coefficients in the correlations are defined per unit volume of aerated liquid, that is, for the liquid–gas mixture.

7.6.2.1 Gas Holdup

The slope of a log–log plot of fractional gas holdup ε (–) against a superficial gas velocity U_G ($\mathrm{L\,T^{-1}}$) decreases gradually at higher gas rates. However, the gas holdup can be predicted by the following empirical dimensionless equation, which includes various liquid properties:

$$\frac{\varepsilon}{(1-\varepsilon)^4} = 0.20(\mathrm{Bo})^{1/8}(\mathrm{Ga})^{1/12}(\mathrm{Fr})^{1.0} \tag{7.40}$$

where (Bo) is the Bond number $= g\,D^2\,\rho/\sigma$ (dimensionless), (Ga) is the Galilei number $= g\,D^3/\nu^2$ (dimensionless), (Fr) is the Froude number $= U_G/(g\,D)^{1/2}$ (dimensionless), g is the gravitational constant ($\mathrm{L\,T^{-2}}$), D is the column

diameter (L), ρ is the liquid density ($M\,L^{-3}$), σ is the surface tension ($M\,T^{-2}$), and v is the liquid kinematic viscosity ($L^2\,T^{-1}$).

7.6.2.2 $k_L a$

Data with four columns, up to 60 cm in diameter, were correlated by the following dimensionless equation:

$$\left(\frac{k_L a D^2}{D_L}\right) = 0.60(\mathrm{Sc})^{0.50}(\mathrm{Bo})^{0.62}(\mathrm{Ga})^{0.31}\varepsilon^{1.1} \tag{7.41}$$

in which D_L is the liquid phase diffusivity ($L^2\,T^{-1}$) and (Sc) is the Schmidt number = (v/D_L) (dimensionless). According to Equation 7.41, $k_L a$ increases with the column diameter D to the 0.17 power. As this trend levels off with larger columns, it is recommended to adopt $k_L a$ values for a 60 cm column when designing larger columns. Data with a large industrial column that was 5.5 m in diameter and 9 m in height agreed with the values calculated by Equation 7.41 for a column diameter of 60 cm [19].

The above equations for ε and $k_L a$ are for nonelectrolyte solutions. For electrolyte solutions, it is suggested that ε and $k_L a$ be increased by approximately 25%. In electrolyte solutions the bubbles are smaller, the gas holdups are larger, and the interfacial areas larger than in nonelectrolyte solutions.

7.6.2.3 Bubble Size

Bubble size distribution was studied by taking photographs of the bubbles in transparent columns of square cross section, after it had been confirmed that a square column gave the same performance as a round column with a diameter equal to the side of the square. The largest fraction of bubbles was in the range of one to several millimeters, mixed with few larger bubbles. As the shapes of bubbles were not spherical, the arithmetic mean of the maximum and minimum dimensions was taken as the bubble size. Except for the relatively narrow region near the gas sparger, or for columns operating in the quiet regime, the average bubble size is minimally affected by the sparger design or its size, mainly because the bubble size is largely controlled by a balance between the coalescence and breakup rates, which in turn depend on the superficial gas velocity and liquid properties. The distribution of bubble sizes was seen to follow the logarithmic normal distribution law. The ratio of calculated values of the volume-surface mean bubble diameter d_{vs} to the column diameter D can be correlated by following dimensionless equation:

$$\left(\frac{d_{vs}}{D}\right) = 26(\mathrm{Bo})^{-0.50}(\mathrm{Ga})^{-0.12}(\mathrm{Fr})^{-0.12} \tag{7.42}$$

7.6.2.4 Interfacial Area a

The gas–liquid interfacial area per unit volume of gas–liquid mixture a ($L^2\,L^{-3}$ or L^{-1}), calculated by Equation 7.26 from the measured values of the fractional gas holdup ε and the volume-surface mean bubble diameter d_{vs}, were correlated

by the following dimensionless equation:

$$(aD) = \left(\frac{1}{3}\right)(\mathrm{Bo})^{0.5}(\mathrm{Ga})^{0.1}\varepsilon^{1.13} \tag{7.43}$$

7.6.2.5 k_L

Values of k_L, obtained by dividing $k_L a$ by a, were correlated by the following dimensionless equation:

$$(\mathrm{Sh}) = \left(\frac{k_L d_{vs}}{D_L}\right) = 0.5\,(\mathrm{Sc})^{1/2}(\mathrm{Bo})^{3/8}(\mathrm{Ga})^{1/4} \tag{7.44}$$

where (Sh) is the Sherwood number. In this equation, d_{vs} is used in place of D in (Bo) and (Ga). According to Equation 7.44, the k_L values vary in proportion to ${D_L}^{1/2}$ and ${d_{vs}}^{1/2}$, but are independent of the liquid kinematic viscosity ν.

7.6.2.6 *Other Correlations for $k_L a$*

Several other correlations are available for $k_L a$ in simple bubble columns without internals, and most of these show approximate agreements. Figure 7.10 compares $k_L a$ values calculated by various correlations for water-oxygen at 20 °C as a function of the superficial gas velocity U_G.

For $k_L a$ with non-Newtonian (excluding viscoelastic) fluids, Equation 7.45 [23], which is based on data with water and aqueous solutions of sucrose and carboxymethylcellulose (CMC) in a 15 cm column, may be useful. Note that $k_L a$ in

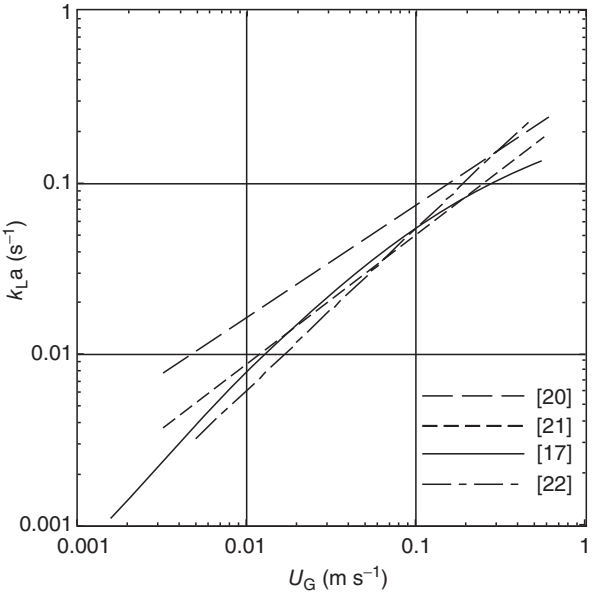

Figure 7.10 Comparison of $k_L a$ by several correlations (water-O_2, 20 °C). Data from [17, 20–22].

this equation is defined per unit volume of clear liquid, without aeration.

$$\left(\frac{k_L a D^2}{D_L}\right) = 0.09\,(\mathrm{Sc})^{0.5}(\mathrm{Bo})^{0.75}(\mathrm{Ga})^{0.39}(\mathrm{Fr})^{1.0} \tag{7.45}$$

For $k_L a$ in bubble columns for non-Newtonian (including viscoelastic) fluids, see Section 12.4.1.

7.6.2.7 $k_L a$ and Gas Holdup for Suspensions and Emulsions

The correlations for $k_L a$ as discussed above are for homogeneous liquids. Bubbling gas–liquid reactors are sometimes used for suspensions, and bioreactors of this type must often handle suspensions of microorganisms, cells, or immobilized cells or enzymes. Occasionally, suspensions of nonbiological particles, to which organisms are attached, are handled. Consequently, it is often necessary to predict how the $k_L a$ values for suspensions will be affected by the system properties and operating conditions. In fermentation with a hydrocarbon substrate, the substrate is usually dispersed as droplets in an aqueous culture medium. Details of $k_L a$ with emulsions are provided in Section 12.4.1.5.

In general, the gas holdups and $k_L a$ for suspensions in bubbling gas–liquid reactors decrease substantially with increasing concentrations of solid particles, possibly because the coalescence of bubbles is promoted by the presence of particles, which in turn results in a larger bubble size and hence a smaller gas–liquid interfacial area. Various empirical correlations have been proposed for the $k_L a$ and gas holdup in slurry bubble columns. Equation 7.46 [24], which is dimensionless and based on data for suspensions with four bubble columns, 10–30 cm in diameter, over a range of particle concentrations from 0 to 200 kg m^{-3} and particle diameter of 50–200 μm, can be used to predict the ratio r of the ordinary $k_L a$ values in bubble columns. This can, in turn, be predicted, for example, by Equation 7.41, for the $k_L a$ values with suspensions.

$$r = 1 + 1.47 \times 10^4 \left(\frac{c_s}{\rho_s}\right)^{0.612} \left(\frac{v_t}{(Dg)^{1/2}}\right)^{0.486} \times \left(\frac{D^2 g \rho_L}{\sigma_L}\right)^{-0.477} \left(\frac{D U_G \rho_L}{\mu_L}\right)^{-0.345} \tag{7.46}$$

where c_s is the average solid concentration in gas-free slurry (kg m^{-3}), D is the column diameter (m), g is the gravitational acceleration (m s^{-2}), U_G is the superficial gas velocity (m s^{-1}), v_t is the terminal velocity of a single particle in a stagnant liquid (m s^{-1}), μ_L is the liquid viscosity (Pa s), ρ_L is the liquid density (kg m^{-3}), ρ_s is the solid density (kg m^{-3}), and σ_L is the liquid surface tension (N m^{-1}).

7.7
Airlift Reactors

In some respects, airlift reactors (airlifts) can be regarded as modifications of the bubble column. Airlift reactors have separate channels for upward and downward fluid flows, whereas the bubble column has no such separate channels. Thus, fluid mixing in bubble columns is more random than in airlift reactors. There are two major types of airlift reactors, namely, the internal loop (IL) and the external loop (EL).

7.7.1
IL Airlifts

The IL airlift reactor shown in Figure 7.11a is a modification of the bubble column equipped with a draft tube (a concentric cylindrical partition) that divides the column into two sections of roughly equal sectional areas. These are the central "riser" for upward fluid flow and the annular "downcomer" for downward fluid flow. Gas is sparged at the bottom of the draft tube. In another type of IL airlift, the gas is sparged at the bottom of the annular space, which acts as the riser, while the central draft tube serves as the downcomer.

The "split-cylinder" IL airlift reactor (not shown in the figure) has a vertical flat partition that divides the column into two halves that act as the riser and downcomer sections. In these IL airlift reactors, as the gas holdup in the downcomer is

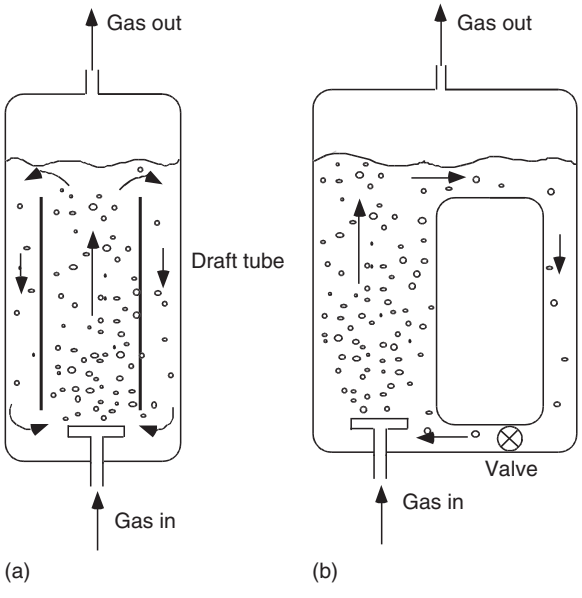

Figure 7.11 Airlift reactors (a) IL airlift and (b) EL airlift.

smaller than that in the riser, the liquid will circulate through the riser and downcomer sections due to differences in the bulk densities of the liquid–gas mixtures in the two sections. The overall values of $k_L a$ for a well-designed IL airlift reactor of both the draft tube and split-cylinder types are approximately equal to those of bubble columns of similar dimensions.

The "deep shaft reactor" is a very tall IL airlift reactor that has vertical partitions, and is built underground for the treatment of biological waste water. This reactor is quite different in its construction and performance from the simple IL airlift reactor with a vertical partition. In the deep-shaft reactor, air is injected into the downcomer and carried down with the flowing liquid. A very large liquid depth is required in order to achieve a sufficiently large driving force for liquid circulation.

7.7.2 EL Airlifts

Figure 7.11b shows an EL airlift reactor , in schematic form. Here, the downcomer is a separate vertical tube that is usually smaller in diameter than the riser, and is connected to the riser by pipes at the top and bottom, thus forming a circuit for liquid circulation. The liquid entering the downcomer tube is almost completely degassed at the top. The liquid circulation rate can be controlled by a valve on the connecting pipe at the bottom. One advantage of the EL airlift reactor is that an efficient heat exchanger can easily be installed on the liquid loop line.

The characteristics of EL airlift reactors [25–27] are quite different from those of the IL airlift reactor. With tubular loop EL airlifts, both the superficial liquid velocity U_L and the superficial gas velocity U_G are important operating parameters. Moreover, U_L increases with increasing U_G and varies with the reactor geometry and liquid properties. U_L can be controlled by a valve at the bottom connecting pipe. The gas holdup, and consequently also $k_L a$, increase with U_G, but at a given U_G they decrease with increasing U_L. For a given gas velocity, the gas holdup and $k_L a$ in the EL airlift reactor are always smaller than in the bubble column reactor, and decrease with increasing liquid velocities. Yet, this is not disadvantageous, as the EL airlift reactor is operated at superficial gas velocities that are two or threefold higher than in the bubble column. Values of $k_L a$ in tubular loop EL airlift reactors at a given U_G are smaller than those in bubble columns and IL airlift reactors fitted with draft tubes.

No general correlations for $k_L a$ are available for EL airlift reactors. However, it has been suggested [28] that, before a production-scale airlift reactor is built, experiments are performed with an airlift that has been scaled down from a production-scale airlift designed with presently available information. The final production-scale airlift should then be designed with the use of the experimental data acquired from the scaled-down airlift reactor.

7.8
Packed-Bed Reactors

The packed bed reactor is a cylindrical, usually vertical, reaction vessel into which particles containing catalyst or enzyme are packed. The reaction proceeds while the fluid containing reactants is passed through the packed bed. In the case of a packed-bed bioreactor, a liquid containing the substrate is passed through a bed of particles of immobilized enzyme or cells.

Consider an idealized simple case of a Michaelis–Menten type bioreaction taking place in a vertical cylindrical packed-bed bioreactor containing immobilized enzyme particles. The effects of mass transfer within and outside the enzyme particles are assumed to be negligible. The reaction rate per differential packed height (m) and per unit horizontal cross-sectional area of the bed (m^2) is given as (cf. Equation 3.28):

$$U\frac{dC_A}{dz} = -\frac{V_{max}C_A}{(K_m + C_A)} \tag{7.47}$$

where U is the superficial fluid velocity through the bed ($m\,s^{-1}$), C_A is the reactant concentration in liquid ($kmol\,m^{-3}$), K_m is the Michaelis constant ($kmol\,m^{-3}$), and V_{max} is the maximum rate of enzyme reaction ($kmol\,m^{-3}\,s^{-1}$).

The required height of the packed bed z can be obtained by integration of Equation 7.47. Thus,

$$z = U\left[\left(\frac{K_m}{V_{max}}\right)\ln\left(\frac{C_{Ai}}{C_{Ao}}\right) + \frac{(C_{Ai} - C_{Ao})}{V_{max}}\right] \tag{7.48}$$

where C_{Ai} and C_{Ao} are the inlet and outlet reactant concentrations ($kmol\,m^{-3}$), respectively. The reaction time t (s) in the packed bed is given as

$$t = \frac{z}{U} \tag{7.49}$$

which should be equal to the reaction time in both the batch reactor and the PFR.

In the case that the mass transfer effects are not negligible, the required height of the packed bed is greater than that without mass transfer effects. In some practices, the ratio of the packed-bed heights without and with the mass transfer effects is defined as the overall effectiveness factor E_{fo} (–), the maximum value of which is unity. However, if the right-hand side of Equation 7.47 is multiplied by E_{fo}, it cannot be integrated simply, since E_{fo} is a function of C_A, U, and other factors. If the reaction is extremely rapid and the liquid phase mass transfer on the particle surface controls the overall rate, then the rate can be estimated by Equation 6.28.

7.9
Microreactors

Microreactors are miniaturized reaction systems with fluid channels of very small dimensions, perhaps 0.05–1 mm [29]. They are a relatively new development, and

at present are used mainly for analytical systems. However, microreactor systems could be useful for small-scale production units, for the following reasons:

- Because of the very small fluid layer thickness of the microchannels, the specific interfacial areas (i.e., the interfacial areas per unit volume of the microreactor systems) are much larger than those of conventional systems.
- Because of the very small fluid channels (Re is very small), the flows in microreactor systems are always laminar. Thus, mass and heat transfers occur solely by molecular diffusion and conduction, respectively. However, due to the very small transfer distances, the coefficients of mass and heat transfer are large. Usually, film coefficients of heat and mass transfer can be estimated using Equations 5.9b and 6.26b, respectively.
- As a result of the first two points, microreactor systems are much more compact than conventional systems of equal production capacity.
- There are no scaling-up problems with microreactor systems. The production capacity can be increased simply by increasing the number of microreactor units used in parallel.

Microreactor systems usually consist of a fluid mixer, a reactor, and a heat exchanger, which is often combined with the reactor. Several types of system are available. Figure 7.12, for example, shows (in schematic form) two types of combined microreactor-heat exchanger. The cross-section of a parallel flow-type microreactor-heat exchanger is shown in Figure 7.12a. For this, microchannels (0.06 mm wide and 0.9 mm deep) are fabricated on both sides of a thin (1.2 mm) metal plate. The channels on one side are for the reaction fluid, while those on the other side are for the heat-transfer fluid, which flows countercurrently to the reaction fluid. The sketch in Figure 7.12b shows a crossflow-type microreactor-heat exchanger with microchannels that are 0.1×0.08 mm in cross section and 10 mm long, fabricated on a metal plate. The material thickness between the two fluids is 0.02–0.025 mm. The reaction plates and heat-transfer plates are stacked alternately, such that both fluids flow crosscurrently to each other. These

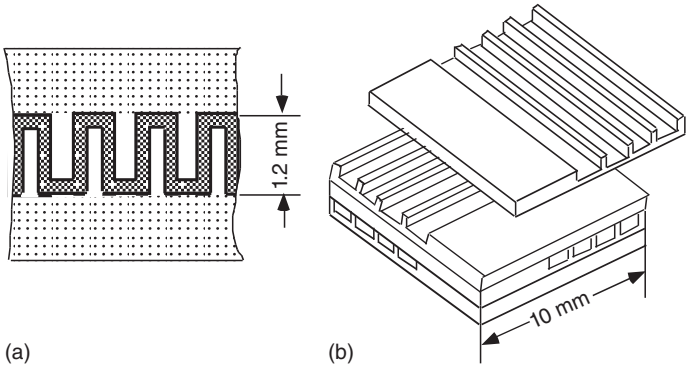

Figure 7.12 Conceptual sketches of two types of microreactor-heat exchanger (a) parallel flow and (b) cross flow.

microreactor systems are normally fabricated from silicon, glass, metals, and other materials, using mechanical, chemical, or physical (e.g., laser) technologies.

Problems

7.1 A reactant A in liquid will be converted to a product P by an irreversible first-order reaction in a CSTR or a PFR reactor with a reactor volume of 0.1 m^3. A feed solution containing 1.0 kmol m^{-3} of A is fed at a flow rate of 0.01 m^3 min^{-1}, and the first-order reaction rate constant is 0.12 min^{-1}.
Calculate the fractional conversions of A in the output stream from the CSTR and PFR.

7.2 The same reaction in Problem 7.1 is proceeding in two CSTR or PFR reactors with a reactor volume of 0.05 m^3 connected in series, as shown in the figure below.

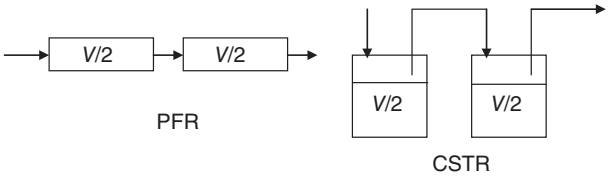

1. Determine the fractional conversions in the output stream from the second reactor.
2. When these reactors are connected in parallel, determine the fractional conversions in the output stream from the second reactor.

7.3 Derive Equation 7.20, where

$$\sinh x = \frac{e^x - e^{-x}}{2}, \cosh x = \frac{e^x + e^{-x}}{2}, \coth x = \frac{\cosh x}{\sinh x}$$

7.4 A reactant in liquid will be converted to a product by an irreversible first-order reaction using spherical catalyst particles that are 0.4 cm in diameter. The first-order reaction rate constant and the effective diffusion coefficient of the reactant in catalyst particles are 0.001 s^{-1} and 1.2×10^{-6} cm^2 s^{-1}, respectively. The liquid film mass transfer resistance of the particles can be neglected.

1. Determine the effectiveness factor for the catalyst particles under the present reaction conditions.
2. How can the effectiveness factor of this catalytic reaction be increased?

7.5 A substrate S will be converted to a product P by an irreversible unimolecular enzyme reaction with the Michaelis constant $K_m = 0.010$ kmol m^{-3} and the maximum rate $V_m = 2.0 \times 10^{-5}$ kmol m^{-3} s^{-1}.

1. A substrate solution of 0.1 kmol m^{-3} is reacted in a stirred-batch reactor using the free enzyme. Determine the initial reaction rate and the conversion of the substrate after 10 min.

2. Immobilized enzyme beads with a diameter of 10 mm containing the same amount of the enzyme above are used in the same stirred-batch reactor. Determine the initial reaction rate of the substrate solution of 0.1 kmol m^{-3}. Assume that the effective diffusion coefficient of the substrate in the catalyst beads is 1.0×10^{-6} cm^2 s^{-1}.
3. How small should the diameter of immobilized enzyme beads be to achieve an effectiveness factor larger than 0.9 under the same reaction conditions as in the case (2)?

7.6 By the dynamic method, the oxygen concentration was measured as shown in Figure P7.6. The static volume of a fermentation broth, the flow rate of air, and the cell concentration were 1 l, 1.5 l min^{-1}, and 3.0 g-dry cell l^{-1}, respectively. Estimate the oxygen consumption rate of the microbes and the volumetric mass transfer coefficient.

7.7 Yeast cells are cultivated under aerobic conditions at 30 °C in an aerated stirred-tank fermentor where air (21 vol% of oxygen) is supplied at a superficial gas velocity of 50 m h^{-1}. The overall volumetric coefficient for oxygen transfer based on the liquid phase concentration is 80 h^{-1}.

1. Determine the oxygen transfer rate per unit volume of a gas-bubble mixture in the unit of g mol-O_2 m^{-3} h^{-1}. Assume that the cells consume oxygen because of respiration, and thus the dissolved oxygen concentration in the medium is essentially zero. Use the solubility of oxygen shown in Table 6.1.
2. If the respiration rate of the cells under the present condition is 0.08 g-O_2 (g dry cell)$^{-1}$ h^{-1}, estimate the cell mass concentration (g dry cell m^{-3}).

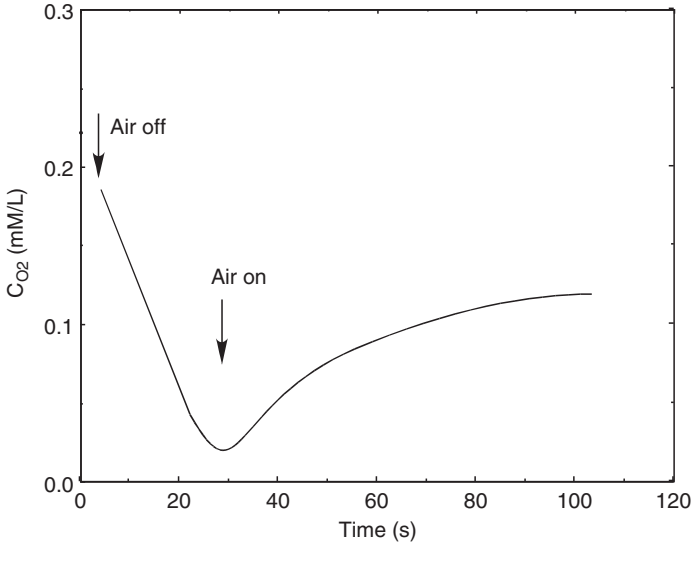

Figure P7.6 Oxygen concentration versus time plot.

7.8 An aerated stirred-tank fermentor equipped with a standard Rushton turbine of the following dimensions contains a liquid with density $\rho = 1010\,\text{kg m}^{-3}$ and viscosity $\mu = 9.8 \times 10^{-4}$ Pa s. The tank diameter D is 0.90 m, liquid depth $H_L = 0.90$ m, impeller diameter $d = 0.30$ m. The oxygen diffusivity in the liquid D_L is $2.10 \times 10^{-5}\,\text{cm}^2\,\text{s}^{-1}$. Estimate the stirrer power required and the volumetric mass transfer coefficient of oxygen (use Equation 7.36b), when air is supplied from the tank bottom at a rate of $0.60\,\text{m}^3\,\text{min}^{-1}$ at a rotational stirrer speed of 120 rpm, that is $2.0\,\text{s}^{-1}$.

7.9 When the fermentor in Problem 7.8 is scaled up to a geometrically similar tank of 1.8 m diameter, show the criteria for scale-up and determine the aeration rate and rotational stirrer speed.

7.10 A 30 cm-diameter bubble column containing water (clear liquid height 2 m) is aerated at a flow rate of $10\,\text{m}^3\,\text{h}^{-1}$. Estimate the volumetric coefficient of oxygen transfer and the average bubble diameter. The values of water viscosity $\mu = 0.001\,\text{kg m}^{-1}\,\text{s}^{-1}$, density $\rho = 1000\,\text{kg m}^{-3}$, and surface tension $\sigma = 75$ dyne cm^{-1} can be used. The oxygen diffusivity in water D_L is $2.10 \times 10^{-5}\,\text{cm}^2\,\text{s}^{-1}$.

References

1. Levenspiel, O. (1972) *Chemical Reaction Engineering*, 2nd edn, John Wiley & Sons, Ltd.
2. Thiele, E.W. (1939) *Ind. Eng. Chem.*, **31**, 916.
3. Van't Riet, K. (1979) *Ind. Eng. Chem. Process Des. Dev.*, **18**, 357.
4. Yoshida, F., Ikeda, A., Imakawa, S., and Miura, Y. (1960) *Ind. Eng. Chem.*, **52**, 435.
5. Taguchi, H. and Humphrey, A.E. (1966) *J. Ferment. Technol.*, **12**, 881.
6. Rushton, J.H., Costich, E.W., and Everett, H.J. (1950) *Chem. Eng. Prog.*, **46**, 395, 467.
7. Nagata, S. (1975) *MIXING Principles and Applications*, John Wiley & Sons, Ltd.
8. Hughmark, G.A. (1980) *Ind. Eng. Chem. Process Des. Dev.*, **19**, 638.
9. Calderbank, P.H. (1958) *Trans. Inst. Chem. Eng.*, **36**, 443.
10. Calderbank, P.H. (1959) *Trans. Inst. Chem. Eng.*, **37**, 173.
11. Yoshida, F. and Miura, Y. (1963) *Ind. Eng. Chem. Process Des. Dev.*, **2**, 263.
12. Yagi, H. and Yoshida, F. (1975) *Ind. Eng. Chem. Process Des. Dev.*, **14**, 488.
13. Hoogendoorm, C.J. and den Hartog, A.P. (1967) *Chem. Eng. Sci.*, **22**, 1689.
14. Kawase, Y., Shimizu, K., Araki, T., and Shimodaira, T. (1997) *Ind. Eng. Chem. Res.*, **36**, 270.
15. Zwietering, T.N. (1958) *Chem. Eng. Sci.*, **8**, 244.
16. Nienow, A.W. (1990) *Chem. Eng. Sci.*, **86**, 61.
17. Akita, K. and Yoshida, F. (1973) *Ind. Eng. Chem. Process Des. Dev.*, **12**, 76.
18. Akita, K. and Yoshida, F. (1974) *Ind. Eng. Chem. Process Des. Dev.*, **13**, 84.
19. Kataoka, H., Takeuchi, H., Nakao, K. *et al.* (1979) *J. Chem. Eng. Jpn.*, **12**, 105.
20. Öztërk, S.S., Schumpe, A., and Deckwer, W.-D. (1987) *AIChE J.*, **33**, 1473.
21. Hikita, H., Asai, S., Tanigawa, K., Segawa, K., and Kitao, M. (1981) *Chem. Eng. J.*, **22**, 61.
22. Kawase, Y., Halard, B., and Moo-Young, M. (1987) *Chem. Eng. Sci.*, **42**, 1609.
23. Nakanoh, M. and Yoshida, F. (1980) *Ind. Eng. Chem. Process Des. Dev.*, **19**, 190.
24. Koide, K., Takazawa, A., Komura, M., and Matsunaga, H. (1984) *J. Chem. Eng. Jpn.*, **17**, 459.

25. Weiland, P. and Onken, U. (1981) *Ger. Chem. Eng.*, **4**, 42.
26. Weiland, P. and Onken, U. (1981) *Ger. Chem. Eng.*, **4**, 174.
27. Weiland, P. (1984) *Ger. Chem. Eng.*, **7**, 374.
28. Choi, P.B. (1990) *Chem. Eng. Prog.*, **86** (12), 32.
29. Ehrfeld, W., Hessel, V., and Löwe, H. (2000) *Microreactors*, Wiley-VCH Verlag GmbH.

Further Reading

Deckwer, W.-D. (1992) *Bubble Column Reactors*, John Wiley & Sons, Ltd.

8
Membrane Processes

8.1
Introduction

In bioprocesses, a variety of apparatus that incorporate artificial (usually polymeric) membranes are often used for both separations and bioreactions. In this chapter, we shall briefly review the general principles of several membrane processes, namely, dialysis, ultrafiltration (UF), microfiltration (MF), and reverse osmosis (RO).

Permeation is a general term meaning the movement of a substance through a solid medium (e.g., a membrane), due to a driving potential such as a difference in concentration, hydraulic pressure, or electric potential, or a combination of these. It is important to understand clearly the driving potential(s) for any particular membrane process.

Only part of the feed solution or suspension supplied to a membrane device will permeate through the membrane; this fraction is referred to as the *permeate*, while the remainder, which does not permeate through the membrane, is called the *retentate*.

Dialysis is a process that is used to separate larger and smaller solute molecules in a solution by utilizing differences in the diffusion rates of larger and smaller solute molecules across a membrane. When a feed solution containing larger and smaller solute molecules is passed on one side of an appropriate membrane, and a solvent (usually water or an appropriate aqueous solution) flows on the other side of the membrane – the *dialysate* – then the molecules of smaller solutes diffuse from the feed side to the solvent side, while the larger solute molecules are retained in the feed solution. In dialysis, those solutes that are dissolved in a membrane, or in the liquid that exists in the minute pores of a membrane, will diffuse through the membrane due to the concentration driving potential rather than to the hydraulic pressure difference. Thus, the pressure on the feed side of the membrane need not be higher than that on the solvent side.

MF is a process that is used to filter very fine particles (smaller than several microns) in a suspension by using a membrane with pores that are smaller than the particles. The driving potential here is the difference in hydraulic pressure.

Biochemical Engineering: A Textbook for Engineers, Chemists and Biologists, Second Edition.
Shigeo Katoh, Jun-ichi Horiuchi, and Fumitake Yoshida.

Companion Website: www.wiley.com\go\katoh\biochem_eng_e2

UF is used to filter any large molecules (e.g., proteins) present in a solution by using an appropriate membrane. Although the driving potential in UF is the hydraulic pressure difference, the mass transfer rates will often affect the rate of UF due to a phenomenon known as "concentration polarization" (this is discussed later in the chapter).

RO is a membrane-based process that is used to remove solutes of relatively low molecular weight that are in solution. As an example, almost pure water can be obtained from sea water by using RO, which will filter out molecules of NaCl and other salts. The driving potential for water permeation is the difference in hydraulic pressure. A pressure that is higher than the osmotic pressure of the solution (which itself could be quite high if the molecular weights of the solutes are small) must be applied to the solution side of the membrane. RO also involves the concentration polarization of solute molecules.

Nanofiltration (NF), a relatively new system, falls between the boundaries of UF and RO, with an upper molecular weight cut-off of approximately 1000 Da. Typical transmembrane pressure (TMP) differences (in bar) are 0.5–7 for UF, 3–10 for NF, and10–100 for RO [1].

Conventional methods for gas separation, such as absorption and distillation, usually involve phase changes. The use of membranes for gas separation seems to show promise due to its lower energy requirement.

Membrane modules (i.e., the standardized unit apparatus for membrane processes) are described at the end of this chapter.

8.2 Dialysis

Figure 8.1 shows, in graphical terms, the concentration gradients of a diffusing solute in the close vicinity and inside of the dialyzer membrane. As discussed in Chapter 6, the sharp concentration gradients in liquids close to the surfaces of the membrane are caused by the liquid film resistances. The solute concentration within the membrane depends on the solubility of the solute in the membrane, or in the liquid in the minute pores of the membrane. The overall mass transfer flux of the solute J_A (kmol h^{-1} m^{-2}) is given as

$$J_A = K_L (C_1 - C_2) \tag{8.1}$$

where K_L is the overall mass transfer coefficient (kmol h^{-1} m^{-2})/(kmol m^{-3}) (i.e., m h^{-1}) and C_1 and C_2 are the bulk solute concentrations (kmol m^{-3}) in the feed and dialysate solutions, respectively.

For a flat membrane, the mass transfer fluxes through the two liquid films on the membrane surfaces and through the membrane should be equal to J_A.

$$J_A = k_{L1}(C_1 - C_{M1}) = k_M (C^*_{M1} - C^*_{M2}) = k_{L2} (C_{M2} - C_2) \tag{8.2}$$

k_{L1} and k_{L2} are the liquid film mass transfer coefficients (m h^{-1}) on the membrane surfaces of the feed side and the dialysate side, respectively; C_{M1} and C_{M2} are

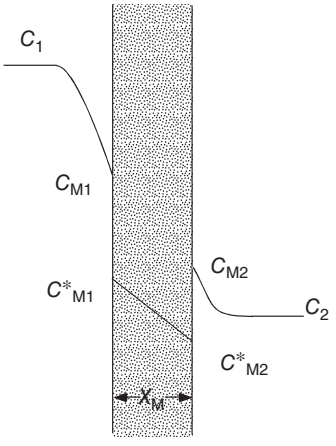

Figure 8.1 Solute concentration gradients in dialysis.

the solute concentrations (kmol m^{-3}) in the feed and dialysate at the membrane surfaces, respectively; C^*_{M1} and C^*_{M2} are the solute concentrations in the membrane (kmol m^{-3}) at its surfaces on the feed side and the dialysate side, respectively. The relationships between C_{M1} and C^*_{M1} and between C^*_{M2} and C_{M2} are given by the solute solubility in the membrane. k_M is the diffusive membrane permeability (m h^{-1}), and should be equal to D_M/x_M, where D_M is the diffusivity of the solute through the membrane (m^2 h^{-1}) and x_M is the membrane thickness (m). D_M varies with membranes and with solutes; for a given membrane, D_M usually decreases with increasing size of solute molecules and increases with temperature.

In the case where the membrane is flat, the overall mass transfer resistance – that is, the sum of the individual mass transfer resistances of the two liquid films and the membrane – is given as

$$\frac{1}{K_L} = \frac{1}{k_{L1}} + \frac{1}{k_M} + \frac{1}{k_{L2}} \tag{8.3}$$

The values of k_L and k_M (especially the latter) decrease with the increasing molecular weights of diffusing solutes. Thus, when a feed solution containing solutes of smaller and larger molecular weights is dialyzed with use of an appropriate membrane, most of the smaller molecular weight solutes will pass through the membrane into the dialysate, while most of the larger molecular weight solutes will be retained in the feed solution.

Dialysis is used on a large scale in some chemical industries. Blood dialyzers, which are used extensively to treat kidney disease patients, are discussed in Chapter 15.

8.3 Ultrafiltration

The driving potential for UF – that is, the filtration of large molecules – is the hydraulic pressure difference. Because of the large molecular weights, and hence the low molar concentrations of solutes, the effect of osmotic pressure is usually minimal in UF; this subject is discussed in Section 8.5.

Figure 8.2 shows data acquired [2] from the UF of an aqueous solution of blood serum proteins in a hollow fiber-type ultrafilter. In this figure, the ordinate is the filtrate flux and the abscissa the TMP (i.e., the hydraulic pressure difference across the membrane). It can be seen from this figure that the filtrate flux J_F for serum solutions increases with TMP at lower TMP values, but becomes independent of the TMP at higher TMP values. In contrast, the J_F for NaCl solutions, using the same apparatus in which case the solute passes into the filtrate, increases linearly with the TMP for all TMP values. The data in the figure also show that, over the range where the J_F for serum solutions is independent of TMP, J_F increases with the wall shear rate γ_w (cf. Example 2.2), which is proportional to the average fluid velocity along the membrane surface for laminar flow, as in this case. These data from serum solutions can be explained if it is assumed that the main hydraulic resistance exists in the protein gel layer formed on the membrane surface and that the resistance increases in proportion to the TMP

The mechanism of such UF can be explained by the following concentration polarization model (cf. Figure 8.3) [3, 4]. In the early stages of UF, the thickness of the gel layer increases with time. However, after the steady state has been reached, the solute diffuses back from the gel layer surface to the bulk of solution; this

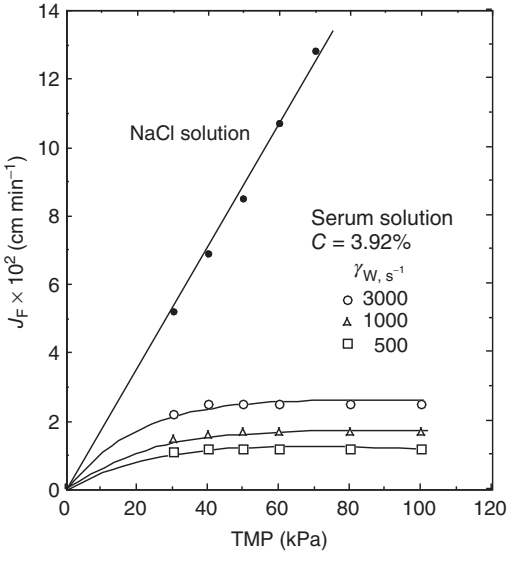

Figure 8.2 Filtrate flux versus TMP in ultrafiltration of serum solutions.

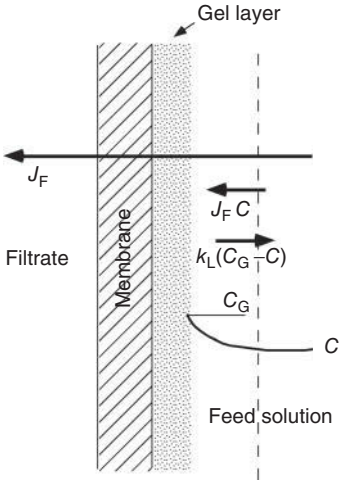

Figure 8.3 Concentration polarization model.

occurs due to the difference between the saturated solute concentration at the gel layer surface and the solute concentration in the bulk of the solution. A dynamic balance is attained, when the rate of back-diffusion of the solute has become equal to the rate of solute carried by the bulk flow of solution toward the membrane. This rate should be equal to the filtrate flux, and consequently the thickness of the gel layer should become constant. Thus, the following dimensionally consistent equation should hold:

$$J_F\, C = D_L \frac{dC}{dx} \tag{8.4}$$

where J_F is the filtrate flux ($L\,T^{-1}$), D_L is the solute diffusivity in solution ($L^2\,T^{-1}$), x is the distance from the gel layer surface (L), and C is the solute concentration in the bulk of feed solution ($M\,L^{-3}$). Integration of Equation 8.4 gives

$$J_F = \left(\frac{D_L}{\Delta x}\right) \ln\left(\frac{C_G}{C}\right) = k_L \ln\left(\frac{C_G}{C}\right) \tag{8.5}$$

where Δx is the effective thickness of laminar liquid film on the gel layer surface, C_G is the saturated solute concentration at the gel layer surface ($M\,L^{-3}$), and k_L is the liquid film mass transfer coefficient for the solute on the gel layer surface ($L\,T^{-1}$), which should vary with the fluid velocity along the membrane and other factors.

Thus, if experiments are performed with solutions of various concentrations C and at a given liquid velocity along the membrane (i.e., at one k_L value), and the experimental values of J_F are plotted against log C on a semi-log paper, then a straight line with a slope of $-k_L$ should be obtained. In addition, it is seen that such straight lines should intersect the abscissa at C_G, because $\ln(C_G/C)$ is zero where $C = C_G$. If such experiments are performed at various liquid velocities, then k_L could be correlated with the liquid velocity and other variables.

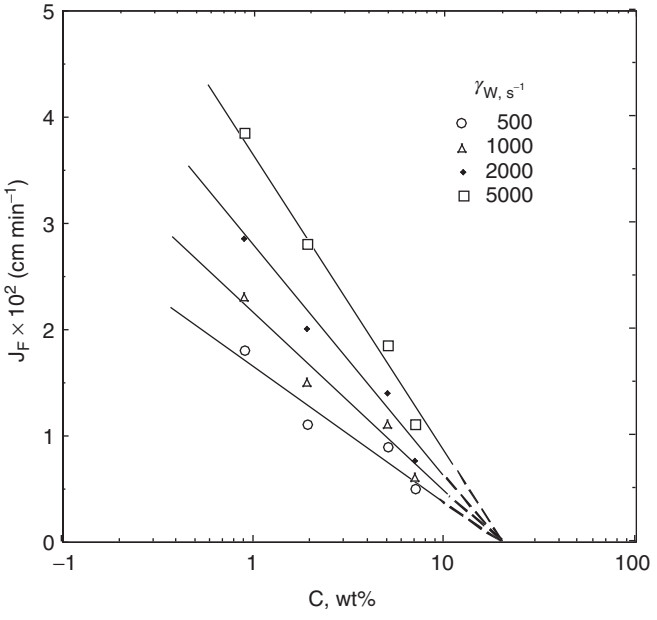

Figure 8.4 Ultrafiltration of serum solutions.

Figure 8.4 shows the data [2] of the UF of serum solutions with a hollow fiber-type ultrafilter, with hollow fibers 16 cm in length and 200 μm in i.d., at four shear rates on the inner surface of the hollow-fiber membrane. Slopes of the straight lines, which converge at a point $C = C_G$ on the abscissa, give k_L values at the shear rates γ_w given in the figure.

The following empirical dimensional equation [5], which is based on data for the UF of diluted blood plasma, can correlate the filtrate flux J_F (cm min^{-1}) averaged over the hollow fiber of length L (cm):

$$J_F(\text{cm min}^{-1}) = 49\left(\frac{\gamma_w {D_L}^2}{L}\right)^{1/3} \ln\left(\frac{C_G}{C}\right) \tag{8.6}$$

The shear rate γ_w (s^{-1}) at the membrane surface is given by $\gamma_w = 8v/d$ (cf. Example 2.2), where v is the average linear velocity (cm s^{-1}), d is the fiber inside diameter (cm), and D_L is the molecular diffusion coefficient (cm^2 s^{-1}); all other symbols are as in Equation 8.4. Hence, Equation 8.6 is most likely applicable to UF in hollow-fiber membranes in general.

8.4 Microfiltration

MF can be categorized between conventional filtration and UF. The process is used to filter very small particles (usually <10 μm in size) from a suspension, by using a membrane with very fine pores. Examples of MF include the separation

of some microorganisms from their suspension and the separation of blood cells from whole blood, using a microporous membrane.

Although the driving potential in MF is the hydraulic pressure gradient, MF flux is often also affected by the fluid velocity along the membrane surface. This is invariably due to the accumulation of filtered particles on the membrane surface – in other words, the concentration polarization of particles.

Equation 8.7 [6] was obtained to correlate the experimental data on membrane plasmapheresis, which is the MF of blood to separate the blood cells from the plasma. The filtrate flux is affected by the blood velocity along the membrane. Since, in plasmapheresis, all of the protein molecules and other solutes will pass into the filtrate, the concentration polarization of protein molecules is inconceivable. In fact, the hydraulic pressure difference in plasmapheresis is smaller than that in the UF of plasma. Thus, the concentration polarization of red blood cells was assumed in deriving Equation 8.7. The shape of the red blood cell is approximately discoid, with a concave area at the central portion, the cells being approximately 1–2.5 μm thick and 7–8.5 μm in diameter. Thus, a value of r (= 0.000257 cm), the radius of the sphere with a volume equal to that of a red blood cell, was used in Equation 8.7.

$$J_F = 4.20\left(\frac{r^4}{L}\right)^{1/3}\gamma_w \ln\left(\frac{C_G}{C}\right) \tag{8.7}$$

Here, J_F is the filtrate flux (cm min^{-1}) averaged over the hollow fiber membrane of length L (cm) and γ_w is the shear rate (s^{-1}) on the membrane surface, as in Equation 8.6. The volumetric percentage of red blood cells (the hematocrit) was taken as C, and its value on the membrane surface, C_G, was assumed to be 95%.

In the case where a liquid suspension of fine particles of radius r (cm) flows along a solid surface at a wall shear rate γ_w (s^{-1}), the effective diffusivity D_E (cm^2 s^{-1}) of particles in the direction perpendicular to the surface can be correlated by the following empirical equation [7]:

$$D_E = 0.025r^2\,\gamma_w \tag{8.8}$$

Equation 8.8 was assumed to hold in deriving Equation 8.7.

Some researchers [8] have suspected that the rate of MF of blood is controlled by the concentration polarization of the platelet (another type of blood cell which is smaller than the red blood cell), such that the effective diffusivity of platelet is affected by the movements of red blood cells.

8.5 Reverse Osmosis

An explanation of the phenomenon of osmosis is provided in most textbooks of physical chemistry. Suppose that a pure solvent and the solvent containing some solute are separated by a membrane that is permeable only for the solvent. In order

to obtain pure solvent from the solution by filtering the solute molecules with the membrane, a pressure which is higher than the osmotic pressure of the solution must be applied to the solution side. If the external (total) pressures of the pure solvent and the solution were equal, however, the solvent would move into the solution through the membrane. This would occur because, due to the presence of the solute, the partial vapor pressure (rigorously activity) of the solvent in the solution would be lower than the vapor pressure of pure solvent. The *osmotic pressure* is the external pressure that must be applied to the solution side to prevent movement of the solvent through the membrane.

It can be shown that the osmotic pressure Π (measured in atm) of a dilute ideal solution is given by the following van't Hoff equation:

$$\Pi V = RT \tag{8.9a}$$

where V (in liter) is the volume of solution containing 1 mol of solute, T is the absolute temperature (K), and R is a constant that is almost identical with the familiar gas law constant (i.e., 0.082 atm l mol^{-1} K^{-1}). Equation 8.9a can also be written as

$$\Pi = RTC \tag{8.9b}$$

where C is the solute concentration (mol l^{-1}). Thus, the osmotic pressures of dilute solutions of a solute vary in proportion to the solute concentration.

From the above relationship, the osmotic pressure of a solution containing 1 mol of solute per liter should be 22.4 atm at 273.15 K. This concentration is called one osmol l^{-1} (i.e., Osm l^{-1}), with one-thousandth of the unit being called a milliosmol (i.e., mOsm l^{-1}). Thus, the osmotic pressure of a 1 mOsm solution would be $22.4 \times 760/1000 = 17$ mmHg.

In RO, the permeate flux J_F (cm s^{-1}) is given as

$$J_F = P_H (\Delta P - \Pi) \tag{8.10}$$

where P_H is the hydraulic permeability of the membrane (cm s^{-1} atm^{-1}) for a solvent and ΔP (atm) is the external pressure difference between the solution and the solvent sides, which must be greater than the osmotic pressure of the solution Π (atm).

There are cases where the concentration polarization of solute must be considered in RO. In such a case, the fraction of the solute permeates through the membrane by diffusion, and the solute flux through the membrane Js (mol cm^{-2} s^{-1}) is given by

$$J_s = J_F\, C_{s1}(1 - \sigma) = k_M(C_{s1} - C_{s2}) \tag{8.11}$$

where J_F is the flux (cm s^{-1}) of the solution that reaches the feed side membrane surface, C_{s1} and C_{s2} are the solute concentrations (mol cm^{-3}) at the feed side membrane surface and in the filtrate (permeate), respectively, σ is the fraction of solute rejected by the membrane (–), and k_M is the diffusive membrane permeability for the solute (cm s^{-1}). The flux of solute (mol cm^{-2} s^{-1}) that returns to the

feed side by concentration polarization is given by

$$J_F\, C_{s1}\, \sigma = k_L(C_{s1} - C_{s0}) \tag{8.12}$$

where k_L is the liquid phase mass transfer coefficient ($cm\, s^{-1}$) on the feed side membrane surface and C_{s0} is the solute concentration in the bulk of the feed solution ($mol\, cm^{-3}$).

RO is widely used for the desalination of sea or saline water, in obtaining pure water for clinical, pharmaceutical, and industrial uses, and also in the food-processing industries.

Example 8.1

Calculate the osmolar concentration and the osmotic pressure of the physiological sodium chloride solution ($9\, g\, l^{-1}$ NaCl aqueous solution). Note: Its osmotic pressure should be almost equal to that of human body fluids (about 6.7 atm).

Solution

Since the molecular weight of NaCl is 58.5, the molar concentration is

$$\frac{9}{58.5} = 0.154\ mol\, l^{-1} = 154\ mmol\, l^{-1}$$

As NaCl dissociates completely into Na^+ and Cl^-, and the ions exert osmotic pressures independently, the total osmolar concentration is

$$154 \times 2 = 308\, mOsm\, l^{-1}$$

The osmotic pressure at 273.15 K is $17 \times 308 = 5236\ mmHg = 6.89\ atm$.

8.6 Membrane Modules

Although many types of membrane modules are used for various membrane processes, they can be categorized as follows. (It should be mentioned here that such membrane modules are occasionally used for gas–liquid systems.)

8.6.1 Flat Membrane

A number of flat membranes are stacked with appropriate supporters (spacers) between the membranes, making alternate channels for the feed (retentate) and the permeate. Meshes, corrugated spacers, porous plates, grooved plates, and so on, can be used as supporters. The channels for feed distribution and permeate collection are built into the device. Rectangular or square membrane sheets are common, but some modules use round membrane sheets.

8.6.2 Spiral Membrane

A flattened membrane tube, or two sheet membranes sealed at both edges (and with a porous backing material inside if necessary), is wound as a spiral with appropriate spacers, such as mesh or corrugated spacers, between the membrane spiral. One of the two fluids – that is, the feed (and retentate) or the permeate – flows inside the wound, flattened membrane tube, while the other fluid flows through the channel containing spacers, in cross flow to the fluid in the wound membrane tube.

8.6.3 Tubular Membrane

Both ends of a number of parallel membrane tubes or porous solid tubes lined with permeable membranes are connected to common header rooms. One of the two headers serves as the entrance of the feed, while the other header serves as the outlet for the retentate. The permeate is collected in the shell enclosing the tube bundle.

8.6.4 Hollow-Fiber Membrane

Hollow fiber refers to a membrane tube of very small diameter (e.g., 200 μm). Such small diameters enable a large membrane area per unit volume of device, as well as operation at somewhat elevated pressures. Hollow-fiber modules are widely used in medical devices such as blood oxygenators and hemodialyzers. The general geometry of the most commonly used hollow-fiber module is similar to that of the tubular membrane, but hollow fibers are used instead of tubular membranes. Both ends of the hollow fibers are supported by header plates and are connected to the header rooms, one of which serves as the feed entrance and the other as the retentate exit. Another type of hollow-fiber module uses a bundle of hollow fibers wound spirally around a core.

▶ Problems

8.1 A buffer solution containing urea flows along one side of a flat membrane and the same buffer solution without urea flows along the other side of the membrane, at an equal flow rate. At different flow rates the overall mass transfer coefficients were obtained as shown in Table P8.1. When the liquid film mass transfer coefficients of both sides increase by one-third power of the averaged flow rate, estimate the diffusive membrane permeability.

Table P8.1 Overall mass transfer coefficient.

Liquid flow rate (cm s^{-1})	Overall mass transfer coefficient K_L (cm s^{-1})
2.0	0.0489
5.0	0.0510
10.0	0.0525
20.0	0.0540

8.2 From the data shown in Figure 8.4 estimate the liquid film mass transfer coefficient of serum protein at each shear rate and compare the dependence on the shear rate with Equation 8.6.

8.3 Blood cells are separated from blood (hematocrit 40%) by microfiltration, using hollow-fiber membranes with an inside diameter of 300 μm and a length of 20 cm. The average flow rate of blood is 5.5 cm s^{-1}. Estimate the filtrate flux.

8.4 Estimate the osmotic pressure of a 3.5 wt% sucrose solution at 293 K.

8.5 If the water flux, J_F, through an RO membrane is 8×10^{-4} cm s^{-1} under a transmembrane pressure $\Delta P = 25$ atm at 25 °C, estimate the water flux of a 2.0 wt% NaCl solution under the same transmembrane pressure and temperature. You may assume that $\sigma = 1.0$ and neglect the effect of the concentration polarization.

8.6 The apparent reflection coefficient ($=(C_{s0} - C_{sp})/C_{s0}$, where C_{sp} is the concentration of solute in the permeate) may depend on the filtrate flux, when the real reflection coefficient σ is constant. Explain the possible reason for this.

References

1. Chen, W., Parma, F., Patkar, A., Elkin, A., and Sen, S. (2004) *Chem. Eng. Prog.*, **102** (12), 12.
2. Okazaki, M. and Yoshida, F. (1976) *Ann. Biomed. Eng.*, **4**, 138.
3. Michaels, A.S. (1968) *Chem. Eng. Prog.*, **64** (12), 31.
4. Porter, M.C. (1972) *Ind. Eng. Chem. Prod. Res. Dev.*, **11**, 234.
5. Colton, C.K., Henderson, L.W., Ford, C.A., and Lysaght, M.J. (1975) *J. Lab. Clin. Med.*, **85**, 355.
6. Zydney, A.L. and Colton, C.K. (1982) *Trans. Am. Soc. Artif. Intern. Organs*, **28**, 408.
7. Eckstein, E.C., Balley, D.G., and Shapiro, A.H. (1977) *J. Fluid Mech.*, **79**, 1191.
8. Malbrancq, J.M., Bouveret, E., and Jaffrin, M.Y. (1984) *Am. Soc. Artif. Intern. Organs J.*, **7**, 16.

Further Reading

Zeman, L.J. and Zydney, A.L. (1996) *Microfiltration and Ultrafiltration*, Marcel Dekker, Inc.

9
Cell–Liquid Separation and Cell Disruption

9.1
Introduction

Since, in bioprocesses, the initial concentrations of target products are usually low, separation and purification by the so-called downstream processing (cf. Chapters 11 and 14) are required to obtain the final products. In most cases, the first step in downstream processing is to separate the cells from the fermentation broth. In those cases where intracellular products are required, the cells are first ruptured to solubilize the products, after which a fraction containing the target product is concentrated by a variety of methods, including extraction, ultrafiltration, salting-out, and aqueous two-phase separation. The schemes used to separate the cells from the broth, and further treatment, are shown diagrammatically in Figure 9.1. The fermentation products may be cells themselves, components of the cells (intracellular products), and/or those materials secreted from cells into the fermentation broth (extracellular products). Intracellular products may exist as solutes in cytoplasm, as components bound to the cell membranes, or as aggregate particles termed inclusion bodies.

The separation schemes vary with the state of the products. For example, intracellular products must first be released by disrupting the cells, while those products bound to cell membranes must be solubilized. As the concentrations of products secreted into the fermentation media are generally very low, the recovery and concentration of such products from dilute media represent the most important steps in downstream processing. In this chapter, several cell-liquid separation methods and cell disruption techniques are discussed.

9.2
Conventional Filtration

The process of filtration separates the particles from a suspension, by forcing a fluid through a filtering medium, or by applying positive pressure to the upstream side or a vacuum to the downstream side. The particles retained on the filtering medium as a deposit are termed "cake," while the fluid that has passed through

Biochemical Engineering: A Textbook for Engineers, Chemists and Biologists, Second Edition.
Shigeo Katoh, Jun-ichi Horiuchi, and Fumitake Yoshida.

Companion Website: www.wiley.com\go\katoh\biochem_eng_e2

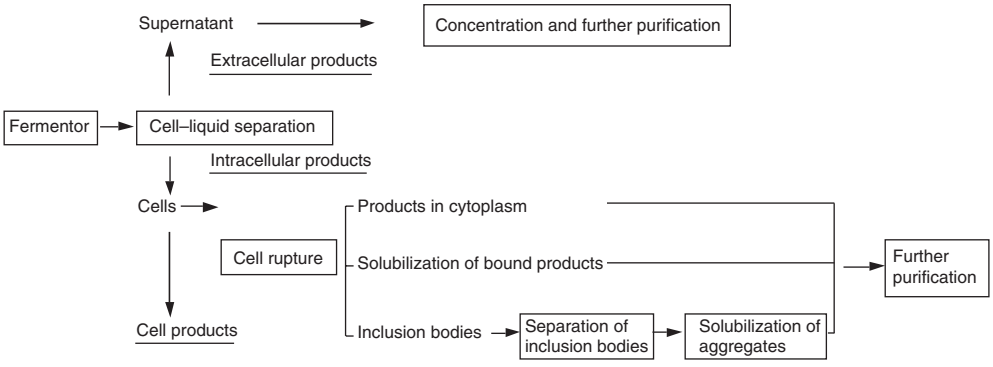

Figure 9.1 Cell–liquid separation and further treatments.

the medium is termed the "filtrate." Conventional filtration, which treats particles larger than several microns in diameter, is used for the separation of relatively large precipitates and microorganisms. Smaller particles can be effectively separated using either centrifugation or microfiltration (Section 9.3).

The two main types of conventional filter used for cell separation are *plate filters* (filter press) and *rotary drum filters*:

- In the plate filter, a cell suspension is filtered through a flat filtering medium by applying a positive pressure, and the cake of deposited cells must be removed batchwise.
- For larger scale filtration, a continuously operated rotary drum filter is usually used. This type of filter has a rotating drum with a horizontal axis, which is covered with a filtering medium and is partially immersed in a liquid–solid feed mixture contained in a reservoir. The feed is filtered through the filtering medium by applying a vacuum to the interior of the drum. The formed cake is washed with water above the reservoir, and then removed using a scraper, knife, or other device as the drum rotates.

The rate of filtration – that is, the rate of permeation of a liquid through a filtering medium – depends on the area of the filtering medium, the viscosity of the liquid, the pressure difference across the filter, and the resistances of the filtering medium and the cake.

As liquid flow through a filter is considered to be laminar, the rate of filtration $\mathrm{d}V_\mathrm{f}/\mathrm{d}t$ ($\mathrm{m^3\,s^{-1}}$) is proportional to the filter area A ($\mathrm{m^2}$) and the pressure difference across the filtering medium ΔP (Pa), and is inversely proportional to the liquid viscosity μ (Pa s) and the sum of the resistances of the filtering medium R_M ($\mathrm{m^{-1}}$) and the cake R_C ($\mathrm{m^{-1}}$). Thus, the filtration flux J_F ($\mathrm{m\,s^{-1}}$) is given by

$$J_\mathrm{F} = \frac{\mathrm{d}V_\mathrm{f}}{A\ \mathrm{d}t} = \frac{\Delta p}{\mu(R_\mathrm{M} + R_\mathrm{C})} \tag{9.1}$$

The resistance of the cake can be correlated with the mass of cake per unit filter area:

$$R_C = \frac{\alpha \rho_c V_f}{A} \tag{9.2}$$

where V_f is the volume of filtrate (m^3), ρ_c is the mass of cake solids per unit volume of filtrate ($kg\,m^{-3}$), and α is the specific cake resistance ($m\,kg^{-1}$). In the case of incompressible cake of relatively large particles ($d_p > 10\,\mu m$), the Kozeny–Carman equation holds for the pressure drop through the cake layer, and the specific cake resistance α is given as:

$$\alpha = \frac{5a^2(1-\varepsilon)}{\varepsilon^3 \rho_s} \tag{9.3}$$

where ρ_s ($kg\,m^{-3}$) is the density of the particle, a is the specific particle surface area per unit cake volume ($m^2\,m^{-3}$), and ϵ is the porosity of the cake (−). In many cases, the cakes from fermentation broths are compressible, and the specific cake resistance will increase with the increasing pressure drop through the cake layer, due to changes in the shape of particles and decrease in the porosity. Thus, the filtration rate rapidly decreases with the progress of filtration, especially in the cases of compressible cakes. Further, fermentation broths containing high concentrations of microorganisms and other biological fluids usually show non-Newtonian behaviors, as stated in Section 2.3. These phenomena will complicate the filtration in bioprocess plants.

9.3 Microfiltration

The cells and cell lysates (fragments of disrupted cells) can be separated from the soluble components by using microfiltration (Chapter 8) with membranes. This separation method offers following advantages:

- It does not depend on any density difference between the cells and the media.
- The closed systems used are free from aerosol formation.
- There is a high retention of cells (>99.9%).
- There is no need for any filter aid.

Depending on the size of cells and debris, and the desired clarity of the filtrate, microfiltration membranes with pore sizes ranging from 0.01 to 10 μm can be used. In cross-flow filtration (CFF; see Figure 9.2b), the liquid flows parallel to the membrane surface and so provides a higher filtration flux than does dead-end filtration (Figure 9.2a), where the liquid path is solely through the membrane. In CFF, a lesser amount of the retained species will accumulate on the membrane surface, as some of the retained species is swept from the membrane surface by the liquid flowing parallel to the surface. The thickness of the microparticle layer on the membrane surface depends on the balance between the particles transported by the bulk flow toward the membrane and the sweeping away of the particle by the

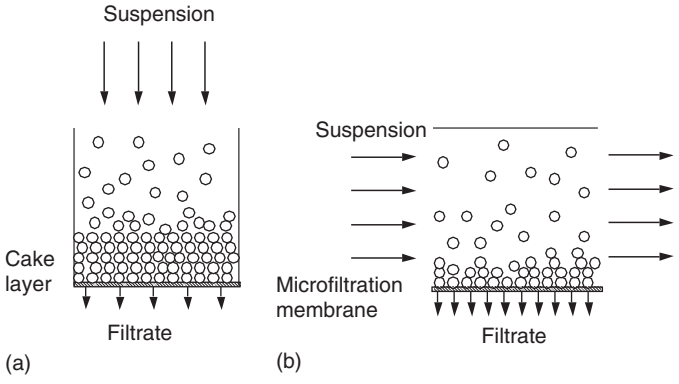

Figure 9.2 Alternative methods of filtration. (a) Dead-end filtration; (b) cross-flow filtration.

cross-flow along the membrane. Similar to the concentration polarization model in ultrafiltration (as described in Section 8.3), an estimation of the filtration flux in microfiltration is possible by using Equation 8.5.

9.4 Centrifugation

In those cases where the particles are small and/or the viscosity of the fluid is high, filtration is not very effective. In such cases, centrifugation is the most common and effective method for separating microorganisms, cells, and precipitates from the fermentation broth. Two major types of centrifuge – the tubular-bowl and the disk-stack – are used for continuous, large-scale operation.

The *tubular centrifuge*, which is shown schematically in Figure 9.3a, incorporates a vertical, hollow cylinder with a diameter on the order of 10 cm, which rotates at between 15 000 and 50 000 rpm. A suspension is fed from the bottom of the cylinder, whereupon the particles, which are deposited on the inner wall of the cylinder under the influence of centrifugal force, are recovered manually in a batchwise manner. Meanwhile, the liquid flows upwards and is discharged continuously from the top of the tube.

The main part of the disk-stack centrifuge is shown schematically in Figure 9.3b. The instrument consists of a stack of conical sheets that rotates on the vertical shaft, with the clearances between the cones being as small as 0.3 mm. The feed is supplied near the bottom center, and passes up through the matching holes in the cones (the liquid paths are shown in Figure 9.3b). The solid particles or heavy liquids that are separated by the centrifugal force move to the edge of the discs, along their under-surfaces, and can be removed either continuously or intermittently, without stopping the machine. Occasionally, particle removal may be carried out in a batchwise manner. The light liquid moves to the central portion of the stack, along the upper surfaces of the discs, and is continuously removed.

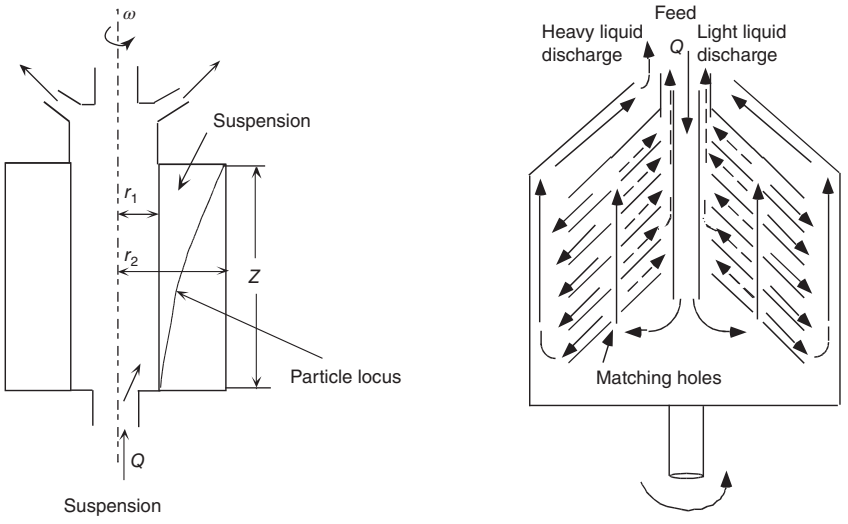

Figure 9.3 Two major types of centrifuges. (a) Tubular-bowl centrifuge; (b) disk-stack centrifuge.

In the "sedimenter" or "gravity settler," the particles in the feed suspension settle due to difference in densities between the particles and the fluid. The settling particle velocity reaches a constant value – the terminal velocity – shortly after the start of sedimentation. The terminal velocity is defined by the following balance of forces acting on the particle:

$$\text{Drag force} = \text{Weight force} - \text{Buoyancy force} \tag{9.4}$$

When the Reynolds number ($d_p\, v_t\, \rho_L/\mu$) is <2 – which is always the case for cell separation – the drag force (kg m s^{-2}) can be given by Stokes law:

$$\text{drag force} = 3\pi d_p v_t \mu \tag{9.5}$$

where d_p is the diameter of the particle (m), v_t is the terminal velocity (m s^{-1}), and μ is the viscosity of the liquid (Pa s). The weight force (kg m s^{-2}) and the buoyancy force (kg m s^{-2}) acting on a particle under the influence of gravity are given by Equation 9.6a, b, respectively.

$$\text{weight force} = \frac{(\pi {d_p}^3 \rho_P g)}{6} \tag{9.6a}$$

$$\text{buoyancy force} = \frac{(\pi {d_p}^3 \rho_L g)}{6} \tag{9.6b}$$

where g is the gravitational acceleration (m s^{-2}), ρ_P is the density of the particle (kg m^{-3}), and ρ_L is the density of the liquid (kg m^{-3}).

The terminal velocity v_t can be estimated from Equations 9.4–9.6b:

$$v_t = \frac{d_p^2(\rho_P - \rho_L)g}{18\mu} \tag{9.7}$$

In the case of a centrifugal separator (i.e., a centrifuge), the acceleration due to centrifugal force, which should be used in place of g, is given as $r\omega^2$, where r is the radial distance from the central rotating axis (m) and ω is the angular velocity of rotation (radian s^{-1}). Thus, the terminal velocity v_t ($m\,s^{-1}$) is given as

$$v_t = \frac{d_p^2(\rho_P - \rho_L)}{18\mu} r\omega^2 \tag{9.8}$$

The sedimentation coefficient, S, as defined by Equation 9.9, is sometimes used:

$$v_t = Sr\omega^2 \tag{9.9}$$

where S (s) is the sedimentation coefficient in the Svedberg unit. The value obtained in water at 20 °C is 10^{-13} s.

Example 9.1

Using a tubular-bowl centrifuge rotating at 3600 rpm, determine the terminal velocity of *Escherichia coli* in a saline solution (density $\rho_L = 1.0\,g\,cm^{-3}$) at a radial distance 10 cm from the axis.

The cell size of *E. coli* is approximately 0.8 μm × 2 μm with a volume of 1.0 μm^3. Its density ρ_P is 1.1 $g\,cm^{-3}$. In calculation, it can be approximated as a sphere of 1.25 μm diameter.

Solution

Substitution of these values into Equation 9.8 gives

$$v_t = \frac{(1.25 \times 10^{-4})^2 \times 0.1}{18 \times 0.01} \times 10 \times (2\pi \times 60)^2 = 1.2 \times 10^{-2} \ \text{cm s}^{-1}$$

In order to separate the particles in a suspension, the maximum allowable flow rate through the tubular-bowl centrifuge, as shown schematically in Figure 9.3a, can be estimated as follows [1]. A suspension is fed to the bottom of the bowl at a volumetric flow rate of Q ($m^3\,s^{-1}$) and the clarified liquid is removed from the top. The sedimentation velocity of particles in the radial direction ($v_t = dr/dt$) can be given by Equations 9.7 and 9.8 with the use of the terminal velocity under gravitational force v_g ($m\,s^{-1}$) and the gravitational acceleration g ($m\,s^{-2}$):

$$v_t = \frac{dr}{dt} = v_g \frac{r\omega^2}{g} \tag{9.10}$$

When the radial distances from the rotational axis of a centrifuge to the liquid surface and the bowl wall are r_1 and r_2, respectively, the axial liquid velocity u ($m\,s^{-1}$) is given by

$$u = \frac{dz}{dt} = \frac{Q}{\pi(r_2^2 - r_1^2)} \tag{9.11}$$

The separated particles should reach the wall when the feed leaves the top end of the tube, as shown by the locus of a particle in Figure 9.3a. The elimination of dt from Equations 9.10 and 9.11 and integration with boundary conditions ($r = r_1$ at $z = 0$ and $r = r_2$ at $z = Z$) give the maximum flow rate for perfect removal of particles from the feed suspension.

$$Q = v_g \frac{\pi Z(r_2^2 - r_1^2)\omega^2}{g \ln(r_2/r_1)} \tag{9.12}$$

The accumulated solids can then be recovered batchwise from the bowl.

9.5 Cell Disruption

In those cases where the intracellular products are required, the cells must first be disrupted. Some products may be present in the solution within the cytoplasm, while others may be insoluble and exist as membrane-bound proteins or small insoluble particles called *inclusion bodies*. In the latter case, these must be solubilized before further purification.

Cell disruption methods can be classified as either nonmechanical or mechanical [2]. Cell walls vary greatly in their strength. Typical mammalian cells are fragile and can be easily ruptured by using a low shearing force or a change in the osmotic pressure. In contrast, many microorganisms such as *E. coli*, yeasts, and plant cells have rigid cell walls, the disruption of which requires high shearing forces or even bead milling. The most frequently used cell rupture techniques, with the mechanical methods arranged in order of increasing strength of the shear force acting on the cell walls, are listed in Table 9.1. Any method used should be sufficiently mild that the desired components are not inactivated. In general, nonmechanical methods are milder and may be used in conjunction with some mild mechanical methods.

Ultrasonication (on the order of 20 kHz) causes high-frequency pressure fluctuations in the liquid, leading to the repeated formation and collapse of bubbles.

Although cell disruption by ultrasonication is used extensively on a laboratory scale, its use on a large scale is limited by the energy available for using a sonicator tip. Bead mills or high-pressure homogenizers are generally used for the large-scale disruption of cell walls. However, the optimum operating conditions must first be determined, using trial-and-error procedures, in order to achieve a high recovery of the desired components.

The separation of cell debris (fragments of cell walls) and organelles from a cell homogenate by centrifugation may often be difficult, essentially because the densities of these are close to that of the solution, which may be highly viscous. Separation by microfiltration represents a possible alternative approach in such a case.

Table 9.1 Methods of cell disruption.

Methods	Treatments
Mechanical methods	
Waring-type blender	Homogenization by stirring blades
Ultrasonics	Application of ultrasonic energy to cell suspensions by sonicator
Bead mills	Mechanical grinding of cell suspensions with grinding media such as glass beads
High pressure homogenization	Discharge of pressurized cell suspension flow through valves involving impingement
Nonmechanical methods	
Osmotic shock	Introduction to solution of low osmolarity
Freezing	Repetition of freezing and melting
Enzymatic digestion	Lysis of cell walls containing polysaccharides by lysozyme
Chemical solubilization	Solubilization of cell walls by surfactants, alkali, or organic solvents

Example 9.2

Using a tubular-bowl centrifuge, calculate the sedimentation velocity of a 70S ribosome (from *E. coli*, diameter 0.02 μm) in water at 20 °C. The rotational speed and distance from the center are 30 000 rpm and 10 cm, respectively.

Solution

By using Equation 9.9, the sedimentation velocity is

$$v_t = 70 \times 10^{-13} \times 10 \times (2\pi \times 500)^2 = 6.9 \times 10^{-4} \ \text{cm s}^{-1}$$

Because of the much smaller size of the ribosome, this value is much lower than that of *E. coli* obtained in Example 9.1.

Problems

9.1 An aqueous suspension is filtered through a plate filter under a constant pressure of 0.2 MPa. After a 10 min filtration, 0.10 m^3 of filtrate is obtained. When the resistance of the filtering medium R_M can be neglected, estimate the volumes of the filtrate after 20 and 30 min.

9.2 Albumin solutions (1, 2, and 5 wt%) are continuously ultrafiltered through a flat plate filter with a channel height of 2 mm. Under cross-flow filtration with a transmembrane pressure of 0.5 MPa, steady-state filtrate fluxes (cm min^{-1}) are obtained as given in Table P9.2.

Table P9.2 Filtrate flux.

		Albumin concentration		
		1 wt%	2 wt%	5 wt%
Liquid flow rate	5 cm s^{-1}	0.018	0.014	0.010
	10 cm s^{-1}	0.022	0.018	0.012

Determine the saturated albumin concentration at the gel-layer surface and the liquid film mass transfer coefficient.

9.3 How long does it take to sediment *E. coli* cells to the bottom of a centrifuge tube (5 cm length) under a centrifugal acceleration of 2000 g? Use the properties of *E. coli* shown in Example 9.1.

9.4 Derive Equation 9.12.

9.5 A suspension of *E. coli* is to be centrifuged in a tubular-bowl centrifuge that has a length of 1 m and is rotating at 15 000 rpm. The radii to the surface (r_1) and bottom (r_2) of the liquid are 5 and 10 cm, respectively. A cell of *E. coli* can be approximated as a 1.25 μm diameter sphere with a density of 1.1 g cm^{-3}. Determine the maximum flow rate for the complete removal of cells.

9.6 How many times g should the centrifugal force be in order to obtain a 10-fold higher sedimentation velocity of a 70S ribosome than that obtained in Example 9.2?

References

1. Doran, P.M. (1995) *Bioprocess Engineering Principles*, Academic Press.
2. Wheelwright, S.M. (1991) *Protein Purification*, Hanser.

10
Sterilization

10.1
Introduction

If a culture medium or a part of the equipment used for fermentation becomes contaminated by living foreign microorganisms, the target microorganisms must grow in competition with the contaminating microorganisms, which will not only consume nutrients but may also produce harmful products. Thus, not only the medium but also all of the fermentation equipment being used, including the tubes and valves, must be sterilized prior to the start of fermentation, so that they are perfectly free from any living microorganisms and spores. In the case of aerobic fermentations, air supplied to the fermentor should also be free from contaminating microorganisms.

Sterilization can be accomplished by several means, including heat, chemicals, radiation (ultraviolet (UV) or γ-ray), and microfiltration. *Heat* is widely used for the sterilization of media and fermentation equipment, while *microfiltration*, using polymeric microporous membranes, can be performed to sterilize the air and media that might contain heat-sensitive components. Among the various heating methods, moist heat (i.e., steam) is highly effective and very economical for performing the sterilization of fermentation set-ups.

10.2
Kinetics of Thermal Death of Cells

In this section, we discuss the kinetics of thermal cell death and sterilization. The rates of thermal death of most microorganisms and spores can be given by Equation 10.1, which is similar in form to the rate equation for the first-order chemical reaction, such as Equation 3.10.

$$-\frac{\mathrm{d}n}{\mathrm{d}t} = k_\mathrm{d} n \tag{10.1}$$

where n is the number of cells in a system. The temperature dependence of the specific death rate k_d is given by Equation 10.2, which is similar to Equation 3.6:

$$k_\mathrm{d} = k_{\mathrm{d}0} \mathrm{e}^{-(E_\mathrm{a}/RT)} \tag{10.2}$$

Biochemical Engineering: A Textbook for Engineers, Chemists and Biologists, Second Edition.
Shigeo Katoh, Jun-ichi Horiuchi, and Fumitake Yoshida.

Companion Website: www.wiley.com\go\katoh\biochem_eng_e2

Combining Equations 10.1 and 10.2, and integrating the resulting equation from time 0 to t gives

$$\ln \frac{n}{n_0} = -k_{d0} \int_0^t e^{-(E_a/RT)} dt \tag{10.3}$$

where E_a is the activation energy for thermal death. For example, E_a for *Escherichia coli* is 530 kJ mol^{-1} [1]. In theory, reducing the number of living cells to absolute zero by heat sterilization would require infinite time. In practical sterilization, the case of contamination must be reduced not to zero, but rather to a very low probability. For example, in order to reduce cases of contamination to 1 in 1000 fermentations, the final cell number n_f must be <0.001. Sterilization conditions are usually determined on the basis on this criterion.

10.3 Batch Heat Sterilization of Culture Media

The batchwise heat sterilization of a culture medium contained in a fermentor consists of heating, holding, and cooling cycles. The heating cycle is carried out by direct steam sparging, electrical heating, or by heat exchange with condensing steam, as shown schematically in Figure 10.1, while the cooling cycle utilizes water. The time–temperature relationships during the heating, holding, and cooling cycles required to integrate Equation 10.3 can be obtained experimentally. In the case where experimental measurements are not practical, theoretical equations [2] can be used, depending on the method used for heating and cooling (Table 10.1).

By applying Equation 10.3 to heating, holding, and cooling cycles, the final number of viable cells n_f can be estimated by

$$\ln \frac{n_f}{n_0} = \ln \frac{n_{heat}}{n_0} + \ln \frac{n_{hold}}{n_{heat}} + \ln \frac{n_f}{n_{hold}} \tag{10.4}$$

where n_0, n_{heat}, and n_{hold} are the numbers of viable cells at the beginning and at the ends of heating and holding cycles, respectively. Since the temperature is kept constant during the holding cycle,

$$\ln \frac{n_{heat}}{n_{hold}} = k_{d0} e^{-(E_a/RT)} t_{hold} \tag{10.5}$$

If the degree of sterilization (n_f/n_0) and the temperature during the holding cycle are given, the holding time can be calculated.

Example 10.1

Derive an equation for the temperature–time relationships of a medium in a fermentor during indirect heating by saturated steam (Figure 10.1c). Use the nomenclature given in Table 10.1.

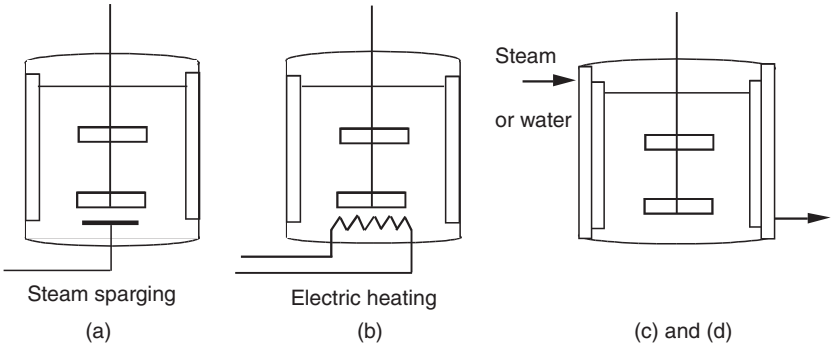

Figure 10.1 Modes of heat transfer for batch sterilization: (a) direct steam sparging, (b) constant rate heating by electric heater, (c) heating by condensing steam (isothermal heat source), and (d) cooling by water (nonisothermal heat sink).

Table 10.1 Temperature versus time relations in batch sterilization by various heating methods.

Heating methods	Temperature (T)–time (t) relations
Heating by direct steam sparging	$T = T_0 + \frac{Hm_s t}{c_p(M+m_s t)}$
Heating with a constant rate of heat flow, for example, electric heating	$T = T_0 + \frac{qt}{c_p M}$
Indirect heating by saturated steam	$T = T_N + (T_0 - T_N)\exp\left(-\frac{UA}{Mc_p}\right)t$

A = area for heat transfer; c_p = specific heat capacity of medium; H = heat content of steam relative to initial medium temperature; m_s = mass flow rate of steam; M = initial mass of medium; q = rate of heat transfer; t = time; T = temperature; T_0 = initial temperature of medium; T_N = temperature of heat source; and U = overall heat transfer coefficient.

Solution

The rate of heat transfer q to the medium at T °C from steam condensing at T_N°C is

$$q = UA(T_N - T)$$

Transferred heat raises the temperature of the medium (mass M and specific heat c_p) at a rate dT/dt. Thus,

$$Mc_p\frac{dT}{dt} = UA(T_N - T)$$

Integration and rearrangement give

$$T = T_N + (T_0 - T_N)\exp\left(-\frac{UA}{Mc_p}\right)t$$

where T_0 is the initial temperature of the medium.

10.4
Continuous Heat Sterilization of Culture Media

Two typical systems of continuous heat sterilization of culture media are shown schematically in Figure 10.2a and b. In the system heated by direct steam injection (Figure 10.2a), the steam heats the medium to a sterilization temperature quickly, and the medium flows through the holding section at a constant temperature, if the heat loss in this section is negligible. The sterile medium is cooled by adiabatic expansion through an expansion valve. In the indirect heating system (Figure 10.2b), the medium is heated indirectly by steam, usually in a plate-and-frame-type heater, before entering the holding section. In both systems, the medium is preheated in a heat exchanger by the hot medium leaving the holding section. In such continuous systems, the medium temperature can be raised more rapidly to the sterilizing temperature than in batch sterilization, and the residence time in the holding section mainly determines the degree of sterilization.

If the flow of the medium in the holding section were an ideal plug flow, the degree of sterilization could be estimated from the average residence time τ_{hold} in the holding section by Equation 10.6:

$$\ln \frac{n_0}{n_f} = k_{d0} e^{-(E_a/RT)} \tau_{\text{hold}} \tag{10.6}$$

The usual velocity distributions in a steady flow of liquid through a tube are shown in Figure 2.4. In either laminar or turbulent flow, the velocity at the tube wall is zero but is maximum at the tube axis. The ratio of the average velocity to the maximum velocity $v/u_{\max}$ is 0.5 for laminar flow and approximately 0.8

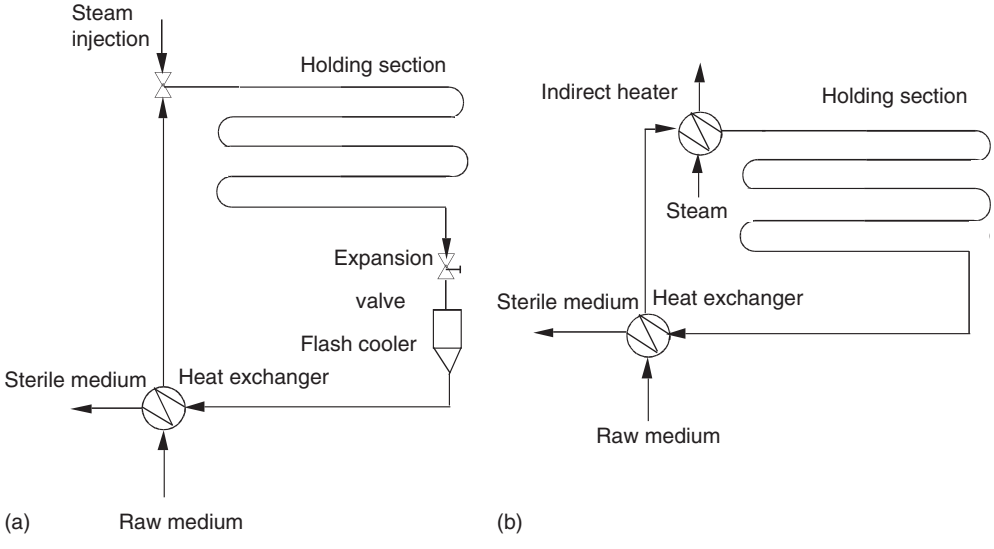

Figure 10.2 Continuous sterilizing systems. (a) Heat exchanger and continuous steam injection and (b) heat exchanger and indirect heater.

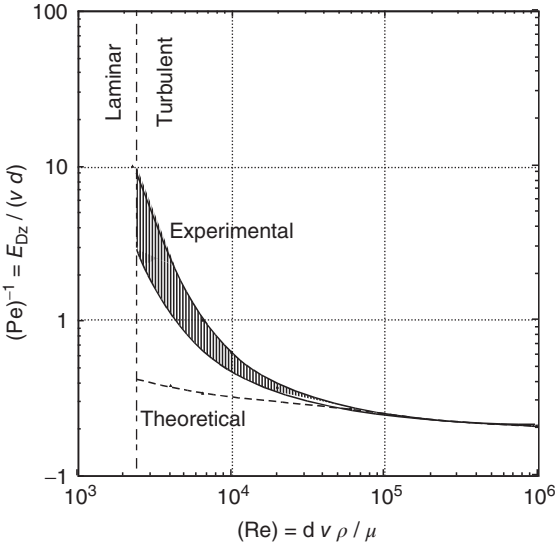

Figure 10.3 Correlation for axial dispersion coefficient in pipe flow, $(\mathrm{Pe})^{-1}$ versus (Re).

for turbulent flow when the Reynolds number is 10^6. Thus, if design calculations of a continuous sterilization unit were based on the average velocity, some portion of a medium would be insufficiently sterilized and might contain living microorganisms.

Deviation from the ideal plug flow can be described by the dispersion model, which uses the axial eddy diffusivity E_{Dz} ($\mathrm{m^2\ s^{-1}}$) as an indicator of the degree of mixing in the flow direction. If the flow in a tube is plug flow, the axial dispersion is zero. On the other hand, if the fluid in a tube is perfectly mixed, the axial dispersion is infinity. For turbulent flow in a tube, the dimensionless Peclet number (Pe) defined by the tube diameter ($v\,d/E_{\mathrm{Dz}}$) is correlated as a function of the Reynolds number, as shown in Figure 10.3 [3]. E_{Dz} is the axial eddy diffusivity, d is the tube diameter, and v is the velocity of liquid averaged over the cross section of the flow channel.

Figure 10.4 [1] shows the results for theoretical calculations [4] for the ratio n, the number of viable cells leaving the holding section of a continuous sterilizer, to n_0, the number of viable cells entering the section, as a function of the Peclet number (Pe), as defined by Equation 10.7, and the dimensionless Damköhler number (Da), as defined by Equation 10.8:

$$(\mathrm{Pe}) = \left(\frac{vL}{E_{\mathrm{Dz}}}\right) \tag{10.7}$$

$$(\mathrm{Da}) = \frac{k_{\mathrm{d}}L}{v} \tag{10.8}$$

where k_{d} is the specific death rate constant (cf. Equation 10.2) and L is the length of the holding tube.

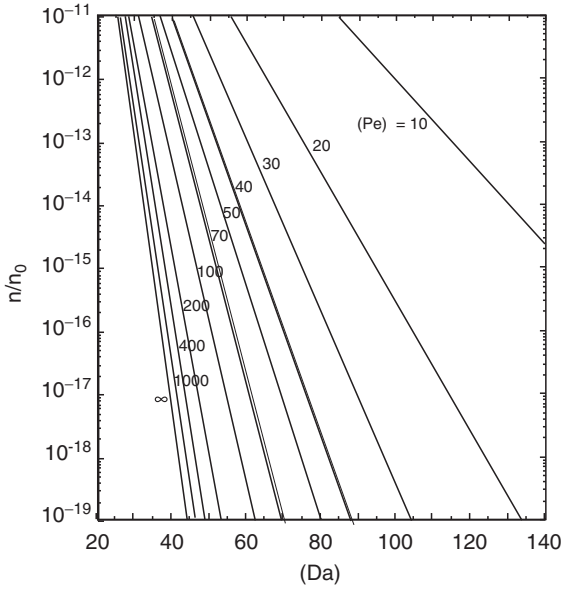

Figure 10.4 Theoretical plots of n/n_o as a function of (Pe) and (Da).

Example 10.2

A medium is to be continuously sterilized at a flow rate of $2\,m^3\,h^{-1}$ in a sterilizer by direct steam injection (Figure 10.2a). The temperature of a holding section is maintained at 120 °C, and the time for heating and cooling can be neglected. The bacterial count of the entering medium, $2 \times 10^{12}\,m^{-3}$, must be reduced to such an extent that only one organism can survive during 30 days of continuous operation. The holding section of the sterilizer is a tube, 0.15 m in internal diameter. The specific death rate of bacterial spores in the medium is $121\,h^{-1}$ at 120 °C, the medium density $\rho = 950\,kg\,m^{-3}$; the medium viscosity: $\mu = 1\,kg\,m^{-1}\,h^{-1}$.

Calculate the required length of the holding section of the sterilizer

a) assuming ideal plug flow;
b) considering the effect of the axial dispersion.

Solution

a)

$$\ln \frac{n_0}{n} = \ln \left\{ \frac{2 \times 10^{12}\,(m^{-3}) \times 2\,(m^3/h) \times 24\,(h/day) \times 30\,(day)}{1} \right\} = 35.6$$

Average holding time:

$$\tau_{\text{hold}} = \ln \frac{n_0}{n} / k_{\text{d}} = 0.294\,\text{h}$$

The average medium velocity in the holding section:

$$v = \frac{2}{(\pi \times 0.075^2)} = 113 \ \text{m} \ \text{h}^{-1}$$

The required length of the holding section:

$$L = 131 \times 0.294 = 33.2\ \text{m}$$

b) The Reynolds number of the medium flowing through the holding tube is

$$(\text{Re}) = \frac{0.15 \times 113 \times 950}{1} = 1.64 \times 10^4$$

From Figure 10.3 (Pe) is approximately 2.5 at $(\text{Re}) = 1.64 \times 10^4$, and

$$E_{\text{Dz}} = \frac{(113 \times 0.15)}{2.5} = 6.8$$

Assuming a length of the holding section of 36 m, the Peclet number is given as

$$(\text{Pe}) = \frac{vL}{E_{\text{Dz}}} = \frac{113 \times 36}{6.8} = 598$$

and

$$(\text{Da}) = \frac{k_{\text{d}} L}{v} = \frac{121 \times 36}{113} = 38.5$$

From Figure 10.4, the value of n/n_0 is about 3×10^{-16} and almost equal to that required in this problem. Thus, the length of the holding section should be 36 m.

10.5 Sterilizing Filtration

Microorganisms in liquids and gases can be removed by microfiltration; hence, air supplied to aerobic fermentors can be sterilized in this way. Membrane filters are often used for the sterilization of liquids, such as culture media for fermentation (especially for tissue culture), and also for the removal of microorganisms from various fermentation products, the heating of which should be avoided.

Sterilizing filtration is usually performed using commercially available membrane filter units of standard design. These are normally installed in special cartridges that often are made from polypropylene. Figure 10.5 [5] shows the sectional views of a membrane filter of folding fan-like structure, which uses a pleated membrane to increase the membrane area.

In selecting a membrane material, its pH compatibility and wettability should be considered. Some hydrophobic membranes require prewetting with

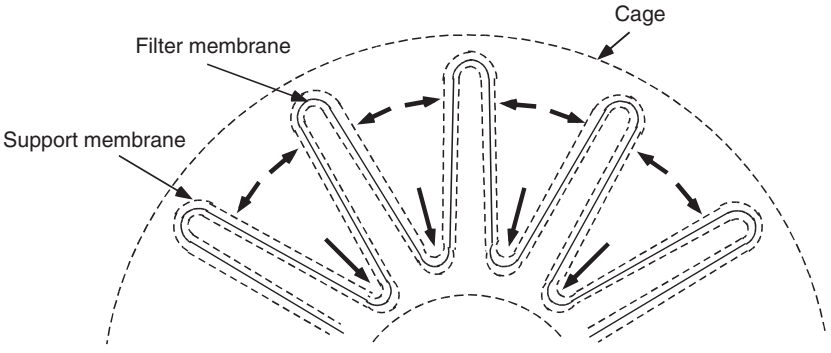

Figure 10.5 Membrane filter of folding fan-like structure.

a low-surface-tension solvent such as alcohol, whereas cartridges containing membranes are often presterilized using gamma irradiation. Such filter systems do not require assembly and steam sterilization.

Naturally, the size of the membrane pores should depend on the size of microbes to be filtered. For example, membranes with 0.2 μm pores are often used to sterilize culture media, while membranes with 0.45 μm pores are often used for the removal of microbes from culture products. It should be noted here that the so-called "pore size" of a membrane is the size of the largest pores on the membrane surface. The sizes of the pores on the surface are not uniform; moreover, the pore sizes usually decrease with increasing depth from the membrane surface. Such a pore size gradient will increase the total filter capacity, as smaller microbes and particles are captured within the inner pores of the membrane.

The so-called "bubble point" of a membrane – a measure of the membrane pore size – can be determined by using standard apparatus. When determining the bubble point of small, disk-shaped membrane samples (47 mm in diameter), the membrane is supported from above by a screen. The disk is then flooded with a liquid, so that a pool of liquid is left on top. Air is then slowly introduced from below, and the pressure increased in a stepwise manner. When the first steady stream of bubbles to emerge from the membrane is observed, that pressure is termed the "bubble point."

The membrane pore size can be calculated from the measured bubble point P_b by using the dimensionally consistent Equation 10.9. This is based on a simplistic model (Figure 10.6) that equates the air pressure in the cylindrical pore to the cosine vector of the surface tension force along the pore surface [6]:

$$P_b = \frac{K2\pi r\sigma \cos\theta}{(\pi r^2)} = \frac{K(2\sigma)\cos\theta}{r} \tag{10.9}$$

where K is the adjustment factor, r is the maximum pore radius (m), σ is the surface tension (N m^{-1}), and θ is the contact angle. The higher the bubble point, the smaller the pore size. The real pore sizes at the membrane surface can be measured using electron microscopy, although in practice the bubble point measurement is much simpler.

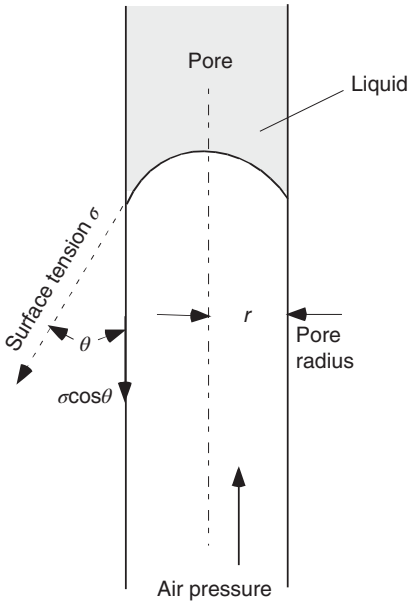

Figure 10.6 Pore size estimation by bubble point measurement.

The degree of removal of microbes of a certain size by a membrane is normally expressed by the reduction ratio, R. For example, if a membrane of a certain pore size is fed 10^7 microbes per cm^2 and it stops them all except one, the value of log reduction ratio log R is 7. It has been shown [7] that a log–log plot of R (ordinate) against the bubble points (abscissa) of a series of membranes will produce a straight line with a slope of 2.

The rates of filtration of microbes (particles) at a constant pressure difference decrease with time due to an accumulation of filtered microbes on the surface and inside the pores of the membrane. Hence, in order to maintain a constant filtration rate, the pressure difference across the membrane should be increased with time due to the increasing filtration resistance. Such data as are required for practical operation can be obtained with fluids containing microbes with the use of real filter units.

Problems

10.1 A culture medium that is contaminated with $10^{10}\ m^{-3}$ microbial spores of microorganisms will be heat-sterilized with steam of 121 °C. At 121 °C, the specific death rate of the spores can be assumed to be $3.2\ min^{-1}$ [1]. When the contamination must be reduced to 1 in 1000 fermentations, estimate the required sterilization time.

10.2 A culture medium weighing 10 000 kg (25 °C) contained in a fermentor is to be sterilized by the direct sparging of saturated steam (0.285 MPa, 132 °C). The flow rate of the injected steam is 1000 kg h^{-1}, and the enthalpies of saturated steam (132 °C) and water (25 °C) are 2723 and 105 kJ kg^{-1}, respectively. The heat capacity of the medium is 4.18 kJ kg^{-1} K^{-1}.
Estimate the time required to heat the medium from 25 to 121 °C.

10.3 When a culture medium flows in a circular tube as a laminar flow, determine the fraction of the medium that passes through the tube with a higher velocity than the averaged linear velocity.

10.4 A medium, which flows through an 80 mm i.d. stainless tube at a flow rate of 1.0 m^3 h^{-1}, is to be continuously sterilized by indirect heating with steam. The temperature of the holding section is maintained at 120 °C. The number of bacterial spores of 10^{11} m^{-3} in the entering medium must be reduced to 0.01 m^{-3}. The specific death rate of the bacterial spores in the medium, medium density, and medium viscosity at 120 °C are 180 h^{-1}, 950 kg m^{-3}, and 1.0 kg m^{-1} h^{-1}, respectively.
Calculate the required length of the holding section considering the effect of the axial dispersion.

References

1. Aiba, S., Humphrey, A.E., and Millis, N.F. (1973) *Biochemical Engineering*, 2nd edn, University of Tokyo Press.
2. Deindoerfer, F.H. and Humphrey, A.E. (1959) *Appl. Microbiol.*, **7**, 256.
3. Levenspiel, O. (1958) *Ind. Eng. Chem.*, **50**, 343.
4. Yagi, S. and Miyauchi, T. (1953) *Kagaku Kogaku*, **17**, 382 (in Japanese).
5. Cardona, M. and Blosse, P. (2005) *Chem. Eng. Prog.*, **101**, 34.
6. Zeman, I.J. and Zydney, A.L. (1996) *Microfiltration and Ultrafiltration*, Marcel Dekker.
7. Johnston, P.R. (2003) *Fluid Sterilization by Filtration*, 3rd edn, Interpharm Press.

11
Adsorption and Chromatography

11.1
Introduction

Adsorption is a physical phenomenon in which some components (*adsorbates*) in a fluid (liquid or gas) move to, and accumulate on, the surface of an appropriate solid (*adsorbent*) that is in contact with the fluid. With the use of suitable adsorbents, desired components or contaminants in fluids can be separated. In bioprocesses, the adsorption of a component in a liquid is widely performed by using a variety of adsorbents, including porous charcoal, silica, polysaccharides, and synthetic resins. Such adsorbents of high adsorption capacities usually have very large surface areas per unit volume. The adsorbates in the fluids are adsorbed at the adsorbent surfaces due to van der Waals, electrostatic, biospecific, or other interactions, and thus become separated from the bulk of the fluid. In practice, adsorption can be performed either batchwise in mixing tanks, or continuously in fixed-bed or fluidized-bed adsorbers. In adsorption calculations, both equilibrium relationships and adsorption rates must be considered.

In gas or liquid column chromatography, the adsorbent particles are packed into a column, after which a small amount of fluid containing several solutes to be separated is applied to the top of the column. Each solute in the applied fluid moves down the column at a rate determined by the distribution coefficient between the adsorbent and the fluid and emerges at the outlet of the column as a separated band. Liquid column chromatography is the most common method used in the separation of proteins and other bioproducts.

11.2
Equilibria in Adsorption

11.2.1
Linear Equilibrium

The simplest expression for adsorption equilibrium, for an adsorbate A, is given as

Biochemical Engineering: A Textbook for Engineers, Chemists and Biologists, Second Edition.
Shigeo Katoh, Jun-ichi Horiuchi, and Fumitake Yoshida.

Companion Website: www.wiley.com\go\katoh\biochem_eng_e2

$$\rho_s \overline{q_A} = K C_A \tag{11.1}$$

where ρ_s is the mass of a unit volume of adsorbent particles (kg-adsorbent m^{-3}), $\overline{q_A}$ is the adsorbed amount of A averaged over the inside surface of the adsorbent (kmol-adsorbate per kg-adsorbent), C_A is the concentration of adsorbate A in the fluid phase (kmol m^{-3}), and K is the distribution coefficient between the fluid and solid phases (–), which usually decreases with increasing temperature. The adsorption equilibria for a constant temperature are known as adsorption isotherms.

11.2.2 Adsorption Isotherms of Langmuir Type and Freundlich Type

Some components in a gas or liquid interact with sites, termed adsorption sites, on a solid surface by virtue of van der Waals forces, electrostatic interactions, or chemical binding forces. The interaction may be selective to specific components in the fluids, depending on the characteristics of both the solid and the components, and thus the specific components are concentrated on the solid surface. It is assumed that adsorbates are reversibly adsorbed at adsorption sites with homogeneous adsorption energy, and that adsorption is under equilibrium at the fluid–adsorbent interface. Let N_s (m^{-2}) be the number of adsorption sites and N_a (m^{-2}) the number of molecules of A adsorbed at equilibrium, both per unit surface area of the adsorbent. Then, the rate of adsorption r (kmol m^{-3} s^{-1}) should be proportional to the concentration of adsorbate A in the fluid phase and the number of unoccupied adsorption sites. Moreover, the rate of desorption should be proportional to the number of occupied sites per unit surface area. Here, we need not consider the effects of mass transfer, as we are discussing equilibrium conditions at the interface. At equilibrium, these two rates should balance. Thus,

$$r = k C_A (N_s - N_a) = k' N_a \tag{11.2}$$

where k (s^{-1}) and k' (kmol m^{-3} s^{-1}) are the adsorption and desorption rate constants, respectively. The ratio of the amount of adsorbed adsorbate $\overline{q_A}$ (kmol-adsorbate per kg-adsorbent) at equilibrium to the maximum capacity of adsorption q_{Am} (kmol-adsorbate per kg-adsorbent) corresponding to complete coverage of adsorption sites is given as the ratio N_a/N_s. Then, from Equation 11.2

$$\frac{N_a}{N_s} = \frac{\overline{q_A}}{q_{Am}} = \frac{a C_A}{1 + a C_A} \tag{11.3}$$

where $a = k/k'$ (m^3 $kmol^{-1}$). This equation is known as the Langmuir-type isotherm, which is shown in Figure 11.1. This isotherm should hold for monolayer adsorption in both gas and liquid phases.

In practice, the following Freundlich-type empirical isotherm can be used for many liquid–solid adsorption systems:

$$\rho_s \overline{q}_A = K'' C_A^{\beta} \tag{11.4}$$

where K'' and β are the empirical constants independent of C_A.

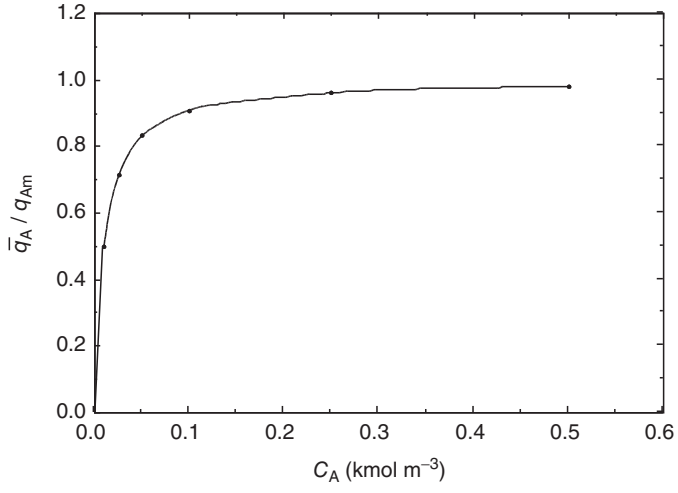

Figure 11.1 Langumuir-type adsorption isotherm.

The isotherms given by Equations 11.1, 11.3, and 11.4, or other types of isotherms, can be used to calculate the equilibrium concentrations of adsorbates in fluid and solid phases in batch and fixed-bed adsorption processes discussed below.

11.3 Rates of Adsorption into Adsorbent Particles

The apparent rates of adsorption into adsorbent particles usually involve the resistances for mass transfer of adsorbate across the fluid film around adsorbent particles and through the pores within particles. Adsorption *per se* at adsorption sites occurs very rapidly, and is not the rate-controlling step in most cases.

Now, we consider a case where an adsorbate in a liquid is adsorbed by adsorbent particles. If the mass transfer across the liquid film around the adsorbent particles is rate controlling, then the adsorption rate is given as

$$\rho_s \frac{d\overline{q_A}}{dt} = k_L a(C_A - C_{Ai}) \tag{11.5}$$

where ρ_s is the mass of adsorbent particles per unit volume (kg m^{-3}), k_L is the liquid phase mass transfer coefficient (m h^{-1}), a is the outside surface area of adsorbent particles per unit liquid volume (m^2 m^{-3}), C_A is the adsorbate concentration in the liquid main body, and C_{Ai} is the liquid phase adsorbate concentration at the liquid–particle interface (kmol m^{-3}). The mass transfer coefficient k_L can be estimated, for example, by Equation 6.28.

In the case where the mass transfer within the pores of adsorbent particles is rate controlling, the driving force for adsorption based on the liquid phase is given

as $(C_A - C_A^*)$, where C_A^* (kmol m^{-3}) $(=\rho_s \overline{q_A}/K)$ is the liquid phase concentration of adsorbate A in equilibrium with the averaged amount of adsorbed A in adsorbent particles $\overline{q_A}$ (kmol per kg-adsorbent) [1]. In adsorption systems, the rate-controlling step usually changes from the mass transfer across the liquid film around the adsorbent particles to the diffusion through the pores of particles as adsorption proceeds. In such cases, the rate of adsorption can be approximated with the use of the overall mass transfer coefficient K_L (m h^{-1}) based on the liquid phase concentration driving force, which is termed the linear driving force assumption:

$$\rho_s \frac{d\overline{q_A}}{dt} = K_L a(C_A - C_A^*) \tag{11.6}$$

In some cases, surface diffusion – that is, the diffusion of adsorbate molecules along the interface in the pores – may contribute substantially to the mass transfer of the adsorbate, and in such cases, the effective diffusivity may become much larger than the case with pore diffusion only.

11.4 Single- and Multistage Operations for Adsorption

In practical operations, a component in a liquid can be adsorbed either batchwise in one mixing tank or in several mixing tanks in series. Such operations are termed single-stage and multistage operations, respectively. For this, the feed liquid containing a component to be separated is mixed with an adsorbent in the tank(s), and equilibrium is reached after sufficient contact time. In this section, we consider both single- and multistage adsorption operations. Suppose that V m^3 of a feed containing A at a concentration C_{A0} and w kg of adsorbent ($q_A = q_{A0}$) are contacted batchwise. The material balance for the solute at adsorption equilibrium is given as

$$w(q_A - q_{A0}) = V(C_{A0} - C_A) \tag{11.7}$$

where q_A is the amount of A adsorbed by unit mass of adsorbent (kmol-adsorbate per kg-adsorbent) and C_A is the equilibrium concentration of adsorbate A in the liquid (kmol m^{-3}). As shown in Figure 11.2, this relationship is represented by a straight line with a slope of $-V/w$ passing through the point, C_{A0}, q_{A0}, while the intersection of the straight line with the equilibrium curve gives values of q_A and C_A. With the use of a large amount of adsorbent, most of the solute can be adsorbed.

In order to increase the recovery of adsorbate by adsorption, and to reduce the amount of adsorbent required to attain a specific recovery, a multistage adsorption operation can be used. In such an operation (as shown in Figure 11.3), a liquid solution is successively contacted at each stage with the adsorbent. In such a scheme, the relationship given by Equation 11.7 can be applied to each stage, with assumptions similar to the single-stage case, and the concentration of the adsorbate in the

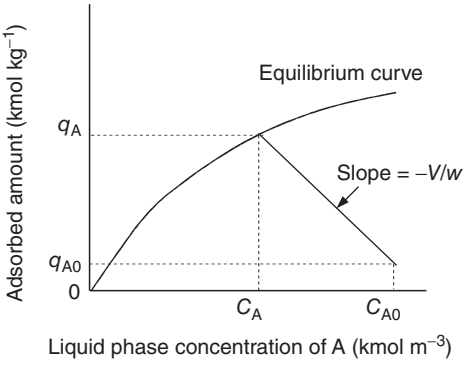

Figure 11.2 Single-stage adsorption process.

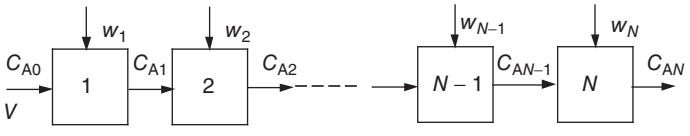

Figure 11.3 Multistage adsorption.

liquid from the Nth stage is given by the following equation, if an equal amount (w/N) of fresh adsorbent ($q_A = 0$) is used in each stage:

$$C_{A,N} = \frac{C_{A0}}{\langle 1 + K(w/NV)\rangle^N} \tag{11.8}$$

Adsorbate recovery increases with increasing number of stages, as shown below.

Example 11.1

For an adsorption system, the distribution coefficient of Equation 11.1 is 3.0 and the feed concentration is C_{A0}. Assuming equilibrium, compare the exit concentrations C_{A1} and C_{A3} in cases (a) and (b).

a) Single-stage adsorption in which the amount of adsorbent used per unit feed volume is 1.0 kg m^{-3}
b) Three-stage adsorption in which the amount of adsorbent used in each stage per unit feed volume is 1/3 kg m^{-3}.

Solution

The concentration of the adsorbate in the liquid from the third stage can be obtained from Equation 11.8:

$$C_{A3} = \frac{C_{A0}}{(1 + 3/3)^3} = \frac{C_{A0}}{8}$$

For single-stage adsorption, C_{A1} is given as

$$C_{A1} = \frac{C_{A0}}{(1+3)}$$

Thus, $C_{A3}/C_{A1} = 1/2$

11.5 Adsorption in Fixed Beds

11.5.1 Fixed-Bed Operation

A variety of adsorber types exists, including stirred tanks (Section 7.4), fixed-bed adsorbers, and fluidized-bed adsorbers. Among these, the fixed-bed adsorbers are the most widely used. In the downflow fixed-bed adsorber (Figure 11.4), a feed solution containing adsorbate(s) at a concentration of C_{A0} is fed continuously to the top of a column packed with adsorbent particles, and flows down at an interstitial liquid velocity u (m s^{-1}) – that is, the liquid velocity through the void of the bed. Initially, adsorption takes place in the adsorption zone in the upper region of the bed, but as the saturation of the adsorbent particles progresses, the adsorption zone moves downward with a velocity that is much slower than that of the feed flowing down the column. When the adsorption zone reaches the bottom of the bed, the adsorbate concentration in the solution coming from the column bottom (i.e., the effluent) begins to increase, and finally becomes equal to the feed concentration C_{A0}. The curve showing the adsorbate concentrations in the effluent plotted against time or the effluent volume – the breakthrough curve – is shown schematically in Figure 11.5.

Usually, the supply of the feed solution is stopped when the ratio of the adsorbate concentration in the effluent to that in the feed has reached a predetermined value (the "break point"). Then, in the elution operation the adsorbate bound to the adsorbent particles is desorbed (i.e., eluted) by supplying a suitable fluid (eluent) that contains no adsorbates. In this way, adsorbent particles are regenerated to their initial conditions. However, in some cases the column may be repacked with new adsorbent particles.

As can be understood from Figure 11.5, the amount of adsorbate lost in the effluent and the extent of the adsorption capacity of the fixed bed utilized at the break point depend on the shape of the breakthrough curve and on the selected break point. In most cases, the time required from the start of feeding to the break point is a sufficient index of the performance of a fixed-bed adsorber. A simplified method to predict the break time is discussed in the following section.

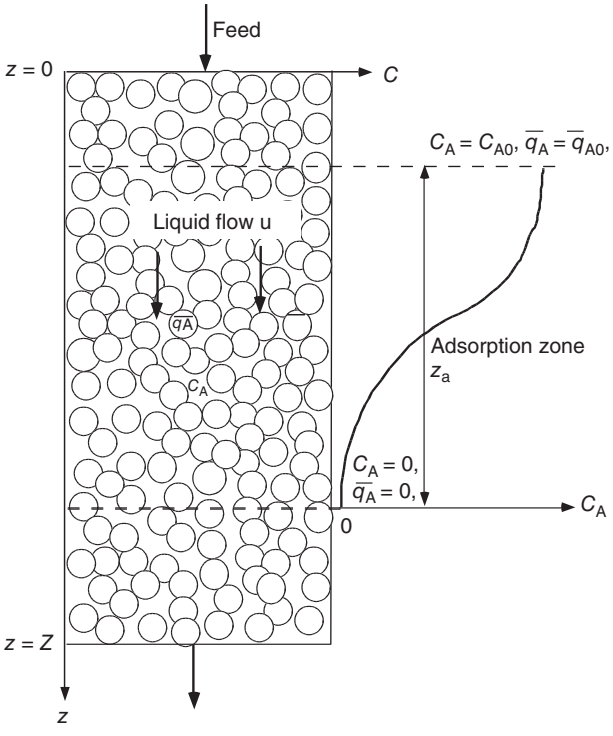

Figure 11.4 Adsorption in fixed bed.

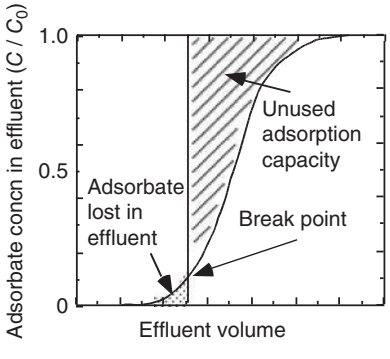

Figure 11.5 Breakthrough curve of fixed-bed adsorber.

11.5.2
Estimation of the Break Point

With favorable adsorption isotherms, in which the slope of adsorption isotherms dq/dc decreases with increasing adsorbate concentration (as shown in Figure 11.1), the moving velocity of the adsorption zone is faster at high

concentrations of the adsorbed component – that is, near the inlet of the bed. Thus, the adsorption zone becomes narrower as adsorption in the bed progresses. On the other hand, a finite rate of mass transfer of the adsorbed component and flow irregularity will broaden the width of the zone. These two compensating effects cause the shape of the adsorption zone to be unchanged through the bed, except in the vicinity of the inlet. This situation is termed the "constant pattern of the adsorption zone."

When the constant pattern of the adsorption zone holds and the amount of an adsorbed is much larger than its concentration in the feed solution, then the velocity of movement of the adsorption zone v_a is given as follows:

$$v_a = \frac{\varepsilon u C_{A0}}{\rho_b q_{A0}} \tag{11.9}$$

where ε is the void fraction of the particle bed (−), u is the interstitial liquid velocity (i.e., the liquid velocity through the void of the bed, m s^{-1}), ρ_b is the packed density of the bed (kg m^{-3}), and q_{A0} is the adsorbed amount of adsorbate equilibrium with the feed concentration C_{A0} (kmol per kg-adsorbent).

Under the constant pattern, the term dq/dC should be constant. The integration of $d\overline{q}_A/dC_A =$ constant with the boundary conditions

$$C_A = 0 \quad q_A = 0$$

$$C_A = C_{A0} \quad q_A = q_{A0}$$

gives the following relation:

$$\overline{q_A} = \frac{q_{A0}}{C_{A0}} C_A \tag{11.10}$$

The time required from the start of feeding to the break point can be estimated with the assumption of the constant pattern stated above. Thus, substitution of Equation 11.10 into Equation 11.6 gives the following equation for the rate of adsorption:

$$\rho_b \frac{d\overline{q_A}}{dt} = \frac{\rho_b q_{A0}}{C_{A0}} \frac{dC_A}{dt} = K_L a (C_A - C_A^*) \tag{11.11}$$

Integration of this equation between the break point and exhaustion point, where the ratio of the adsorbate concentration in the effluent to that in the feed becomes a value of (1 − the ratio at the break point), gives

$$t_E - t_B = \frac{\rho_b q_{A0}}{\overline{K_L a} C_{A0}} \int_{c_{AB}}^{c_{AE}} \frac{dC_A}{C_A - C_A^*} \tag{11.12}$$

where the subscripts B and E indicate the break and exhaustion points, respectively. The averaged value of the overall volumetric coefficient $\overline{K_L a}$ can be used for practical calculation, although this varies with the progress of adsorption. The velocity of the movement of the adsorption zone under constant pattern

conditions is given by Equation 11.9, and thus the break time t_B is given by approximating that the fractional residual capacity of the adsorption zone is 0.5.

$$t_B = \frac{Z - \frac{z_a}{2}}{v_a} = \frac{\rho_b q_{A0}}{\varepsilon u C_{A0}} \left[Z - \frac{\varepsilon u}{2\overline{K_L a}} \int_{C_B}^{C_E} \frac{dC_A}{C_A - C_A^*} \right] \tag{11.13}$$

where z_a is the length of the adsorption zone given as $v_a\,(t_E - t_B)$. Numerical integration of the above equation is possible in cases where the Langmuir and Freundlich isotherms hold.

Example 11.2

An adsorbate A is adsorbed in a fixed-bed adsorber that is of 25 cm height and packed with active charcoal particles of 0.6 mm diameter. The concentration of A in a feed solution C_A is 1.1 mol m^{-3}, and the feed is supplied to the adsorber at an interstitial velocity of 1.6 m h^{-1}. The adsorption equilibrium of A is given by the following Freundlich-type isotherm.

$$\rho_b \overline{q} = 1270 C_A^{0.11}$$

where the units of ρ_b, $\overline{q}$, and C_A are kg m^{-3}, mol kg^{-1}, and mol m^{-3}, respectively.

The packed density of the bed, the void fraction of the particle bed, and the density of the feed solution are 386 kg m^{-3}, 0.5, and 1000 kg m^{-3}, respectively. The averaged overall volumetric coefficient of mass transfer $K_L a$ is 9.2 h^{-1}, and a constant pattern of the adsorption zone can be assumed in this case.

Estimate the break point at which the concentration of A in the effluent becomes 0.1 C_{A0}.

Solution

From the Freundlich-type isotherm

$$\frac{\overline{q_A}}{q_{A0}} = \left(\frac{C_A^*}{C_{A0}} \right)^{0.11}$$

where C_A^* is the liquid phase concentration of A in equilibrium with q_A. Since the assumption of the constant pattern holds, Equation 11.10 is substituted in the above equation.

$$\frac{C_A^*}{C_{A0}} = \left(\frac{C_A}{C_{A0}} \right)^{\frac{1}{0.11}}$$

Substitution of C_A into the integral term of Equation 11.13 and integration from $C_{AB} = 0.1 C_{A0}$ to $C_{AE} = 0.9 C_{A0}$ give

$$\int_{C_B}^{C_E} \frac{dC_A}{C_A - C_A^*} = \ln\left(\frac{0.9}{0.1}\right) + \left(\frac{0.11}{0.89}\right) \ln\left\langle \frac{1 - 0.1^{8.1}}{1 - 0.9^{8.1}} \right\rangle = 2.26$$

Substitution of the above and other known values into Equation 11.13 gives

$$t_B = \frac{1283}{0.5 \times 1.6 \times 1.1} \times \left(0.25 - \frac{0.5 \times 1.6 \times 2.26}{2 \times 9.2}\right) = 221 \text{ h}$$

11.6 Separation by Chromatography

11.6.1 Chromatography for Bioseparation

Liquid column chromatography is the most commonly used method in bioseparation. As shown in Figure 11.6, the adsorbent particles are packed into a column as the stationary phase, and a fluid is continuously supplied to the column as the mobile phase. For separation, a small amount of solution containing several

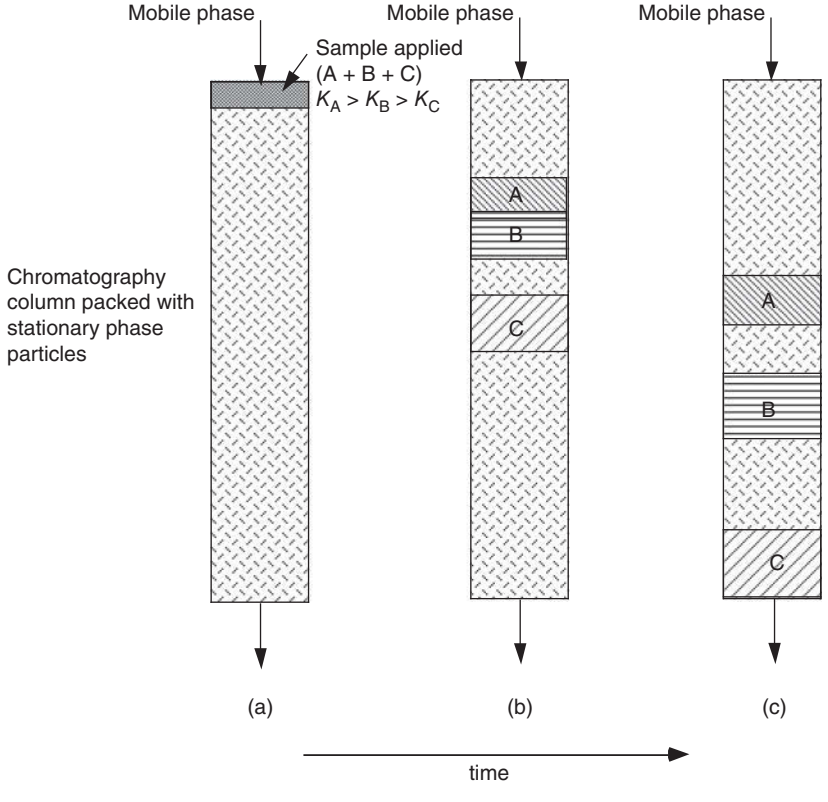

Figure 11.6 Schematic diagram showing the chromatographic separation of solutes with different distribution coefficients.

Table 11.1 Liquid column chromatography used in bioseparation.

Liquid chromatography	Mechanism of partition	Elution method	Characteristics
Gel filtration chromatography (GFC)	Size and shape of molecule	Isocratic	Relatively long column for separation Separation under mild condition High recovery
Ion-exchange chromatography (IEC)	Electrostatic interaction	Gradient Stepwise	Short column, wide applicability Separation depending on elution conditions High capacity
Hydrophobic interaction chromatography (HIC)	Hydrophobic interaction	Gradient Stepwise	Adsorption at high salt concentration
Affinity chromatography (AFC)	Biospecific interaction	Stepwise	High selectivity High capacity

solutes is supplied to the column (Figure 11.6a). Each solute in the applied solution moves down the column with the mobile phase liquid at a rate determined by the distribution coefficient between the stationary and mobile phases (Figure 11.6b), and then emerges from the column as a separated band (Figure 11.6c). Depending on the type of adsorbent packed as the stationary phase and on the nature of the interaction between the solutes and the stationary phase, several types of chromatography may be used for bioseparations, as listed in Table 11.1.

Chromatography is operated in several ways, depending on the strength of the interaction (affinity) between the solutes and the stationary phase. In the case where the interaction is relatively weak – as in gel chromatography (Section 11.6.4) – the solutes are eluted by a mobile phase of a constant composition (*isocratic elution*). With increasing interaction – that is, with increasing distribution coefficient – it becomes necessary to alter the composition of the mobile phase in order to decrease the interaction, because elution with an isocratic elution requires a very long time. Subsequent changes in the ionic strength, pH, and so on, of the mobile phase can be either stepwise (stepwise elution) or continuous (gradient elution). In the case where the interaction is high and selective (as in bioaffinity chromatography), a specific solute can be selectively adsorbed by the stationary phase until the adsorbent is almost saturated, and can then be eluted by a stepwise change of the mobile phase to weaken the interaction between the solute and the stationary phase. Such an operation can be regarded as selective adsorption and desorption in a fixed-bed adsorber, as noted in Section 11.5.

The performance of a chromatographic system is generally evaluated by the time required for the elution of each solute (*retention time*) and the width of the elution curve (*peak width*), which represents the concentration profile of each solute in the effluent from a column. Although several models are used for evaluation, the equilibrium, stage, and rate models are discussed here.

11.6.2 General Theories on Chromatography

11.6.2.1 Equilibrium Model

In this model, the rate of migration of each solute along with the mobile phase through the column is obtained on the assumptions of instantaneous equilibrium of solute distribution between the mobile and the stationary phases, with no axial mixing. The distribution coefficient K is assumed to be independent of the concentration (linear isotherm), and is given by the following equation:

$$C_S = KC \tag{11.14}$$

where C_S (kmol per m^3-bed) and C (kmol m^{-3}) are the concentrations of a solute in the stationary and the mobile phases, respectively. The fraction of the total solute that exists in the mobile phase is given by

$$X_s = \frac{C\varepsilon}{C\varepsilon + C_s(1-\varepsilon)} = \frac{1}{1+EK} \tag{11.15}$$

where ε (−) is the interparticle void fraction and $E = (1-\varepsilon)/\varepsilon$. The moving rate of the solute dz/dt (m s^{-1}) along with the mobile phase through the column is proportional to X_s and the interstitial fluid velocity u (m s^{-1}).

$$\frac{dz}{dt} = X_s u = \frac{u}{1+EK} \tag{11.16}$$

If the value of K is independent of the concentration, then the time required to elute the solute from a column of length Z (m) (retention time t_R) is given as

$$t_R = \frac{Z(1+EK)}{u} \tag{11.17}$$

The volume of the mobile phase fluid that flows out of the column during the time t_R – that is, the elution volume V_R (m^3) is given as

$$\begin{aligned} V_R &= V_0 + K(V_t - V_0) \\ &= V_0 (1 + EK) \end{aligned} \tag{11.18}$$

where V_0 (m^3) is the interparticle void volume and V_t (m^3) is the total bed volume.

Solutes flow out in the order of increasing distribution coefficients, and thus can be separated. Although a sample is applied as a narrow band, the effects of finite mass transfer rate and flow irregularities in practical chromatography result in band broadening, which may make the separation among eluted bands of solutes insufficient. These points must be taken into consideration when evaluating separation among eluted bands, and can be treated by one of the following two models, namely, the stage model or the rate model.

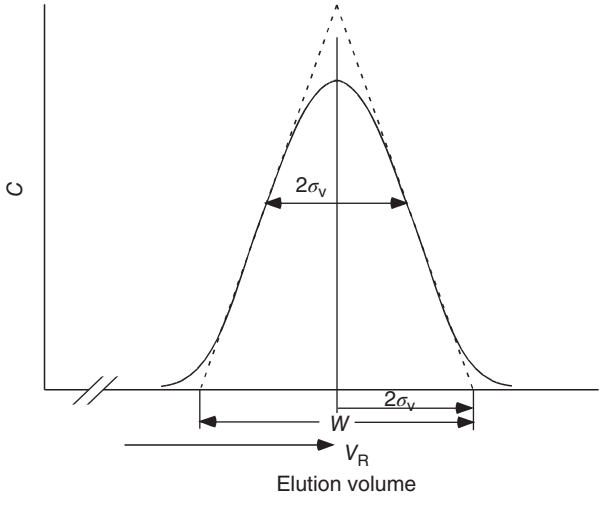

Figure 11.7 Elution curve and parameters for evaluation of *N*.

11.6.2.2 **Stage Model**

The performance of a chromatography column can be expressed by the concept of the theoretical stage at which the equilibrium of solutes distribution between the mobile and stationary phases is reached. For chromatography columns, the height of packing equivalent to one equilibrium stage (i.e., the column height divided by the number of theoretical stages N) is defined as the height equivalent to an equilibrium stage, Hs (m). However, in this text, the term HETP (height equivalent to the theoretical plate) is not used in order to avoid confusion with the HETP of packed columns for distillation and absorption.

The shape of the elution curve for a pulse injection can be approximated by the Gaussian error curve for $N > 100$, which is almost the case for column chromatography [2]. The value of N can be calculated from the elution volume V_R (m^3) and the peak width W (m^3), which is obtained by extending tangents from the sides of the elution curve to the baseline and is equal to four times the standard deviation σ_v (m^3) $= (V_R{}^2/N)^{1/2}$, as shown in Figure 11.7.

$$H\text{s} = \frac{Z}{N} = \frac{Z}{(V_R/\sigma_v)^2} = \frac{Z}{16(V_R/W)^2} \tag{11.19}$$

With a larger N, the width of the elution curve becomes narrower at a given V_R, and a better resolution will be attained. The dependence of the value of N on the characteristics of packing material and operating conditions is not clear with the stage model, because the value of N is obtained empirically. The dependence of Hs on these parameters can be obtained by the following rate model.

11.6.2.3 **Rate Model**

This treatment is based on the two differential material balance equations on a fixed bed and packed particles. Although these equations, together with an

adsorption isotherm and suitable boundary and initial conditions, describe precisely the performance of chromatography, the complexity of their mathematical treatment sometimes makes them insolvable. If the distribution coefficient K given by Equation 11.1 is constant, then Hs can be correlated to several parameters by the use of the first absolute moment and the second central moment, as given by Equation 11.20 [3].

$$Hs = \frac{Z}{N} = \frac{2D_z}{u} + \frac{2ur_0^2EK}{15(1+EK)^2}\left(\frac{1}{D_{eff}} + \frac{5K}{k_L r_0}\right) \tag{11.20}$$

where D_z is the axial eddy diffusivity ($m^2\ s^{-1}$), which is a measure of mixing along the axial direction of a column, D_{eff} is the effective diffusivity of the solute in adsorbent particles ($m^2\ s^{-1}$), k_L is the liquid phase mass transfer coefficient outside particles ($m\ h^{-1}$), and r_0 is the radius of particles of the stationary phase (m).

The first term of the right-hand side of Equation 11.20 shows the contribution of axial mixing of the mobile phase fluid to band broadening, and is independent of the fluid velocity and proportional to r_0 in the range of the packed particle Reynolds number below 2. The second term is the contribution of mass transfer, and decreases in line with a decrease in the fluid velocity and r_0. Therefore, columns packed with particles of a smaller diameter show a higher resolution, which leads to high efficiency associated with high-performance liquid chromatography (HPLC).

11.6.3 Resolution Between Two Elution Curves

Since the concentration profile of a solute in the effluent from a chromatography column can be approximated by the Gaussian error curve, the peak width W (m^3) can be obtained by extending tangents at inflection points of the elution curve to the base line and is given by

$$W = \frac{4V_R}{(N)^{1/2}} = 4\sigma_v \tag{11.21}$$

where V_R (m^3) is the elution volume, N is the number of theoretical plates, and σ_v is the standard deviation based on elution volume (m^3). The separation of the two successive curves of solutes 1 and 2 can be evaluated by the resolution R_S, as defined by the following equation:

$$R_S = \frac{V_{R,2} - V_{R,1}}{(W_1 + W_2)/2} \tag{11.22}$$

Values of $V_{R,2}$ and $V_{R,1}$ given by Equation 11.18 are substituted into Equation 11.22 and, if W_1 is approximated as equal to W_2, then substitution of Equation 11.21 into Equation 11.22 gives

$$R_S = \frac{E(K_2 - K_1)N^{1/2}}{4(1+EK_1)} \tag{11.23}$$

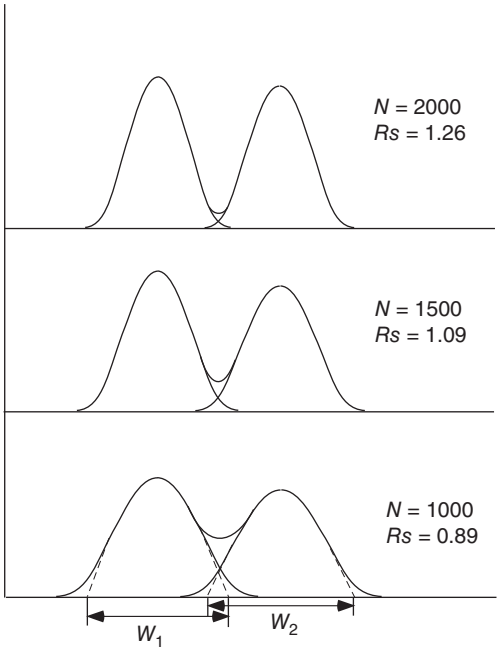

Figure 11.8 Resolution of two elution curves at three theoretical plates, interparticle void fraction = 0.36.

Thus, resolution increases in proportion to $N^{1/2}$. In order to attain good resolution between two curves, the difference in the distribution coefficients of two solutes and/or the number of theoretical plates should be large. As seen from Equation 11.19, resolution is proportional also to $(Z/H\text{s})^{1/2}$. The separation behaviors of two curves with change in the number of theoretical plates are shown in Figure 11.8 [4]. For any given difference between the values of K_1 and K_2 in Equation 11.23, larger values of N lead to a higher resolution, as shown in Figure 11.8. In order to attain good separation in chromatography – that is, a good recovery and high purity of a target – the value of the resolution between the target and a contaminant must be above 1.2.

11.6.4
Gel Chromatography

Gel chromatography, as a separation method, is based on the size of molecules, which in turn determines the extent of their diffusion into the pores of gel particles packed as a stationary phase. Large molecules are excluded from most of the pores, whereas small molecules can diffuse further into the stationary phase.

Thus, smaller molecules take a longer time to move down the column and are retarded in terms of their emergence from the column.

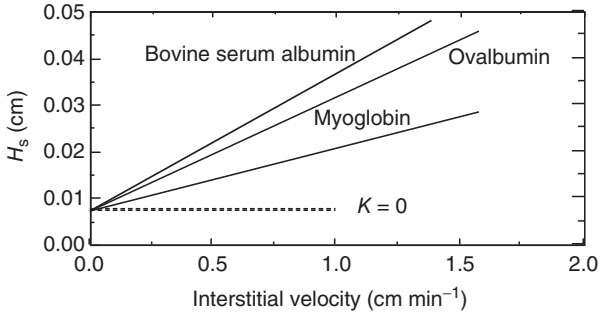

Figure 11.9 Effects of liquid velocity and molecular weight on *Hs* in gel chromatography (d_p: 44 μm, 1.6 × 30 cm column).

In gel chromatography, the distribution coefficient K is little affected by the concentration of solutes, pH, ionic strength, and so on, and is considered to be constant. Therefore, the results obtained in Section 11.6.2 for constant K can be applied to evaluate the performance of gel chromatography. Figure 11.9 shows the increase in Hs with the liquid velocity in gel chromatography packed with gel particles of 44 μm diameter [4]. The values of Hs increase linearly with the velocity, and the slopes of the lines become steeper with an increase in molecular weights, as predicted by Equation 11.20.

Gel chromatography can be applied to desalting and buffer exchange, in which the composition of electrolytes (small molecules) in a buffer containing proteins or other bioproducts (large molecules) is changed. It can also be used for the separation of bioproducts with different molecular sizes, and for determining molecular weights. Gel chromatography is operated by isocratic elution, and the recovery of products is generally high, although it has the disadvantage of the eluted products being diluted. Consequently, processes that have a more concentrating effect, such as ultrafiltration and ion-exchange chromatography (IEC), are generally combined with gel chromatography for bioseparation.

Example 11.3

A chromatography column of 10 mm i.d. and 100 mm height was packed with particles for gel chromatography. The interparticle void fraction ε was 0.20. A small amount of a protein solution was applied to the column and elution performed in an isocratic manner with a mobile phase at a flow rate of 0.5 cm^3 min^{-1}. The distribution coefficient K of a protein was 0.7. An elution curve of the Gaussian type was obtained, and the peak width W was 1.30 cm^3. Calculate the Hs value of this column for this protein sample.

Solution

The elution volume of the protein is calculated by Equation 11.18 with the values of K and $E = (1 - \varepsilon)/\varepsilon$.

$$V_R = 1.57(1 + 4 \times 0.7) = 5.97 \text{ cm}^3$$

Equation 11.19 gives the Hs value as follows:

$$H\text{s} = \frac{10}{16(5.97/1.3)^2} = 0.030 \text{ cm}$$

11.6.5 Affinity Chromatography

Complementary structures of biological materials, especially those of proteins, often result in specific recognitions and various types of biological affinity. These include many pairs of substances, such as enzyme–inhibitor, enzyme–substrate (analog), enzyme–coenzyme, hormone–receptor, and antigen–antibody, as summarized in Table 11.2. Thus, bioaffinity represents a useful approach to separating specific biological materials.

When separating by affinity chromatography (AFC) (which utilizes specific bioaffinity), one of the interacting components (the *ligand*) is immobilized onto an insoluble, porous support as a specific adsorbent, whereupon the other component is selectively adsorbed onto the ligand. Polysaccharides, such as agarose, dextran, and cellulose, are widely used as supports. AFC (which is shown schematically in Figure 11.10) generally uses a fixed bed that is packed with the

Table 11.2 Pairs of biomaterials interacting with bioaffinity.

Enzyme	Inhibitor
	Substrate
	Substrate-analog
	Coenzyme
Hormone	Receptor
Antigen	Antibody
Antibody	Protein A, protein G
Polysaccharide	Lectin
Coagulation factor	Heparin
DNA (RNA)	Complemental DNA (RNA)
NAD(P) dependent enzyme	Synthetic dye
Histidine containing protein	Chelated heavy metal
Antibody	Peptide

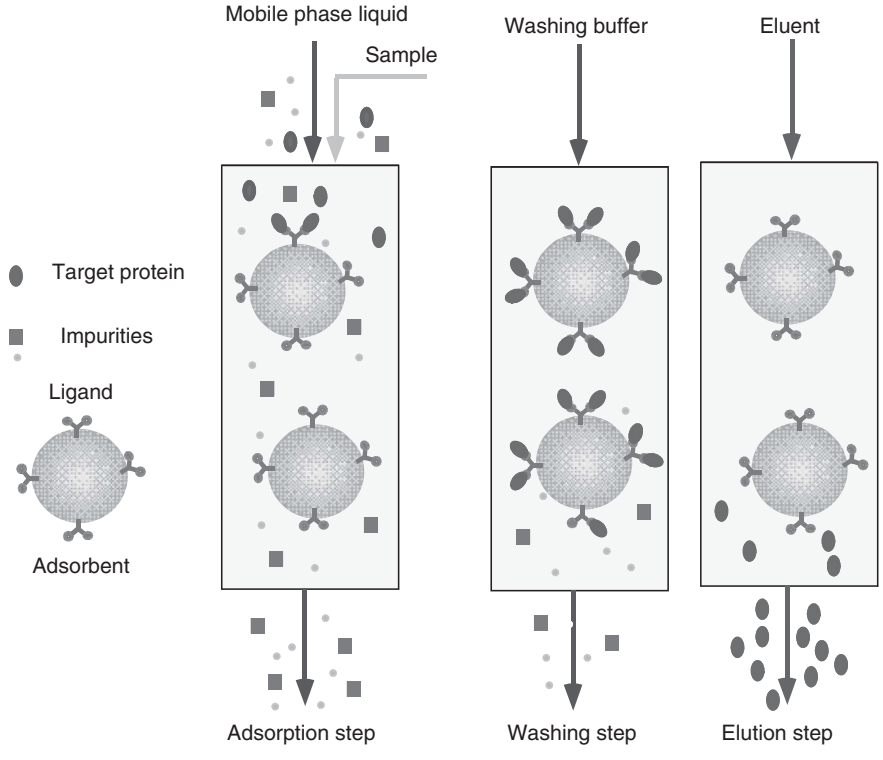

Figure 11.10 Scheme of affinity chromatography.

specific adsorbent thus formed. When equilibration with a buffer solution has been reached in a packed column, a crude solution is applied to the column. Any component that interacts with the coupled ligand will be selectively adsorbed by the adsorbent, while contaminants in the feed solution will flow through the column; this is the *adsorption step*. As the amount of the adsorbed component increases, the component will begin to appear in the effluent solution from the column (*breakthrough*). The supply of the feed solution is generally stopped at a predetermined ratio (0.1 or 0.05, at the break point) of the concentration of the adsorbed component in the effluent to that in the feed. The column is then washed with a buffer solution (*washing step*). Finally, the adsorbed component is eluted by altering the pH or ionic strength, or by using a specific eluent (*elution step*).

As shown in Figure 11.10, the operations in AFC are regarded as highly specific adsorption and desorption steps. Thus, the overall performance is much affected by the break point, an estimation of which can be made as described in Section 11.5.2.

11.7
Biorecognition Assay

11.7.1
Antigen Recognition by an Antibody

Specific recognitions between pairs of biological materials can be utilized for biological assay, as well as for the specific separation of biological materials stated in Section 11.6.5. Among many pairs of biological materials, the antigen–antibody interactions are highly specific and strong; thus, these are widely used for biological assays, and are referred to as immunological assays. Antibodies are produced in the mammalian body by infection from pathogens, or from invasion by exogenous materials, in order to bind specifically to them and to detoxify them. In humans, there are five types (classes) of antibodies (IgM, IgD, IgG, IgA, and IgE), and among them IgG and its derivatives are the most widely used in immunological assay.

Antibodies (IgGs, molecular weight approximately 150 kD) are Y-shaped molecules consisting of two identical heavy chains and two identical light chains linked by disulfide bonds, as schematically shown in Figure 11.11. Each heavy chain has four domains (three constant regions and one variable region), and each light chain has two domains (constant and variable regions). While the amino acid sequences of the constant regions are less variable among IgG molecules, those of the two variable regions in the heavy chain and the light chain, which produce antigen-binding sites, vary among antibody molecules. This makes it possible to produce a large repertoire of antibody molecules against a wide variety of antigens. Thus, the antibody–antigen interaction has high specificity and sensitivity, and it can be used for the immunological assay of many kinds of biological materials. In the case of antigens with a large molecular weight, antibody molecules generally only recognize a specific part of the antigen termed the "epitope."

As the antigen-binding site consists of two variable regions from the heavy and light chains, it is possible to create a genetically engineered molecule that is referred to as a "single-chain Fv" (scFv) antibody, in which two variable regions are linked by a polypeptide linker. The schematic structure of an scFv is shown in Figure 11.11. An scFv molecule has the ability to selectively bind a target antigen, but it lacks the other biological activities of IgG. Recently, scFv molecules have been produced by the fermentation of recombinant *Escherichia coli* and are used for immunological assay.

11.7.2
Enzyme-Linked Immunosorbent Assay (ELISA)

Among the many immunological assay methods, the enzyme-linked immunosorbent assay methods (ELISA) are the most popular methods. ELISA can detect both antigen molecules and antibody molecules with only a slight modification of the procedure. The direct-binding and sandwich methods that are used for the

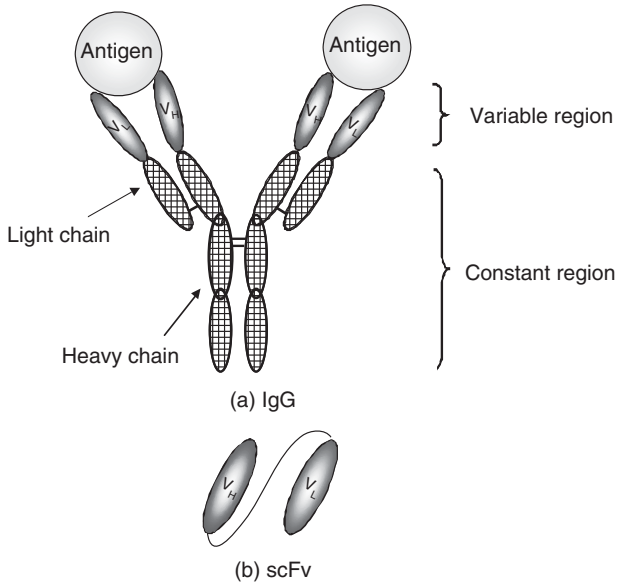

Figure 11.11 Immunoglobulin G and scFv. (a) IgG and (b) scFv.

detection of antigen molecules are explained in this section. In both methods, an enzyme is linked chemically to an antibody specific to a target antigen, and assay procedures are performed using a microtiter plate (approximately 128 mm × 86 mm), made of polystyrene or polyethylene, with 96 wells (each well of approximately 6.5 mm diameter and 12 mm depth). In Figure 11.12, ELISA procedures are shown schematically for one well of the microtiter plate.

Using the direct-binding method (Figure 11.12a), a small amount of sample solution (e.g., 100 μl per well) containing an unknown concentration of an antigen to be measured was added to a well, and the antigen molecules were bound to the plastic surface of the well. After washing with a suitable buffer solution, the plastic surface of the well was coated by inactive protein molecules, such as bovine serum albumin, to block the nonspecific adsorption of other proteins. After washing, an enzyme-linked antibody was added into the well and bound to the antigen on the surface of the well. After further washing, the binding of the antibody was detected through a reaction of the linked enzyme, which converted a colorless substrate to a colored product during incubation for a predetermined time. The absorbance of the colored product in the well was measured using a spectrophotometer. By comparing the absorbance with a standard calibration curve, which was obtained under the same procedures using antigen solutions of known concentrations, we were able to determine the concentration of the antigen in the samples. A typical example of such a calibration curve is shown in Figure 11.13a.

When using the sandwich method (Figure 11.12b), the antibody molecules specific to a target antigen were first bound to the surface of a well. Then, after washing

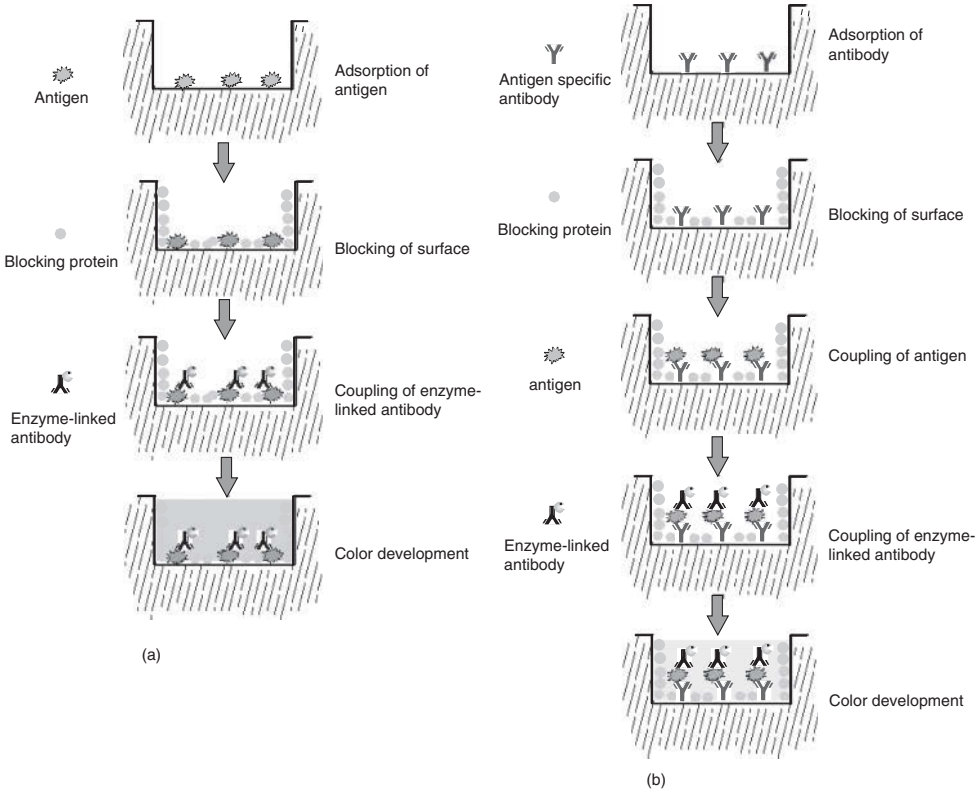

Figure 11.12 Schematic figures of ELISA: (a) direct-binding method and (b) sandwich method.

and blocking, a sample solution was added, and antigen molecules in the sample were bound to the antibody on the surface of the well. The binding of the antigen was detected using an enzyme-linked antibody that recognized another epitope, which was not detected by the first antibody, on the antigen molecule. Color development by similar procedures in the direct-binding method was used to determine the bound amount of the second antibody, which can be related to the amount of the antigen in the sample. The concentration of the antigen in the sample was obtained with the use of a calibration curve.

In the sandwich method, the first antibody molecules bound to the surface of a well can concentrate the antigen in a sample because of the high density with which they are adsorbed onto the surface of the well and the strong binding affinity to the antigen. Therefore, if antibody molecules with similar binding affinities are used, the sandwich method leads to a higher sensitivity to the target compared with the direct-binding method (Figure 11.13b).

Because of the increase in the number of samples and the need for high-sensitivity detection, high-throughput, and high-sensitivity immunological assay

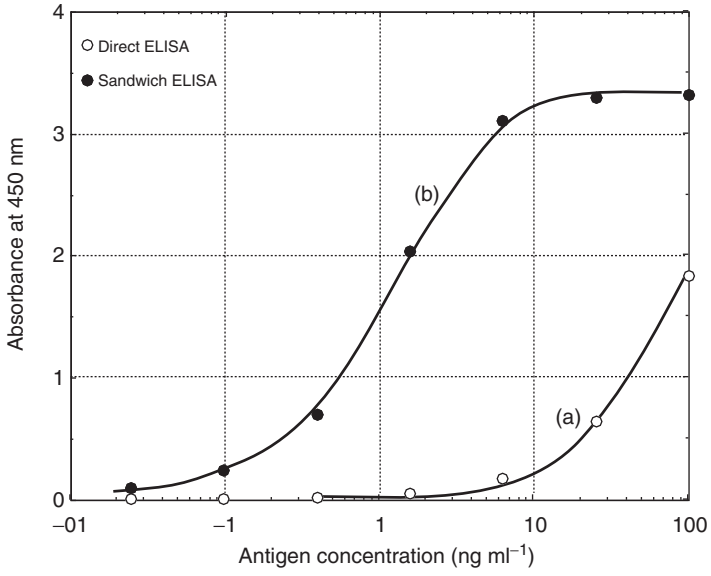

Figure 11.13 Calibration curves of direct and sandwich ELISA.

methods are required. Microblotting and microchip methods were developed to satisfy these requirements.

▶ Problems

11.1 A solution of 1 m^3 of A at a concentration of 200 g m^{-3} is contacted batchwise with 1.0 kg of fresh adsorbent ($q_{A0} = 0$).
Estimate the equilibrium concentration of the solution. An adsorption isotherm of the Freundlich type is given as

$$q_A\,(\text{g-adsorbate per kg-adsorbent}) = 120\,C_A{}^{0.11}$$

where C_A (g m^{-3}) is the equilibrium concentration of A.

11.2 By single- or three-stage adsorption with an adsorbent, 95% of an adsorbate A in an aqueous solution of C_{A0} needs to be recovered. When the linear adsorption equilibrium is given as

$$q_A = 2.5\,C_A$$

obtain the ratio of the required amount of the adsorbent in single-stage adsorption to that for three-stage adsorption.

11.3 Derive the following adsorption isotherm for an A–B gas mixture of two components, each of which follows the Langmuir-type isotherm:

$$q_A = \frac{q_{Am} a p_A}{1 + a p_A + b p_B}$$

where p_A and p_B are the partial pressures of A and B, respectively, and a and b are constants.

11.4 When the height of the adsorbent bed is 50 cm, under the same operating conditions given in Example 11.2, estimate the break point ($C_A = 0.1\ C_{A0}$) and the length of the adsorption zone z_a.

11.5 A 1.0 cm-i.d. and 50 cm-long chromatography column is packed with gel beads that are 100 μm in diameter. The interparticle void fraction ε is 0.27, and the flow rate of the mobile phase is 20 $cm^3\ h^{-1}$. A retention volume of 20 cm^3 and a peak width W of 1.8 cm^3 were obtained for a protein sample.
Calculate the distribution coefficient K and the Hs value for this protein sample.

11.6 Two proteins in a sample were separated in a gel chromatography column, but the resolution between the two eluted curves was insufficient.
Propose strategies in order to improve the resolution between these two proteins using gel chromatography separation.

11.7 Why does the sandwich ELISA method generally show a higher degree of sensitivity compared with the direct-binding ELISA method?

References

1. Hall, K.R., Eagleton, L.C., Acrivos, A., and Vermeulen, T. (1944) *Ind. Eng. Chem. Fundam.*, **5**, 212.
2. van Deemter, J.J. (1956) *Chem. Eng. Sci.*, **5**, 271.
3. Kubin, M. (1975) *J. Chromatogr.*, **108**, 1.
4. Yamamoto, S., Nomura, M., and Sano, Y. (1987) *J. Chromatogr.*, **394**, 363.

Scopes, R.K. (1994) *Protein Purification – Principles and Practice*, 3rd edn, Springer-Verlag.

Turková, J. (1978) *Affinity Chromatography*, Elsevier.

Wheelwright, S.M. (1991) *Protein Purification*, Hanser.

Further Reading

King, C.J. (1974) *Separation Processes*, McGraw-Hill.

Part III
Practical Aspects in Bioengineering

Biochemical Engineering: A Textbook for Engineers, Chemists and Biologists, Second Edition.
Shigeo Katoh, Jun-ichi Horiuchi, and Fumitake Yoshida.

Companion Website: www.wiley.com\go\katoh\biochem_eng_e2

12
Fermentor Engineering

12.1
Introduction

The term "fermentation," as originally defined by biochemists, means "anaerobic microbial reactions"; hence, according to this original definition, the microbial reaction for wine making is fermentation. However, within the broader industrial sense of the term, fermentation is taken to mean anaerobic as well as aerobic microbial reactions for the production of a variety of useful substances. In this chapter, we use the term fermentation in the broader sense, and include, for example, processes such as the productions of antibiotics, of microbial biomass as a protein source, and of organic acids and amino acids using microorganisms. All of these are regarded as fermentations, and so the bioreactors used for such processes can be called "fermentors." Although the term "bioreactor" is often considered synonymous with fermentor, not all bioreactors are fermentors. The general physical characteristics of bioreactors are discussed in Chapter 7.

As with other industrial chemical processes, the types of laboratory apparatus used for basic research in fermentation or for seed culture, are often different from those of industrial fermentors. For microbial cultures with media volumes of up to perhaps 30 l, glass fermentors equipped with a stirrer (which often is magnetically driven to avoid contamination), and with an air sparger in the case of aerobic fermentation, are widely used. Visual observation is easy with such glass fermentors, the temperature can be controlled by immersing the fermentor in a water bath, and the sparging air can be sterilized using a glass-wool filter or a membrane filter. This type of laboratory fermentor is capable of providing basic biochemical data, but is not large enough to provide the engineering data that are valuable for design purposes. Fermentors of the pilot-plant scale – that is, sized between basic research and industrial fermentors – are often used to obtain the engineering data required when designing an industrial fermentor.

Two major types of fermentors are widely used in industry. The *stirred tank*, with or without aeration (e.g., air sparging) is most widely used for aerobic and anaerobic fermentations, respectively. The *bubble column* (tower fermentor) and its modifications, such as airlifts, are used only for aerobic fermentations, especially of a large scale. The important operating variables of the sparged (aerated)

Biochemical Engineering: A Textbook for Engineers, Chemists and Biologists, Second Edition.
Shigeo Katoh, Jun-ichi Horiuchi, and Fumitake Yoshida.

Companion Website: www.wiley.com\go\katoh\biochem_eng_e2

stirred tank are the rotational stirrer speed and the aeration rate, whereas for the bubble column it is the aeration rate that determines the degree of liquid mixing, as well as the rates of mass transfer.

Stirred tanks with volumes up to a few hundred cubic meters are frequently used. The bubble columns are more practical as large fermentors in the case of aerobic fermentations. The major types of gas sparger include, among others, the single nozzle and the ring sparger (i.e., a circular, perforated tube). Some stirred-tank fermentors will incorporate a mechanical foam breaker that rotates around the stirrer shaft over the free liquid surface. Occasionally, an antifoam agent is added to the broth (i.e., the culture medium containing microbial cells) in order to lower its surface tension. Some bubble columns and airlifts will have large empty spaces above the free liquid surface so as to reduce entrainment of any liquid droplets carried over by the gas stream.

The main reasons for mixing the liquids in the fermentors with a rotating stirrer and/or gas sparging are to

- equalize the composition of the broth as much as possible;
- enhance heat transfer between the heat-transfer surface and the broth, and to equalize the temperature of the broth as much as possible. Depending on whether the bioreaction is exothermic or endothermic, the broth should be cooled or heated via a heat-transfer medium, such as cold water, steam, and other heat-transfer fluids;
- increase the rates of mass transfer of substrates, dissolved gases, and products between the liquid media and the suspended fine particles, such as microbial cells or immobilized cells or enzymes suspended in the medium;
- increase the rates of gas–liquid mass transfer at the bubble surfaces in the case of gas-sparged fermentors.

Details of the mixing time in stirred tanks and its estimation are provided in Section 7.4.4.

Most industrial fermentors incorporate heat-transfer surfaces, which include: (i) an external jacket or external coil; (ii) an internal coil immersed in the liquid; and (iii) an external heat exchanger, through which the liquid is recirculated by a pump. With small-scale fermentors, approach (i) is common, whereas approach (iii) is sometimes used with large-scale fermentors. These heat transfer surfaces are used for

- heating the medium up to the fermentation temperature at the start of fermentation;
- keeping the fermentation temperature constant by removing the heat produced by the reaction, as well as by mechanical stirring;
- batch medium sterilization before the start of fermentation. Normally, steam is used as the heating medium, and water as the cooling medium.

Details of heat transfer in fermentors are provided in Chapter 5.

Industrial fermentors, as well as pipings, pipe fittings, and valves, and all parts that come into contact with the culture media and sterilized air are usually constructed from stainless steel. All of the inside surfaces should be smooth and easily polished in order to help maintain aseptic conditions. All fermentors (other than the glass type) must incorporate glass windows for visual observation. Naturally, all fermentors should have a variety of fluid inlets and outlets, as well as ports for sampling and instrument insertion. Live steam is often used to sterilize the inside surfaces of the fermentor, pipings, fittings, and valves.

Instrumentation for measuring and controlling the temperature, pressure, flow rates, and fluid compositions, including oxygen partial pressure, is necessary for fermentor operation. (Details of instrumentation and control for fermentation are provided in Chapter 13.)

12.2
Stirrer Power Requirements for Non-Newtonian Liquids

Some fermentation broths are highly viscous, and many are non-Newtonian liquids that follow Equation 2.6. For liquids with viscosities up to approximately 50 Pa s, impellers (Figure 7.7a–c) can be used, but for more viscous liquids special types of impeller, such as the helical ribbon-type and anchor-type, are often used.

When estimating the stirrer power requirements for non-Newtonian liquids, correlations of the power number versus the Reynolds number (Re; see Figure 7.8) for Newtonian liquids are very useful. In fact, Figure 7.8 for Newtonian liquids can be used at least for the laminar range, if appropriate values of the apparent viscosity μ_a are used in calculating the Reynolds number. Experimental data for various non-Newtonian fluids with the six-blade turbine for the range of (Re) below 10 were correlated by the following empirical Equation 12.1 [1]:

$$N_p = 71/(\mathrm{Re}) \tag{12.1}$$

where N_p is the dimensionless power number, that is,

$$N_p = \frac{P}{(\rho N^3 d^5)} \tag{12.2}$$

and

$$(\mathrm{Re}) = \frac{N d^2 \rho}{\mu_a} \tag{12.3}$$

in which P is the power requirement ($\mathrm{M\,L^2\,T^{-3}}$), d is the impeller diameter (L), N is the impeller rotational speed ($\mathrm{T^{-1}}$), ρ is the liquid density ($\mathrm{M\,L^{-3}}$), and μ_a is the apparent liquid viscosity defined by Equation 2.6 (all in consistent units). From the above equations

$$P = 71 \mu_a d^3 N^2 \tag{12.4}$$

Although local values of the shear rate in a stirred liquid may not be uniform, the effective shear rate S_{eff} ($\mathrm{s^{-1}}$) was found to be a sole function of the impeller

rotational speed N (s^{-1}), regardless of the ratio of the impeller diameter to tank diameter (d/D), and was given by the following empirical equation [1].

$$S_{\text{eff}} = k_s N \tag{12.5}$$

where S_{eff} is the effective shear rate (s^{-1}) and k_s is a dimensionless empirical constant. (Note that k_s is different from the consistency index K in Equation 2.6.) The values of k_s vary according to different authors; values of 11.5 for the disc turbine, 11 for the straight-blade turbine and pitched-blade turbine, 24.5 for the anchor-type impeller ($d/D = 0.98$), and 29.4 for the helical ribbon-type impeller ($d/D = 0.96$) have been reported [2]. The substitution of S_{eff} for (du/dy) in Equation 2.6 gives Equation 12.6 for the apparent viscosity μ_a:

$$\mu_a = K(S_{\text{eff}})^{n-1} \tag{12.6}$$

Values of the consistency index K and the flow behavior index n for a non-Newtonian fluid can be determined experimentally. For pseudoplastic fluids, $n < 1$.

Example 12.1

Estimate the stirrer power requirement P for a tank fermentor, 1.8 m in diameter, containing a viscous non-Newtonian broth, of which the consistency index $K = 124$, flow behavior index $n = 0.537$, density $\rho = 1050\ \text{kg m}^{-3}$, stirred by a pitched-blade, turbine-type impeller of diameter $d = 0.6$ m, with a rotational speed N of $1\ \text{s}^{-1}$.

Solution

Since k_s for a pitched-blade turbine is 11, the effective shear rate S_{eff} is given by Equation 12.5 as

$$S_{\text{eff}} = 11 \times 1 = 11\ \text{s}^{-1}$$

Equation 12.6 gives the apparent viscosity

$$\mu_a = 124 \times 11^{(0.537-1)} = 124/3.04 = 40.8\ \text{Pa s}$$

Then,

$$(\text{Re}) = \frac{0.6^2 \times 1 \times 1050}{40.8} = 9.26$$

This is in the laminar range. The power requirement P is given by Equation 12.4:

$$P = 71 \times 40.8 \times 0.6^3 \times 1^2 = 625\ \text{W}$$

12.3 Heat Transfer in Fermentors

Heat transfer is an important aspect of fermentor operation. In the case where a medium is heat-sterilized *in situ* within the fermentor, live steam is either bubbled through the medium, or is passed through the coil or the outer jacket of the fermentor. In the former case, an allowance should be made for dilution of the medium by the steam condensate. In either case, the sterilization time consists of the three periods: (i) a heating period; (ii) a holding period; and (iii) a cooling period. The temperature is held constant during the holding period. Sterilization rates during these three periods can be calculated using the equations given in Chapter 10.

At the start of the batch fermentor operation, the broth must be heated to the fermentation temperature, which is usually in the range of 30–37 °C, by passing steam or warm water through the coil or the outer jacket.

During fermentation, the broth must be maintained at the fermentation temperature by removing any heat generated by the biochemical reaction(s), or which has dissipated from the mechanical energy input associated with stirring. Such cooling is usually achieved by passing water through the helical coil or the external jacket.

The rates of heat transfer between the fermentation broth and the heat-transfer fluid (such as steam or cooling water flowing through the external jacket or the coil) can be estimated from the data provided in Chapter 5. For example, the film coefficient of heat transfer to or from the broth contained in a jacketed or coiled stirred-tank fermentor can be estimated using Equation 5.13. In the case of non-Newtonian liquids, the apparent viscosity, as defined by Equation 2.6, should be used.

Although the effects of gas sparging and the presence of microbial cells or minute particles on the broth film coefficient are not clear, they are unlikely to decrease the film coefficient. The film coefficient for condensing steam is relatively large, and can simply be assumed (as noted in Section 5.4.4). The film coefficient for cooling water can be estimated from the relationships provided in Section 5.4.1. The resistance of the metal wall of the coil or tank is not large, unless the wall is very thick. However, resistances due to dirt (cf. Table 5.1) are often not negligible. From these individual heat-transfer resistances, the overall heat transfer coefficient U can be calculated using Equation 5.15. It should be noted that the overall resistance $1/U$ is often controlled by the largest individual resistance, in case other individual resistances are much smaller. For example, with a broth the film resistance will be much larger than other individual resistances, and the overall coefficient U will become almost equal to the broth film heat transfer coefficient. In such cases, it is better to use U-values that are based on the area for larger heat transfer resistance.

It should be mentioned here that the cooling coil can also be used for *in situ* media sterilization, by passing steam through its structure.

Example 12.2

A fermentation broth contained in a batch-operated stirred-tank fermentor, 2.4 m in inside diameter D, is equipped with a paddle-type stirrer of diameter (L) of 0.8 m that rotates at a speed $N = 4\,s^{-1}$. The broth temperature is maintained at 30 °C with cooling water at 15 °C, which flows through a stainless steel helical coil that has a 50 mm outside diameter and is 5 mm thick. The maximum rate of heat evolution by biochemical reactions, plus dissipation of mechanical energy input by the stirrer, is 51 000 kcal h^{-1}, although the rate varies with time. The physical properties of the broth at 30 °C were density $\rho = 1000\,kg\,m^{-3}$, viscosity $\mu = 0.013$ Pa s, specific heat $c_p = 0.90$ kcal kg^{-1} °C^{-1}, and thermal conductivity $\kappa = 0.49$ kcal h^{-1} m^{-1} °C^{-1} = 0.000136 kcal s^{-1} m^{-1} °C^{-1}.

Calculate the total length of the stainless steel helical coil that should be installed in the fermentor.

Solution

In the case where the exit temperature of cooling water is 25 °C, the flow rate of water is

$$\frac{51\ 000}{(25-15)} = 5100\ \text{kg}\ \text{h}^{-1}$$

and the average water temperature is 20 °C. As the inside sectional area of the tube is 12.56 cm^2, the average velocity of water through the coil tube is

$$\frac{5100 \times 1000}{(12.56\ \times\ 3600)} = 113\ \text{cm}\ \text{s}^{-1} = 1.13\ \text{m}\ \text{s}^{-1}$$

The water-side film coefficient of heat transfer h_w is calculated by Equation 5.8c.

$$h_w = (3210 + 43 \times 20)\frac{1.13^{0.8}}{4^{0.2}} = 3400\ \text{kcal}\ \text{h}^{-1}\ \text{m}^{-2}\ ^\circ\text{C}^{-1}$$

The broth-side film coefficient of heat transfer h_B is estimated by Equation 5.13 for coiled vessels. Thus

$$(\text{Nu}) = 0.87(\text{Re})^{2/3}(\text{Pr})^{1/3}$$

$$(\text{Re}) = \left(\frac{L^2 N\rho}{\mu}\right) = \frac{0.8^2 \times 4 \times 1000}{0.013} = 197\,000\ (\text{Re})^{2/3} = 3400$$

$$(\text{Pr}) = \left(\frac{c_p \mu}{\kappa}\right) = \frac{0.90 \times 0.013}{0.000136} = 86\ (\text{Pr})^{1/3} = 4.40$$

$$(\text{Nu}) = \left(\frac{h_B D}{\kappa}\right) = 0.87 \times 3400 \times 4.40 = 13\,020$$

$$h_B = \frac{13\,020 \times 0.49}{2.4} = 2660 \text{ kcal h}^{-1}\text{ m}^{-2}\,^\circ\text{C}^{-1}$$

As the thermal conductivity of stainless steel is 13 kcal h^{-1} m^{-1} °C^{-1}, the heat transfer resistance of the tube wall is

$$\frac{0.005}{13} = 0.00038\,^\circ\text{C h m}^2\text{ kcal}^{-1}$$

A fouling factor of 2000 kcal h^{-1} m^{-2} °C^{-1} is assumed. The overall heat transfer resistance $1/U$ based on the outer tube surface is

$$\frac{1}{U} = \frac{1}{2660} + 0.00038 + \frac{1}{[3400(4/5)]} + \frac{1}{2000} = 0.00162$$

$$U = 616 \text{ kcal h}^{-1}\text{ m}^{-2}\,^\circ\text{C}^{-1}$$

The log mean of the temperature differences 15 and 5 °C at both ends of the cooling coil is

$$\Delta t_{lm} = \frac{(15-5)}{\ln(15/5)} = 9.1\,^\circ\text{C}$$

The required heat transfer area (outer tube surface) A is

$$A = \frac{51\,000}{(616 \times 9.1)} = 9.10 \text{ m}^2$$

The required total length L of the coil is

$$L = \frac{9.10}{(0.05\pi)} = 58.0 \text{ m}$$

12.4
Gas–Liquid Mass Transfer in Fermentors

Gas–liquid mass transfer plays a very important role in aerobic fermentation. The rate of oxygen transfer from the sparged air to the microbial cells suspended in the broth or the rate of transfer of carbon dioxide (produced by respiration) from the cells to the air often controls the rate of aerobic fermentation. Thus, a correct knowledge of such gas–liquid mass transfer is required when designing and/or operating an aerobic fermentor.

Resistances to the mass transfer of oxygen and carbon dioxide (and also of substrates and products) at the cell surface can be neglected because of the minute size of the cells, which may be only a few microns. The existence of liquid films or the renewal of a liquid surface around these fine particles is inconceivable. The compositions of the broths in well-mixed fermentors can, in practical terms, be assumed uniform. In other words, mass transfer resistance through the main body of the broth may be considered negligible.

Thus, when dealing with gas transfer in aerobic fermentors, it is important to consider only the resistance at the gas–liquid interface, usually at the surface of gas bubbles. As the solubility of oxygen in water is relatively low (cf. Section 6.2 and Table 6.1), we can neglect the gas-phase resistance when dealing with oxygen absorption into the aqueous media, and consider only the liquid film mass transfer coefficient k_L and the volumetric coefficient $k_L a$, which are practically equal to K_L and $K_L a$, respectively. Although carbon dioxide is considerably more soluble in water than oxygen, we can also consider that the liquid film resistance will control the rate of carbon dioxide desorption from the aqueous media.

Standard correlations for $k_L a$ in an aerated stirred tank and the bubble column were provided in Chapter 7. However, such correlations were obtained under simplified conditions and may not be applicable to real fermentors without modifications. Various factors that are not taken into account in those standard correlations may influence the $k_L a$ values in aerobic fermentors used in practice.

12.4.1 Special Factors Affecting $k_L a$

12.4.1.1 Effects of Electrolytes

It is a well-known fact that bubbles produced by mechanical force in electrolyte solutions are much smaller than those in pure water. This can be explained by reduction of the rate of bubble coalescence due to an electrostatic potential at the surface of aqueous electrolyte solutions. Thus, $k_L a$ values in aerated stirred tanks obtained by the sulfite oxidation method are larger than those obtained by physical absorption into pure water, in the same apparatus, and at the same gas rate and stirrer speed [3]. Quantitative relationships between $k_L a$ values and the ionic strength are available [4]. Recently published data on $k_L a$ were obtained mostly by physical absorption or desorption with pure water.

Culture media usually contain some electrolytes, and in this respect the values of $k_L a$ in these media might be closer to those obtained by the sulfite oxidation method than to those obtained by experiments with pure water.

12.4.1.2 Enhancement Factor

Since respiration by microorganisms involves biochemical reactions, oxygen absorption into a fermentation broth can be regarded as a case of gas absorption with a chemical reaction (as discussed in Section 6.5). If the rate of the respiration reaction were to be fairly rapid, we should multiply k_L by the enhancement factor E (–). However, theoretical calculations and experimental results [5] with aerated stirred fermentors on oxygen absorption into fermentation broth containing resting and growing cells have shown that the enhancement factor is only slightly or negligibly larger than unity, even when an accumulation of microorganisms at or near the gas–liquid interface is assumed. Thus, except for extreme cases, the effect of respiration of microorganisms on $k_L a$ can, in practical terms, be ignored.

12.4.1.3 Presence of Cells

Fermentation broths are suspensions of microbial cells in a culture media. Although we need not consider the enhancement factor E for respiration reactions (as noted above), the physical presence *per se* of microbial cells in the broth will affect the $k_L a$ values in bubbling-type fermentors. The rates of oxygen absorption into aqueous suspensions of sterilized yeast cells were measured in (i) an unaerated stirred tank with a known free gas–liquid interfacial area; (ii) a bubble column; and (iii) an aerated stirred tank [6]. Data acquired with scheme (i) showed that the k_L values were only minimally affected by the presence of cells, whereas for schemes (ii) and (iii), the gas holdup and $k_L a$ values were decreased somewhat with increasing cell concentrations, because of smaller a due to increased bubble sizes.

12.4.1.4 Effects of Antifoam Agents and Surfactants

In order to suppress excessive foaming above the free liquid surface in fermentors, due to materials such as proteins being produced during culture, antifoam agents (i.e., surfactants which reduce the surface tension) are often added to culture media. The use of mechanical foam breakers is preferred in the case of stirred-tank fermentors, however. The effects on $k_L a$ and gas holdup of adding antifoam agents were studied with the same apparatus as was used to study the effects of sterilized cells [6]. Values of k_L obtained in the stirred vessel with a free liquid surface varied little with the addition of a surfactant. In contrast, the values of $k_L a$ and gas holdup in the bubble column and in the aerated stirred tank were decreased greatly on adding very small amounts (<10 ppm) of surfactant (Figure 12.1a). Photographic studies conducted with the bubble column showed that bubbles in pure water were relatively uniform in size, whereas in water that contained a surfactant a small number of very large bubbles mingled with a large number of very fine bubbles. As large bubbles rise fast, while fine bubbles rise very slowly, the contribution of the very fine bubbles to mass transfer seems negligible because of their very slow rising velocity and long residence time. Thus, the $k_L a$ for a mixture of a few large bubbles and many fine bubbles should be smaller than that for bubbles of a uniform size. The same can be said about the gas holdup.

Variations in $k_L a$ and gas holdup in sterilized cell suspensions following the addition of a surfactant are shown in Figure 12.1b and c, respectively [6]. When a very small amount of surfactant was added to the cell suspension, both the $k_L a$ and gas holdup were seen to increase in line with cell concentration. This situation occurred because the amount of surfactant available at the gas–liquid interface was reduced due to it having been adsorbed by the cells. However, when a sufficient quantity of surfactant was added, there was no effect of cell concentration on either $k_L a$ or gas holdup.

12.4.1.5 $k_L a$ in Emulsions

The volumetric coefficient $k_L a$ for oxygen absorption into oil-in-water emulsions is of interest in connection with fermentation using hydrocarbon substrates. Experimental results [7] have shown that such emulsions can be categorized

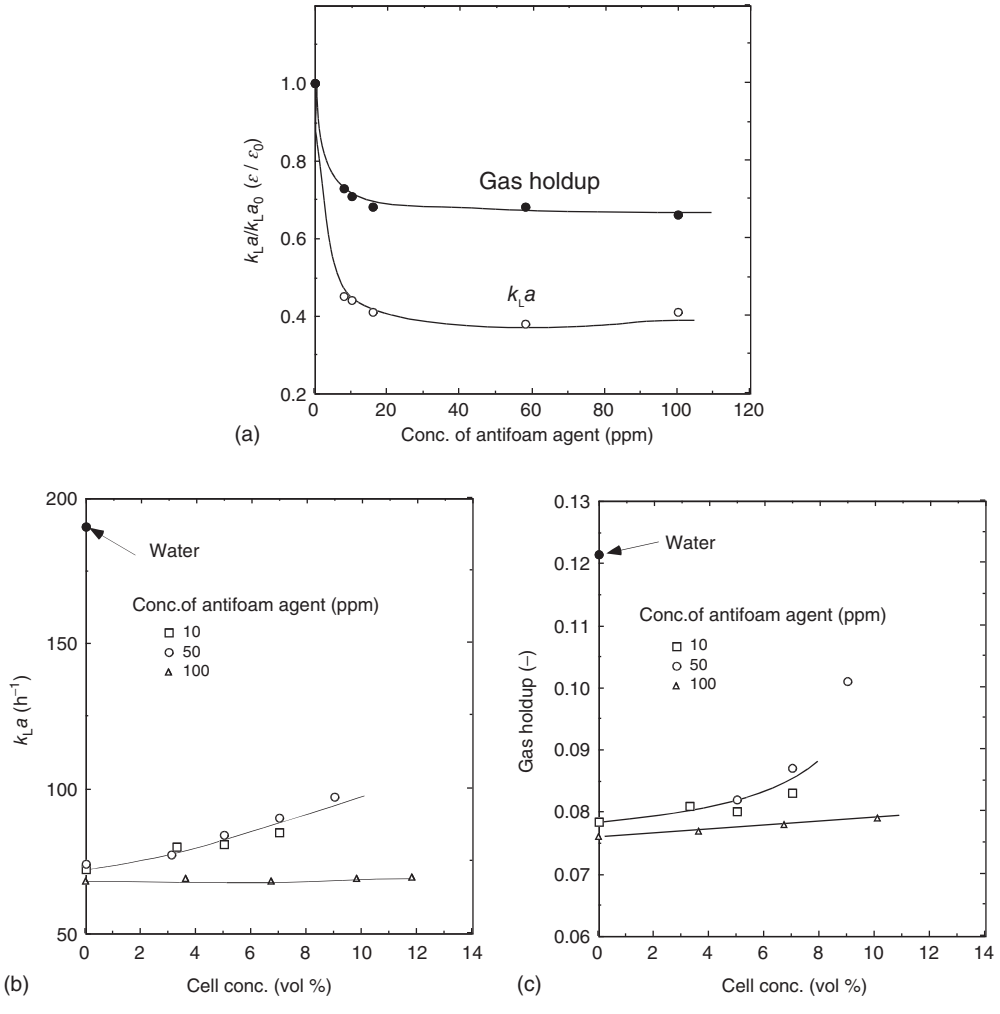

Figure 12.1 (a) Relative values of k_La and gas holdup for water in a bubble column. (b) k_La for cell suspensions in a bubble column. (c) Gas holdup for cell suspensions in a bubble column.

into two major groups, depending on the values of the spreading coefficient s (dyne cm^{-1}) defined as

$$s = \sigma_w - (\sigma_h + \sigma_{h-w}) \tag{12.7}$$

where σ_w is the water surface tension (dyne cm^{-1}), σ_h is the oil surface tension (dyne cm^{-1}), and σ_{h-w} is the oil–water interfacial tension (dyne cm^{-1}).

In the group with negative spreading coefficients (e.g., kerosene-in-water and paraffin-in-water emulsions), the values of k_La in both stirred tanks and bubble columns decrease linearly with an increasing oil fraction. This effect is most

likely due to the formation of lens-like oil droplets over the gas–liquid interface. Subsequent slower oxygen diffusion through the droplets, and/or slower rates of surface renewal at the gas–liquid surface, may result in a decrease in $k_L a$.

In the group with positive spreading coefficients (e.g., toluene-in-water and oleic acid-in-water emulsions), the values of $k_L a$ in both stirred tanks and bubble columns decrease upon the addition of a very small amount of "oil," and then increase with increasing oil fraction. In such systems, the oils tend to spread over the gas–liquid interface as thin films, providing additional mass transfer resistance and consequently lower k_L values. Any increase in $k_L a$ value upon the further addition of oils could be explained by an increased specific interfacial area a due to a lowered surface tension and consequent smaller bubble sizes.

12.4.1.6 $k_L a$ in Non-Newtonian Liquids

The effects of broth viscosity on $k_L a$ in aerated stirred tanks and bubble columns is apparent from Equations 7.37 and 7.41, respectively. These equations can be applied to ordinary non-Newtonian liquids with the use of apparent viscosity μ_a, as defined by Equation 2.6. Although liquid-phase diffusivity generally decreases with increasing viscosity, it should be noted that at equal temperatures, the gas diffusivities in aqueous polymer solutions are almost equal to those in water.

Some fermentation broths are non-Newtonian due to the presence of microbial mycelia or fermentation products, such as polysaccharides. In some cases, a small amount of water-soluble polymer may be added to the broth to reduce stirrer power requirements, or to protect the microbes against excessive shear forces. These additives may develop non-Newtonian viscosity or even viscoelasticity of the broth, which in turn will affect the aeration characteristics of the fermentor. Viscoelastic liquids exhibit elasticity superimposed on viscosity. The elastic constant, an index of elasticity, is defined as the ratio of stress (Pa) to strain (−), while viscosity is shear stress divided by shear rate (Equation 2.4). The relaxation time (s) is viscosity (Pa s) divided by the elastic constant (Pa).

Values of $k_L a$ for viscoelastic liquids in aerated stirred tanks are substantially smaller than those in inelastic liquids. Moreover, less breakage of gas bubbles in the vicinity of the impeller occurs in viscoelastic liquids. The following dimensionless equation [8] (a modified form of Equation 7.37) can be used to correlate $k_L a$ in sparged stirred tanks for non-Newtonian (including viscoelastic) liquids:

$$\left(\frac{k_L a d^2}{D_L}\right) = 0.060\left(\frac{d^2 N\rho}{\mu_a}\right)^{1.5}\left(\frac{dN^2}{g}\right)^{0.19}\left(\frac{\mu_a}{\rho D_L}\right)^{0.5} \times \left(\frac{\mu_a U_G}{\sigma}\right)^{0.6}\left(\frac{Nd}{U_G}\right)^{0.32}[1 + 2.0\,(\lambda N)^{0.5}]^{-0.67} \tag{12.8}$$

in which λ is the relaxation time, all other symbols are the same as in Equation 7.37. The dimensionless product (λN) can be called the Deborah number or the Weissenberg number.

Correlations for $k_L a$ in bubble columns such as Equation 7.41 should hold for non-Newtonian fluids with use of apparent viscosity μ_a. To estimate the effective shear rate S_{eff} (s^{-1}), which is necessary to calculate μ_a by Equation 2.6, the

following empirical equation [9] is useful.

$$S_{\text{eff}} = 50U_G \quad (U_G > 4 \text{ cm s}^{-1}) \tag{12.9}$$

in which U_G (cm s^{-1}) is the superficial gas velocity in the bubble column.

Values of k_La in bubble columns decrease with increasing values of liquid viscoelasticity. In viscoelastic liquids, relatively large bubbles mingle with a large number of very fine bubbles <1 mm in diameter, whereas most bubbles in water are more uniform in size. As very fine bubbles contribute less to mass transfer, the k_La values in viscoelastic liquids are smaller than those in inelastic liquids. Equation 12.10 [10], which is a modified form of Equation 7.45, can correlate k_La values in bubble columns for non-Newtonian liquids, including viscoelastic liquids.

$$\frac{k_L\underline{a}D^2}{D_L} = 0.09(\text{Sc})^{0.5}(\text{Bo})^{0.75}(\text{Ga})^{0.39}(\text{Fr})^{1.0} \times\left[1 + 0.13(\text{De})^{0.55}\right]^{-1} \tag{12.10}$$

$$(\text{De}) = \frac{\lambda U_B}{d_{vs}} \tag{12.11}$$

in which (De) is the Deborah number, λ is the relaxation time (s), U_B is the average bubble rise velocity (cm s^{-1}), and d_{vs} is the volume-surface mean bubble diameter (cm) calculated by Equation 7.42. All other symbols are the same as in Equation 7.45. The average bubble rise velocity U_B (cm s^{-1}) in Equation 12.11 can be calculated by the following relationship:

$$U_B = \frac{U_G(1+\varepsilon)}{\varepsilon} \tag{12.12}$$

where U_G is the superficial gas velocity (cm s^{-1}) and ε is the gas holdup (–). It should be noted that k_La in both Equation 12.10 and in Equation 7.45 is based on the clear liquid volume, excluding bubbles.

12.4.2 Desorption of Carbon Dioxide

Carbon dioxide produced in an aerobic fermentor should be desorbed from the broth into the exit gas. Figure 12.2 [11] shows, as an example, variations with time of the dissolved CO_2 and oxygen concentrations in the broth, CO_2 partial pressure in the exit gas, and the cell concentration during batch culture of a bacterium in a stirred fermentor. It can be seen that CO_2 levels in the broth and in the exit gas increase, while the dissolved oxygen (DO) concentration in the broth decreases.

Carbon dioxide in aqueous solutions exist in three forms: (i) physically dissolved CO_2; (ii) bicarbonate ion HCO_3^-; and (iii) carbonate ion CO_3^{-2}. In the physiological range of pH the latter form can be neglected. The bicarbonate ion HCO_3^- is produced by the following hydration reaction:

$$H_2O + CO_2 \rightarrow HCO_3^- + H^+$$

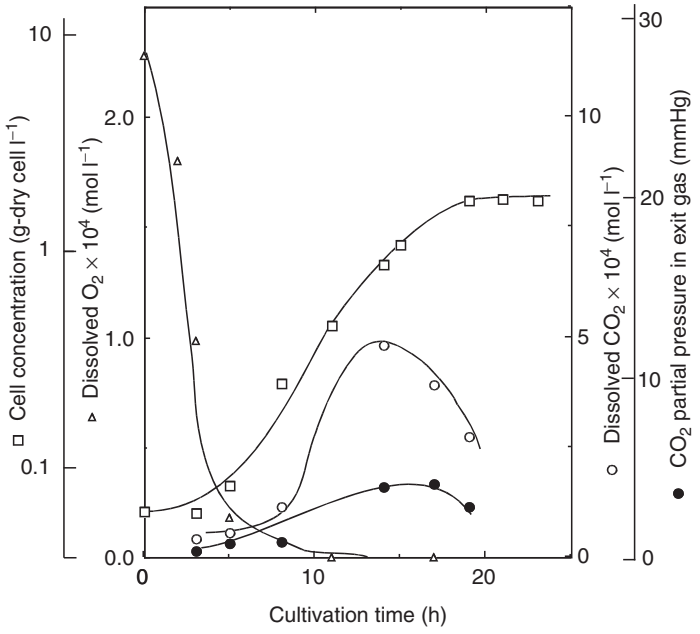

Figure 12.2 Concentration changes during batch culture of a bacterium.

This reaction is rather slow in the absence of the enzyme carbonic anhydrase, which is usually the case with fermentation broths, although this enzyme exists in the red blood cells. Thus, any increase of k_L for CO_2 desorption from fermentation broths due to simultaneous diffusion of HCO_3^- seems negligible.

The partial pressure of CO_2 in the gas phase can be measured by, for example, using an infrared CO_2 analyzer. The concentration of CO_2 dissolved in the broth can be determined indirectly by the so-called "tubing method," in which nitrogen gas is passed through a coiled small tube, made from a CO_2 permeable material, immersed in the broth; the CO_2 partial pressure in the emerging gas can then be analyzed. If a sufficient quantity of nitrogen is passed through the tube, the amount of CO_2 diffusing into the nitrogen stream should be proportional to the dissolved CO_2 concentration in the broth, and independent of the bicarbonate ion concentration.

The values of k_La for CO_2 desorption in a stirred-tank fermentor, calculated from the experimental data on physically dissolved CO_2 concentration (obtained by the above-mentioned method) and the CO_2 partial pressure in the gas phase, agreed well with the k_La values estimated from the k_La for O_2 absorption in the same fermentor, but corrected for any differences in the liquid-phase diffusivities [11]. Perfect mixing in the liquid phase can be assumed when calculating the mean driving potential. In the case of large industrial fermentors, it can practically be assumed that the CO_2 partial pressure in the exit gas is in equilibrium with the concentration of CO_2 that is physically dissolved in the broth. The assumption of either a plug flow or perfect mixing in the gas phase does not have any major effect

on the calculated values of the mean driving potential, and hence in the calculated values of $k_L a$.

12.5 Criteria for Scaling-Up Fermentors

Few steps are available for the so-called "scale-up" of fermentors, starting from the glass apparatus used in fundamental research investigations. Usually, chemical engineers are responsible for building and testing pilot-scale fermentors (usually with capacities of 100 – 1000 l), and subsequently for designing industrial-scale fermentors based on data acquired from the pilot-scale system. In most cases, the pilot-scale and industrial fermentors will be of the same type, but with a several hundred-fold difference in terms of their relative capacities. The size of the stirred tank, whether unaerated or aerated, or of the bubble column to obtain engineering data that would be useful for design purposes, should be at least 20 cm in diameter, and preferably larger.

For anaerobic fermentation, the unaerated stirred tank discussed in Section 7.4 is used almost exclusively. One criterion for scaling-up this type of bioreactor is the power input per unit liquid volume of geometrically similar vessels, which should be proportional to $N^3 L^2$ for the turbulent range and to N^2 for the laminar range, where N is the rotational stirrer speed and L is the representative length of the vessel.

In order to minimize any physical damage to the cells, the product of the diameter d and the rotational speed N of the impeller – which should be proportional to the tip speed of the impeller and hence to the shear rate at the impeller tip – becomes an important criterion for scale-up.

If the rate of heat transfer to or from the broth is important, then the heat transfer area per unit volume of broth should be considered. As the surface area and the liquid volume will vary in proportion to the square and cube of the representative length of vessels, respectively, the heat transfer area of jacketed vessels may become insufficient with larger vessels. Thus, the use of internal coils, or perhaps an external heat exchanger, may become necessary with larger fermentors.

Aerated stirred tanks, bubble columns, and airlifts are usually used for aerobic fermentations. One criterion of scaling-up aerated stirred tank fermentor is $k_L a$, approximate values of which can be estimated by Equation 7.36a or b. For the turbulent range, a general correlation for $k_L a$ in aerated stirred fermentors is of the following type [3]:

$$k_L a = c U_G{}^m (N^3 L^2)^n \tag{12.13}$$

where U_G is the superficial gas velocity over the cross-sectional area of the tank, N is the rotational stirrer speed, and L is the representative length of geometrically similar stirred tanks. For the turbulent regime ($N^3 L^2$) should be proportional to the power requirement per unit liquid volume. One practice in scaling-up this type of fermentors is to keep the superficial gas velocity U_G equal in both fermentors.

In general, a U_G value in excess of 0.6 m s^{-1} should be avoided so as not to allow excessive liquid entrainment [12]. The so-called VVM (gas volume per volume of liquid per minute), which sometimes is used as a criterion for scale-up, is not necessarily reasonable, because an equal VVM might also result in an excessive U_G in larger fermentors. Keeping ($N^3 L^2$) equal might also result in an excessive power requirement and cause damage to the cells in large fermentors. In such cases, the product (NL), which is proportional to the impeller tip speed, can be made equal, if a reduction in $k_L a$ values is permitted. Maintaining the oxygen transfer rate per unit liquid volume (i.e., $k_L a$ multiplied by the mean liquid concentration driving potential ΔC_m) seems equally reasonable. To attain this criterion, many combinations of the agitator power per unit liquid volume and the gas rate are possible. For a range of gas rates, the sum of gas compressor power plus agitator power becomes almost minimal [12].

The main operating factor of a bubble column fermentor is the superficial gas velocity U_G over the column cross section, which should be kept equal in scaling up. As mentioned in connection with Equation 7.41, $k_L a$ in bubble columns <60 cm in diameter will increase with the column diameter D to the power of 0.17. As this trend levels off with larger columns, it is recommended that $k_L a$ values estimated for a 60 cm column are used. If heat transfer is a problem, then heat transfer coils within the column, or even an external heat exchanger, may become necessary when operating a large, industrial bubble column-type fermentor. Scale-up of an internal loop airlift-type fermentor can be achieved in the same way as for bubble column-type fermentors; for external loop airlifts see Section 7.7.

Example 12.3

Two geometrically similar stirred tanks with flat-blade turbine impellers of the following dimensions are to be operated at 30 °C as pilot-scale and production-scale aerobic fermentors.

Scale	Tank diameter and liquid depth (m)	Impeller diameter (m)	Liquid volume (m^3)
Pilot	0.6	0.24	0.170
Production	2.0	0.8	6.28

Satisfactory results were obtained with the pilot-scale fermentor at a rotational impeller speed N of 1.5 s^{-1} and air rate (30 °C) of 0.5 m^3 min^{-1}. The density and viscosity of the broth are 1050 kg m^{-3} and 0.002 Pa s, respectively. Data from the turbine impellers [3] showed that $k_L a$ can be correlated by Equation 12.13, with values $m = n = 2/3$. Using $k_L a$ as the scale-up criterion, estimate the impeller speed and the air rate for the production-scale fermentor that will give results comparable with the pilot-scale data.

Solution

In the pilot-scale fermentor: $U_G = 0.5/[(\pi/4)\ (0.6)^2 \times 60] = 0.0295\ \mathrm{m\ s^{-1}}$.
At equal U_G, the air rate to the production-scale fermentor should be

$$0.0295 \times 60 \times \left(\frac{\pi}{4}\right)(2.0)^2 = 5.56\ \mathrm{m^3\ min^{-1}}$$

With the pilot fermentor $N^3\ L^2 = 1.5^3 \times 0.6^2 = 1.215$.
With this equal value of $N^3\ L^2$ and $L^2 = 2.0^2 = 4$ for the production fermentor, the production fermentor should be operated at

$$N^3 = \frac{1.215}{4} = 0.304 \quad N = 0.672\ \mathrm{s^{-1}}$$

Incidentally, the impeller tip speeds in the pilot and production fementors are calculated as 1.13 and 1.69 $\mathrm{m\ s^{-1}}$, respectively.

A survey [13] of nearly 500 industrial stirred-tank fermentors revealed the following overall averages: tank height/diameter ratio = 1.8; working volume/total volume = 0.7; agitator power/unit liquid volume = 6 $\mathrm{kW\ m^{-3}}$ (2 $\mathrm{kW\ m^{-3}}$ for larger fermentors); impeller diameter/tank diameter = 0.38; impeller tip speed = 5.5 $\mathrm{m\ s^{-1}}$. These data were mainly for microbial fermentors, but include some data on animal cell culture fermentors. According to the same authors, the averages for animal cell culture fermentors were as follows: average impeller tip speed = 0.5–2 $\mathrm{m\ s^{-1}}$; the stirrer power per unit liquid volume = one order-of-magnitude smaller than those for microbial fermentors.

12.6 Modes of Fermentor Operation

Batch operation of fermentors is much more common than continuous operation, although theories for continuous operation are well established (as will be indicated later in this section). The reasons for this are as follows:

1) The operating conditions of batch fermentors can be more easily adjusted to required specific conditions, as the fermentation proceeds.
2) The capacities of batch fermentors are usually large enough, especially in cases where the products are expensive.
3) In the case of batch operation, damages by the so-called "contamination" – that is, the entry of unwanted organisms into the systems, with resultant spoilage of the products – is limited to the particular batch that was contaminated.

In the fed-batch operation of fermentors (which is also commonly practiced), the feed is added either continuously or intermittently to the fermentor, without any product withdrawal, the aim being to avoid any excessive fluctuations of oxygen demand, substrate consumption, and other variable operating conditions.

12.6.1 Batch Operation

In addition to the several phases of batch cell culture discussed in Chapter 4, the practical operation of a batch fermentor includes the pre-culture operations, such as cleaning and sterilizing the fermentor, charging the culture medium, feeding the seed culture, and post-culture operations, such as discharging the fermentor content for product recovery. Consequently, the total operation time for a batch fermentor will be substantially longer than the culture time *per se*. Procedures for sterilizing the medium and sparging air are provided in Chapter 10.

The kinetics of cell growth was discussed in Chapter 4. By combining Equations 4.2 and 4.6, we obtain:

$$\frac{dC_x}{dt} = \mu C_x = \left[\frac{\mu_{max} C_s}{(K_s + C_s)}\right] C_x \tag{12.14}$$

This equation provides the rate of cell growth as a function of the substrate concentration C_s. In case the cell mass is the required product (an example is baker's yeast), the cell yield with respect to the substrate, Y_{xS}, as defined by Equation 4.4, is of interest.

In the case where a product (e.g., ethanol) is required, then the rate of product formation, r_p (kmol h^{-1} (unit mass of cell)$^{-1}$), and the product yield with respect to the substrate Y_{pS}, as well as the cell yield, should be of interest. Then, for unit volume of the fermentor,

$$\frac{dC_s}{dt} = -\left(\frac{\mu}{Y_{xS}} + \frac{r_p}{Y_{pS}}\right) C_x \tag{12.15}$$

in which C_x, a function of time, is given for the exponential growth phase by Equation 4.5, where C_{x0} is the initial cell concentration. A combination of the two equations, and integration, give the following equation for the batch culture time for the exponential growth phase t_b:

$$t_b = \left(\frac{1}{\mu_{max}}\right) \ln\left[1 + \frac{(C_{s0} - C_{sf})}{\{(1/Y_{xS} + r_p/\mu_{max} Y_{pS})\, C_{x0}\}}\right] \tag{12.16}$$

where C_{s0} and C_{sf} are the initial and final substrate concentrations, respectively.

In case only cells are the required product, Equation 12.16 is simplified to

$$t_b = \left(\frac{1}{\mu_{max}}\right) \ln\left[1 + \frac{(C_{s0} - C_{sf})\, Y_{xS}}{C_{x0}}\right] \tag{12.17}$$

12.6.2 Fed-Batch Operation

In a fed-batch culture (semi-batch culture, see Figure 7.1b), a fresh medium that contains a substrate but no cells is fed to the fermentor, without product removal. The fed-batch operation has special importance in biotechnology, as it is the most

frequently used in industrial-scale microbial and animal cell cultures. The fed-batch operation is regarded as a type of *batch* operation where a medium containing a substrate is *fed* into a fermentor without product harvest. In fed-batch culture, the fresh medium is fed to the fermentor either continuously or intermittently. The feed rate is controlled by monitoring, for example, the DO concentration, the glucose concentration, and other parameters. Naturally, the volume of the liquid in the fermentor V (m^3) increases with time. The feed rate F ($m^3\,h^{-1}$), though not necessarily constant, when divided by V is defined as the dilution rate D (h^{-1}). Thus,

$$D = \frac{F}{V} \tag{12.18}$$

where

$$F = \frac{dV}{dt} \tag{12.19}$$

Usually D decreases with time, but not necessarily at a constant rate.

The increase in the total cell mass per unit time is given as

$$\frac{d(C_x V)}{dt} = \frac{C_x dV}{dt} + \frac{V dC_x}{dt} = \mu C_x V \tag{12.20}$$

where C_x is the cell concentration ($kg\,m^{-3}$) and μ is the specific growth rate defined by Equation 4.2. Combining Equations 12.19 and 12.20 and dividing by V, we obtain

$$\frac{dC_x}{dt} = C_x(\mu - D) \tag{12.21}$$

Thus, if D is made equal to μ, the cell concentration would not vary with time. For a given substrate concentration in the fermentor C_s, μ is given by the Monod equation (i.e., Equation 4.6). Alternatively, we can adjust the substrate concentration C_s for a given value of μ. Practical operation usually starts as batch culture and, when an appropriate cell concentration is reached, the operation is switched to a fed-batch culture.

The total substrate balance for the whole fermentor is given as:

$$\begin{aligned}\frac{d(C_s V)}{dt} &= \left(\frac{V dC_s}{dt} + \frac{C_s dV}{dt}\right) \\ &= FC_{si} - \left(\frac{\mu}{Y_{xS}} + \frac{r_p}{Y_{pS}}\right) C_x V\end{aligned} \tag{12.22}$$

where C_{si} is the substrate concentration in the feed, which is higher than the substrate concentration in the fermentor content C_s. Combining Equations 12.19 and 12.22 and dividing by V, we obtain

$$\frac{dC_s}{dt} = D(C_{si} - C_s) - \left(\frac{\mu}{Y_{xS}} + \frac{r_p}{Y_{pS}}\right) C_x \tag{12.23}$$

Fed-batch culture is not a steady-state process, as the liquid volume in the fermentor increases with time and withdrawal of products is not continuous. However, the feed rate and the concentrations of cells and substrate in the broth in a fermentor can be made steady.

The characteristics of the fed-batch culture, shown by Equations 12.21 and 12.23, make it possible to keep the concentrations of the substrate and/or the cell at the desired values. For example, after a batch culture, a feed medium that contains the substrate at a high concentration can be fed, either continuously or intermittently, to the fermentor under a fed-batch operation. The values of the dilution rate and the substrate concentration in the feed medium can be determined using Equation 12.23. Thus, by using the fed-batch operation, the yield and/or productivity can be greatly improved in a variety of areas of biotechnology by controlling the concentrations of substrate and cell. Some examples of where the fed-batch operation can be effectively used are as follows.

1) *High Cell Density Culture*: The fed-batch operation that maintains the substrate concentration at a suitable value for a high cell-growth rate can achieve a high cell concentration ($50-100\,g\,l^{-1}$).
2) *Avoiding Substrate Inhibition, Enzymatic Inhibition, and Catabolite Repression*: When using the fed-batch operation, the concentration of a substrate can be kept at a low value so that substrate inhibition, enzymatic inhibition, or catabolite repression is practically avoided, which results in high productivity [14].
3) *Cultivation of Auxotrophic Mutant*: Microbial processes that use an auxotrophic mutant require control of the concentration of a required nutrient. The fed-batch operation is effective in controlling its concentration by regulating the feeding rate of the required nutrient [15].

Control of the concentrations of substrates and/or cells can be accomplished in many ways (Chapter 13). For example, the feeding of the substrate can be started when the DO concentration rises to a lower predetermined value, which is an indication of inactive respiration of the cell caused by the substrate depression, and then the feeding is halted when the DO reaches an upper DO set point, usually 30–50% of the saturated DO. By repeating this procedure, the substrate concentration is kept approximately at a constant value, and the cells continue to grow to a high cell concentration. Figure 12.3 shows the time course of yeast fermentation by batch and the DO-stat fed-batch culture using glycerol as a limiting substrate [16].

12.6.3 Continuous Operation

Suppose that a well-mixed stirred tank is being used as a fed-batch fermentor at a constant feed rate F ($m^3\,h^{-1}$), substrate concentration in the feed C_{si} ($kg\,m^{-3}$), and at a dilution rate D equal to the specific cell growth rate μ. The cell concentration C_x ($kg\,m^{-3}$) and the substrate concentration C_s ($kg\,m^{-3}$) in the fermentor do not

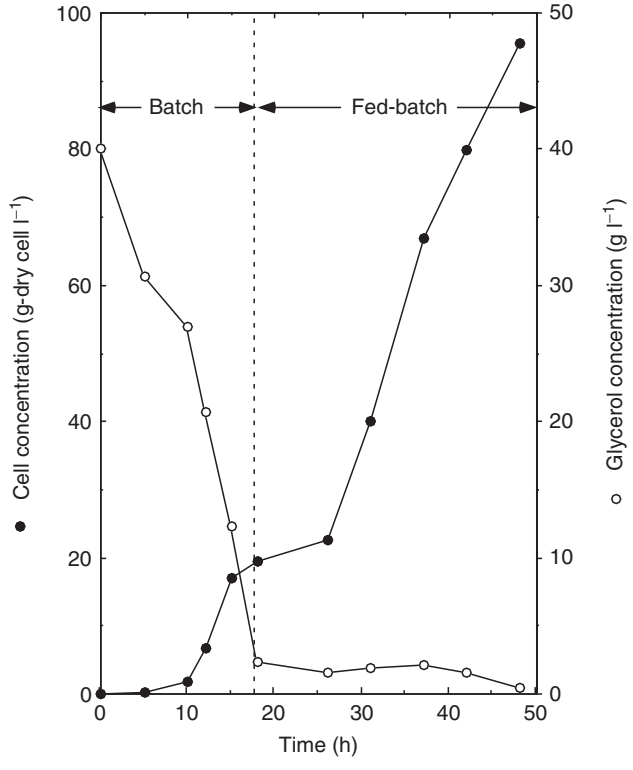

Figure 12.3 Fed-batch culture of yeast cells (on-off DO-stat).

vary with time. This is not a steady-state process, as aforementioned. Then, by switching the mode of operation, part of the broth in the tank is continuously withdrawn as product at a rate P ($m^3\ h^{-1}$) equal to the feed rate F. The values of the C_x and C_s in the withdrawn product should be equal to those in the tank, as the content of the tank is well mixed. The volume of the broth in the tank V becomes constant as P equals F. The operation has now become continuous and steady.

As mentioned in Section 7.2.1, a well-mixed stirred-tank reactor, when used continuously, is termed a continuous stirred-tank reactor (CSTR). Similarly, a well-mixed stirred-tank fermentor used continuously is termed a continuous stirred-tank fermentor (CSTF). If cell death is neglected, the cell balance for a CSTF is given as

$$PC_x = FC_x = \mu C_x V \tag{12.24}$$

From Equations 12.24 and 12.18

$$\mu = D \tag{12.25}$$

The reciprocal of D is the residence time τ of the liquid in the fermentor:

$$\frac{1}{D} = \frac{V}{F} = \tau \tag{12.26}$$

Combination of Equation 12.25 and the Monod equation (Equation 4.6) gives

$$C_s = \frac{K_s D}{(\mu_{max} - D)} \tag{12.27}$$

The cell yield Y_{xS} is defined as

$$Y_{xS} = \frac{C_x}{(C_{si} - C_s)} \tag{12.28}$$

From Equations 12.28 and 12.27, we obtain

$$C_x = Y_{xS}\left[C_{si} - \frac{K_s D}{(\mu_{max} - D)}\right] \tag{12.29}$$

The cell productivity DC_x – the amount of cells produced per unit time per unit fermentor volume – can be calculated from the above relationships.

In the situation where the left-hand side of Equation 12.24 (i.e., the amount of cells withdrawn from the fermentor per unit time) is greater than the right-hand side (i.e., the cells produced in the fermentor per unit time), continuous operation will become impossible. This is the range where D is greater than μ, as can be seen by dividing both sides of Equation 12.24 by V; and such a condition is referred to as a "washout."

Figure 12.4 shows how the concentrations of cells and the substrate and the productivity vary with the dilution rate under steady conditions. Here, the calculated values (all made dimensionless) of the substrate concentration, $C_s^* = C_s/C_{si}$, cell concentration $C_x^* = C_x/(Y_{xS}\, C_{si})$, and productivity DC_x^*/μ_{max} at $\kappa = K_s/C_{si} = 0.01$ are plotted against the dimensionless dilution rate D/μ_{max}. Although it can be seen that productivity is highest in the region where D nears μ_{max}, the operation becomes unstable in this region.

There are two possible ways of operating a CSTF:

- In the *chemostat*, the dilution rate is set at a fixed value, and the rate of cell growth then adjusts itself to the set dilution rate. This type of operation is relatively easy to carry out, but becomes unstable in the region near the washout point.
- In the *turbidostat*, P and F are kept equal but the dilution rate D is automatically adjusted to a preset cell concentration in the product by continuously measuring its turbidity. Compared to chemostat, turbidostat operation can be more stable in the region near the washout point, but requires more expensive instruments and automatic control systems.

12.6.4 Operation of Enzyme Reactors

Bioreactors that use enzymes but not microbial cells could be regarded as fermentors in the broadest sense. Although their modes of operation are similar to those of microbial fermentors, fed-batch operation is seldom practiced for enzyme reactors. The basic equations for batch and continuous reactors for

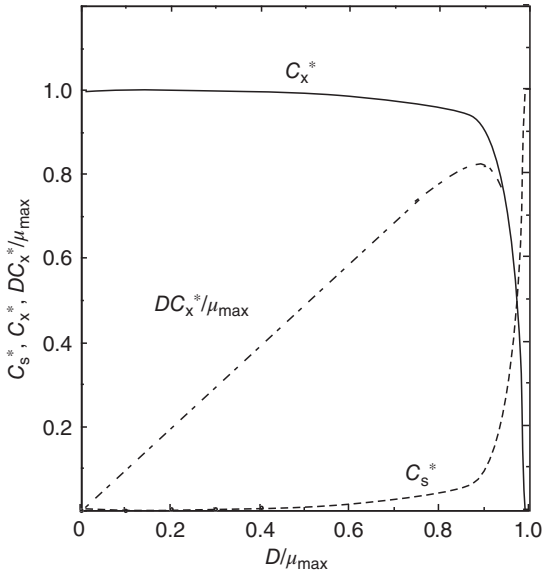

Figure 12.4 Dimensionless concentrations of cells and the substrate and the productivity at $\kappa = 0.01$.

enzyme reactions can be derived by combining material balance relationships and the Michaelis–Menten equation for enzyme reactions.

For batch enzyme reactors, we have

$$\frac{dC_s}{dt} = \frac{V_{max}C_s}{(K_m + C_s)} \tag{12.30}$$

where C_s is the reactant concentration, V_{max} is the maximum reaction rate, and K_m is the Michaelis constant.

For continuous enzyme reactors, that is, CSTR for enzyme reactions, we have Equations 12.31 and 12.32:

$$F(C_{si} - C_s) = \frac{VV_{max}C_s}{(K_m + C_s)} \tag{12.31}$$

$$D(C_{si} - C_s) = \frac{V_{max}C_s}{(K_m + C_s)} \tag{12.32}$$

where F is the feed rate, V is the reactor volume, and D is the dilution rate. In the case where an immobilized enzyme is used, the right-hand sides of Equations 12.31 and 12.32 should be multiplied by the total effectiveness factor E_f.

12.7
Fermentors for Animal Cell Culture

Animal cells, and in particular mammalian cells, are cultured on industrial scale to produce vaccines, interferons, and monoclonal antibodies for diagnostic and therapeutic uses, among others materials.

Animal cells are extremely fragile as they do not possess a cell wall, as do plant cells, and grow much more slowly than microbial cells. Animal cells can be allocated to two groups: (i) anchorage-independent cells, which can grow independently, without attachment surfaces and (ii) anchorage-dependent cells, which grow on solid surfaces. Tissue cells belong to the latter group.

For industrial-scale animal cell culture, stirred tanks can be used for both anchorage-independent and anchorage-dependent cells. The latter are sometimes cultured on the surface of the so-called "microcarriers" suspended in the medium, a variety of which are available commercially. These microcarriers include solid or porous spheres (0.1 to a few millimeters in diameter) composed of synthetic polymers, cellulose, gelatin, or other materials. Anchorage-dependent cells can also be cultured in stirred tanks without microcarriers, although the cell damage caused by shear forces and bubbling must be minimized by using a very low impeller tip speed ($0.5-1\,\mathrm{m\,s^{-1}}$) and reducing the degree of bubbling by using pure oxygen for aeration.

One method of culturing anchorage-dependent tissue cells is to use a bed of packings, on the surface of which the cells grow and through which the culture medium can be passed. Hollow fibers can also be used in this role; here, as the medium is passed through either the inside or the outside of the hollow fibers, the cells grow on the other side. These systems have been used to culture liver cells to create a bioartificial liver (Section 15.4.2).

▶ Problems

12.1 A fermentation broth contained in a batch-operated, stirred-tank fermentor, with a diameter D of 1.5 m, equipped with a flat-blade paddle with a diameter of 0.5 m, is rotated at a speed $N = 3\,\mathrm{s^{-1}}$. The broth temperature is maintained at 30 °C with cooling water at 15 °C, which flows through a stainless steel helical coil, with an outside diameter of 40 mm and a thickness of 5 mm. The heat evolution by biochemical reactions is $2.5 \times 10^4\,\mathrm{kJ\,h^{-1}}$, and dissipation of mechanical energy input by the stirrer is 3.5 kW. Physical properties of the broth at 30 °C: density $\rho = 1050\,\mathrm{kg\,m^{-3}}$, viscosity $\mu = 0.004\,\mathrm{Pa\,s}$, specific heat $c_p = 4.2\,\mathrm{kJ\,kg^{-1}\,°C^{-1}}$, thermal conductivity $\kappa = 2.1\,\mathrm{kJ\,h^{-1}\,m^{-1}\,°C^{-1}}$. The thermal conductivity of stainless steel is $55\,\mathrm{kJ\,h^{-1}\,m^{-1}\,°C^{-1}}$.
Calculate the total length of the helical stainless steel coil that should be installed for the fermentor to function adequately.

12.2 Estimate the liquid-phase volumetric coefficient of oxygen transfer for a stirred-tank fermentor with a diameter of 1.8 m, containing a viscous non-Newtonian broth, with consistency index $K = 0.39$, flow behavior index $n = 0.74$,

density $\rho = 1020\,\mathrm{kg\,m^{-3}}$, surface tension $\sigma = 0.075\,\mathrm{N\,m^{-1}}$, oxygen diffusivity $D_L = 2.1 \times 10^{-9}\,\mathrm{m^2\,s^{-1}}$, superficial gas velocity $U_G = 25\,\mathrm{m\,h^{-1}}$, stirred by a flat-blade turbine of diameter $d = 0.6\,\mathrm{m}$, with a rotational speed N of $1\,\mathrm{s^{-1}}$. An effective shear rate is given by $(\mathrm{d}u/\mathrm{d}y) = 11.5\,N$.

12.3 Estimate the liquid-phase volumetric coefficient of oxygen transfer for a bubble column fermentor, 0.8 m in diameter 9.0 m in height (clear liquid), containing the same liquid as in Problem 12.2. The superficial gas velocity is $150\,\mathrm{m\,h^{-1}}$.

12.4 For an animal cell culture, satisfactory results were obtained with a pilot fermentor, 0.3 m in diameter, with a liquid height of 0.3 m (clear liquid), at a rotational impeller speed N of $1.0\,\mathrm{s^{-1}}$ (impeller diameter 0.1 m) and an air rate (30 °C) of $0.02\,\mathrm{m^3\,min^{-1}}$. The density and viscosity of the broth are $1020\,\mathrm{kg\,m^{-3}}$ and 0.002 Pa s, respectively. The $k_L a$ value can be correlated by Equation 7.36b. When $k_L a$ is used as the scale-up criterion, and the allowable impeller tip speed is $0.5\,\mathrm{m\,s^{-1}}$, estimate the maximum diameter of a geometrically similar stirred tank.

12.5 *Saccharomyces cerevisiae* can grow at a constant specific growth rate of $0.24\,\mathrm{h^{-1}}$ from 2.0 to 0.1 wt% glucose in YEPD medium. It is inoculated at a concentration of 0.01 kg dry-cell $\mathrm{m^{-3}}$, and the cell yield is constant at 0.45 kg dry-cells kg-glucose^{-1}. For how long does the exponential growth phase continue, starting from 2.0 wt% glucose?

12.6 Determine the value of the dilution rate where the maximum cell productivity is obtained in chemostat continuous cultivation.

References

1. Metzner, A.B. and Otto, R.E. (1957) *AIChE J.*, **3**, 3.
2. Bakker, A. and Gates, L.E. (1995) *Chem. Eng. Prog.*, **91** (12), 25.
3. Yoshida, F., Ikeda, A., Imakawa, S., and Miura, Y. (1960) *Ind. Eng. Chem.*, **52**, 435.
4. Robinson, C.W. and Wilke, C.R. (1973) *Biotechnol. Bioeng.*, **15**, 755.
5. Yagi, H. and Yoshida, F. (1975) *Biotechnol. Bioeng.*, **17**, 1083.
6. Yagi, H. and Yoshida, F.J. (1974) *Ferment. Technol.*, **52**, 905.
7. Yoshida, F., Yamane, T., and Miyamoto, Y. (1970) *Ind. Eng. Chem. Proc. Des. Dev.*, **9**, 570.
8. Yagi, H. and Yoshida, F. (1975) *Ind. Eng. Chem. Proc. Des. Dev.*, **14**, 488.
9. Nishikawa, M., Kato, H., and Hashimoto, K. (1977) *Ind. Eng. Chem. Proc. Des. Dev.*, **16**, 133.
10. Nakanoh, M. and Yoshida, F. (1980) *Ind. Eng. Chem. Proc. Des. Dev.*, **19**, 190.
11. Yagi, H. and Yoshida, F. (1977) *Biotechnol. Bioeng.*, **19**, 801.
12. Benz, G.T. (2003) *Chem. Eng. Prog.*, **99** (5), 32.
13. Murakami, S., Nakamoto, R., and Matsuoka, T. (2000) *Kagaku Kogaku Ronbun.*, **26**, 557 (in Japanese).

14. Horiuchi, J., Kamasawa, M., Miyakawa, H., and Kishimoto, M. (1993) *J. Ferment. Bioeng.*, **76**, 212.
15. Tada, K., Kishimoto, M., Omasa, T., Katakura, Y., and Suga, K. (2000) *J. Biosci. Bioeng.*, **90**, 674.
16. Lee, C.Y., Lee, S.J. , Jung, K.H., Katoh, S., and Lee, E.K. (2003) *Process Biochem.*, **38**, 1147.

Further Reading

Aiba, S., Humphrey, A.E., and Millis, N.F. (1973) *Biochemical Engineering*, University of Tokyo Press.
Doran, P.M. (1995) *Bioprocess Engineering Principles*, Academic Press.

13
Instrumentation and Control of Bioprocesses

13.1
Introduction

As with refining and petrochemical processes, bioprocesses must be operated automatically so as to achieve a consistent production of various bioproducts in a cost-effective way. In particular, there is a strong demand to optimize bioprocesses by controlling them automatically to promote labor-saving operations. To achieve this, it is necessary to understand what is happening in a bioreactor (instrumentation) and to properly manipulate the control variables that affect the performance of a bioreactor operation (control).

The following steps are used to operate a bioprocess plant.

1) A control strategy is established, and set-points for control variables are determined (pH, temperature, feed rate, dissolved oxygen (DO), etc.). These are predetermined through laboratory experiments and day-to-day operation.
2) Process variables are measured via instrumentation and the use of sensors and measuring devices.
3) Deviation between the set-point and the measured process variable must be strictly monitored.
4) Deviation between set-point and variables is mitigated via control of the process.

There are several barriers to the successful control of bioprocesses due to particular circumstances that are related to their characteristics: the complexities of microbial metabolisms, the nonlinearity of microbial reactions, the frequent use of batch and fed-batch operations, and the limited availability of sterilizable online sensors for important process variables such as cell and product concentrations. Furthermore, it is difficult to construct mathematical models that can predict the entire range of batch or fed-batch operations that many fermentation processes require.

We can easily imagine the difficulties by comparing bioprocesses with chemical processes that require an inorganic catalyst. For example, the cell concentration in a fermentation process corresponds to the catalyst concentration in a chemical process, which is usually kept at an almost constant state during the chemical

Biochemical Engineering: A Textbook for Engineers, Chemists and Biologists, Second Edition.
Shigeo Katoh, Jun-ichi Horiuchi, and Fumitake Yoshida.

Companion Website: www.wiley.com\go\katoh\biochem_eng_e2

reaction. Cell concentrations, however, typically increase by several tens to hundred times during batch and fed-batch operations as a result of cell growth, and there is no effective way to measure the cell concentration automatically in real time. This means that in order to operate bioprocesses automatically, it must be accomplished with no knowledge of the changes to a critical parameter such as cell concentration.

To overcome this difficulty, many challenges have been met in the fields of bioprocess control. In this chapter, the basic principles of the instrumentation and control of bioprocess are explained.

13.2 Instrumentation of Bioprocesses

In process industries, the following variables are usually measured and monitored through instrumentation.

1) Quality and quantity of raw material and products
2) Utility consumption (power, steam, water, etc.)
3) Process variables (temperature, pH, etc.)
4) Analyses of process safety and environmental protection.

These data are utilized for process control, improvement of product quality, the saving of raw material and energy, and an assurance of safety. In this section, we focus on the measurement of process variables as the basis of bioprocess control.

The instrumentation of processing plants is fully computerized these days, and the use of distributed control systems (DCS) along with advanced network systems makes plant operations highly reliable.

In this section, we describe the instrumentation for monitoring the current status of bioprocess plants, focusing on the measurement of process variables as the basis of bioprocess control.

13.2.1 Process Variables and Sensors in Bioprocess Operations

A process variable is a parameter of the current status of a process under operation, and, therefore, the measurement of process variables is a key to understanding what is happening in a bioreactor and to being able to control the process. Most of the sensors used for the measurements of process variables are inserted into the culture broth of a bioreactor. These must have qualities that will allow them to be repeatedly sterilized (autoclavable) in order to prevent microbial contamination in bioreactors. Naturally, all the sensors must be calibrated before sterilization.

Process variables measured in bioprocess instrumentation can be categorized into one of three groups: physical, chemical, and biochemical variables. Table 13.1 summarizes these three types of variables.

Table 13.1 Process variables measured and estimated in bioprocess instrumentation.

Type of variable	Process variable (primary measurement)	Device	Process variable (secondary information)
Physical	Temperature	Resistance thermometer	Heat generation rate
	Power consumption	Wattmeter	
	Pressure	Pressure gauge	
	Agitation speed		$k_L a$
	Foam	Foaming sensor	
	Viscosity	Rotational viscometer	
	Turbidity	Laser/optical turbidity probe	Specific growth rate
	Gas flow rate	Floatmeter/mass flow meter	Oxygen uptake rate
	Liquid flow rate	Flow meter/weight	
Chemical	pH	Sterilizable pH probe	NH_3 control
	ORP		
	DO		Carbon source requirement
	CO_2/O_2 in off-gas	Infrared spectrophotometer/galvanic cell	RQ, CO_2 evolution rate
Biochemical	Volatile matters	Tubing sensor	
	Glucose	Enzyme thermister	Glucose consumption rate
	NADH	Enzyme thermister	
	Organic acids	Enzyme thermister	

Furthermore, using the primary measurements to obtain the secondary process variables (so-called "gateway sensor") is a form of bioprocess control. For example, the measurement of optical density (primary measurement) can be used for the estimation of cell concentration, and, subsequently, the time course of cell concentration can be employed for the estimation of specific growth rate (secondary

information). Examples of secondary information obtained from primary measurements are shown in Table 13.1.

13.2.1.1 Physical Variables

Temperature The temperature in a bioreactor is an important parameter in any bioprocess, because all microorganisms and enzymes have an optimal temperature at which they function most efficiently. For example, optimal temperature for cell growth is 37 °C for *Escherichia coli* and 30 °C for *Saccharomyces sp*, respectively. Although there are many types of devices for temperature measurements, metal-resistance thermometers or thermistor thermometers are used most often for bioprocess instrumentation. The data of temperature is sufficiently reliable and mainly used for the temperature control of bioreactors and for the estimation of the heat generation in a large-scale aerobic fermentor such as in yeast production or in industrial beer fermentation.

Power Consumption Power consumption sometimes becomes important in industrial bioprocesses, because the power used for aeration and agitation can be highly expensive. The cost of power consumption occupies approximately 15–20% of total production cost in aerobic fermentation processes.

Pressure Most bioreactors are operated at normal atmospheric pressure; however, in some cases with high oxygen requirements, such as high-density cultivation, a bioreactor must be pressurized in order to enhance the oxygen transfer rate. In such cases, the control of vessel pressure is essential.

Agitation The speed of agitation is closely related to the mixing characteristics of a bioreactor and to the oxygen transfer rate ($k_L a$). Careful control of agitation speed is required when using filamentous microorganisms or animal cells, because they are very sensitive to shearing stress.

Foaming In most aerobic microbial processes, some foaming is inevitable. To limit the amount of foaming, an anti-foaming agent (silicone type or alcohol type) is intermittently added into the culture broth. A foaming sensor is required for proper addition of the anti-foaming agent. Without foaming prevention, microorganisms in a fermentation broth will be washed out with foam along with exhaust gas. It is noted that the addition of an anti-foaming agent temporarily decreases the oxygen transfer rate ($k_L a$, refer to Sections 7.4.3 and 12.4.1.4) of a bioreactor because anti-foaming agents depress the generation of dispersed bubbles, which means the decrease of "a" in $k_L a$.

Viscosity The viscosity of a broth is monitored by a rotational viscometer in some fermentation processes that use filamentous bacteria such as in antibiotics production where the viscosity of the culture broth increases as fermentation progresses. Increase in the viscosity of a culture broth results in a decrease in the oxygen transfer rate and the increase of power consumption.

Turbidity Many studies have been focused on developing a sterilizable probe to measure the turbidity of the culture broth, because the turbidity can be an index of cell concentration, which is one of the most important parameters in bioprocess operations. Sterilizable laser or optical turbidity probes are now available and are being used successfully [1]. However, the accuracy of the measurements is insufficient for industrial applications, because the outputs from the probes are affected by some factors including the absorbance of the broth and the bubbles caused by aeration.

Gas-Flow Rate Gas flow rate is measured by a floating meter or a mass flow meter that can measure flow rate independent of pressure and temperature effects. Based on the measurements by flow meters, the flow rate is controlled manually or automatically by manipulating a flow control valve. Gas-flow rate is used to calculate the oxygen uptake rate, the RQ (respiratory quotient) and the CO_2 evolution rate. Biogas-generation rate is measured using a volumetric flow meter in anaerobic digestion (methane fermentation) to monitor methane generation.

Liquid-Flow Rate Liquid flow rate is measured when a medium is fed into a bioreactor in continuous and fed-batch operation. The flow rate of cooling water is also monitored in industrial bioprocessing plants.

13.2.1.2 Chemical Variables

pH The pH in a bioreactor is also an important variable, because all microorganisms or enzymes have pH that is optimal for growth. Sterilizable pH combination electrodes are widely used in bioprocessing instrumentation. pH data are usually reliable and are used mainly to control the pH of a bioreactor. The pH is usually controlled by the addition of acid (HCl, H_2SO_4) and alkali (NaOH, NH_3) solutions that are added automatically; however, CO_2 gas is sometimes used in animal cell culture to avoid cell damage from the addition of acid or alkali agents. The measurement of pH is also used to control NH_3 feeding in glutamic acid fermentation [2].

Oxidation-Reduction Potential Oxidation-reduction potential (ORP) is measured by an ORP probe, which is effective to monitor the redox potential of a bioreactor operated under microaerobic conditions that cannot be successfully measured by a DO probe. The measurements of redox are sometimes influenced by changes in the pH and mineral concentrations of a culture broth.

Dissolved Oxygen The metabolic behavior of a microorganism drastically changes depending on the concentration of the oxygen in a bioreactor. For example, yeasts (facultative microorganism) produce ethanol (alcohol beverage) under anaerobic conditions, but they become baker's yeast under aerobic conditions. Therefore, DO concentration is also a key parameter in aerobic bioprocesses and in activated sludge processes that are widely used for sewage treatment. DO is measured by

sterilizable galvanic or polarographic DO probes that are effectively employed in practical applications. The measurement of DO helps in maintaining DO in a bioreactor and in determining the oxygen transfer rate ($k_L a$, h^{-1}). A sudden increase in DO during aerobic fermentation often suggests the lack of a carbon source (glucose) in a bioreactor. It should be noted that the dissolution of oxygen into a culture broth is easily influenced by the agitation conditions, the operating pressure of a bioreactor, the partial pressure of oxygen in the supply gas, and the temperature.

CO_2/O_2 in the Off-Gas CO_2 evolution from a bioreactor is closely related to the physiological state and the activity of microorganisms in a bioreactor because CO_2 evolves as a result of catabolism and respiration by microorganisms or cells. Therefore, it is helpful to measure the content of CO_2/O_2 in the exhaust gas in order to understand the physiological climate of a bioreactor. The CO_2 and O_2 content in the exhaust gas are taken from the streamline and analyzed by infrared spectrophotometer (CO_2) and galvanic cell probe (O_2). The wet off-gas must be desiccated before being introduced into the gas analyzer.

The analysis of CO_2 and O_2 content is widely employed in industrial bioprocesses. For example, the O_2 consumption rate is known to be proportional to the heat generation and respiration rates. The CO_2 evolution rate and total CO_2 evolution can be an index for the estimation of the carbon source consumption rate and total carbon source consumption. The data are also used for the calculation of the RQ, which is discussed later.

13.2.1.3 Biochemical Variables

Tubing Sensors for Volatile Matter Measurement Several volatile matters such as methanol, aldehyde, and volatile acids are used as substrates, or appear as metabolites in the culture broth. To measure them, a tubing sensor method has been developed [3]. A length of tubing made of sterilizable, hydrophobic, and gas-permeable material such as Teflon is immersed in the culture broth. The tube is connected to a gas analyzer such as gas chromatography, and a carrier gas is continuously provided through the tubing. Volatile matters dissolved in a culture broth are diffused into the tube, transported via carrier gas and detected by the analyzer. The amount of materials diffused into the tube during a certain period is regarded as proportional to the concentration of volatile matters in the broth. This is a useful way to determine volatile matters that cannot otherwise be measured online; however, there are several drawbacks such as the high cost of equipment, a delayed response, and the long-term stability of the tubing, which can be compromised by fouling.

Biosensors Enzymatic analysis of components and products from bioprocesses is widely utilized because this type of analysis is both selective and sensitive. To use enzymes for the automatic analysis and instrumentation of bioprocesses, various sensors using enzymatic reactions, the so-called "biosensors," have been

developed [4]. Biosensors comprise a reaction device that immobilizes an enzyme for a specific reactant and an electrical device to detect the resultant product. They are currently combined on a small chip such as an enzyme thermistor in an electrode. For example, the analysis of blood glucose concentrations in health examination uses this type of biosensor. The biosensor immobilizes glucose oxidase, which converts glucose into gluconolactone and H_2O_2 in proportion to glucose concentration, which can then be electrically detected. This process greatly simplifies the labor involved with analysis; however, at the moment, most biosensors are not sterilizable, and, therefore, they are mainly used off-line in bioprocess control.

13.3 Control of Bioprocesses

The goal of bioprocess control is to maintain important process variables in a bioreactor at a desired level regardless of time-dependent environmental changes. Process control will be performed by the following two steps based on the information obtained through the instrumentation.

1) A check of the deviation between the set point and the measured process variable.
2) Manipulation of the control variable so as to dissolve the deviation.

Process control can be done manually or automatically. Needless to say, current refinery and petrochemical process plants are fully automated; however, it should be noted that manual control by experienced operators still occupies an important portion of bioprocess control due to the difficulties, as previously described.

13.3.1 Schematic View of Instrumentation and Control of Bioprocesses

Figure 13.1 is a schematic representation of a fully instrumented bioreactor system for an industrial-scale fed-batch culture. The system comprises a bioreactor equipped with sensors and pumps, an A/D converter, and a local controller that is linked to a DCS. The current status of a bioreactor is monitored by various sensors as previously mentioned. The analog signal from sensors are converted to digital data by the A/D converter, and sent to the local controller that performs a control action to control a process variable properly. The digital data are also logged or sent to a LAN system through the DCS.

A set-point control is mainly used to control process variables such as temperature and pH. For example, temperature is controlled by heating and cooling by cooling water, and pH is maintained by the addition of acid and alkali. The modification of a set-point will be done manually or by the DCS, which works as a supervisory system.

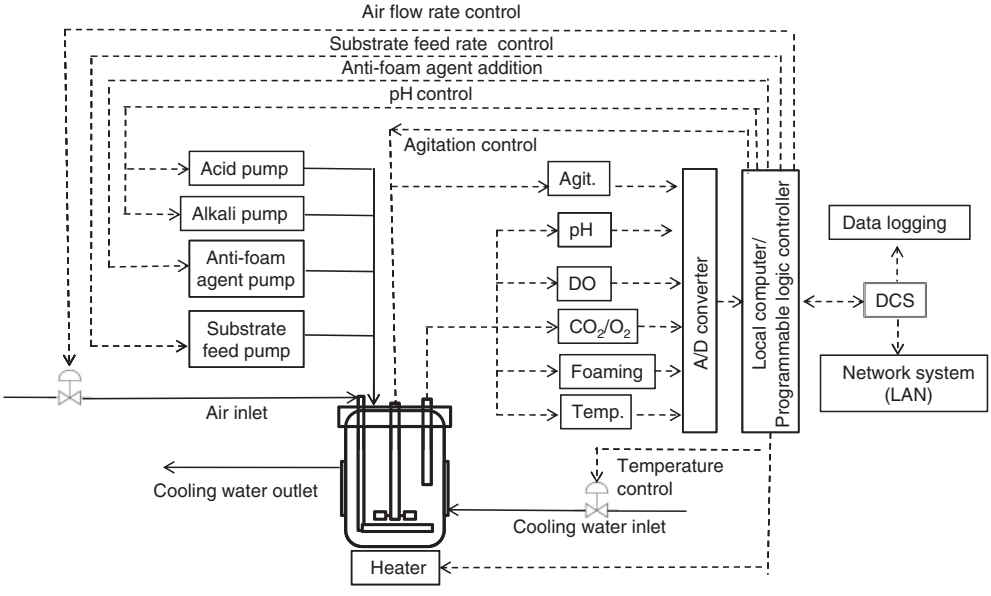

Figure 13.1 Schematic representation of a fully instrumented bioreactor system for an industrial-scale fed-batch culture (solid line – fluid flow and air flow; dotted line – analog/digital signals).

13.3.2 Principles of Control Systems Used for Bioprocesses

13.3.2.1 Closed-Loop System with Feedback

A closed-loop system with feedback, which is illustrated in Figure 13.2, is the central feature of a control system in bioprocess control, as well as in other processing industries. First, a set-point is established for a process variable. Then, the process variable measured in a bioreactor is compared with the set-point value to determine a deviation ε. Based on the deviation, a controller uses an algorithm to calculate an output signal O that determines a control action to manipulate a control variable. By repeating this cycle during operation, successful process control is performed. The controller can be the operator when manual control is being employed.

Suppose the objective is to control the temperature of a bioreactor. The temperature of a bioreactor is measured by instrumentation and compared with a set-point value. Based on the difference between the measured and the set-point temperature, the flow rate of cooling water into a fermentor jacket is increased or decreased by manipulating a control valve of cooling water until the difference between the measured and the set-point temperature becomes zero. By repeating this operation, the temperature of a bioreactor can be kept constant regardless of changes in the outer temperature or from the internal generation of heat.

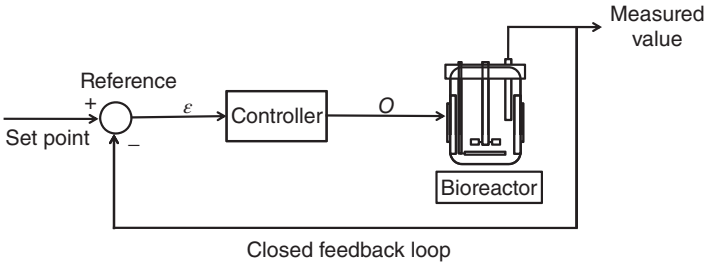

Figure 13.2 Block diagram of a closed feedback control system.

13.3.2.2 **Algorithms for Manipulation of Control Variables**

We know that the temperature control of the shower in a bathroom is not so easy. To have a comfortable shower, a hot water valve needs to be manipulated carefully (control action); however, we usually rely on a trial and error action until the proper temperature of a shower is achieved. How can we achieve the most comfortable shower temperature more quickly? This is a common problem in the control action of many processes that are controlled by a feedback loop. The difficulty comes from a delay in the response, which naturally exists in any process – in other words, the dynamic characteristics of a process. Therefore, the control action should be determined based on the dynamics of the process. In particular, some bioprocesses are known to have serious delays in response.

There are two frequently used algorithms to determine the control action in a feedback control system for bioprocess control, an on–off (two-positioned) control, and a PID (proportional-integral-derivative) control.

On–Off (Two-Positioned) Control An on–off (two-positioned) controller is an algorithm that has two manipulating actions: completely ON or completely OFF. Here, the controller gives the ON signal when the deviation exceeds a threshold value and the OFF signal when the deviation falls below another threshold value. Automatic on–off valves or switches are usually employed in actual processing plants in order to perform on–off (two-positioned) control.

Figure 13.3 illustrates a typical control action (below) and the response of a process variable (above) in an on–off control system. As a result of on–off control, the response of a process variable inevitably becomes oscillatory around a set-point (overshoot and hunting). Thus, the precise control of a process variable is difficult to achieve using an on–off control system, and, therefore, the on–off control can be applicable only when the minimum and maximum values of the response are acceptable for successful operation of the bioprocess. To decrease the oscillation around a set-point, a differential gap (or a dead zone) is normally used to determine a threshold value.

For example, when the set-point of a bioreactor temperature is 37 °C, if cooling water is ON at 39 °C and OFF at 35 °C, the differential gap (2 h in Figure 13.3) is 4 °C. The proper differential gap is usually determined by trial and error, but once

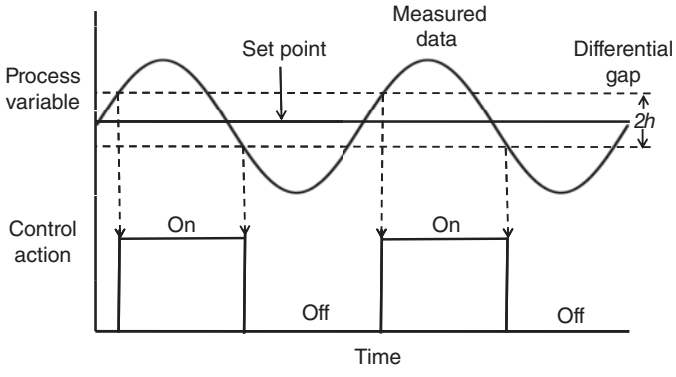

Figure 13.3 Control action and response of an on–off controller with differential gaps.

the proper differential gap for each process variable is established, the accuracy of control will be significantly improved.

The on–off control is a simple and cheap algorithm for manipulating a control variable, and, therefore, it has been applied to bioprocess controls such as temperature control and pH control.

Proportional-Integral-Derivative Control The most common algorithm for control action in the feedback loop of processing industries is the PID control, which is a combination of proportional action (P), integral action (I), and differential action (D).

First, the deviation ε between the set-point and the measured process variable is calculated.

$$\varepsilon = \text{set-point} - \text{measured value} \tag{13.1}$$

To improve the accuracy of ε, a data smoothing method such as a moving average is applied to the measured data as required.

A proportional action (P action) provides an output signal O in proportion to the deviation ε according to the following equation.

$$O = O_0 + K_p \varepsilon \tag{13.2}$$

where, K_p is the proportional gain and O_0 is the control action when the deviation (ε) is zero. By choosing K_p properly, successful control can be achieved. P action is apparently similar to the manual action by an operator and is the basis of a feedback control system. However, a steady-state deviation between the set-point and the measured process variable, the so-called "off-set" is observed in many cases (Figure 13.6). Generally, the increase of K_p decreases the off-set, while the stability of the system becomes spoiled. Furthermore, the response of P action is usually not so quick.

An integral action (I action) gives an output signal O in proportion to the integration (sum) of the deviation ε according to the following equation.

$$O = O_0 + \frac{K_P}{T_I}\int \varepsilon dt \tag{13.3}$$

where T_I is an integration time constant. By introducing the integral action, an off-set in a P action is effectively canceled since the $\int \varepsilon dt$ increases as far as the off-set exists. I action is usually used in combination with P action as a PI control.

A differential action (D action) provides an output signal O in proportion to the derivative of the deviation ε − that is, the changing rate of ε according to the following equation.

$$O = O_0 + K_P T_D \frac{d\varepsilon}{dt} \tag{13.4}$$

where, T_D is a differential time constant. As can be seen in the equation, a differential action works only when the deviation of ε is changing. If the changing rate of ε is high, the output signal will be larger, resulting in a quicker response of the output. Actually, the D action cannot be used independently since $d\varepsilon/dt$ is calculated based on the change of ε that contributes P action and I action.

However, the ideal control algorithm would have no overshoot, no offset, and a quick response characteristic. For this purpose, a proportional action (P), an integral action (I), and a differential action (D) were combined as a PID controller as follows.

$$O = O_0 + K_P\left(\varepsilon + \frac{1}{T_I}\int \varepsilon dt + T_D\frac{d\varepsilon}{dt}\right) \tag{13.5}$$

Figure 13.4 shows a conceptual diagram of a PID algorithm in the feedback control of a bioreactor. First, a set-point and parameters K_p, T_I, and T_D are given to a PID controller. During operation, the process variable in a bioreactor is measured and returned to determine ε. Then, a proportional action (P), an integral action (I), and a differential action (D) are calculated independently. Finally, they are combined according to Equation 13.5, and the output O is determined. The O (normalized between 0 and 1) is used to manipulate control equipment such as a control valve that can actuate the opening of a valve in response to the O value. By repeating this operation at certain intervals during operation, PID control is performed. Automatic control valves are usually equipped in actual process plants in order to perform the PID control.

A key to the successful application of a PID control is the tuning of parameters, K_p, T_I, and T_D in Equation 13.5. To tune them properly, the Ziegler–Nichols method is used, which includes an ultimate-gain method and a step-response method.

The ultimate gain method is performed by the following steps.

1) Set only the P control by setting $T_I = \infty$ and $T_D = 0$;
2) increase K_p until continuous oscillations occur;

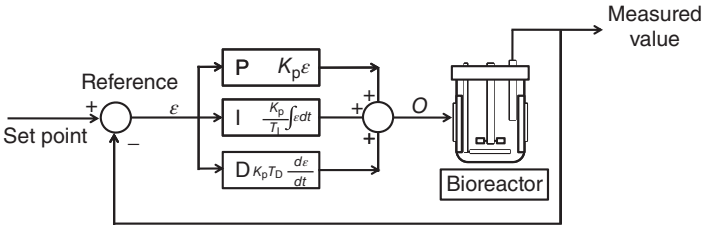

Figure 13.4 Block diagram of a PID controller.

3) record the ultimate gain of K_p when oscillations occur as K_c and the oscillation cycle time, T_c; and
4) Determine parameters according to Table 13.2.

The step response method uses the process response to the step change of input as illustrated below.

The step response method is performed using the following steps.

1) Draw a straight slope line (dotted line in Figure 13.5) so as to fit a step response curve.
2) Determine the slope, R, of the slope line and a lag time, L, as graphically shown in Figure 13.5.
3) Determine the parameters according to Table 13.3.

Figure 13.6 compares the typical response of P, PI, and PID controllers against the step change of a set-point. As can be seen, a well-tuned PID controller realizes

Table 13.2 Determination of parameters of PID control by ultimate gain method.

	K_p	T_I	T_d
P control	$0.5K_c$	∞	0
PI control	$0.45K_c$	$0.83\ T_c$	0
PID control	$0.6K_c$	$0.5\ T_c$	$0.125\ T_c$

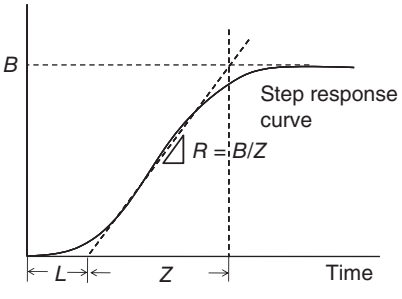

Figure 13.5 Step response curve for the determination of PID parameters.

Table 13.3 Determination of parameters of PID control by step response method.

	K_p	T_I	T_d
P control	$1/LR$	∞	0
PI control	$0.9/LR$	$3.5L$	0
PID control	$1.2/LR$	$2.0L$	$0.5L$

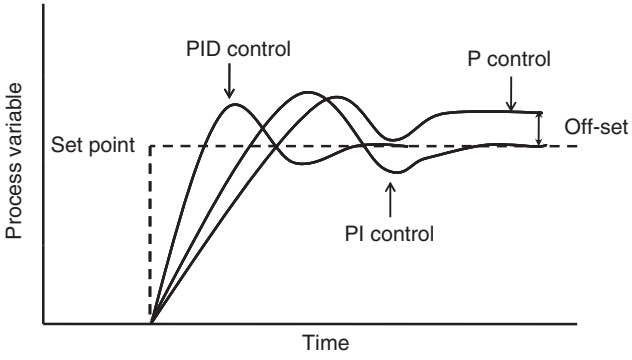

Figure 13.6 Responses of a P controller, a PI controller, and a PID controller for the step change of set-points.

a quick response with minimum off-set. For more information, please refer to the Further Reading section at the end of the chapter.

13.3.3 Examples of Bioprocess Control

Table 13.4 summarizes the typical applications of automatic control in bioprocess operation.

13.3.3.1 pH and Temperature Control

As previously mentioned, the control of pH and temperature is of great importance in any bioprocess, since all biocatalysts have their optimal pH and temperature for cell growth and product formation. pH is usually controlled by an alkali/acid addition using an on–off control (laboratory-scale) or a PID control (industrial scale) based on a signal from a pH probe, although the CO_2 gas is supplied for the pH control of animal cell culture since the addition of alkali/acid causes serious damages against mammalian cells. Temperature is also controlled by an on–off control (laboratory-scale) or a PID control (industrial scale); however, the PID control is essential for the temperature control of a large-scale aerobic bioreactor due to the delayed response and a difficulty in removing heat generated in a bioreactor accompanied with biological reactions.

Table 13.4 Typical applications of automatic control in bioprocess operation.

Bioprocess	Strategy	Process variable	Control variable	Method
Various	pH control	pH	Alkali/acid addition	ON–OFF control, PID
Animal cell culture	pH control	pH	CO_2 supply	PID
Various	Temperature control	Temperature	Heater/cooling water	ON–OFF control, PID
Aerobic processes	DO control	DO	Agitation, aeration rate, internal pressure	PID
Baker's yeast production by fed-batch operation	RQ control	CO_2/O_2	Glucose feed rate	PID
Glutamic acid fermentation by fed-batch operation	pH stat	pH	NH_3 supply	ON–OFF control, PID
		Total CO_2 evolution	Glucose feed rate	PID
High density culture of *E. coli*	DO stat	DO	Glucose feed rate	ON–OFF control, PID

13.3.3.2 DO Control

In aerobic fermentations, DO control is extremely important as previously mentioned. In many cases, the lower limits of DO, which becomes the set-point of DO in a control system, is experimentally determined for each case. For example, it is known that critical oxygen concentrations to maintain aerobic metabolism are approximately 0.008 mmol l^{-1} for *E. coli* and 0.004 mmol l^{-1} for *Saccharomyces sp*. Then, the agitation rate and/or aeration rate are increased so as not to lower the set-point during cultivation. Naturally, an increase in the agitation rate and/or in the aeration rate will increase the $k_L a$ in a bioreactor. The manipulation of the agitation rate and aeration rate is achieved according to the PID algorithm. However, a complicated algorithm will be required when the agitation rate, the aeration rate, and the operating pressure are simultaneously manipulated for DO control.

13.3.3.3 Respiratory Quotient

RQ is the molar ratio of CO_2 that evolves from the consumed O_2 during fermentation and can be defined as follows [5, 6].

$$\mathrm{RQ} = \frac{\text{evolved } CO_2 \text{ (M)}}{\text{consumed } O_2 \text{ (M)}} \tag{13.6}$$

If an aerobic metabolism is dominant in a fermentor, the RQ value becomes 1.0 according to the following chemical equation.

$$C_6H_{12}O_6 + 6O_2 \rightarrow 6CO_2 + 6H_2O$$

However, if an anaerobic metabolism such as ethanol fermentation occurs in a fermentor in the presence of high concentration of glucose, the RQ value becomes larger than 1.0, known as the Crabtree effect. This is because CO_2 evolves without O_2 consumption as follows.

$$C_6H_{12}O_6 \rightarrow 2C_2H_5OH + 2CO_2$$

Thus, the RQ value can be used to estimate the metabolic status in an aerobic bioreactor. In practice, the RQ value can be determined based on the analysis of CO_2 and O_2 in the off-gas from a bioreactor. There may be difficulty in calculating the RQ due to the noise of measured data when the CO_2 content in the off-gas is relatively low compared with the O_2 content in the supply of air (20.91%).

The RQ control, where the sugar-feeding rate is controlled so as to maintain the RQ value at approximately 1.0, is the distinct control method in aerobic fed-batch cultivation such as with baker's yeast production. By keeping the RQ at 1.0 during the fed-batch operation, cell production with a high yield will be achieved.

13.3.3.4 pH Stat

When an NH_3 solution is used as a nitrogen source of fermentation, the consumption of NH_3 decreases the pH of the culture broth. A pH stat control utilizes the pH change as a process variable where the NH_3 addition is manipulated so as to keep the pH value constant during fermentation. The pH stat is often employed in a fed-batch cultivation of industrial glutamic acid production (high NH_3 consuming fermentation) using molasses as a feedstock.

13.3.3.5 DO Stat

A DO stat is used to manipulate the glucose feed rate of a fed-batch culture with a high oxygen requirement such as a high cell density culture of *E. coli*. Glucose feeding, which will decrease the DO value in a fermentor, is on when the DO value exceeds an upper set-point. Glucose feeding is off when the DO value falls below the lower set-point. This regime is repeated until the end of fermentation. By using the DO stat, unfavorable byproduct formations such as acetic acid can be prevented.

13.4 Advanced Control of Bioprocesses

The physiological state and concentration of microorganisms in a batch or a fed-batch process change as a fermentation progresses; therefore, it is desirable to determine current control strategy (set-point) in real time based on current process variables. However, the limited availability of online sensors to measure

important variables and the lack of a mathematical model that can cover the entire range of fermentation processes make it extremely difficult.

To overcome these difficulties, various advanced control methods specialized in bioprocess control have been developed.

13.4.1 Optimization and Control of Bioprocesses

Mathematical optimization always requires a deterministic process model to predict the future behavior of a process. However, as previously mentioned, it is difficult to construct mathematical models that can cover the entire range of fermentation due to the complexity of intracellular metabolic reactions. As an alternative to the deterministic mathematical models, Kishimoto *et al.* proposed a statistical procedure that uses linear multiple regression models [7], as shown below, instead of a deterministic mathematical model such as a Monod equation.

$$\mu = \mu_a + a_1(X - X_e) + a_2(S - S_e) \tag{13.7}$$

$$\gamma = \gamma_b + b_1(X - X_e) + b_2(S - S_e) \tag{13.8}$$

$$\rho = \rho_c + c_1(X - X_e) + c_2(S - S_e) \tag{13.9}$$

Here, μ, ν, and ρ represent a specific growth rate, a specific substrate consumption rate, and a specific product formation rate, respectively. X_e and S_e are the mean values of data used for regression analysis and a_i, b_i, and c_i are the coefficients in the regression models that are determined based on selected operating data in a database. This model was linked with the dynamic programming method and successfully applied to the simulation and online optimization of glutamic acid production and Baker's yeast production.

13.4.2 Application of Artificial Intelligence (AI) Technology to Bioprocess Control

The operational conditions of industrial fermentation processes are often optimized through knowledge gained during repeated operations under the control of highly skilled operators. While such empirical knowledge-based operations can be considered useful from a practical viewpoint, it is difficult to adapt them to computer control because the skills involved often cannot be quantified or incorporated into a traditional control system. To overcome this shortcoming, artificial intelligence (AI) approaches including fuzzy control, artificial neural network (ANN), and expert systems have been introduced into the modeling and control of bioprocesses over the last two decades [8].

13.4.2.1 Fuzzy Control

Fuzzy control, which is based on fuzzy sets theory proposed by Zadeh [9], can easily utilize empirical knowledge gained from skilled operators by employing

membership functions and IF ~ THEN rules and can infer in a manner similar to humans based on min–max operation. Fuzzy modeling and control have been extensively examined in various biological processes, in which qualitative information such as operators' know-how or physiological states of microorganisms plays significant roles in the actual operation [10]. It has proved to be effective for the online control of various biological processes and recently, several industrial applications of fuzzy control, including large-scale fermentor control [11], have been reported.

13.4.2.2 **Artificial Neural Network**

An ANN is an information technology inspired by the mechanisms of the neuronal system in the brain. The ANN has been extensively applied to the modeling of various biological processes because of its superior ability to model nonlinear and multivariable systems. The ANN is a data-driven model, which can be constructed by a learning procedure such as a back propagation algorithm employing input–output data; therefore, it requires only operating data in order to establish a model. The ANN approach was useful and successfully applied to the modeling where detailed information on the biological phenomena or the reaction mechanism is not sufficiently available [12].

13.4.2.3 **Expert System**

An expert system is a computer program to reproduce a problem-solving manner according to an expert's knowledge and inference procedures in a computer system. Expert systems have been used for fault diagnosis in bioprocess operations, the improvement of medium composition, and the optimization of culture conditions, since it can handle a large amount of information and data concerning bioprocess operation and optimization [13].

▶ Problems

13.1 Summarize the difference between bioprocesses and chemical processes in terms of process control.

13.2 Give the operating principle of the following sensors in a few sentences.
a. Resistance thermometer
b. Galvanic dissolved oxygen probe
c. pH electrode.

13.3 Explain the reason why a proportional control (P action) results in the off-set between the set-point and the measured process variable at a steady state.

13.4 Determine the parameters, K_p, T_I, and T_D in PID controller by the ultimate gain method when the ultimate gain K_c and the oscillation cycle time, T_c, are 4.0 and 30 s, respectively.

13.5 Calculate RQ value based on the analysis of the inlet air and the exhaust gas as follows.

– *Inlet Air*: O_2, 20.90%; CO_2, 0.01%
– *Outlet Gas*: O_2, 18.30%; CO_2, 2.90%.

References

1. Zhong, J.-J., Fujiyama, K., Seki, T., and Yoshida, T. (1993) *Biotechnol. Bioeng.*, **42**, 542.
2. Nakamura, T., Kuratani, T., and Morita, Y. (1985) Fuzzy control application to glutamic acid fermentation. Proceedings of IFAC Modelling and Control of Biotechnology Processes, pp. 211–215.
3. Dairaku, K. and Yamane, T. (1979) *Biotechnol. Bioeng.*, **21**, 1671.
4. Clarke, D.J., Blake-Coleman, B.C., Calder, M.R., Carr, R.J.G., and Moody, S.C. (1984) *J. Biotechnol.*, **1**, 135.
5. Aiba, S., Nagai, S., and Nishizawa, Y. (1976) *Biotechnol. Bioeng.*, **18**, 1001.
6. Wang, H., Cooney, C.L., and Wang, D.I.C. (1977) *Biotechnol. Bioeng.*, **19**, 69.
7. Kishimoto, M., Yoshida, T., and Taguchi, H. (1981) *J. Ferment. Bioeng.*, **59**, 43.
8. Konstantinov, K.B. and Yoshida, T. (2004) *Biotechnol. Bioeng.*, **39**, 479.
9. Zadeh, L.A. (1965) *Inf. Control*, **8**, 338.
10. Horiuchi, J. (2002) *J. Biosci. Bioeng.*, **94**, 574.
11. Horiuchi, J. and Hiraga, K. (1999) *J. Biosci. Bioeng.*, **87**, 365.
12. Karim, M.N., Yoshida, T., Rivera, S.L., Saucedo, V.M., Eikens, B., and Oh, G.-S. (1997) *J. Ferment. Bioeng.*, **83**, 1.
13. Kishimoto, M. and Suzuki, H. (1995) *J. Ferment. Bioeng.*, **80**, 58.

Further Reading

Aiba, S., Humphrey, A.E., and Mills, N.F. (1973) *Biochemical Engineering*, 2nd edn, University of Tokyo Press.

Bailey, J.E. and Ollis, D.F. (1986) *Biochemical Engineering Fundamentals*, 2nd edn, McGraw-Hill.

Dunn, I.J., Heinzle, E., Ingham, J., and Prenosil, J.E. (2003) *Biological Reaction Engineering*, 2nd edn, Wiley-VCH Verlag GmbH.

Leigh, J.R. (1987) *Modelling and Control of Fermentation Processes*, IEE Control Engineering Series, vol. 31, Peter Peregrious Ltd.

Shuler, M.L. and Kargi, F. (2002) *Bioprocess Engineering, Basic Concepts*, 2nd edn, Prentice Hall PTR.

Stanbury, P.F., Whitaker, A., and Hall, S.J. (1995) *Principles of Fermentation Technology*, 2nd edn, Pergamon.

Yamane, T. and Shioya, S. (1997) *Intelligent Control of Bioprocesses*, Kyoritsu Shuppan Co., Ltd. (in Japanses).

14
Downstream Operations in Bioprocesses

14.1
Introduction

Certain foodstuffs and pharmaceutical materials are produced by fermentations that include the culture of cells or microorganisms. When the initial concentrations of these products are low, a subsequent separation and purification by the so-called "downstream processing" is required to obtain them in their final form. In many cases, a high level of purity and biological safety are essential for these products. It is also vital that their biological properties are retained, as these may be lost if the processes were to be conducted at an inappropriate temperature or pH, or under incorrect ionic conditions. Consequently, only a limited number of techniques and operating conditions can be applied to the separation of these bioactive materials. Very often, many separation steps (as shown schematically in Figure 14.1) are required to achieve the requirements of high purity and biological safety during industrial bioprocessing. Thus, downstream processing may often account for a large proportion of the production costs.

It should be pointed out here that most biochemical separation methods that have been developed in research laboratories cannot necessarily be practiced on an industrial scale, so as to achieve high recovery levels. Rather, innovative approaches are often necessary in these industrial processes to achieve separations that ensure high purity and good recovery of the target product.

Figure 14.2 [1] shows, as an example, several steps in the production of interferon α. In the first step, *Escherichia coli* (which actually produces the interferon) is obtained genetically, and a strain with high productivity is then selected (screened). Next, the strain is cultivated first on a small scale (flask culture), and then increasingly on larger scales, usually with approximately 10-fold increases in culture volume at each step. For large-scale cultivation, fermentors such as have been described in Chapters 7 and 12 are used. Following fermentation, a series of procedures that are collectively referred to as "downstream processing" are introduced, which involve the ultimate separation and purification of the interferon. Through these stages, the various unit operations that have been described in Chapters 8, 9, and 11 are utilized, the aim being to satisfy the requirements of both high purity and biological safety of the product.

Biochemical Engineering: A Textbook for Engineers, Chemists and Biologists, Second Edition.
Shigeo Katoh, Jun-ichi Horiuchi, and Fumitake Yoshida.

Companion Website: www.wiley.com\go\katoh\biochem_eng_e2

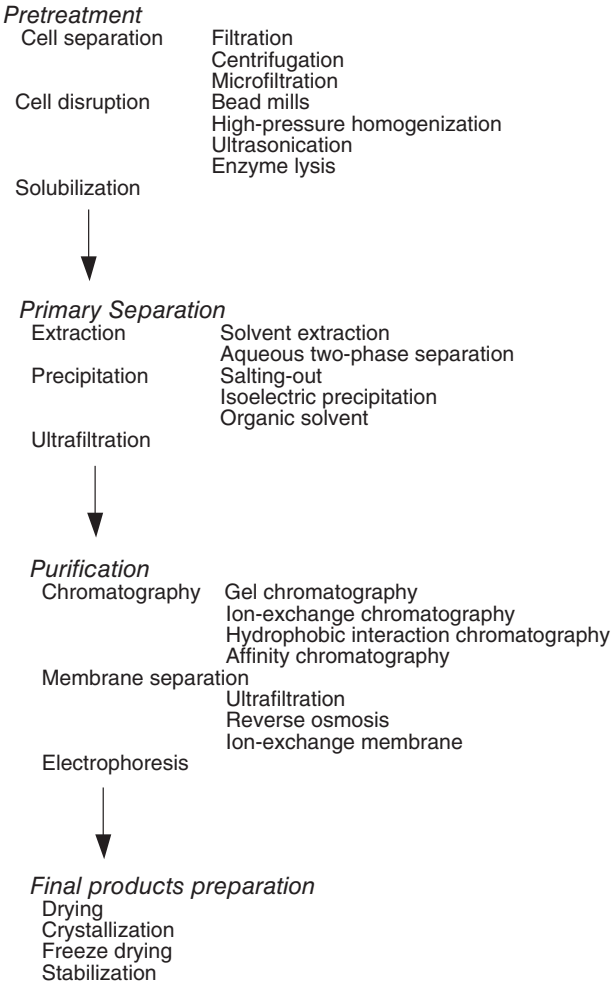

Figure 14.1 Main steps in downstream processing.

The interferon is produced within the *E. coli* cells, which must first be separated from the culture media by using centrifugation. The isolated cells are then solubilized by cell disruption, after which the fraction containing interferon is concentrated by salting-out. Two subsequent procedures using immunoaffinity and cation-exchange chromatography raise the purity of the interferon 1000-fold.

An alternative approach is taken in the production of monosodium glutamate (MSG) which, unlike interferon, is secreted into the fermentation broth. The stages of downstream processing for MSG are shown in Figure 14.3. Again, a variety of unit operations, including centrifugation, crystallization, vaporization, and fixed-bed adsorption, are used in this process.

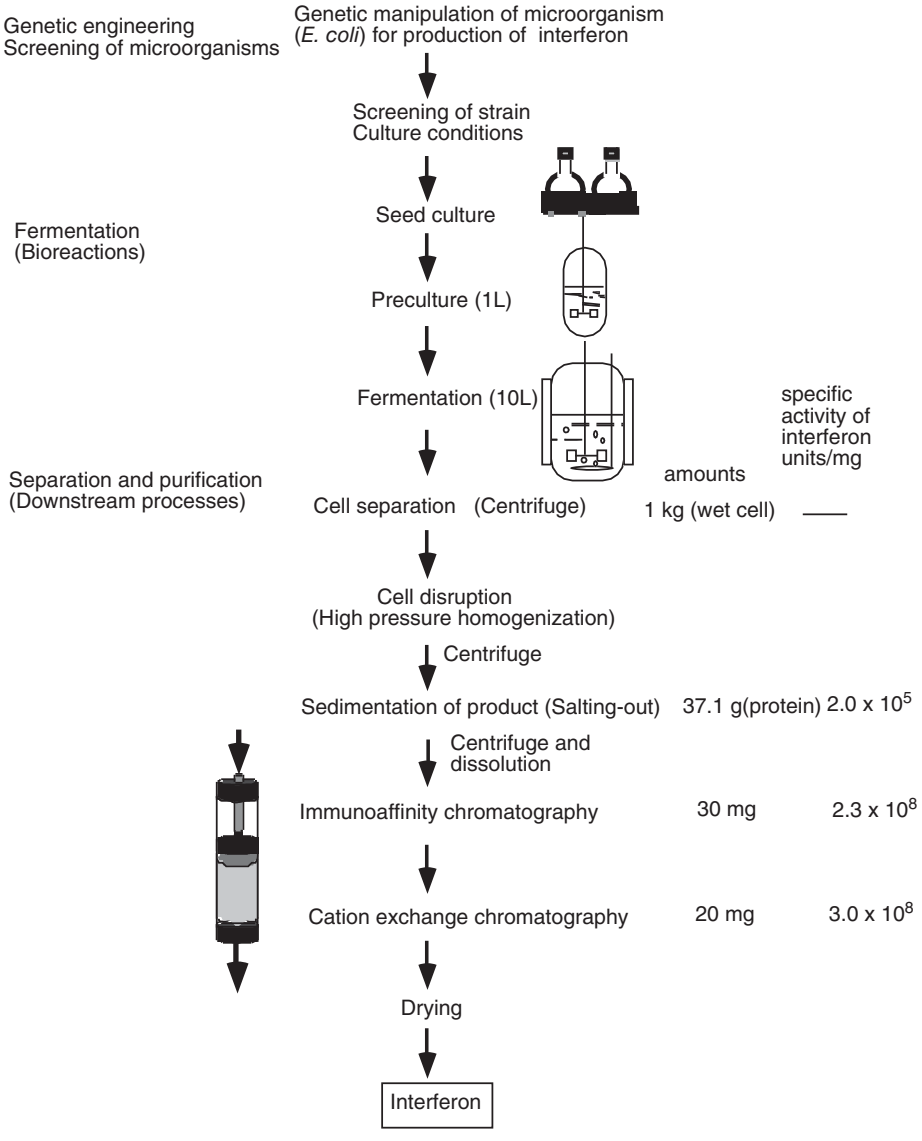

Figure 14.2 The steps of interferon α production.

When planning an industrial-scale bioprocess, the main requirement is to scale up each of the process steps. As the principles of the unit operations used in these downstream processes have been outlined in previous chapters, at this point we discuss only examples of practical applications and scaling-up methods of two unit operations that are frequently used in downstream processes: (i) cell separation by filtration and microfiltration and (ii) chromatography for fine purification of the target products.

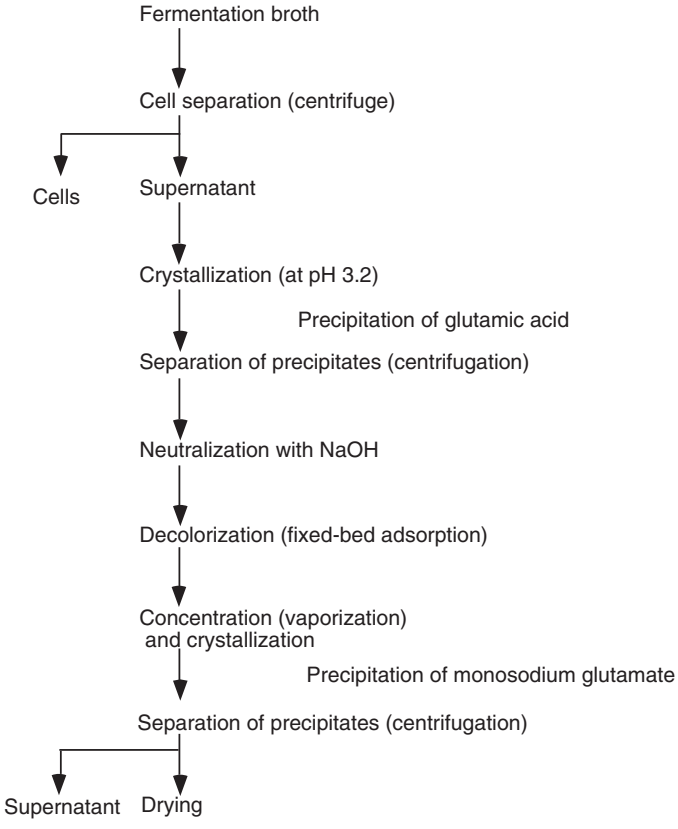

Figure 14.3 Separation steps for monosodium glutamate.

14.2
Separation of Microorganisms by Filtration and Microfiltration

14.2.1
Dead-End Filtration

In conventional filtration systems used for cell separation, plate filters (e.g., a filter press) and/or rotary drum filters are normally used (cf. Chapter 9). The filtrate fluxes in these filters decrease with time due to an increase in the resistance of the cake R_C (m^{-1}), as shown by Equation 9.1. If the cake on the filtering medium is incompressible, then R_C can be calculated using Equation 9.2, with the value of the specific cake resistance α ($m\,kg^{-1}$) given by the Kozeny–Carman equation (Equation 9.3). For many microorganisms, however, the values of α obtained by dead-end filtration (cf. Section 9.3) are larger than those calculated by Equation 9.3, as shown in Figure 14.4 [2]. The volume–surface diameter (the abscissa of Figure 14.4) can be obtained as: (6× volume of microorganism/surface

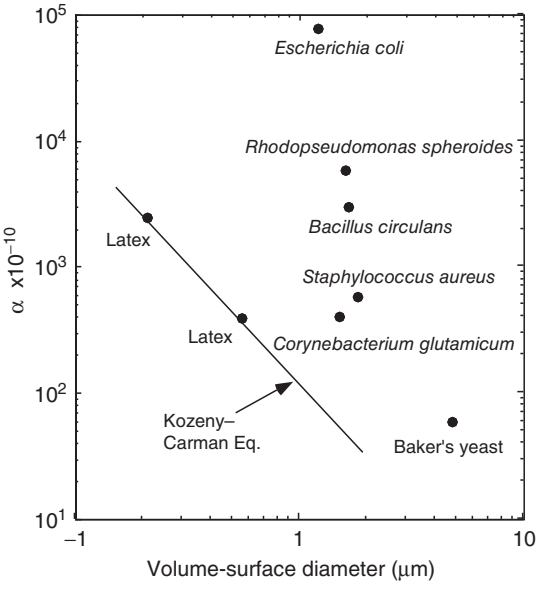

Figure 14.4 Specific cake resistance of several microorganisms measured by dead-end filtration.

area of microorganism). Bacillar (rod-like shaped) microorganisms such as *Bacillus* and *Escherichia* show larger values of α than do cocci (microorganisms of spherical shape, such as baker's yeast and *Corynebacterium*) because the porosities of the cake ε (–) of the former microorganisms are smaller than those of the latter. In many cases, the cakes prepared from microorganisms are compressible, such that the pressure drop through the cake layer increases with increasing specific cake resistance, due to change in the shape of the particles. If the resistance of the filtering medium R_M (m^{-1}) is small compared to R_C, then the value of the specific cake resistance α ($m\,kg^{-1}$) will be approximately constant under a constant filtration pressure drop ΔP (Pa). Then, Equation 9.2 is substituted into Equation 9.1, and integration from the start of filtration to time t (s) gives

$$\left(\frac{V_f}{A}\right)^2 + \frac{2R_M V_f}{\alpha \rho_c A} = \frac{2\Delta p}{\alpha \rho_c \mu} t \tag{14.1}$$

where V_f is the volume of the filtrate (m^3), A is the filter area (m^2), ρ_c is the mass of cake solids per unit volume of filtrate ($kg\,m^{-3}$), and μ is the liquid viscosity (Pa s). By this equation the filtrate flux at time t (s) can be estimated for dead end conventional filtration and microfiltration.

Example 14.1

A suspension of baker's yeast ($\rho_c = 10\,kg\,m^{-3}$, $\mu = 0.001\,kg\,m^{-1}\,s^{-1}$) is filtered with a dead end filter (filter area = $1\,m^2$) at a constant filtration pressure difference of 0.1 MPa.

Calculate the volume of filtrate versus time relationship, when the specific cake resistance of baker's yeast α and the resistance of the filtering medium R_M are $7 \times 10^{11}\,m\,kg^{-1}$ and $3.5 \times 10^{10}\,m^{-1}$, respectively. How long does it take to obtain $0.5\,m^3$ of filtrate?

Solution

Equation 14.1 gives

$$\left(\frac{V_f}{A}\right)^2 + \frac{2 \times 3.5 \times 10^{10} V_f}{7 \times 10^{11} \times 10 A} = \frac{2 \times 10^5}{7 \times 10^{11} \times 10 \times 10^{-3}} t$$

As shown in Figure 14.5, a plot of the filtrate volume V_f versus time t gives a parabolic curve.

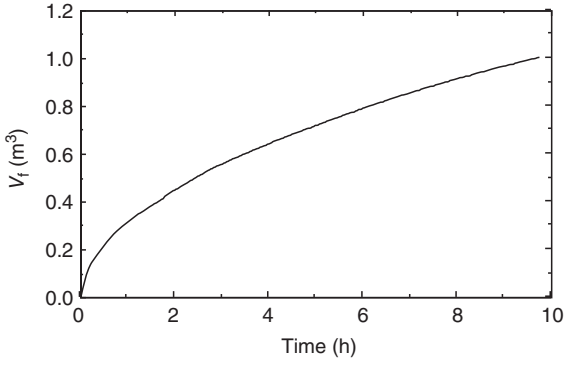

Figure 14.5 Volume of filtrate plotted against time. Constant filtration pressure: 0.1 MPa. Concentration of Baker's yeast suspension: $10\,kg\,m^{-3}$.

When $V_f = 0.5\,m^3$, t is given as 2.48 h = 149 min.

The average filtrate flux from the start of filtration to 149 min is $5.6 \times 10^{-5}\,m^3\,m^{-2}\,s^{-1}$.

14.2.2 Cross Flow Filtration

As stated in Chapter 9, cross-flow filtration (CFF) provides a higher efficiency than dead-end filtration, as some of particles retained on the membrane surface are swept off by the liquid flowing parallel to the surface. As shown by a solid line in Figure 14.6 [3], filtrate flux decreases with time from the start of filtration due to an accumulation of filtered particles on the membrane surface, as in the case of dead-end filtration. The flux then reaches an almost constant value, where

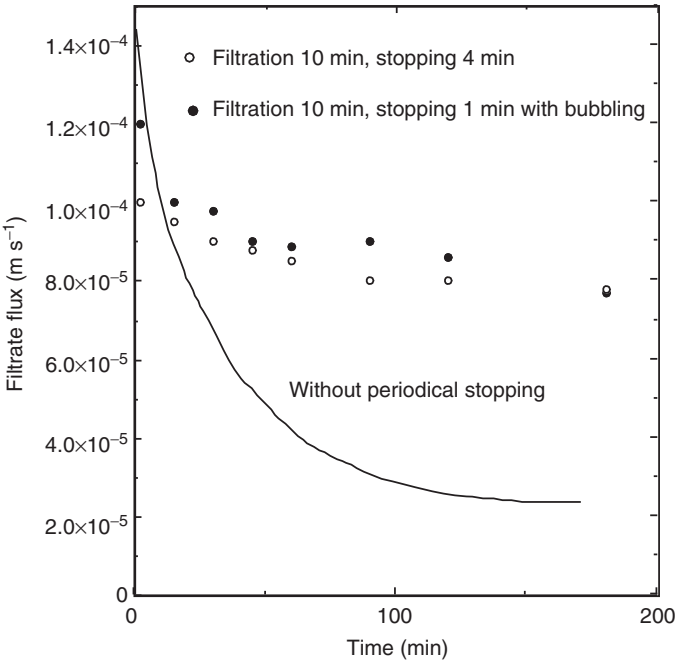

Figure 14.6 Cross-flow filtration flux of baker's yeast suspension. Cell concentration: 7%. Transmembrane pressure: 0.49 bar. Flow rate: 0.5 m s^{-1}.

the accumulation of filtered particles on the membrane surface due to filtration is balanced by a sweeping-off of the particles. While the earlier stage can be treated similarly to dead-end filtration, in the later stages the filtrate flux J_F in CFF modules often depends on the shear rate, and can be expressed by Equation 14.2:

$$J_F \propto \gamma_w{}^n \tag{14.2}$$

where $n = 0.63 - 0.88$ for suspensions of yeast cells [4].

The estimation of a steady-state value of the CFF filtrate flux in general is difficult because it is affected by many factors, including the type of membrane module, the characteristics of the membranes and suspensions, and the operating conditions. For example, it has been reported that the specific cake resistance of cocci in CFF was equal to the value obtained by dead-end filtration. However, the cake resistance became much larger in the CFF of bacillar microorganisms because the cells became aligned along the streamline of the liquid. This leads to the porosity of the cake being less than that of a cake composed of randomly stacked cells. Furthermore, particulate contaminants and antifoam agents in the cell suspensions may increase the specific cake resistance. Thus, in many cases the filtrate fluxes must be measured experimentally using small-scale membrane modules in order to obtain basic data for the scale up of CFF modules.

Several methods to increase the steady-state filtrate flux of cell suspensions in CFF have been reported. Among these, backwashing with pressurized air during CFF is most common. It has been reported that the average filtrate flux was increased from 8.3×10^{-6} to 1.2×10^{-5} m s^{-1} by backwashing for 5 s every 5 min during the CFF of *E. coli* [5]. The periodic stopping of permeation flow during CFF is also effective to increase the flux, as shown in Figure 14.6 [3]. In such an operation, a valve at the filtrate outlet was periodically closed, with or without introduction of air bubbles into the filtration module. The filtrate flux after 3 h was fourfold higher than that without periodic stopping.

14.3 Separation by Chromatography

14.3.1 Factors Affecting the Performance of Chromatography Columns

Liquid chromatography can be operated under mild conditions in terms of pH, ionic strength, polarity of liquid, and temperature. The apparatus used is simple in construction and easily scaled up. Moreover, many types of interaction between the adsorbent (the stationary phase) and solutes to be separated can be utilized, as shown in Table 11.1. Liquid chromatography can be operated isocratically, stepwise, and with gradient changes in the mobile phase composition. Since the performance of chromatography columns was discussed, with use of several models and on the basis of retention time and the width of elution curves, in Chapter 11, we will at this point discuss some of the factors that affect the performance of chromatography columns.

In order to estimate resolution among peaks eluted from a chromatography column, those factors that affect N must first be elucidated. By definition, a low value of Hs will result in a large number of theoretical plates for a given column length. As discussed in Chapter 11, Equation 11.20 obtained by the rate model shows the effects of axial mixing of the mobile phase fluid and mass transfer of solutes on Hs.

14.3.1.1 Velocity of Mobile Phase and Diffusivities of Solutes

As the first term of the right-hand side of Equation 11.20 is independent of fluid velocity and is proportional to the radius r_0 (m) of particles packed as the stationary phase under usual conditions in chromatography separation, Hs (m) will increase linearly with the interstitial velocity of the mobile phase u (m s^{-1}), as shown in Figure 11.9. With a decrease in the effective diffusivities of solutes D_{eff} (m^2 s^{-1}), Hs for a given velocity will increases, while the intercept of the straight lines on the y-axis, which corresponds to the value of the first term of Equation 11.20, is constant for different solutes. The value of the intercept will depend on the radius of packed particles, but does not vary with the effective diffusivity of the solute.

14.3.1.2 Radius of Packed Particles

To clarify the effect of radius of packed particles on Hs, Equation 11.20 can be rearranged as follows, in case the liquid film mass transfer resistance is negligible:

$$\frac{Hs}{2r_0} = \frac{D_z}{ur_0} + \frac{2ur_0EK}{30(1+EK)^2D_{eff}} \tag{14.3}$$

When the effective diffusivity of solutes D_{eff} can be approximated by the diffusivity in water, D, multiplied by a constant that includes the effects of particle porosity and tortuosity of pores in particles, Equation 14.3 can be written as follows:

$$\frac{Hs}{2r_0} = A + B\nu \tag{14.4}$$

where $\nu = (2\ r_0\ u)/D$. In Figure 14.7, the left-hand side of Equation 14.4 is plotted against ν for several diameters of gel particles [6]. The intercept is approximately 2 – that is, twice the particle diameter. The Hs for various solutes with different diffusivities can be correlated using this equation, which indicates the effects of the velocity of mobile phase, solute diffusivity, and radius of packed particles on Hs. This correlation indicates that packed particles with a small diameter are useful for attaining high separation efficiency because operation at high velocity without any loss of resolution is possible. A high-performance liquid chromatography (HPLC) analysis, in which particles with diameters of 3–5 µm are used as the stationary phase, shows the high resolution of eluted curves at relatively high velocities of the mobile phase.

14.3.1.3 Sample Volume Injected

In industrial-scale chromatography, one very desirable aspect is the ability to handle large amounts of samples, without any increase in Hs. For sample volumes of

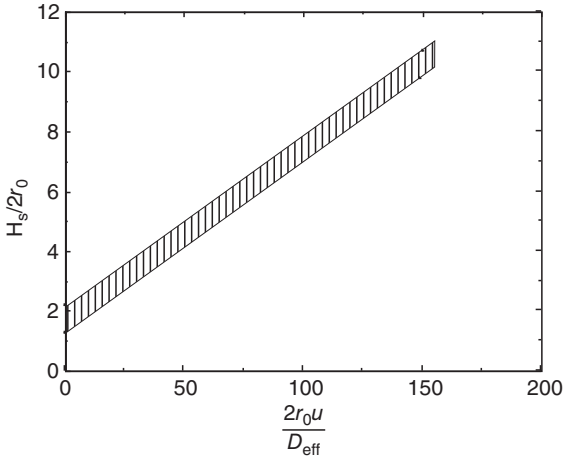

Figure 14.7 $Hs/2r_0$ plotted against $2r_0\ u/D_{eff}$. r_0: 17–37 µm; solute: myoglobin, ovalbumin, bovine serum albumin. Temperature: 10, 20, 40 °C.

up to a small percentage of the total column volume, Hs remains constant, but it then increases with the sample volume. It has been reported that the effect of sample volume on Hs should rather be treated as the effect of the sample injection time t_0 (s) [7].

$$Hs = \frac{Z(\sigma_t^2 + t_0^2/12)}{(t_R + t_0/2)^2} \tag{14.5}$$

where Z is the column height (m), σ_t^2 is the dispersion of elution curve at a small sample volume (s^2), and t_R is the retention time (s). The dispersion σ_t^2 is obtained from the peak width ($4\sigma_t$) of an elution curve on the plot of solute concentrations versus time. From the relative magnitudes of σ_t^2 and $t_0^2/12$, a suitable injection time t_0 without significant loss of resolution can be determined.

14.3.1.4 Column Diameter

The effect of the column diameter on the shapes of elution curves was studied with the use of hard particles (Toyopearl HW55F) for gel chromatography [7] and soft particles (Matrix Blue A) for affinity chromatography [8]. The results showed that Hs did not vary for column diameters of 1.0–9.0 cm in the former case, nor for column diameters of 1.65–18.4 cm in the latter case.

When soft compressible particles are used, the pressure drop increases substantially with the velocity of the mobile phase above a certain velocity because of compression of the particles, thus limiting the allowable velocity. Such compression of particles becomes significant with increases in the column diameter.

Example 14.2

In a gel chromatography column packed with particles of average radius 22 μm at an interstitial velocity of 1.2 cm min^{-1} of the mobile phase, two peaks show poor separation characteristics, that is, $R_S = 0.85$.

a) What velocity of the mobile phase should be applied to attain good separation (R_S above 1.2) with the same column length?
b) What length of a column should be used to obtain $R_S = 1.2$ at the same velocity?
   The linear correlation of $h = Hs/2r_0$ versus ν shown in Figure 14.7 can be applied to this system, and the diffusivities of these solutes of 7×10^{-7} cm^2 s^{-1} can be used.

Solution

Under the present conditions

$$\nu = \frac{(2r_0\, u)}{D} = \frac{(2 \times 0.0022 \times 1.2)}{(60 \times 7 \times 10^{-7})} = 125$$

From Figure 14.7

$$h = \frac{Hs}{(2 \times 0.0022)} = 9.0 \quad Hs = 0.040$$

a) R_S increases in proportion to $(Hs)^{-1/2}$. Thus, the value of Hs must be lower than 0.020 to obtain a resolution R_S larger than 1.2. Again, from Figure 14.7

$$\nu = 46$$

Then,

$$u = 0.0073 \text{ cm s}^{-1} = 0.44 \text{ cm min}^{-1}$$

b) At the same value of Hs, R_S increases in proportion to $N^{1/2}$, that is, $Z^{1/2}$. To increase the value of R_S from 0.85 to 1.2, the column should be $(1.2/0/85)^2 = 2.0$ times longer.

14.3.2 Scale-Up of Chromatography Columns

The scale-up of chromatography separation means increasing the recovered amount of a target that satisfies the required purity per unit time. This can be achieved by simply increasing the column diameter, and also by shortening the time required for separation, and/or by increasing the sample volume applied to a column [9].

The scale-up of chromatography operated in isocratic elution can be carried out as follows.

The simplest way of scaling-up of chromatography is to simply increase the column diameter. In this case, good care must be taken of the distribution of the mobile phase liquid over the cross section of the column. When particles of the same dimension and characteristics are packed in a larger-diameter column with the same height, the linear velocity and the sample volume per unit cross-sectional area should be kept unchanged to obtain the same resolution.

When the radius of particles packed and/or the column height are changed, the number of theoretical plates of a large-scale column must be kept equal to that of a small column; that is,

$$N_L = N_S = \left(\frac{Z}{Hs}\right)_{L \text{ or } S} \tag{14.6}$$

From a correlation similar to Figure 14.7, the velocity of the mobile phase for the scaled up column to obtain the equal value of N_L can be determined. In the case where particles with a smaller radius are used, an operation with a higher interstitial velocity will be possible to attain the same resolution with the same column height, and thus this increases the productivity. The resolution between a target and a contaminant can be estimated by Equation 11.23 to calculate the purity and recovery of the target.

In chromatography separations operated under gradient elution, one simple method of obtaining an equal peak width of a specific solute in columns of different dimensions is to keep the numbers of theoretical stages of both columns equal.

14.4
Separation in Fixed-Beds

In the downstream processing of bioprocesses, fixed-bed adsorbers are used extensively both for the recovery of a target and for the removal of contaminants. Moreover, their performance can be estimated from the breakthrough curve, as stated in Chapter 11. The break time t_B is given by Equation 11.13, and the extent of the adsorption capacity of the fixed bed utilized at the break point and loss of adsorbate can be calculated from the break time and the adsorption equilibrium. Affinity chromatography, as well as some ion-exchange chromatography, are operated as specific adsorption and desorption steps, and the overall performance is affected by the column capacity available at the break point and the total operation time.

The scale-up of a fixed-bed separation may be carried out by increasing the diameter of a column, the length of the packed bed, and/or the flow rate of the feed solution. The pressure drop through the column limits the length of the packed bed. The amount of adsorbate treated per unit time and the unit sectional area of a column will increase with the linear velocity of the feed. However, the slope of the breakthrough curve becomes gentle with an increase in the velocity, when the intraparticle resistance of solute transfer is dominant, and thus the fraction of the column capacity available at the break point will decrease. Therefore, the linear velocity at which the maximum rate of treatment is reached depends on the column length. When soft compressible particles are used, the maximum velocity is limited due to a rapid increase in the pressure drop. Figure 14.8 shows the purification rates (mg h^{-1}) of bovine serum albumin by affinity chromatography with antibody ligands coupled to two different packed materials, namely, soft particles made from agarose, and hard particles as used in HPLC [10]. The purification rate increases with the linear velocity of the mobile phase, while the maximum rate depends on the characteristics of the packed particles.

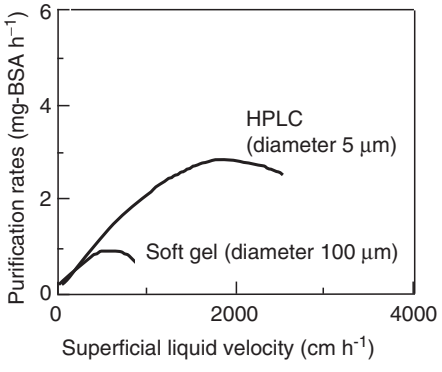

Figure 14.8 Calculated purification rates with two support materials. Concentration of BSA in feed: 0.05 mg cm^{-3}. Adsorption capacity: 0.9 mg-BSA cm^{-3}-bed, 4.6 × 100 mm column.

Example 14.3

Calculate the fractional residual capacity at the break point for the fixed-bed of Example 11.2. The fractional residual capacity of the adsorption zone can be approximated as 0.5.

Estimate the residual capacity, when the interstitial velocity is doubled. It can be assumed that the averaged overall volumetric coefficient increases with the interstitial velocity to the power of 0.2.

Solution

The length of the adsorption zone is given as

$$z_a = \frac{\varepsilon u}{K_L a} \int_{C_B}^{C_E} \frac{dC_A}{C_A - C_A^*}$$

$$z_a = \frac{0.5 \times 1.6}{9.2} \times 2.26 = 0.196 \text{ m}$$

Since the fractional residual capacity of the adsorption zone is 0.5 and the bed height is 0.25 m, the residual capacity is given as

$$\frac{(0.196 \times 0.5)}{0.25} \times 100 = 39.3\%$$

At the interstitial velocity of 3.2 m h^{-1} the overall volumetric coefficient is

$$9.2 \times 2^{0.2} = 10.7 \text{ h}^{-1}$$

Thus,

$$z_a = \frac{0.5 \times 3.2}{10.7} \times 2.26 = 0.338 \text{ m}$$

The residual capacity is

$$\frac{(0.338 \times 0.5)}{0.25} \times 100 = 67.6\%$$

Two-thirds of the adsorption capacity is not utilized at the break point in this case.

14.5 Sanitation in Downstream Processes

As bioproducts must be pure and safe, they must be free from contamination with viruses, microorganisms, and pyrogens; an example of the latter is the lipopolysaccharides from gram-negative bacteria, which cause fevers to develop in mammals. In downstream processes, these types of contaminant must be avoided and eliminated. The equipment used, including the tubes, tube fittings, valves, and gaskets, must be made from safe materials, and be easily cleaned by washing and sterilization in place. In case these materials are not resistant to steam sterilization, then

sanitizing chemicals, such as 0.1 – 0.5 mol l^{-1} NaOH solution, sodium hypochlorite, and detergents, can be used for the sterilization of microorganisms, the inactivation of viruses, and the removal of any proteins that have adsorbed onto the equipment surfaces. In these procedures, the design details and materials to be used, as well as the actual operations, must follow any authoritative regulations.

Problems

14.1 A suspension of baker's yeast ($\rho_c = 20\,kg\,m^{-3}$, $\mu = 0.0012\,kg\,m^{-1}\,s^{-1}$) is filtered with a dead-end filter (filter area = 1 m^2) at a constant filtration pressure. Neglecting the resistance of the filtering medium, determine the filtration pressure difference ΔP to obtain 0.5 m^3 of filtrate after 2.5 h.

14.2 In the case where only the length of a gel chromatography column is doubled, how is the resolution of two solutes changed under the same operating conditions with the same packed beads? The linear correlation of $h = Hs/2r_0$ versus ν shown in Figure 14.7 can be applied to this system.

14.3 Derive Equation 14.5.

14.4 For a scale-up of gel chromatography, the diameter of the packed beads will be increased from 44 to 75 μm. How much should the velocity of the mobile phase in the scaled-up column be reduced to attain the same resolution as the small column ($Hs = 0.22$ mm) with the same column length? The linear correlation of h versus ν shown in Figure 14.7 can be applied to this system.

14.5 When the height of the adsorbent bed is 50 cm under the same operating conditions given in Example 11.2, estimate the residual capacity.

References

1. Staehelin, T., Hobbs, D.S., Kung, H., Lai, C.-Y., and Pestka, S. (1981) *J. Biol. Chem.*, **256**, 9750.
2. Nakanishi, K., Tadokoro, T., and Matsuno, R. (1987) *Chem. Eng. Commun.*, **62**, 187.
3. Tanaka, T., Itoh, H., Itoh, K., and Nakanishi, K. (1995) *Biotechnol. Bioeng.*, **47**, 401.
4. Tanaka, T., Tsuneyoshi, S., Kitazawa, W., and Nakanishi, K. (1997) *Sep. Sci. Technol.*, **32**, 1885.
5. Kroner, K.H., Schütte, H., Hustedt, H., and Kula, M.R. (1987) *Process Biochem.*, **22**, 67.
6. Yamamoto, S., Nomura, M., and Sano, Y. (1987) *J. Chromatogr.*, **394**, 363.
7. Yamamoto, S., Nomura, M., and Sano, Y. (1986) *J. Chem. Eng. Jpn.*, **19**, 227.
8. Katoh, S. (1987) *Trends Biotechnol.*, **5**, 328.
9. Janson, J.-C. and Hedman, P. (1982) *Adv. Biochem. Eng.*, **25** (Chromatography Special Edition), 43.
10. Katoh, S., Terashima, M., Majima, T. *et al.* (1994) *J. Ferment. Bioeng.*, **78**, 246.

Further Reading

King, C.J. (1971) *Separation Processes*, McGraw-Hill.

LeRoith, D., Shiloach, J., and Leahy, T.M. (eds) (1985) *Purification of Fermentation Products – Application to Large-Scale Processes*, ACS Symposium Series, vol. 271, American Chemical Society.

Scopes, R.K. (1994) *Protein Purification – Principles and Practice*, Springer-Verlag.

Turkova, J. (1978) *Affinity Chromatography*, Elsevier Scientific Publishing Co.

Wheelwright, S.M. (1991) *Protein Purification*, Hanser.

15
Medical Devices

15.1
Introduction

One type of medical device – the so-called artificial organs – can be designed and/or evaluated on the basis of chemical engineering principles. For example, the "artificial kidney" is a membrane device, mainly a dialyzer, which is capable of cleaning the blood of patients with chronic kidney diseases. Likewise, a "blood oxygenator" is used outside the body during surgery for oxygen transfer to, and CO_2 removal from, the blood. The "bioartificial liver" is a bioreactor that performs the liver functions of patients with liver failure, by using liver cells.

For details of the physiology and anatomy of human internal organs, the reader should refer to medical textbooks [1, 2].

15.2
Blood and Its Circulation

15.2.1
Blood and Its Components

Roughly speaking, 60% of a human being's body weight is water, of which 40% is contained within the cells (intracellular fluid) and 20% outside the cells (extracellular fluid). The extracellular water consists of the water in the interstitial fluids (15% of body weight) – that is, fluid in the interstices between cells and blood vessels – and the water in the blood plasma (5% of the body weight). *Plasma*, the liquid portion of the blood, is an aqueous solution of very many organic and inorganic substances. *Blood* is a suspension in plasma of various blood corpuscles, such as *erythrocytes* (red blood cells), *leukocytes* (white blood cells), *platelets*, and others.

The volumetric percentage of erythrocytes in whole blood is called the *hematocrit*, the values of which are 42–45% in healthy men and 38–42% in women. In man, a $1\,cm^3$ blood sample will contain approximately 5×10^9 erythrocytes,

Biochemical Engineering: A Textbook for Engineers, Chemists and Biologists, Second Edition.
Shigeo Katoh, Jun-ichi Horiuchi, and Fumitake Yoshida.

Companion Website: www.wiley.com\go\katoh\biochem_eng_e2

with leukocyte and platelet numbers being approximately 1/600 and 1/20 that of erythrocytes, respectively.

The erythrocyte is disc-shaped, 7.5 – 8.5 μm in diameter, and 1 – 2.5 μm thick, but is thinner at its central region. Functionally, erythrocytes contain hemoglobin, which combines very rapidly with oxygen (as discussed later).

There are various types of leukocytes, the main function of which is to protect against infection. *Macrophages*, one type of leukocytes, engulf and digest various foreign particles and bacteria that have passed into the interstitial spaces. Lymphocytes exist as two types: (i) B cells, which produce antibodies (i.e., various immunoglobulins) and (ii) T cells, which destroy foreign cells, activate macrophages, and regulate the production of antibodies by B cells. *Complements* are proteins in plasma that assist the functions of antibodies in a variety of ways.

Clotting – the coagulation of blood – involves a series of very complicated chain reactions that are assisted by enzymes. In the final stage of blood clotting, the protein *fibrinogen*, which is soluble in plasma, becomes an insoluble fibrin, which encloses the red cells and platelets, with the latter component playing an important role in the clotting process. If a blood vessel is injured, clotting must occur to stop further bleeding. However, clotting must not occur in blood that is flowing through the blood vessels or through artificial organs. Within the blood vessels, blood does not coagulate due to the existence of antithrombin and other anticoagulants. *Serum* is the plasma from which fibrinogen has been removed during the process of clotting, and can be obtained by stirring and then centrifuging the clotted blood.

Heparin, an anticoagulant that is widely used to prevent blood coagulation flowing through artificial organs, is a mucopolysaccharide that is obtained from the liver or lung of animals. It is also possible to prevent blood clotting *in vitro* by the addition of oxalic acid or citric acid; these combine with the Ca^{2+} ions that are required in clotting reactions and block the process.

Hemolysis is the leakage of hemoglobin into liquid such as plasma, and is due to disruption of the erythrocytes. Within the body, hemolysis may be caused by some diseases or poisons, whereas hemolysis outside the body, as in artificial organs, is caused by physical or chemical factors. If erythrocytes are placed in water, hemolysis will occur as the cells rupture due to the difference in osmotic pressure between water and the intracellular liquid. Hemolysis in artificial organs and their accessories occurs due to a variety of physical factors, including turbulence, shear, and changes of pressure and velocity. It is difficult, however, to obtain any quantitative correlation between the rates of hemolysis and such physical factors.

The body fluids can be regarded as buffer solutions, with the normal pH values of the extracellular fluids (including blood) and intracellular fluids being 7.4 and 7.2, respectively.

Plasma or serum can be regarded as a Newtonian fluid. The viscosity of plasma at 37 °C is approximately 1.2 cp. In contrast, whole blood shows non-Newtonian behavior, its viscosity decreasing with an increasing shear rate, but with a decreasing hematocrit.

15.2.2
Blood Circulation

The circulation of blood was discovered and reported by W. Harvey in 1628. Figure 15.1 is a simplified diagram showing the main flows of blood in the human body. The heart consists of four compartments, but for simplicity we can consider the heart as a combination of two blood pumps, the *right heart* and the *left heart*. The blood coming from various parts of the body is propelled by the right heart pump through the lung (pulmonary) artery to the lungs, where the blood absorbs oxygen from the air and desorbs carbon dioxide into the air. The oxygenated blood returns from the lungs through the pulmonary vein to the left heart. This blood circulation through the lungs is called the "lesser circulation." The blood vessels that carry blood toward the various organs and tissues are known as *arteries*, whereas blood vessels carrying blood from the organs and tissues toward the heart are called *veins*.

As shown in the figure, the blood from the left heart is pumped through the arteries to the various organs and tissues from where, after exchanging various substances, it is returned through the veins to the right heart. This blood circulation is called the "major circulation."

In Figure 15.1 only the large arteries and veins are shown. However, in the organs and tissues, the arteries branch into many smaller blood vessels – the *arterioles* – which further branch into many fine blood vessels that range from 5 to 20 μm in inner diameter, and are termed *capillaries*. Various nutrients and

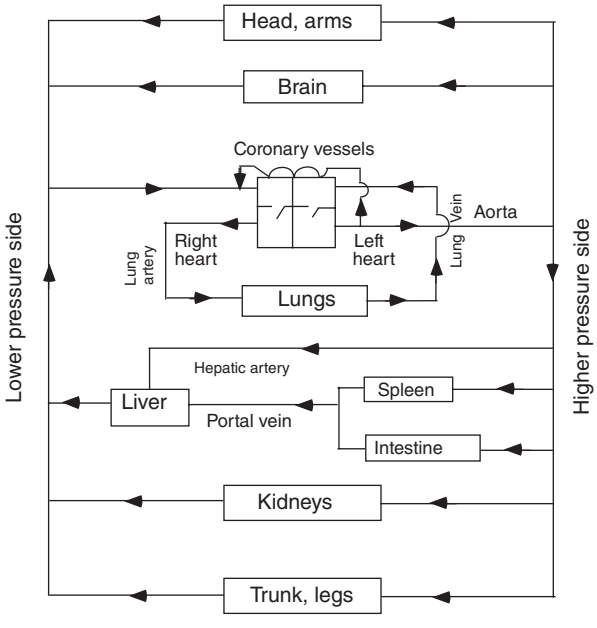

Figure 15.1 Simplified blood flow diagram.

other required substances are transported from the arterial blood through the walls of the arterial capillaries into tissues and organs. In contrast, waste products and unrequired substances produced by the organs and tissues are transported to the venous blood through the walls of the venous capillaries, which combine into *venules*, and then into larger veins.

The *spleen* is an organ, the main functions of which are the formation and purification of blood. Blood from the spleen and intestine is passed through the portal vein to the liver for further reactions. The functions of the lungs, kidneys, and liver are described later in the chapter. The *coronary arteries*, which branch from the aorta, supply blood to the muscles of the heart.

The flow rate of blood through the heart is approximately $4-5\,\mathrm{l\,min^{-1}}$ for adults. The typical mean blood velocity through the aorta (which is the largest artery with a diameter of 2–3 cm), when pumped from the left heart, is approximately $25\,\mathrm{cm\,s^{-1}}$ (mean); the maximum velocity is approximately $60\,\mathrm{cm\,s^{-1}}$. The Reynolds number for the maximum velocity is about 3000. In general, the blood flow through arteries and veins is laminar in nature. In capillaries, the typical blood velocity is $0.5-1\,\mathrm{mm\,s^{-1}}$, and the Reynolds number is on the order of 0.001.

15.3 Oxygenation of Blood

15.3.1 Use of Blood Oxygenators

The function of the lung is to absorb oxygen into the blood for distribution to the various parts of the body, while simultaneously desorbing carbon dioxide from the venous blood that is received from the organs and tissues. The lungs consist of a pair of spongy, sac-like organs, in which the air passages end in very small hemi-spherical sacs known as *alveoli*. The total surface area of the alveolar walls in both lungs is approximately $90\,\mathrm{m^2}$. The alveolar walls are surrounded by capillaries, such that the gas transfer between the blood and the alveolar gas occurs through the alveolar wall, the interstitial fluid, capillary membrane, plasma, and the erythrocyte membrane.

The term "artificial lung," which is often used as the synonym for a blood oxygenator, is sometimes confused by laymen with the "respirator," which is a mechanical device used for artificial respiration. For this reason, we will not use the term artificial lung in this book. As the human lungs are very closely connected to the heart, it is difficult to bypass only the heart during heart surgery. The so-called "heart–lung machine," which performs the functions of the heart and lungs, may be used for several hours during heart surgery. The system consists of a blood pump, a blood oxygenator, and a heat exchanger, where the blood oxygenator performs the functions of lungs – that is, to absorb oxygen into, and desorb carbon dioxide from, the blood.

Occasionally, the blood oxygenator may be used continuously for several days, or even for a few weeks, to assist the lung functions of patients suffering from acute severe respiratory diseases.

15.3.2 Oxygen in Blood

The absorption of oxygen into the blood is not simple physical gas absorption. Rather, it is gas absorption with chemical reactions, known as "oxygenation." Oxygenation is not oxidation, since Fe^{2+} in hemoglobin is not oxidized. Oxygenation involves very rapid, reversible, loose reactions between oxygen and the hemoglobin contained in the erythrocytes. Typically, the hemoglobin concentration in blood is 15 g dl^{-1}, when the hematocrit is 42%.

Hemoglobin, a protein with a molecular weight of 68 000 Da, consists of four subunits with a molecular weight of 17 000 Da. Oxygenation proceeds in the following four steps:

1) $hb_4 + O_2 = hb_4O_2$
2) $hb_4O_2 + O_2 = hb_4O_4$
3) $hb_4O_4 + O_2 = hb_4O_6$
4) $hb_4O_6 + O_2 = hb_4O_8$.

where hb indicates one subunit of the hemoglobin molecule. From the above relations and the law of mass action, the following Adair equation [3] is obtained:

$$\frac{y}{100} = \frac{K_1p + 2K_1K_2p^2 + 3K_1K_2K_3p^3 + 4K_1K_2K_3K_4p^4}{4(1 + K_1p + K_1K_2p^2 + K_1K_2K_3p^3 + K_1K_2K_3K_4p^4)} \tag{15.1}$$

where y is the oxygen saturation (%), p is the oxygen partial pressure (mmHg), and K's are the equilibrium constants (−) of the above four reactions: (1) to (4). Their values at pH = 7.4 are $K_1 = 0.066$, $K_2 = 0.018$, $K_3 = 0.010$, and $K_4 = 0.36$ [4]. The increase in K values with pH is given by Equation 15.2 [5].

$$\log K = \log K(\text{at pH} = 7.2) + 0.48(\text{pH} - 7.2) \tag{15.2}$$

in which K values at pH = 7.2 are as follows.

$$K_1 = 0.0415,\ K_2 = 0.0095,\ K_3 = 0.0335,\ K_4 = 0.103.$$

From the practical point of view, the following empirical equation of Hill [6] is more convenient.

$$\frac{y}{100} = \frac{Hp^n}{(1 + Hp^n)} \tag{15.3a}$$

where y is the oxygen saturation (%) and p is the oxygen partial pressure (mmHg). Values of the empirical constants H and n vary with pCO_2 (hence pH) and temperature. Equation 15.3a can be transformed into Equation 15.3b.

$$\log\left[\frac{y}{(1-y)}\right] = \log H + n\log p \tag{15.3b}$$

Thus, plotting experimental values of the left-hand side of Equation 15.3b against those of log p gives the values of H and n, which are functions of pH and temperature.

Figure 15.2 [7] is the so-called "oxyhemoglobin dissociation curve," which correlates hemoglobin saturation y (%) with the oxygen partial pressure pO_2 (mmHg). Hemoglobin is approximately 75% saturated at a pO_2 of 40 mmHg (venous blood) and approximately 97% saturated at a pO_2 of 90 mmHg (arterial blood). As shown in Figure 15.2, lower pH (higher pCO_2) in tissues makes y smaller for a given pO_2, resulting in more oxygen transfer from blood to tissues (the Bohr effect).

Table 15.1 lists the partial pressures (mmHg) of oxygen, carbon dioxide, water, and nitrogen in the inspired air, expired air, air in alveoli, arterial blood, blood in tissues, and venous blood.

15.3.3 Carbon Dioxide in Blood

When the partial pressure of CO_2 is 40 mmHg, 100 cm^3 of blood at 37 °C contains 50 cm^3 of CO_2, 44 cm^3 of which as bicarbonate ions HCO_3^-, 3 cm^3

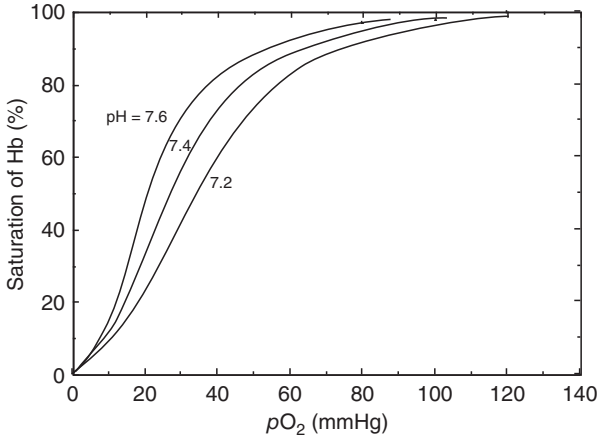

Figure 15.2 Oxyhemoglobin dissociation curve.

Table 15.1 Partial pressures of gases in the body (mmHg).

Gases	O_2	CO_2	H_2O	N_2
Inspired air	158	0.3	5.7	596
Expired gas	116	32	47	565
Alveolar gas	100	40	47	573
Arterial blood	95	40	47	578
Blood in tissue	40	46	47	627
Venous blood	40	46	47	627

as physically dissolved CO_2, and the remainder as compounds with proteins such as hemoglobin. The bicarbonate ion is produced by the following reversible reactions:

$$CO_2 + H_2O \rightleftarrows H_2CO_3 \rightleftarrows H^+ + HCO_3^-$$
$$\text{(A)} \qquad \text{(B)}$$

Reaction (B) is very rapid. Reaction (A) is slow, but becomes very rapid in the presence of the enzyme carbonic anhydrase, which exists in the erythrocytes. Carbon dioxide produced by the gas exchange in tissues moves into the erythrocytes, while bicarbonate ions produced by reactions (A) and (B) in the erythrocytes move out into the plasma.

Carbonic acid, H_2CO_3, is a weak acid that dissociates by the above reaction (B). In general, a solution of a weak acid HA that dissociates into H^+ and A^- will serves as a buffer solution. Thus, respiration in lungs contributes to physiological buffer actions.

The normal value of pH of the extracellular fluids at 37 °C is about 7.4, while that of the intracellular fluids is about 7.2. This can be explained by the buffering action of carbonic acid. In general, when a weak acid HA dissociates into H^+ and A^-, the following relationship holds:

$$\frac{[H^+][A^-]}{[HA]} = K$$

where K is the dissociation equilibrium constant. From this relationship the following Henderson–Hasselbalch equation for pH is obtained:

$$\text{pH} = -\log[H^+] = \log\left[\frac{1}{K}\right] + \log\left\{\frac{[A^-]}{[HA]}\right\} \tag{15.4}$$

Most of the CO_2 in blood exists as HCO_3^- produced by the dissociation of H_2CO_3. For this dissociation reaction, the values of $\log[1/K] = \text{pK}$ at 37 °C is 6.10. The ratio $[HCO_3^-]/[H_2CO_3]$ at 37 °C is maintained at approximately 20 by the respiration in the lungs. Then, Equation 15.4 gives pH = 7.4.

Most of the CO_2 that is physically absorbed by blood becomes H_2CO_3 by the above-mentioned reaction (A), in the presence of carbonic anhydrase. Thus, $[H_2CO_3]$ is practically equal to $[CO_2]$, which should be proportional to the partial pressure of CO_2, that is, pCO_2.

Even if H^+ is added to blood, it decreases HCO_3^- producing H_2CO_3, which is expired in the lungs as CO_2 and H_2O. The total CO_2 concentration, which can be determined by chemical analysis, is the sum of $[HCO_3^-]$ and $[CO_2]$, and the latter should be proportional to the partial pressure of CO_2, that is, pCO_2.

$$[CO_2] = s\, pCO_2$$

where the value of s at 37 °C is $(0.0314\,\text{mmol}\,\text{l}^{-1})/(pCO_2\ \text{mmHg})$. Thus, the following equation is obtained from Equation 15.4 for pH of blood at 37 °C.

$$\text{pH} = 6.10 + \log\left\{\frac{[\text{total } CO_2 - s\, pCO_2]}{s\, pCO_2}\right\} \tag{15.5}$$

15.3.4 Types of Blood Oxygenators

Blood oxygenators are gas–liquid bioreactors. During heart surgery, the blood that flows through the heart and lungs is bypassed through the heart–lung machine, which is used outside the body and consists mainly of a blood oxygenator and a blood pump. Since about 1950, many types of blood oxygenator have been developed and used. The early models of blood oxygenator included (i) the bubble-type, in which oxygen was bubbled through the blood; (ii) the blood film-type, in which blood films formed on the surface of rotating disks were brought into contact with oxygen; and (iii) the sheet-type, in which blood and oxygen flowed through channels that were separated by flat sheets of gas-permeable membranes. Each of these early models had to be assembled and sterilized every time before use. The bubble-type also required a section for the complete removal of any fine gas bubbles remaining in the blood, while the sheet-type was quite large because of the poor gas permeability of the early membranes. For all of these early blood oxygenators, separate heat exchangers were required to control the blood temperature.

Recently developed blood oxygenators are disposable, used only once, and can be presterilized and coated with anticoagulant (e.g., heparin) when they are constructed. Normally, membranes with high gas permeabilities, such as silicone rubber membranes, are used. In the case of microporous membranes, which are also used widely, the membrane materials themselves are not gas permeable, but gas–liquid interfaces are formed in the pores of the membrane. The blood does not leak from the pores for at least several hours, due to its surface tension. Composite membranes consisting of microporous polypropylene and silicone rubber have also been developed.

Hollow-fiber (capillary)-type membrane oxygenators are the most widely used today, and comprise two main types: (i) those where blood flow occurs inside the capillaries and (ii) those where there is a cross-flow of blood outside the capillaries. Although in the first type the blood flow is always laminar, the second type has been used more extensively in recent times, as the mass transfer coefficients are higher due to blood turbulence outside capillaries and hence the membrane area can be smaller. Figure 15.3 shows an example of the cross-flow type membrane oxygenator, with a built-in heat exchanger for controlling the blood temperature.

All of the above-mentioned blood oxygenators are used outside the body, and hence are referred to as "extracorporeal" oxygenators. They are mainly used for heart surgery, which can last for up to several hours. However, blood oxygenators are occasionally used extracorporeally to assist the pulmonary function of the patients in *acute respiratory failure* (*ARF*) for extended periods of up to a few weeks. This use of extracorporeal oxygenators is known as *extracorporeal membrane oxygenation* (*ECMO*).

Intracorporeal oxygenators are an entirely different type of blood oxygenator that can be used within the body to temporarily and partially assist the lung functions of patients with serious pulmonary diseases. No blood pump is necessary,

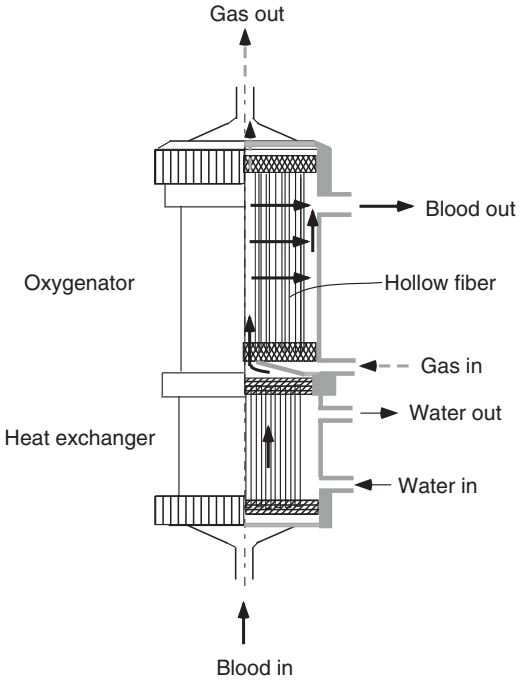

Figure 15.3 Hollow-fiber-type membrane oxygenator.

but a supply of oxygen-rich gas is required. Some suggestions have also been made regarding the implantation of an oxygenator within the body; in the case of the *VOX* (*intravascular oxygenator*), a series of clinical tests was performed, whereby woven capillaries of hollow fibers were inserted into the lower large vein leading to the right heart, and oxygen gas was passed through the capillaries and blood flowed outside the capillaries. Although these devices might be referred to as "artificial lungs," they cannot totally substitute for the functions of natural lungs.

15.3.5 Oxygen Transfer Rates in Blood Oxygenators

The gas-phase resistance for oxygen transfer in blood oxygenation is always negligible. With modern membrane-type blood oxygenators, the mass transfer resistance of membranes is usually much smaller than that of the blood phase. Hence, we need to consider only the blood phase mass transfer.

15.3.5.1 Laminar Blood Flow

In the case where the blood flow is laminar, as within hollow-fiber oxygenators, the rates of blood oxygenation can be predicted on a theoretical basis. Due to the shape of the oxyhemoglobin dissociation curve and the fact that the oxygen partial

pressure in most blood oxygenators is normally around 700 mmHg, the oxygenation reaction in such blood oxygenators is completed within the extremely thin reaction front, which advances into the unreacted zone as the reaction proceeds, with the necessary oxygen being supplied by diffusion through the oxygenated blood. Based on the advancing-front model, Lightfoot [8] obtained some useful solutions. For laminar blood flow through hollow fibers,

$$z^+ = \frac{3}{8} - \frac{1}{2}\left(\eta^2 - \frac{\eta^4}{4}\right) + \left(\eta^2 - \frac{\eta^4}{2}\right)\ln \eta \tag{15.6}$$

where z^+ is the dimensionless fiber length defined by

$$z^+ = \frac{(C_W - C_S)}{C_{Hb}} \frac{D_{O_2}}{d^2} \frac{z}{u} = \frac{(C_W - C_S)z}{C_{Hb}(\mathrm{Re})(\mathrm{Sc})d} \tag{15.7}$$

in which C_W and C_S are oxygen concentrations at the fiber wall and at the reaction front, respectively. C_{Hb} is the unreacted hemoglobin concentration, D_{O_2} is the oxygen diffusivity through saturated blood, z is the fiber length, d is the inside fiber diameter, and u is the average blood velocity through the hollow fiber (all in consistent units). η is the ratio of the distance r of the reaction front from the fiber axis to the inside radius of the fibers R; that is, $\eta = r/R$. In the case where blood flows through the hollow fibers, the ratio f of the decrease in unreacted hemoglobin to the hemoglobin entering the fiber is given by

$$f = 1 - 2\eta^2 + \eta^4 \tag{15.8}$$

where

$$f = \frac{(Q_0 - Q)}{Q_0} \tag{15.9}$$

Q is the flow rate of unreacted hemoglobin and Q_0 its value at the fiber entrance. Oxygen diffusivity through oxygenated blood D_{O_2} at 37 °C can be estimated, for example, by Equation 15.10 [9] or by Figure 15.4a

$$D_{O_2}(\mathrm{cm^2\,s^{-1}}) = (2.13 - 0.0092\ \mathrm{Ht}) \times 10^{-5} \tag{15.10}$$

where Ht is the hematocrit (%).

15.3.5.2 Turbulent Blood Flow

In the case where the blood flow is turbulent, we can use the concept of enhancement factor E for the case of liquid-phase mass transfer with a chemical reaction (Section 6.5). Thus,

$$k_B^* = E k_B \tag{15.11}$$

The value of the liquid phase mass transfer coefficient k_B can be obtained from the experimental data for physical absorption of oxygen into blood saturated with oxygen, or estimated from the data with the same apparatus for physical oxygen absorption into water or a reference liquid or solution with known physical properties. Mass transfer coefficients for liquids flowing through or across tubes or hollow fibers can usually be correlated by equations, such as Equation 6.26a for

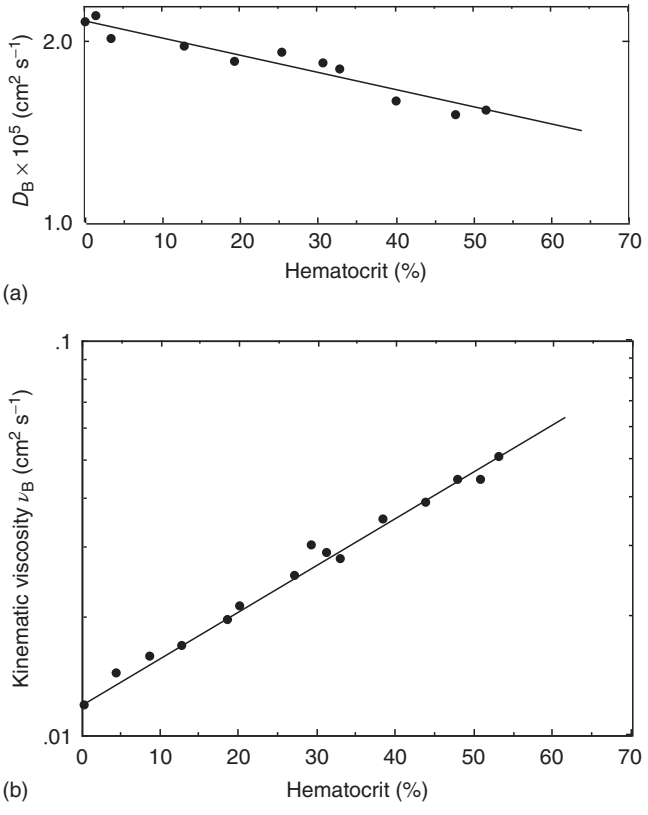

Figure 15.4 Diffusivity of oxygen in blood D_B (a) and kinematic viscosity of blood ν_B (b) at 37 °C.

laminar flow through tubes and Equation 6.27a for turbulent flow outside and across tubes. For the latter case,

$$\frac{k_B}{k_0} = \left(\frac{D_{O_2B}}{D_{O_20}}\right)^{2/3} \left(\frac{\nu_B}{\nu_0}\right)^{-1/3} \tag{15.12}$$

in which D_{O_2} is the oxygen diffusivity (cm^2 s^{-1}), ν is the kinematic viscosity (cm^2 s^{-1}), and subscript B is for blood and subscript 0 for reference liquid. Experimental values of kinematic viscosity of blood ν_B at 37 °C are shown in Figure 15.4b [9] as a function of hematocrit Ht (%).

Experimental values of the enhancement factor E for blood oxygenation under turbulent conditions are shown in Figure 15.5 [9]. Note that values of E shown in this figure were obtained with completely deoxygenated blood and hemoglobin solutions at the oxygen pressure at the interface p_i of 714 mmHg. The concentration of unsaturated hemoglobin should decrease as oxygenation proceeds. Taking this into account, the following concept of the effective hematocrit Ht* was proposed [10, 11].

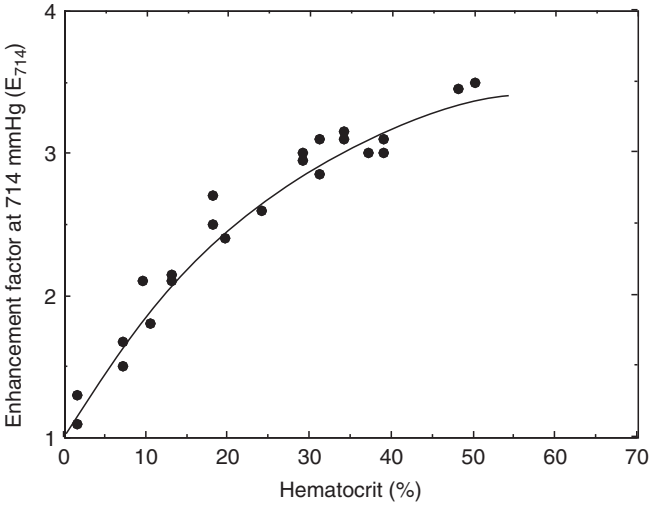

Figure 15.5 Enhancement factor for blood oxygenation.

$$\mathrm{Ht}^* = (1 - y)\mathrm{Ht} \tag{15.13}$$

in which y is the fractional oxygen saturation of blood (–). Thus, the effective hematocrit is the hematocrit corresponding to the unreacted fraction of hemoglobin conceived for convenience. It is reasonable to assume that, for partially saturated blood, the correlation shown in Figure 15.5 holds for Ht* rather than for Ht. The correlation of Figure 15.5 can be represented by the following empirical equation [10, 11].

$$E_{714} = 1 + 11.8\left(\frac{\mathrm{Ht}^*}{100}\right)^{0.8} - 8.9\left(\frac{\mathrm{Ht}^*}{100}\right) \tag{15.14}$$

in which E_{714} is the E value for the oxygen partial pressure at the interface p_i of 714 mmHg. It can be shown that E values for other p_i values can be estimated by the following relationship [9]:

$$E = E_{714}\left(\frac{714}{p_i}\right)^{1/3} \tag{15.15}$$

The overall coefficient of oxygen transfer based on the blood phase K_B (cm s^{-1}), neglecting the gas phase resistance, is given as

$$\frac{1}{K_B} = \frac{\alpha}{K_G} = \frac{1}{k_M} + \frac{1}{k_B^*} \tag{15.16}$$

where K_G is the overall oxygen transfer coefficient based on gas phase (mol or cm^3 min^{-1} cm^{-2} atm^{-1} or mmHg^{-1}), α is the physical oxygen solubility in blood (mol or cm^3 cm^{-3} atm^{-1} or mmHg^{-1}), and k_M is the diffusive oxygen permeability of the membrane (cm min^{-1}).

The flux of oxygen transfer per unit membrane area J_{O_2} (mol or $cm^3\ min^{-1}\ cm^{-2}$) is given by

$$J_{O_2} = K_B(C^* - C) = K_G(p - p^*) \tag{15.17}$$

in which C is the oxygen concentration in blood (mol or $cm^3\ cm^{-3}$), C^* is the fictitious value of C in equilibrium with the oxygen partial pressure in the gas phase p (atm or mmHg), and p^* is the fictitious value of p in equilibrium with C.

As the overall driving potentials $(C^* - C)$ as well as $(p - p^*)$ vary over the membrane surface, some appropriate mean driving potential $(C^* - C)_m$ or $(p - p^*)_m$ should be used in calculating the total rate of oxygen transfer I_{O2} (mol or $cm^3\ min^{-1}$). Thus,

$$I_{O_2} = K_B A(C^* - C)_m = K_G A(p - p^*)_m \tag{15.18}$$

For physical oxygen absorption into an inert liquid (e.g., water), the logarithmic mean, or even the arithmetic mean if the ratio of the driving potentials at both ends is <2, driving potentials can be used. This is not appropriate in calculating the rate of oxygen transfer in membrane oxygenators, as the slope of the oxyhemoglobin dissociation curve varies greatly with the oxygen partial pressure, and values of the enhancement factor E and hence the blood phase mass transfer coefficient $k_B^* = E\,k_B$ will vary as the oxygenation proceeds. The following rigorous method [10, 11] of calculating the required membrane area can be applied to any type of membrane oxygenator.

Let A be the total membrane area (m^2) and dA an infinitesimal increase of A in the blood flow direction. Oxygen saturation y (–) and oxygen partial pressure p (mmHg) increase by dy and dp, respectively, in the membrane area dA. The increase in the oxygen content of blood dN ($cm^3\ cm^{-3}\ min^{-1}$) on dA is given by

$$dN = Q_B\left[\beta\left(\frac{Ht}{100}\right)dy + \alpha dp\right] \tag{15.19}$$

where Q_B is the blood flow rate ($cm^3\ min^{-1}$), Ht is the hematocrit (%), β is the amount of oxygen that combines chemically with the unit volume of red blood cells ($0.451\ cm^3\ cm^{-3}$ at 37 °C), and α is the physical oxygen solubility in blood ($2.82 \times 10^{-5}\ cm^3\ cm^{-3}\ mmHg^{-1}$) at 37 °C. The rate of oxygen transfer to blood through the membrane area dA should be equal to

$$dN = Ek_B\alpha(p_i - p)dA \tag{15.20}$$

where p_i is the pO_2 at the membrane surface. From Equations 15.19 and 15.20, we obtain

$$A = \frac{Q_B}{k_B}\int_{p1}^{p2}\frac{\beta(Ht/100)(dy/dp) + \alpha}{E\alpha(p_i - p)}dp \tag{15.21a}$$

where p_1 and p_2 are p_{O_2} of blood entering and leaving the membrane surface. Values of (dy/dp) can be obtained by differentiating Equation 15.1 or 15.3a. In case the membrane resistance is not negligible, p_i can be estimated by the following relationship and Equation 15.14.

$$(p^* - p_i)k_M = Ek_B(p_i - p) \tag{15.22}$$

where p^* is the p_{O_2} in the gas phase and k_M is the diffusive membrane permeability. The integral of Equation 15.21a can be called the "number of transfer units" (N_M) of the membrane blood oxygenators [10, 11]. Thus, Equation 15.21a can be written as

$$\frac{A}{(N_M)} = \text{ATU} = \frac{Q_B}{k_B} \tag{15.21b}$$

which defines ATU as the "area per transfer unit" of the membrane oxygenators [11]. The smaller the value of ATU, the more efficient the blood oxygenator. Rigorous calculations using the NTU and ATU concepts give rigorous results, but involve graphical integrations. An approximate method, such as that given in Example 15.1, would be simpler. Both rigorous and approximate methods require experimental data on physical oxygen absorption into water, or into a reference liquid (e.g., 0.1% CMC (carboxylmethyl cellulose) solution) that shows kinematic viscosity almost equal to that of blood. The liquid-phase physical oxygen transfer coefficient k_L (cm min^{-1}) for a reference liquid can be obtained as (cf. Section 6.2)

$$k_L = \frac{Q_L \alpha (p_2 - p_1)}{[A(\Delta p)_m \alpha]} \tag{15.23}$$

where Q_L is the liquid flow rate (cm^3 min^{-1}), p_2 and p_1 are the outlet and inlet oxygen partial pressures (mmHg) in the reference liquid, respectively, A is the liquid-side membrane area (cm^2), $(\Delta p)_m$ is the logarithmic mean oxygen partial pressure difference (mmHg), and α is the physical oxygen solubility in liquid (cm^3 cm^{-3} mmHg^{-1}).

Example 15.1

In a hollow-fiber-type membrane blood oxygenator, the blood flows outside and across the hollow fibers. The total membrane area (outside fibers) is 4 m^2. From the data on physical oxygen absorption into water at 20 °C, the following empirical equation (a) for the water-phase oxygen transfer coefficient k_w (cm min^{-1}) in this particular oxygenator at 20 °C was obtained.

$$k_w = 0.106 Q_w{}^{0.6} \tag{a}$$

where Q_w is the water flow rate (l min^{-1}). The oxygen partial pressure in the gas phase is 710 mmHg, and the diffusive membrane resistance can be neglected. Estimate how much venous blood (Ht = 40%, $y = 0.70$) can be oxygenated to arterial blood ($y = 0.97$) with the use of this oxygenator. At 37 °C, the oxygen content of the blood increases by 0.0168 cm^3 cm^{-3}blood with increase in the fractional oxygen saturation $\Delta y = 0.1$.

Solution

The required total membrane area is subdivided into three zones 1, 2, and 3 by the ranges of oxygen saturation y.

Blood phase-oxygen transfer coefficient k_B is estimated by Equations 15.11 – 15.13. Oxygen diffusivity in water at 20 °C, $D_{O_2W} = 2.07 \times 10^{-5}$ cm^2 s^{-1}; kinematic viscosity of water at 20 °C, $\nu_w = 0.010$ cm^2 s^{-1}; oxygen diffusivity in blood at 37 °C, $D_{O_2B} = 1.76 \times 10^{-5}$ cm^2 s^{-1}; kinematic viscosity of blood at 37 °C, $\nu_B = 0.0256$ cm^2 s^{-1}.

By Equation 15.12

$$\frac{k_B}{k_w} = \frac{(1.76/2.07)^{2/3}}{(0.0256/0.010)^{1/3}} = 0.656 \qquad \text{(b)}$$

The enhancement factor E for each zone is estimated by Equations 15.13 and 15.14.

After several trials, a blood flow rate of 5 l min^{-1} is assumed. Then, by Equation a

$$k_w = 0.278 \text{ cm min}^{-1}$$

and by Equation b

$$k_B = 0.278 \times 0.656 = 0.182 \text{ cm min}^{-1}$$

Calculations for the three zones are summarized as follows:

	Zone 1	Zone 2	Zone 3
y	0.70 – 0.80	0.80 – 0.90	0.90 – 0.97
y_m	0.75	0.85	0.94
pO_2 at y_m (mmHg)	40	52	70
Effective Ht* (%)	10	6	2.4
E	1.98	1.71	1.38
$E\,k_B$	0.360	0.311	0.251
$K_G = \alpha E\,k_B$	10.15×10^{-6}	8.77×10^{-6}	7.08×10^{-6}
$(\Delta p)_m$ (mmHg)	670	658	640
O_2 transfer (cm^3 min^{-1})	84.0	84.0	58.8
$A = Q_o/K_G\,(\Delta p)_m$ (m^2)	1.24	1.46	1.30

The total membrane area required is 4.00 m^2. Thus, this oxygenator with 4 m^2 membrane area can oxygenate 5 l min^{-1} of blood, as assumed.

15.3.6
Carbon Dioxide Transfer Rates in Blood Oxygenators

As mentioned in Section 15.3.3, most CO_2 in blood exists as HCO_3^-. In evaluating the CO_2 desorption performance of blood oxygenators, we must always consider the simultaneous diffusion of HCO_3^-, the rate of which is greater than that of physically dissolved CO_2. Experimental data on the rates of CO_2 desorption

from blood and hemoglobin solutions in membrane oxygenators agreed well with the values that were theoretically predicted, taking into account the simultaneous diffusion of HCO_3^- [12].

The driving potential for CO_2 transfer in the natural lung is the difference between pCO_2 of the venous blood (46 mmHg) and that in the alveolar gas (40 mmHg), as can be seen from Table 15.1. The CO_2 transfer rates in blood oxygenators should correspond to those of oxygen transfer, the driving force for which is much larger than in the natural lung, because the pO_2 in the gas phase is usually over 700 mmHg. However, the physical solubility of CO_2 in blood is about 20-fold larger than that of oxygen, and more CO_2 is transferred as HCO_3^-. At the blood–gas interface, HCO_3^- is desorbed as CO_2 gas. Thus, the usual practice with gas–liquid direct contact-type oxygenators, such as the bubble-type, would be to add some CO_2 gas to the gas supplied to the oxygenator in order to suppress excessive CO_2 desorption.

In membrane-type oxygenators, the CO_2 passes through the membrane only as CO_2. Although the CO_2 permeabilities of most membranes are several-fold greater than those for O_2, the driving potential for CO_2 transfer is much smaller than that for O_2 transfer. Thus, if the membrane permeability for CO_2 is not high enough, then an insufficient CO_2 removal rate would become a problem. However, this is not the case with most membranes used today, including microporous membranes. Difficulties in CO_2 removal reported with membrane oxygenators are often due to too-low gas rates, resulting in too-high CO_2 content in the gas phase and hence too-small a driving potential for CO_2 transfer. In such a case, increasing the gas flow rates would solve the problem. In most cases, membrane-type oxygenators with sufficient membrane areas for oxygen transfer encounter no problems with CO_2 removal.

15.4 Artificial Kidney

The hemodialyzer, also known as the artificial kidney, is a device that is used outside the body to remove the so-called the uremic toxins, such as urea and creatinine, from the blood of patients with kidney disease. While it is a crude device compared to the exquisite human kidney, many patients who are unable to receive a kidney transplant can survive for long periods with the use of this device.

15.4.1 Human Kidney Functions

The main functions of the human kidney are the formation and excretion of urine, and control of the composition of body fluids. Details of the structure and functions of the human kidney may be found in textbooks of physiology [1] or biomedical engineering [13]. Each of the two human kidneys contains approximately one million units of tubules (nephrons), each 20–30 μm in diameter, and with a total

length of 4–7 cm. Each tubule begins blindly with a renal corpuscle, which consists of the *glomerulus* (about 200 μm in diameter) and the surrounding capsule, which is connected to the *proximal convoluted tubule*, the descending and ascending limbs of the hairpin-shaped *loop of Henle*, the *distal convoluted tubule*, and finally to the *collecting tubule*. The glomerulus, a tuft of arterial capillaries, acts as a blood filter, and the composition of the glomerular filtrate changes as the filtrate flows through the above-mentioned sections of the tubule, and finally becomes urine. Changes in filtrate compositions occur due to the exchange of components with the blood coming from the glomerulus that flows through the capillaries surrounding tubule and hairpin-shaped capillaries alongside the loop of Henle.

The total blood flow rate through the two kidneys is approximately $1200\,cm^3\,min^{-1}$, which is about one-fourth of the total cardiac output. The glomeruli filter out all blood corpuscles and most molecules with molecular weight above 70 000–80 000 Da. The *glomerular filtration rate* (*GFR*) is approximately $125\,cm^3\,min^{-1}$ (i.e., 180 l per day), which is approximately one-fifth of the rate at which plasma enters the kidneys. As the volume of urine excreted daily is approximately 1–1.5 l, most of the water in the glomerular filtrate is reabsorbed into the blood. Not only the filtrate volume but also the concentrations of all components of the filtrate undergo adjustments as the filtrate flows through the tubules, with unrequired metabolic products (such as urea) being excreted into the urine. Thus, it can be said that the general function of the kidney is to finely control the compositions of the body fluids at appropriate levels.

The mechanisms of transfer of molecules and ions across the wall of tubules are more complicated than in the artificial apparatus. In addition to osmosis and simple passive transport (*viz*., ordinary downhill mass transfer due to concentration gradients), renal mass transfer involves active transport (*viz*., uphill mass transport against gradients). The mechanism of active transport, which often occurs in living systems, is beyond the scope of this text. Active transport requires a certain amount of energy, as can be seen from the fact that live kidneys require an efficient oxygen supply.

As is evident from the major difference between the GFR and the rate of urine production, the majority of the water in the filtrate is reabsorbed into the blood in the capillaries, by osmosis through the wall of the tubule and the interstitial fluid. This reabsorption of water occurs mostly in the proximal tubule, although some is also reabsorbed in the distal tubule and collecting duct.

At the proximal tubule, the concentrations of glucose, proteins, and amino acids decrease greatly due to reabsorption by active transport into the capillary blood. Na^+, K^+, Cl^-, and HCO_3^- are also reabsorbed by active transport, although their concentrations vary minimally due to the large decrease in the water flow rate.

The loop of Henle consists of a descending limb that connects to the proximal tubule, and an ascending limb that connects to the distal tubule. The wall of the descending limb is water permeable, whereas the wall of the ascending limb is not. Na^+, K^+, Cl^-, and HCO_3^- that are reabsorbed by active transport across the wall of the ascending limb diffuse through the interstitial fluid into the fluid in the descending limb by passive transport. The concentrations of these ions are

decreased substantially in the ascending limb, but are increased in the descending limb.

In the distal tubule and collecting duct, some Na^+ is either actively transported out or exchanged for K^+, H^+, $NH_4{}^+$, and water moves out by osmosis. Thus, the ion concentrations and pH of the body fluids are maintained at appropriate levels.

A 1 l volume of urine from a healthy person contains approximately 1800 mg of urea, 200 mg of creatinine, 130 mEq of Na^+, 130 mEq of Cl^-, and lesser amounts of other ions. The concentrations of urea and creatinine, both of which are breakdown products of protein metabolism, are increased in the tubular fluid during flow through the tubule, due to a decrease in water flow rate.

The GFR can be measured by injecting into blood vessel a substance x, which is neither reabsorbed nor secreted in the tubule, and measuring its concentration in the urine. Inulin, a polymer of fructose, is extensively used to measure the GFR. Let V be the urine flow rate, ($cm^3\ min^{-1}$), U_x the concentration of x in urine, and P_x the concentration of x in plasma. Then, $GFR = U_x\ V/P_x$. This is the volume of plasma per unit time, ($cm^3\ min^{-1}$), from which x is totally removed, leading to the following concept of clearance.

Clearance of the kidney with respect to some particular substance (e.g., urea) is defined as the conceptual volume of plasma per unit time, ($cm^3\ min^{-1}$) from which the substance is completely removed. Thus, clearance for x, Cl_x, ($cm^3\ min^{-1}$), is defined as

$$Cl_x = \frac{U_x V}{P_x} \tag{15.24}$$

where U_x is the concentration of x in urine, ($mg\ dl^{-1}$), V is the urine flow rate, ($cm^3\ min^{-1}$), and P_x is the concentration of x in plasma, ($mg\ dl^{-1}$). For example, if the urea concentrations in plasma and in urine are 34 and 1450 $mg\ dl^{-1}$, respectively, and the urine flow rate is 1.3 $cm^3\ min^{-1}$, then the urea clearance can be calculated as follows:

$$Cl_x = \frac{1450 \times 1.3}{34} = 55\ cm^3\ min^{-1}$$

Clearance for a substance is equal to the GFR, only if neither reabsorption nor secretion of the substance occurs during its flow through the tubule. Clearance for a substance decreases with increasing reabsorption of the substance in the tubule.

In the cases of kidney disease, due to the impaired function of the glomeruli and/or tubules, urea, creatinine, and other substances that would normally be excreted into the urine would accumulate in the blood of the patient, causing various symptoms and disorders.

15.4.2 Artificial Kidneys

15.4.2.1 Hemodialyzer

The main form of artificial kidney is the *hemodialyzer*, which uses semipermeable membranes to remove urea and other metabolic wastes, as well as some water

and ions, from the blood of patients with kidney diseases. Compared to the human kidney, the hemodialyzer is a very crude device for use outside the body. Unlike the kidney, in which both active and passive transport of various substances occurs, the hemodialyzer depends only on the passive transport of substances between the blood and the dialysate solution, across an artificial semipermeable membrane. Urea, creatinine, and other metabolic products move into the dialysate by diffusive mass transfer, that is, by concentration difference. Some water must be removed from the body fluid into the dialysate. This can be achieved either by (i) making the hydrostatic pressure of the blood side slightly higher than that of the dialysate side or (ii) adding glucose or another sugar to the dialysate to make its osmolarity slightly higher than that of the body fluid, so that water moves into the dialysate by osmosis (cf. Section 8.5).

Although the initial proposals and studies of hemodialyzers date back to the early twentieth century, it was not until 1945 that Kolff used a hemodialyzer in a clinical situation. This was a long cellophane tube wound around a rotating drum that was immersed in a dialysate solution. The earlier models of hemodialyzers, such as the rotating-drum and flat-membrane types, were bulky and nondisposable. A pre-sterilized, disposable dialyzer of the coil (Kolff) type, in which blood flowed through a coil of flattened membrane tube, while the dialysate flowed through the interstices in the coil in the axial direction, first appeared in 1956. Disposable hemodialyzers of the hollow-fiber and flat-membrane types were first marketed during the early 1970s. Today, the hollow-fiber hemodialyzer is the most widely used, due mainly to its compactness and high efficiency. For example, a dialyzer of this type uses approximately 10 000 hollow fibers, each of some 200 μm internal diameter and 100–250 mm length. In this system, the blood flows through the fibers, and the dialysate outside the fibers.

The blood of the patient, withdrawn from an artery near the wrist, is allowed to flow through the blood circuit, which includes the dialyzer, usually a blood pump plus monitoring instruments, and is returned to a nearby vein. The connections to the blood vessels are made via the so-called "subcutaneous arteriovenous shunt"; this involves an artificial tube that connects the artery and vein underneath the wrist skin.

A dialysate solution of a composition appropriate to the patient is prepared by diluting with water one of concentrated dialysates of standard compositions that are available commercially. Typical compositions of diluted dialysates are as follows: Na^+: 130–140 mEq l^{-1}, K^+: 2–2.5 mEq l^{-1}, Ca^{2+}: 2.5–3.5 mEq l^{-1}, Mg^{2+}: 1.0–1.5 mEq l^{-1}, Cl^-: 100–110 mEq l^{-1}, HCO_3^-: 30–35 mEq l^{-1}, glucose: 0 or 1–2 g l^{-1}, osmolarity: 270–300 mOsm l^{-1}. Electrolytes are added to the dialysate mainly to prevent electrolytes in the body fluid from moving into the dialysate, and sometimes to control the concentration of some ions such as Na^+ in the body fluid at an appropriate level.

The dialysate solution is recirculated through the hemodyalyzer system. In hospitals where multiple patients are treated, central dialysate supply systems are normally used. The flow rates of blood and dialysate through a hollow-fiber-type

dialyzer are approximately 200–300 and 500 $cm^3\ min^{-1}$, respectively. The more recently developed hemodialyzers have all been disposable; that is, they are presterilized and used only once. Normally, a patient undergoes dialysis for 4–5 h per day, for 3 days each week.

Operationally, dialysis (cf. Section 8.2) utilizes differences in the diffusion rates of various substances across a membrane between two liquid phases. The diffusivities of substances in the membrane and liquid phases (particularly the former) decrease with increasing molecular sizes of the diffusing substances. Thus, with any hemodialyzer, the rates of removal of uremic toxins from the blood will decrease with increasing molecular size, although sharp separation at a particular molecular weight is difficult. In contrast, proteins (e.g., albumin) should be retained in the patient's blood. In the human kidney, small amounts of albumin present in the glomerular filtrate are reabsorbed in the proximal tubule.

Hemodialysis, which involves some transfer of water due to differences in the hydrostatic or osmotic pressure, is often referred to as *hemodiafiltration* (*HDF*).

15.4.2.2 **Hemofiltration**

In the *hemofiltration* (*HF*) (i.e., ultrafiltration; see Section 8.3) of blood, using an appropriate membrane, all of the solutes in plasma below a certain molecular weight will pass into the filtrate at the same rate, irrespective of their molecular sizes, as occurs in the human kidney glomeruli. Since its first proposal in 1967 [14], HF has been studied extensively [15–17]. Although a dialysate solution is not used in HF, the correct amount of substitution fluid must be added to the blood of the patient, either before or after filtration, to replace all the necessary blood constituents that are lost in the filtrate. This substitution fluid must be absolutely sterile, as it is mixed with the patient's blood. For these reasons, HF is more expensive to perform than hemodialysis, and so is not generally used to the same extent.

15.4.2.3 **Peritoneal Dialysis**

As an artificial dialyzer is not used in peritoneal dialysis, use of the term "artificial kidney" might not be appropriate in this case. In peritoneal dialysis,the dialysate solution is infused into the peritoneal cavity of the patient and later discharged. Uremic toxins in the blood are removed as the blood flows through the capillaries in the peritoneum to the dialysate by diffusion. Water is removed by adding glucose to the dialysate, thereby making the osmolarity of dialysate higher than that of the blood.

In *continuous ambulatory peritoneal dialysis* (*CAPD*), approximately 2 l of dialysate solution is infused into the patient's peritoneal cavity, and is exchanged with new dialysate about four times each day. The patient need not stay in bed, as with ordinary hemodialysis, but it is difficult to continue CAPD for many years due to the formation of peritoneal adhesions.

15.4.3
Mass Transfer in Hemodialyzers (cf. 8.2)

In the situation where the effect of filtration – that is, water movement across the membrane due to the difference in hydrostatic pressure and/or osmolarity – can be neglected, the overall resistance for mass transfer in hemodialyzers with flat membranes is given as

$$\frac{1}{K_L} = \frac{1}{k_B} + \frac{1}{k_M} + \frac{1}{k_D} \tag{15.25}$$

where K_L is the overall mass transfer coefficient (cm min^{-1}), k_B is the blood phase mass transfer coefficient (cm min^{-1}), k_M is the diffusive membrane permeability (cm min^{-1}), and k_D is the dialysate phase mass transfer coefficient (cm min^{-1}). Equation 15.25 holds for each of the diffusing components. The blood phase mass transfer coefficient k_B and the dialysate phase mass transfer coefficient k_D can generally be estimated when the design and operating conditions of the hemodialyzer are known (cf. Chapter 6). The diffusive membrane permeability k_M varies with the material and thickness of the membrane, and with the diffusing components. This must be experimentally determined by using an appropriate apparatus under standard conditions.

Many membrane materials have been developed and are used for hemodialyzers. Today, these include regenerated cellulose, cellulose acetate, polyacrylonitrile, poly(methylmethacrylate), vinyl alcohol-ethylene copolymer, polysulfone, polyamide, and others.

The relative magnitudes of the three terms on the right-hand side of Equation 15.25 vary with the diffusing substance, the flow conditions of both fluids, and especially with the membrane material and thickness. With the hollow-fiber-type hemodialyzers that are widely used today, membrane resistance usually takes a substantial fraction of the total resistance, and the fraction increases with increasing molecular weight of the diffusing component.

One widely used performance index of hemodialyzers is that of clearance, defined similarly to that of the human kidney. The clearance of a hemodialyzer is the conceptual volume of blood (cm^3 min^{-1}) from which a uremic substance is completely removed by hemodialysis. Let Q_B (cm^3 min^{-1}) be the blood flow rate through the dialyzer, Q_D (cm^3 min^{-1}) the dialysate flow rate, and C_B and C_D (mg cm^{-3}) the concentrations of a uremic substance in the blood and the dialysate, respectively, with the subscripts i and o indicating values at the inlet and outlet, respectively. The rate of transfer of the substance in the dialyzer w (mg min^{-1}) is then given as

$$w = Q_B(C_{Bi} - C_{Bo}) = Q_D(C_{Do} - C_{Di}) \tag{15.26}$$

The clearance of the hemodialyzer Cl (cm^3 min^{-1}) for the substance is defined as

$$\mathrm{Cl} = \frac{w}{C_{Bi}} = \frac{Q_B(C_{Bi} - C_{Bo})}{C_{Bi}} = \frac{Q_D(C_{Do} - C_{Di})}{C_{Bi}} \tag{15.27}$$

From the mass transfer relations (cf. Chapter 6),

$$w = K_L A(\Delta C)_{lm} = \frac{K_L A(\Delta C_1 - \Delta C_2)}{\ln(\Delta C_1/\Delta C_2)} \tag{15.28}$$

where A (cm^2) is the membrane area. In the case of hollow fiber membranes, A is the inside or outside area of the fiber with which K_L is defined and $(\Delta C)_{lm}$ is the logarithmic mean (cf. Section 5.3) of the concentration difference at one end of the dialyzer, ΔC_1, and that at the other end, ΔC_2. In theory, the log mean can be used only for the cases of (i) countercurrent flow; (ii) parallel-current flow; and (iii) one phase completely mixed. However, in the case where the ratio of the concentration differences at both ends is <2, the simple arithmetic mean could practically be used, as the difference between the two mean values is less than a small percentage.

Another index of hemodialyzer performance is the *dialysance*, ($cm^3\,min^{-1}$), defined as

$$\mathrm{Dl} = \frac{w}{(C_{Bi} - C_{Di})} = \frac{K_L A(\Delta C)_{lm}}{(C_{Bi} - C_{Di})} \tag{15.29}$$

Note that the denominator is $(C_{Bi} - C_{Di})$ in place of C_{Bi} in Equation 15.27. Dialysance is the conceptual volume of blood ($cm^3\,min^{-1}$) from which a uremic substance is removed down to a concentration equal to its concentration in the entering dialysate. In case the entering dialysate does not contain the substance, dialysance is equal to clearance.

It should be noted also that the values of clearance and dialysance may vary with the particular uremic substance, such as urea and creatinine, with which clearance and dialysance are defined. From Equations 15.26 and 15.29

$$E = \frac{\mathrm{Dl}}{Q_B} = \frac{(C_{Bi} - C_{Bo})}{(C_{Bi} - C_{Di})} \tag{15.30}$$

which defines the extraction ratio E.

Combining Equations 15.27–15.30 and further manipulation results in the following relationships [18]:

1) *For Counter Flow*:

$$E = \frac{\{1 - \exp[N_M(1 - Z)]\}}{\{Z - \exp[N_M(1 - Z)]\}} \tag{15.31}$$

2) *For Parallel Flow*:

$$E = \frac{\{1 - \exp[-N_M(1 + Z)]\}}{(1 + Z)} \tag{15.32}$$

where

$$N_M \text{ (number of transfer units)} = \frac{K_L A}{Q_B} \tag{15.33}$$

$$Z \text{ (flow ratio)} = \frac{Q_B}{Q_D} \tag{15.34}$$

In the above relationships, the effect of the so-called "filtration" – that is, the permeation of water across the membrane – on the clearance and dialysance has been neglected. In the case where the Q_F ($cm^3\,min^{-1}$) of water moves from the blood phase to the dialysate across the membrane, the clearance of a hemodialyzer with respect to a uremic substance Cl^* is given as

$$\begin{aligned} Cl^* &= \frac{(Q_{Bi}C_{Bi} - Q_{Bo}C_{Bo})}{C_{Bi}} \\ &= \frac{\{(Q_{Bo} + Q_F)C_{Bi} - Q_{Bo}C_{Bo}\}}{C_{Bi}} \\ &= \{(C_{Bi} - C_{Bo})Q_{Bo}/C_{Bi}\} + Q_F \end{aligned} \tag{15.35}$$

Example 15.2

In a hollow-fiber-type hemodialyzer of the following specifications, $200\,cm^3\,min^{-1}$ of blood (inside fibers) and $500\,cm^3\,min^{-1}$ of dialysate (outside fibers) flow countercurrently.

Hollow fiber inside diameter = 212 μm

Membrane thickness = 20.7 μm

Effective length of hollow fibers: $L = 16.8\,cm$

Inside diameter of the shell: $D_i = 2.86\,cm$

Total membrane area (based on i.d.): $A = 7400\,cm^2$

Diffusive membrane permeability (based on i.d.) : $k_M = 0.00116\,cm\,s^{-1}$

Calculate the overall mass transfer coefficient K_L (based on the hollow-fiber inside diameter) and the dialysance of the hemodialyzer for urea, neglecting the effect of water permeation.

Data: Urea diffusivity in blood: $D_B = 0.507 \times 10^{-5} cm^2 s^{-1}$

Urea diffusivity in dialysate: $D_D = 1.37 \times 10^{-5} cm^2 s^{-1}$

Blood viscosity: $\mu_B = 0.027\ g\ cm^{-1} s^{-1}$

Blood density: $\rho_B = 1.056\ g\ cm^{-3}$

Solution

For simplicity, it is assumed that the dialysate flows parallel to the hollow fibers, although the real flow pattern is not so simple.

Number of hollow fibers:

$$n = \frac{7400}{(\pi \times 0.0212 \times 16.8)} = 6617$$

The blood phase urea transfer coefficient k_B is estimated as follows:
Volumetric blood flow rate through one hollow fiber:

$$F_B = \frac{200}{(60 \times 6617)} = 5.04 \times 10^{-4}\,\text{cm}^3\,\text{s}^{-1}$$

Blood velocity through hollow fibers:

$$v_B = \frac{5.04 \times 10^{-4}}{[(\pi/4)(0.0212)^2]} = 1.428\ \text{cm s}^{-1}$$

$$\text{Blood Reynolds number} = (\text{Re})_B = \frac{(0.0212)(1.428)(1.056)}{0.027} = 1.184$$

The blood-side mass transfer coefficient k_B is estimated by Equation 6.26b.
Since $(F_B/D_B L) = 5.04 \times 10^{-4}/[(0.507 \times 10^{-5})\ (16.8)] = 5.91 < 10$ it can be assumed that $(\text{Sh}) = k_B d/D_B = 3.66$
Then $k_B = (3.66)(0.507 \times 10^{-5})/(0.0212) = 8.75 \times 10^{-4}\,\text{cm s}^{-1}$.
The dialysate phase urea transfer coefficient k_D is estimated as follows.
Sectional area of the dialysate channel:

$$S = \left(\frac{\pi}{4}\right)(2.86^2 - 6618 \times 0.0253^2) = 3.096\ \text{cm}^2$$

Equivalent diameter of the dialysate channel:

$$d_E = \frac{4S}{(\text{wetted perimeter})} = \frac{4(3.096)}{[\pi(0.0253)6,617 + 2.86\pi]}$$
$$= 0.0232\ \text{cm} = 232\,\mu\text{m}$$

Dialysate velocity through the channel:

$$u_D = \frac{500}{(60)\ (3.096)} = 2.69\ \text{cm s}^{-1}$$

Dialysate Reynolds number:

$$(\text{Re})_D = \frac{d_E u_D \rho_D}{\mu_D} = \frac{(0.0232)(2.69)\ (1.00)}{(0.01)} = 6.25$$

Hence, it is assumed that $(\text{Sh}) = (k_D d_E/D_D) = 3.66$.

$$k_D = \frac{3.66 D_D}{d_E} = \frac{(3.66)(1.37 \times 10^{-5})}{0.0232}$$
$$= 2.16 \times 10^{-3}\text{cm s}^{-1}(\text{based on fiber o.d.})$$

The overall urea transfer coefficient K_L: (based on fiber i.d.)

$$\frac{1}{K_L} = \frac{1}{k_B} + \frac{1}{k_M} + \frac{1}{[k_D(252/212)]}$$
$$= 1140 + 862 + 389 = 2391\ \text{s cm}^{-1}$$

$$K_L = 0.000418\ \text{cm s}^{-1} = 0.0251\ \text{cm min}^{-1}$$

$$N_M = \frac{K_L A}{Q_B} = \frac{(0.0251)(7400)}{200} = 0.929$$

$$Z = \frac{Q_B}{Q_D} = \frac{200}{500} = 0.4$$

Equation 15.31 gives the extraction ratio:

$$E = \frac{[1 - \exp(0.929 \times 0.6)]}{[0.4 - \exp(0.929 \times 0.6)]} = 0.554$$

Dyalysance for urea is given by Equation 15.30:

$$\mathrm{Dl} = Q_B E = 200 \times 0.554 = 111 \text{ cm}^3 \text{ min}^{-1}$$

15.5 Bioartificial Liver

15.5.1 Human Liver

In humans, the liver is the largest organ, typically weighing 1.2–1.6 kg. The many functions of the liver are performed by the liver cells, or *hepatocytes*. One important function of the liver is the secretion of *bile*, which is essential for the digestion and absorption of lipids in the intestine. Bile, when collected through the bile capillaries by the bile ducts that unite with the hepatic duct, is either transferred to the *gallbladder* or enters the *duodenum* directly. Other functions performed by liver cells, through contact with blood, include the metabolism and storage of carbohydrates, the detoxication of drugs and toxins, the manufacture of plasma proteins, the formation of urea, and the metabolism of fat, among many others. The liver can, therefore, be regarded as the complex "chemical factory" of the human body.

Two main blood vessels (Figure 15.1) enter the liver: the *hepatic artery* carries oxygen-rich blood directly from the heart, while the *hepatic portal vein* carries blood from the spleen and nutrient-rich blood from the intestine. On leaving the liver, the blood is returned to the heart via the hepatic vein.

The liver contains an enormous number of hepatocytes that perform the various functions noted above. The hepatocytes are contained within minute units known as *hepatic lobules*, in which the cell layers (which are one or two cells thick) are in contact with networks of minute blood channels – the *sinusoids* – which ultimately join the venous capillaries. Capillaries carrying blood from the hepatic artery and the portal vein empty separately into the sinusoids. The walls of sinusoids and liver cells are incomplete, and blood is brought into direct contact with the hepatocytes.

Bile is an aqueous solution of bile salts, inorganic salts, bile pigments, fats, cholesterol, and others. The physiology of bile secretion is not simple, as it involves the active excretion of organic solutes from the blood to the bile. Bile is collected directly from the liver cells through separate channels, without being mixed with blood. The liver cell membrane incorporates extremely fine passages that permit bile secretion.

15.5.2 Bioartificial Liver Devices

Although certain simple functions of the liver, such as the removal of some toxins, can be performed by using dialysis and adsorption with activated charcoal, it is clear that such a simple artificial approach cannot perform the complex functions of the liver, and that any practical liver support system must use living hepatocytes. It should be mentioned at this point that hepatocytes have an anchorage-dependent nature; that is, they require a form of "anchor" (i.e., a solid surface or scaffold) on which to grow. Thus, the use of single-cell suspensions is not appropriate for liver cell culture, and liver cells attached to solid surfaces are normally used. Encapsulated liver cells and spheroids (i.e., spherical aggregates of liver cells) may also be used for this purpose.

In recent years, many investigations have been conducted, including clinical trials, with bioartificial liver devices using either animal or human liver cells. Likewise, many reports have been made with various designs of bioartificial liver device [19]. However, there are no established liver support systems that can be used routinely in the same way as hemodialyzers or blood oxygenators. Today, bioartificial liver devices can be used to assist the liver functions of patients with liver failure on only a partial and/or a temporary basis. Moreover, none of these devices can excrete bile, as does the human liver.

It should be noted here that the bioartificial liver device is not only a bioreactor but also a mass transfer device. The mass transfer of various nutrients from the blood into the liver cells, and also the transfer of many products of biochemical reactions from the cells into the bloodstream, should be efficient processes. In human liver, the oxygen-rich blood is delivered via the hepatic artery, and bioartificial devices should be so designed that the oxygen can be easily delivered to the cells.

In order to sustain life, a bioartificial liver device should contain at least 10–30% of the normal liver mass (i.e., 150–450 g of cells in the case of an adult). In a bioartificial liver device, the animal or human liver cells can conceivably be cultured and used in several forms, including (i) independent single-cell suspensions; (ii) spheroid (i.e., globular) aggregates of cells of 100–150 μm diameter; (iii) cylindroid, rod-like aggregates of cells of 100–150 μm diameter; (iv) encapsulated cells; and (v) cells attached to solid surfaces, such as microcarriers, flat surfaces, and the inside or outside of hollow fibers. In order to facilitate mass transfer, a direct contact between the cells and the blood seems preferable. Among the various types of bioartificial liver devices tested to date, four distinct groups can be identified [19]:

1) *Hollow Fibers*. The general configuration of the hollow-fiber apparatus is similar to that of hemodialyzers and blood oxygenators. Hepatocytes or microcarrier-attached hepatocytes are cultured either inside the hollow fibers or in the extra-fiber spaces, and the patient's blood is passed outside or inside the fibers. A bioartificial liver of this type, using 1.5 mm o.d. hollow fibers with 1.5 mm clearance between them, and with tissue-like aggregates of animal hepatocytes cultured in the extra-fiber spaces, can maintain liver functions for a few months [20].
2) *Flat Plates*. In this case, the hepatocytes are cultured on multilayered solid sheets, between which the blood is passed through narrow channels. This configuration, with direct blood-cell contact, somewhat resembles that of the human liver. However, scale-up is not easy because of the possible maldistribution of blood, and the existence of large dead spaces.
3) *Packed Bed*. Here, the hepatocytes are cultured on the inside surfaces of small pieces of highly porous resin that are packed randomly in a vertical cylindrical reactor [21]. A high cell density can be attained, as the cells grow in the minute pores of the resin. The cells are in direct contact with the blood.
4) *Encapsulation and Suspension*. In this case, encapsulated spheroids of hepatocytes are contacted with blood in fluidized-bed, spouted-bed, and/or packed-bed systems. The mass transfer resistance should be high with encapsulated cells. However, the use of a suspension would lead to excessive shear forces being exerted on the cells.

The bioartificial liver support systems tested to date have been shown to perform liver functions on only a partial and/or temporary basis. The development of a true "bioartificial liver" will require more fundamental studies to be conducted, and in this regard "tissue engineering" involving nanobiotechnology will undoubtedly play an important role. Tissue engineering applies the principles of engineering and biology to the development of biological substitutes that restore, maintain, or improve tissue functions [22]. To date, the regeneration of skin, cornea, and other tissues has been studied by tissue engineers. The structure of the bioartificial liver devices mentioned above differs notably from that of the natural liver. Hence, the culture of liver tissue, which is more similar to the human liver, using hepatocytes to create an implantable, bioartificial liver, should be the target of tissue engineering research.

▶ Problems

15.1 The pH of a blood sample is 7.40 at 310 K, and its total CO_2 concentration is 25.2 mmol l^{-1}. Estimate the partial pressure of CO_2 for this blood sample.

15.2 A hollow-fiber-type membrane blood oxygenator, in which blood flows inside the hollow fibers, has a total membrane area (outside fibers) of 4.3 m^2. The inside diameter, membrane thickness, and length of the hollow fibers are 200 μm, 25 μm, and 13 cm, respectively. When venous blood (Ht = 40%, pO_2 = 36 mmHg)

is supplied to the oxygenator at a flow rate of $4.0\,l\,min^{-1}$ and 310 K, estimate the oxygen saturation of the blood at the exit by the advancing front model. The partial pressure of oxygen in the gas phase is 710 mmHg, and the diffusive membrane resistance can be neglected.

15.3 For the situation in Problem 15.2, calculate the pressure drop through the hollow fibers. The density of blood is $1.05\,g\,cm^{-3}$ at Ht = 40%.

15.4 In a hollow-fiber-type hemodialyzer, $200\,cm^3\,min^{-1}$ of blood (inside fibers) and $500\,cm^3\,min^{-1}$ of dialysate (outside fibers) flow countercurrently. The urea concentrations of the inlet blood, outlet blood, and outlet dialysate are 100, 20, and $32\,mg\,dl^{-1}$, respectively. Calculate the clearance for urea.

15.5 In a hollow-fiber-type hemodialyzer of the total membrane area (based on o.d.) $A = 1\,m^2$, $200\,cm^3\,min^{-1}$ of blood (inside fibers) and $500\,cm^3\,min^{-1}$ of dialysate (outside fibers) flow countercurrently. The overall mass transfer coefficient K_L for urea (based on the outside diameter of the hollow fiber) is $0.030\,cm\,min^{-1}$. Estimate the dialysance for urea.

References

1. Ganong, W.F. (1989) *Medical Physiology*, 14th edn, Lange Medical Publications.
2. Kahle, W., Leonhardt, H., and Platzer, W. (1986) *Color Atlas and Textbook of Human Anatomy*, vol. 2, Internal Organs, Thieme, Stuttgart and New York.
3. Adair, G.S. (1925) *J. Biol. Chem.*, **63**, 515.
4. Lambertsen, C.T., Bunce, P.L., Drabkin, D.L., and Schmidt, C.F. (1952) *J. Appl. Physiol.*, **4**, 873.
5. Ohshima, N. and Yoshida, F. (1971) *Bull. Heart Inst. Jpn.*, **13**, 14.
6. Hill, A.V. (1921) *Biochem. J.*, **15**, 577.
7. Comroe, J.H. (1970) *Physiology of Respiration*, Year Book Medicine Publications.
8. Lightfoot, E.N. (1968) *AIChE J.*, **14**, 669.
9. Katoh, S. and Yoshida, F. (1972) *Chem. Eng. J.*, **3**, 276.
10. Shimizu, S. and Yoshida, F. (1981) *Jinko Zoki*, **10**, 179 (in Japanese).
11. Yoshida, F. (1993) *Artif. Organs Today*, **2**, 273.
12. Katoh, S. and Yoshida, F. (1978) *Ann. Biomed. Eng.*, **6**, 48.
13. Cooney, D.O. (1976) *Biomedical Engineering Principles*, Marcel Dekker, Inc.
14. Henderson, L.W., Besarab, A., Michaels, A., and Bluemle, L.W. Jr., (1967) *Trans. Am. Soc. Artif. Intern. Organs*, **13**, 216.
15. Colton, C.K. (1975) *J. Lab. Clin. Med.*, **85**, 355.
16. Porter, M.C. (1972) *Ind. Eng. Chem. Prod. Res. Dev.*, **11**, 234.
17. Okazaki, M. and Yoshida, F. (1976) *Ann. Biomed. Eng.*, **4**, 138.
18. Michaels, A.S. (1968) *Chem. Eng. Prog.*, **64**, 31.
19. Allen, J.W., Hassanein, T., and Bhatia, S.N. (2001) *Hematology*, **34**, 447.
20. Funatsu, K. *et al.* (2001) *Artif. Organs*, **25**, 194.
21. Ohshima, N., Yanagi, K., and Miyoshi, H. (1997) *Artif. Organs*, **21**, 1169.
22. Langer, R. and Vacanti, J.P. (1993) *Science*, **260**, 920.

Appendix A: Conversion Factors for Units

Parameter (dimension)

Length (L)	Meter (m)	Centimeter (cm)	Inch (in)	Foot (ft)
	1	1.00000E + 02	3.93701E + 01	3.28084E + 00
	1.00000E − 02	1	3.93701E − 01	3.28084E − 02
	2.54000E − 02	2.54000E + 00	1	8.33333E − 02
	3.04800E − 01	3.04800E + 01	1.20000E + 01	1

Mass (M)	Kilogram (kg)	Gram (g)	Ounce (oz)	Pound (lb)
	1	1.00000E + 03	3.52740E + 01	2.20462E + 00
	1.00000E − 03	1	3.52740E − 02	2.20462E − 03
	2.83495E − 02	2.83495E + 01	1	6.25000E − 02
	4.53592E − 01	4.53592E + 02	1.60000E + 01	1

Density (ML^{-3})	$kg \cdot m^{-3}$	$g \cdot cm^{-3}$	$lb \cdot in^{-3}$	$lb \cdot ft^{-3}$
	1	1.00000E − 03	3.61273E − 05	6.24280E − 02
	1.00000E + 03	1	3.61273E − 02	6.24280E + 01
	2.76799E + 04	2.76799E + 01	1	1.72800E + 03
	1.60185E + 01	1.60185E − 02	5.78704E − 04	1

Force (MLT^{-2})	N	dyn	kg_f	lb_f
	1	1.00000E + 05	1.01972E − 01	2.24809E − 01
	9.80665E + 00	9.80665E + 05	1	2.20462E + 00
	4.44822E + 00	4.44822E + 05	4.53592E − 01	1

Biochemical Engineering: A Textbook for Engineers, Chemists and Biologists, Second Edition.
Shigeo Katoh, Jun-ichi Horiuchi, and Fumitake Yoshida.

Companion Website: www.wiley.com\go\katoh\biochem_eng_e2

Pressure ($ML^{-1}T^{-2}$)	Pa	bar	atm	mmHg (torr)	$lb_f \cdot in^{-2}$ (psi)
	1	1.00000E − 05	9.86923E − 06	7.50062E − 03	1.45038E − 04
	1.00000E + 05	1	9.86923E − 01	7.50062E + 02	1.45038E + 01
	1.01325E + 05	1.01325E + 00	1	7.60000E + 02	1.46960E + 01
	1.33322E + 02	1.33322E − 03	1.31580E − 03	1	1.93368E − 02
	6.89476E + 03	6.89476E − 02	6.80460E − 02	5.17150E + 01	1

Energy (ML^2T^{-2})	*J*	erg	cal_{th}	Btu_{th}	kWh
	1	1.00000E + 07	2.39006E − 01	9.48452E − 04	2.77778E − 07
	1.00000E − 07	1	2.39006E − 08	9.48452E − 11	2.77778E − 14
	4.18400E + 00	4.18400E + 07	1	3.96832E − 03	1.16222E − 06
	1.05435E + 03	1.05435E + 10	2.51996E + 02	1	2.92875E − 04
	3.60000E + 06	3.60000E + 13	8.60421E + 05	3.41443E + 03	1

Heat conductivity ($MLT^{-3}\theta^{-1}$)	$W\,m^{-1}\,K^{-1}$	$kcal_{th}\,m^{-1}\,h^{-1}\,°C^{-1}$	$Btu_{th}\,ft^{-1}\,h^{-1}\,°F^{-1}$
	1	8.60421E − 01	5.78176E − 01
	1.16222E + 00	1	6.71968E − 01
	1.72958E + 00	1.48817E + 00	1

Viscosity ($ML^{-1}T^{-1}$)	Pa s ($kg\,m^{-1}\,s^{-1}$)	poise ($g\,cm^{-1}\,s^{-1}$)
	1	1.00000E + 01
	1.00000E − 01	1

Appendix B: Solutions to the Problems

Chapter 1

1.1 (a) $[M\,L^{-1}\,T^{-2}]$, Pa
(b) $[M\,L^{2}\,T^{-3}]$, J s^{-1} (W)
(c) $[L\,T^{-2}\,\theta]$, J kg^{-1} K^{-1}

1.2 $[M\,L^{-1}\,T^{-2}]/[L] = [M\,L^{-3}]\,[L\,T^{-2}]$ Therefore, it is dimensionally sound.

1.3 (a) bar $cm^3 = 0.1$ J,
(b) 1.744×10^5 Pa

1.4 The weight of a body is the gravitational force acting on the body, that is, (mass) × (gravitational acceleration, g). Strictly speaking, weight will vary slightly with locations and altitudes on the Earth. See Section 1.2.

1.5 At $x = 0.01$, $p_{NH_3} = 2.70 \times 0.01 = 0.027$ atm,

$$\text{molar concentration of pure water} = \frac{998}{18.01} = 55.41\ \text{kmol m}^{-3}$$

$$\text{molar concentration of } NH_3 \text{ in water} = 55.41 \times 0.01 = 0.554\ \text{kmol m}^{-3}$$

$$H = \frac{0.027}{0.554} = 0.0487\ \text{atm m}^3\,\text{kmol}^{-1}$$

$$m = \frac{0.027}{0.01} = 2.70$$

1.6 Assuming the ideal gas law, the total mole number of 200 m^3 (air + methane) is 8318 mol. The mole number of methane to be removed is

$$8318 \times 0.20 \times 0.99 = 1647\ \text{mol h}^{-1}$$

The mole fraction of methane in water under equilibrium at a partial pressure of 0.20 atm is

$$x = \frac{p}{H} = \frac{0.20}{(3.76 \times 10^4)} = 5.32 \times 10^{-6}$$

$$\text{mole number of methane in water} = 5.5410 \times 5.32 \times 10^{-6} = 0.295\ \text{mol m}^{-3}$$

Biochemical Engineering: A Textbook for Engineers, Chemists and Biologists, Second Edition.
Shigeo Katoh, Jun-ichi Horiuchi, and Fumitake Yoshida.

Companion Website: www.wiley.com\go\katoh\biochem_eng_e2

The minimum amount of water needed is

$$\frac{1647}{0.295} = 5580 \text{ m}^3\text{h}^{-1}$$

1.7 (a) PE $= 1.0 \times 9.8 \times 10 = 98$ J

(b) KE $= 1.0 \times \frac{u^2}{2} = 98$ J $\quad u = 14$ m s^{-1}.

1.8 2403 kg h^{-1}

1.9 33%

Chapter 2

2.1 The heat transfer rate for the radial direction is $Q = -\kappa A(\mathrm{d}T/\mathrm{d}r)$.

For the tube length L, the area A at $r = r$ is; $A = 2\pi rL$.
Thus, $Q = 2\pi\kappa rL(\mathrm{d}T/\mathrm{d}r)$ and integration with the inside surface temperature T_i (°C) at $r = r_\mathrm{i}$ and outside temperature T_o (°C) at $r = r_\mathrm{o}$ gives

$$Q = 2\pi\kappa L\frac{(T_\mathrm{i} - T_\mathrm{o})}{\ln(r_\mathrm{o}/\, r_\mathrm{i})}$$

2.2 By interpolation, the viscosity of water at 37 °C is 0.69×10^{-3} Pa s

$$\frac{(2.1 \times 10^{-9} \times 1.00 \times 10^{-3})}{293} = \frac{(D_{\text{at } 37\,^\circ\text{C}} \times 0.69 \times 10^{-3})}{310}$$

$$D_{\text{at } 37\,^\circ\text{C}} = 3.2 \times 10^{-9} \text{ m}^2 \text{ s}^{-1}$$

2.3 From the force balance acting on an imaginary coaxial fluid cylinder of radius r and length L, the velocity distribution in laminar flow through a straight round tube is given as follows,

$$\pi r^2 \Delta P = -2\pi rL\mu\frac{\mathrm{d}u}{\mathrm{d}r}$$

$$\frac{\mathrm{d}u}{\mathrm{d}r} = -\frac{1}{2}\frac{\Delta P}{L\mu}r$$

$$u = -\frac{\Delta P}{L\mu}\frac{r^2}{4} + C$$

At $\quad r = r_\mathrm{i} \quad u = 0$

$$u = \frac{\Delta P r_\mathrm{i}^2}{4L\mu}\left(1 - \frac{r^2}{r_\mathrm{i}^2}\right)$$

Total volumetric flow rate is

$$F = \int_0^{r_\mathrm{i}} 2\pi ru\mathrm{d}r = \frac{\pi\Delta P r_\mathrm{i}^4}{8L\mu}$$

Averaged flow rate v

$$v = \frac{F}{(\pi r_\mathrm{i}^2)} = \frac{\Delta P r_\mathrm{i}^2}{8L\mu}$$

Therefore, $\frac{u}{v} = 2\left(1 - \frac{r^2}{r_i^2}\right)$ Equation (2.8)

and $v = \frac{F}{(\pi r_i^2)} = \frac{\Delta P r_i^2}{8L\mu}$ Equation (2.9)

2.4 The flow is laminar, and thus by using Equations 2.10 and 2.12,

$$\Delta P = 7.02 \times 10^3 \text{ kPa}$$

2.5

$$k_{Gp}\left(\frac{17.5}{760} - \frac{15}{760}\right) = \frac{0.0041 \times 10^4}{18.01}$$

$$k_{Gp} = 692 \text{ mol h}^{-1} \text{ m}^{-2} \text{ atm}^{-1} = 0.692 \text{ kmol h}^{-1} \text{ m}^{-2} \text{ atm}^{-1}.$$

From Example 2.4

$$k_{Gc} = 0.0821 \times (273 + 22.5) \times k_{Gp} = 6.8 \text{ m h}^{-1}$$

$$\Delta y_f = \frac{D_{H_2O}}{k_{Gc}} = \left(\frac{0.25 \times 3600/10\,000}{16.8}\right) = 5.36 \times 10^{-3} \text{ m}$$
$$= 5.36 \text{ mm}$$

2.6 From Equation 2.17

$$\Delta y_f = \frac{\kappa}{h} = 239 \text{ μm}$$

2.7 From Equation 2.6

$$\tau = 0.415\ (60)^{1.23} = 63.9 \text{ Pa} \quad \mu_a = \frac{63.9}{60} = 1.07 \text{ Pa s}$$

Chapter 3

3.1 According to Equation 3.7, $\ln(k)$ is plotted against $1/T$. From the slope $(-E_a/T)$ of the straight line

$$E_a = 8010 \times 8.31$$
$$= 6.66 \times 10^4 \text{ kJ kmol}^{-1}$$

3.2 By use of Equation 3.11, $\ln(C_{A0}/C_A)$ is plotted against t.

First-order, $k = 0.0161 \text{ min}^{-1}$

3.3 If the reactants A and B are introduced in the stoichiometric ratio, the following equations hold, that is, $C_{A0} = C_{B0}$ and $C_A = C_B$.

$$-r_A = -\frac{dC_A}{dt} = kC_A{}^2$$

By integration with the initial condition, at $t = 0$, $C_A = C_{A0}$.

$$\frac{1}{C_A} - \frac{1}{C_{A0}} = \frac{1}{C_{A0}} \frac{x_A}{1 - x_A} = kt$$

3.4 By plotting $1/C_A - 1/C_{A0}$ against t,

$$\text{Second-order, } k = 0.012 \text{ m}^3 \text{ kmol}^{-1} \text{ s}^{-1}$$

3.5 11.5 min

3.6 1. $0.046 \text{ mol m}^{-3} \text{ min}^{-1}$
2. $0.046 \text{ unit cm}^{-3}$

3.7 $K\text{m} = 2.5 \text{ mol m}^{-3}$, $V\text{max} = 8.1 \times 10^{-6} \text{ mol m}^{-3} \text{ s}^{-1}$

3.8 From the Lineweaver–Burk plot,
Competitive inhibition,
$K\text{m} = 4.9 \text{ mmol l}^{-1}$, $V\text{max} = 2.20 \text{ mmol l}^{-1} \text{ min}^{-1}$

3.9 1. By comparing the calculated values with the use of Equation 3.42 and an assumed value of K_m with the reaction rates in Table P3.9,

$$K_m = 60 \text{ mol m}^{-3}$$

Chapter 4

4.1 1. $\mu = \ln 2/t_d = 1.39 \text{ h}^{-1}$
2. From Equation 4.5, $t = 3.3$ h

4.2 1. $\mu_{max} = 1.61 \text{ h}^{-1}$
2. $t_d = 0.43$ h
3. $t = 1.4$ h

4.3 1. $\mu_{max} = 0.16 \text{ h}^{-1}$

4.4 $\mu_{max} = 0.05 \text{ h}^{-1}$

4.5 1. $\mu_{max} = 0.15 \text{ h}^{-1}$
2. From Equation 4.4, $Y_{xS} = 0.43$ (kg dry cells formed)/(kg substrate consumed)

4.6 $C_x = 1.6$ g dry cells l^{-1} $\mu = 0.5 \text{ h}^{-1}$

Chapter 5

5.1 $U_o = 188 \text{ kcal h}^{-1} \text{ m}^{-2} \text{ °C}^{-1}$

5.2
(i) From heat balance $t_2 = 55$ °C
(ii) $(\Delta t)_{lm} = 37.4$ °C

$A = Q/(U\ (\Delta t)_{lm}) = 6.88 \text{ m}^2$

5.3 Under turbulent flow Equation 5.8a is used.

$$h = 61.8 \text{ J s}^{-1} \text{ m}^{-2} \text{ °C}^{-1} = 220 \text{ kJ h}^{-1} \text{ m}^{-2} \text{ °C}^{-1}$$

5.4 The water-side coefficient of heat transfer is

$$h_i = 3465 \text{ kcal h}^{-1} \text{ m}^{-2} \text{ °C}^{-1}$$

The steam-side coefficient of heat transfer is converted to h_{si} based on the inside tube surface.

$$h_{si} = 2000 \times \frac{30}{25} = 2400 \text{ kcal h}^{-1} \text{ m}^{-2} \text{ °C}^{-1}$$

We use the thermal conductivity of stainless steel of 14 kcal h^{-1} m^{-2} °C^{-1} and Equation 5.4,

$$\frac{1}{U_i} = \frac{1}{3465} + \frac{1}{5000} + \frac{0.0025}{14} + \frac{1}{2400}$$
$$= 0.00109$$
$$U_i = 920 \text{ kcal } h^{-1} \text{ } m^{-2} \text{ °}C^{-1}$$

5.5 Methanol side, from Equation 5.8,

$$h_{im} = \left(\frac{0.18}{0.046}\right) \times 0.023 \times (2.13 \times 10^4)^{0.8} \times (5.21)^{1/3} = 452 \text{ kcal } h^{-1}$$

Water side

$$h_{ow} = 1434 \text{ kcal } h^{-1} \text{ } m^{-2} \text{ °}C^{-1}$$

The overall heat transfer coefficient based on the outer surface of the inner tube U_o

$$U_o = 320 \text{ kcal } h^{-1} \text{ } m^{-2} \text{ °}C^{-1}$$

The required heat transfer area is

$$A_o = \frac{[0.62 \times 780 \times 1.0 \times \pi/4 \times (0.046)^2 \times 30 \times 3600]}{(320 \times 20)}$$
$$= 13.6 \text{ } m^2$$

The required total length of the tube

$$L = 86 \text{ m}$$

5.6 By use of Equation 5.13

$$h = 290 \text{ kcal } h^{-1} \text{ } m^{-2} \text{ °}C^{-1}$$

Chapter 6

6.1 The solubility of SO_2 at 76 mmHg is 1.27 kg-SO_2/100 kg-H_2O
We can assume the ideal gas behavior of the gas mixture.
The mole number of SO_2 to be removed is

$$1.343 \text{ kmol} = 86.03 \text{ kg-}SO_2$$

The amount of water required is

$$6770 \text{ kg-}H_2O h^{-1}$$

6.2 $k_{Gc} = 204 \text{ m } h^{-1}$

6.3 1.

$$\frac{1}{(mk_G)} = \frac{1}{K_L} - \frac{1}{k_L}$$
$$m = \frac{(H_m)}{RT} = 2.02 \times 10^{-3}$$
$$k_{Gc} = 1.64 \times 10^{-2} \text{m } s^{-1}$$

2.

$$\frac{[1/(mk_G)]}{(1/K_L)} = \frac{(2.7\times10^{-5})}{(3.32\times10^{-5})} = 0.81$$

81%

6.4 Similar to Equation 6.11,

$$\frac{1}{K_{Gp}} = \frac{1}{k_{Gp}} + \frac{H_m}{k_L} = \frac{1}{1.10} + \frac{0.0461}{0.34}$$
$$= 1.0447 \text{ kmol}^{-1}\text{m}^2 \cdot \text{h} \cdot \text{atm}$$

$$K_{Gp} = 0.96 \text{ kmol m}^{-2} \cdot \text{h}^{-1} \cdot \text{atm}^{-1}$$

$$K_{Gc} = RTK_{Gp} = 22.7 \text{ m h}^{-1}$$

percentage of gas film resistance： 87%

6.5 Average contact time = 0.4/20 = 0.02 s
From Equation 6.18

$$k_L = 2\left(\frac{D}{\pi t}\right)^{1/2} = 2\times\left(\frac{2.1\times10^{-9}}{(\pi\times0.02)}\right)^{1/2}$$
$$= 3.66\times10^{-4} \text{ m s}^{-1}$$

6.6 When the concentrations are expressed by $X = x/(1-x)$ and $Y = y/(1-y)$, the operating line becomes a straight line.
From mass balance $U_G'(0.009-0.001) = U_L'(0.08-0)$

$$\frac{U_G'}{U_L'} = 10$$

From Equation 6.51,

$$H_{OG} = H_G + \frac{H_L m U_G'}{U_L'} = 0.45 + 0.06\times10\times0.3 = 0.63 \text{ m}$$

$$N_{OG} = \frac{(Y_B - Y_T)}{(\Delta Y)_{lm}} = 3.59$$

From Equation 6.47, $Z = H_{OG}\times N_{OG} = 0.63\times3.59 = 2.26$ m

6.7 From Equation 6.50,

$$k_L a = \frac{U_L}{H_L} = 66.7 \text{ h}^{-1}$$

6.8 See Section 6.7.3 and Figure 6.5.

Chapter 7

7.1 CSTR $x_A = 0.55$, PFR $x_A = 0.70$

7.2 1. For PFR, the fractional conversion is the same, and $x_A = 0.70$.

$$\text{CSTR} \quad x_{A2} = 0.61$$

2.

$$\text{CSTR} \quad x_A = 0.55, \qquad \text{PFR} \quad x_A = 0.70$$

7.3

$$E_f = \frac{4\pi R^2 D_{eff}\left(\frac{dC_A}{dr}\right)_{r=R}}{\frac{4}{3}\pi R^3 k C_{Ab}} = \frac{1}{3\varphi^2}\left(\frac{dC_A^*}{dr^*}\right)_{r^*=1}$$

$$\frac{dC_A^*}{dr^*}(\text{at } r^* = 1) = 3\phi \coth 3\phi - 1$$

$E_f = \frac{3\phi \coth 3\phi - 1}{3\phi^2}$ This is Equation (7.20).

7.4 From Equation 7.17,
$\phi = 1.92$, by use of Equation 7.20 or Figure 7.4 $E_f = 0.43$

7.5 1. From Equation 3.28, $r_p = 1.82 \times 10^{-5}$ kmol m^{-3} s^{-1}, $x_A = 0.11$

2. $\phi = 7.45$, $C_{Ab}/K_m = 10$
From Figure 7.5 $E_f = 0.50$
The initial reaction rate is

$$1.82 \times 10^{-5} \times 0.50 = 9.1 \times 10^{-6} \text{ kmol m}^{-3} \text{ s}^{-1}$$

3. $d < 0.4$ cm

7.6 From the slope of the first straight line in Figure P7.6

$$dC_L/dt = q_o C_x = 8.2 \times 10^{-3} \text{ mM l}^{-1} \text{ s}^{-1}$$

According to Equation 7.29, $dC_L/dt + q_o C_x$ is plotted against C_L.
From the slope of the straight line, $K_L a = 0.038\ \text{s}^{-1} = 137\ \text{h}^{-1}$

7.7 1. Mole fraction of oxygen in equilibrium with air
$2.0 \times 10^{-5} \times 0.21 = 4.2 \times 10^{-6}$
0.233 mol m^{-3}
oxygen transfer rate $= 80 \times 0.233 = 18.64$ mol m^{-3} h^{-1}

2. 7460 g dry cells m^{-3}.

7.8 By use of Equation 7.32, $P_0 = 6 \times 1010 \times 2^3 \times 0.3^5 = 118$ W
By use of Equation 7.34, $\log(P_G/P_0) = -0.296$
$P_G = 60$ W
By use of Equation 7.37, $k_L a = 0.0331\ \text{s}^{-1} = 119\ \text{h}^{-1}$

7.9 To keep the $k_L a$ value constant, P_G/V and U_G should be kept constant.
Under turbulent conditions P_G/V is proportional to $N^3 L^2$.

$$N = 1.26\ \text{s}^{-1} = 76 \text{ rpm}$$
$$\text{aeration rate} \quad 0.6 \times 4 = 2.4\ \text{m}^3 \cdot \text{min}^{-1}$$

7.10 From Equation 7.41,
$k_L a = 91\ \text{h}^{-1}$

From Equation 7.42,

$$\left(\frac{d_{vs}}{D}\right) = 0.0160,\ d_{vs} = 0.0160 \times 0.30 = 0.0048\ \text{m} = 4.8\ \text{mm}$$

Chapter 8

8.1 If $1/K_L$ is plotted against $1/u^{1/3}$, a straight line will be obtained and the intersection with y-axis gives $1/k_M$. $k_M = 0.060\ \text{cm s}^{-1}$

8.2 The slopes of the straight lines in Figure 8.4 give $-k_L$.

Shear rate (s^{-1})	k_L ($cm\ min^{-1}$)
5000	1.18×10^{-2}
2000	0.94×10^{-2}
1000	0.73×10^{-2}
500	0.56×10^{-2}

These values are roughly proportional to one-third power of the shear rate.

8.3 From Equation 8.7, $J_F = 3.2 \times 10^{-2}\ \text{cm min}^{-1}$

8.4 $\Pi = RT\,C = 0.08206 \times 293 \times 0.10 = 2.4\ \text{atm}$

8.5 The solute concentration is

$$2 \times \frac{20}{58.4} = 0.685\ \text{mol l}^{-1}$$

The osmotic pressure is

$$\Pi = RT\ \times\ 0.685 = 16.75\ \text{atm}$$

$$J_F = 8 \times 10^{-4} \times \frac{(25 - 16.75)}{25} = 2.65 \times 10^{-4}\text{cm s}^{-1}$$

8.6 See Section 8.5 as for the concentration polarization.

Chapter 9

9.1 As R_M is neglected, V_f is proportional to $t^{1/2}$.

20 min	$0.10 \times 2^{1/2} = 0.14\ \text{m}^3$
30 min	$0.10 \times 3^{1/2} = 0.17\ \text{m}^3$

9.2 The filtration fluxes ($cm\ min^{-1}$) are plotted against $\ln C$ similar to Figure 8.4.

Saturated albumin concentration 30 wt%	
Liquid film mass transfer coefficient	
$5\ \text{cm s}^{-1}$	$5.3 \times 10^{-3}\ \text{cm min}^{-1}$
$10\ \text{cm s}^{-1}$	$6.4 \times 10^{-3}\ \text{cm min}^{-1}$

9.3 $t = 294\ \text{s} = 4.9\ \text{min}$

9.4 Elimination of dt from Equations 9.10 and 9.11 gives

$$\frac{dz}{dt} = \frac{dz}{dr}\frac{dr}{dt} = \frac{dz}{dr}\frac{v_g\omega^2}{g}r = \frac{Q}{\pi(r_2^2 - r_1^2)}$$

Integration with boundary conditions ($r = r_1$ at $z = 0$ and $r = r_2$ at $z = Z$) gives Equation 9.12.

9.5 By use of Equation 9.12,

$$Q = 726\ \text{cm}^3\text{s}^{-1} = 2.6\ \text{m}^3\text{h}^{-1}$$

9.6 95 000 rpm, thus 10^6 g

Chapter 10

10.1 By use of Equation 10.3, $t = 10.1\ \text{min}$

10.2 For heating by direct sparging of steam in Table 10.1, $t = 1.81\ \text{h}$

10.3 The velocity distribution in a tube is given by Equation 2.8. Thus,

$$u = v \text{ at } r = 0.707r_i$$

0.75

10.4 Assuming a length of the holding section of 35 m

$$(\text{Pe}) = \frac{vL}{E_{Dz}} = 1100$$

$$(\text{Da}) = \frac{k_d L}{v} = 32$$

From Figure 10.4, the value of n/n_0 is about 10^{-13} is equal to that required in this problem.

Chapter 11

11.1 $C_A = 27.3\ \text{g m}^{-3}$

11.2 For single-stage $0.05 = \frac{1}{(1+2.5\ w)}$

For three-stage $0.05 = \frac{1}{(1+2.5\ w')3}$

$\frac{w}{3w'} = 3.7$

11.3 Similar to the derivation of Equation 11.2

$$k_A p_A(N_s - N_a - N_b) = k'_A N_a$$

$$k_B p_B(N_s - N_a - N_b) = k'_B N_b$$

Therfore,

$$ap_A(N_s - N_a - N_b) = N_a$$

$$bp_B(N_s - N_a - N_b) = N_b$$

where $a = k_A/k'_A$ and $b = k_B/k'_B$.
Addition of these equations gives

$$1 + ap_A + bp_B = \frac{N_s}{(N_s - N_a - N_b)}$$

Substituting this to

$$ap_A(N_s - N_a - N_b) = N_a$$

Thus,

$$N_a = \frac{N_s a\, p_A}{(1 + ap_A + bp_B)}$$

11.4 586 h, 0.20 m

11.5 By use of Equation 11.18,

$$V_R = V_0 + K(V_t - V_0), K = 0.33$$

Equation 11.19, $Hs = 0.025$

11.6 See Sections 11.6.3 and 11.6.4 for the resolution.

11.7 See Section 11.7.2 for the sandwich method.

Chapter 12

12.1 The heat to be removed is $(1.26 + 2.5) \times 10^4$ kJ h^{-1}.
If we assume that cooling water leaves the coil at 25 °C, the flow rate F of cooling water is 0.90 m^3 h^{-1}. The heat transfer coefficient inside the tube = 5200 kJ h^{-1} m^{-2} °C^{-1}; the heat transfer coefficient at the surface of the coiled tube = 12 700 kJ h^{-1} m^{-2} °C^{-1}; the overall coefficient based on the outer surface are = 2350 kJ h^{-1} m^{-2} °C^{-1}.
As the mean temperature difference is 10 °C, the required surface area is 1.6 m^2. Thus the required tube length is 12.7 m.

12.2 By use of Equation 2.6, $\mu_a = 0.21$ Pa s
By use of Equation 12.8, $k_L a = 6.6$ h^{-1}

12.3 The effective shear rate is given by Equation 12.9, $S_{eff} = 50\, U_G = 208$ s^{-1}. By use of Equation 2.6, $\mu_a = 0.097$ Pa s. By use of Equation 7.45, $k_L a = 45$ h^{-1}

12.4 If values of P_G/V and U_G are kept constant, $k_L a$ becomes constant. If we can assume P_G/P_0 is roughly constant at the same U_G, from Equation 7.32 P_G/V is proportional to $N^3 d^2$.

$$N^3 d^2 = 1^3 \times 0.1^2$$

πNd must be smaller than 0.5 m s^{-1}

$$N \times \left(\frac{0.5}{3.14}\right)^2 = 0.01 \quad N = 0.39 \text{ s}^{-1}$$

Therefore, $d = 0.5/(3.14 \times 0.39) = 0.41$ m

$$D = \text{d} \times 3 = 1.2 \text{ m}$$

12.5 By use of Equation 12.17, $t_b = 28$ h

12.6 The cell productivity in chemostat is given as

$$DC_x = Y_{xs}\left[\frac{C_{si} - K_s D}{(\mu_{max} - D)}\right]$$

Differentiate this equation with D and set equal to zero.
When

$$D = \mu_{max}\left(1 - \sqrt{1 - \frac{C_{si}}{C_{si} + K_S}}\right)$$

$$= \mu_{max}\left(1 - \sqrt{\frac{K_S}{C_{si} + K_S}}\right)$$

the productivity becomes maximum.

Chapter 13

13.1

	Chemical processes	Bioprocesses
Type of process	Continuous	Batch/fed-batch
Size of plant	Large	Small
Catalyst	Inorganic catalyst	Enzyme/microorganism
Type of operation	Steady state	Nonsteady state
Operating conditions	High pressure, high temperature and acidic/basic condition	Normal pressure, moderate temperature, and neutral pH
Sterilization	Not required	Required
Sensors	Sufficiently available	Limited

13.2 (a) Resistance thermometer
A resistance thermometer is a temperature measuring device based on the principle that the resistance of metals proportionally increases as the temperature of a metal increases.
(a) Galvanic dissolved oxygen probe
A galvanic dissolved oxygen probe measures the partial pressure of oxygen by use of an electrode based on the following reactions.

$$\text{Cathode } \frac{1}{2}O_2 + H_2O + 2e^- \rightarrow 2OH^-$$

$$\text{Anode (galvanic) } Pb \rightarrow Pb^{2+} + 2e^-$$

The resulting electric current is proportional to the oxygen flux to the cathode through the oxygen-permeable membrane that separates the electrode from a culture medium.

(i) pH electrode

pH electrode measures hydrogen ion activity based on an electric potential difference between a reference electrode and a glass electrode assembled in a sensor probe.

13.3 Suppose the temperature control of a bioreactor using heat supply with a proportional controller. When a proportional controller is tuned at a set point of 30 °C, as long as the set point remains constant, the temperature will remain at 30 °C successfully. Then, if the set point is changed to 40 °C, the proportional controller increases the output (heat supply) proportional to the error (temperature difference). Consequently, a heat supply will continue until the temperature gets to 40 °C and would be off at 40 °C. However, the temperature of a bioreactor will not reach 40 °C because a heat loss from the bioreactor increases due to the temperature increase. Finally, the heat supply matches the heat loss, at this point, the temperature error will remain constant; therefore, proportional controller will keep its output constant. Now the system keeps in a steady state, but the temperature of a bioreactor is below its set point. This residual error is called Offset.

13.4 By use of Table 13.2, K_p, $T_{I,}$ and T_D are 2.4, 15, and 3.75 s, respectively.

13.5 From the ideal gas law, the molar mass of the gas is proportional to the volume of the gas under constant pressure and constant temperature, therefore, by use of Equation 13.6,

$$\mathrm{RQ} = \frac{(2.9 - 0.01)}{(20.90 - 18.30)} = \frac{2.89}{2.60} = 1.11$$

Chapter 14

14.1 By use of Equation 14.1 and α of 7×10^{11} m kg^{-1},

$$\Delta p = 2.3 \times 10^5 \text{ Pa} = 2.3 \text{ atm}$$

14.2 From Equation 11.23, the resolution is proportional to $Z^{1/2}$, and thus it increase by $2^{1/2}$.

14.3 According to the rate model, the effect of a sample volume on the dispersion of elution curve based on time is given
$\sigma_t{}^2 = \sigma_{t_0}{}^2 + \frac{t_0{}^2}{12}$ (Derivation is shown in Kubin, M., J. Chromatogr., **108**, 1 (1975). reference 3 in Chapter 11)
The retention time including the effect of the loading time of a sample is

$$t_R = t_{R0} + \frac{t_0}{2}$$

When Hs is defined based on the retention time, Equation 11.19 becomes

$$Hs = \frac{Z\sigma_t{}^2}{t_R{}^2} = \frac{Z(\sigma_{t_0}{}^2 + t_0{}^2/12)}{(t_{R_0} + t_0/2)^2}$$

14.4 From Figure 14.7,

for the column packed with the small particles, $2r_0u/D_{eff} = 65$

for the column packed with the small particles, $2r_0u'/D_{eff} = 25$

Therefore, $u'/u = (0.044 \times 25)/(0.075 \times 65) = 0.23$

14.5 From Equations 11.9 and 11.12,
$z_a = 0.196$ m
The residual capacity is

$$\frac{(0.196 \times 0.5\ )}{0.5} \times 100 = 19.6\%$$

Chapter 15

15.1 By use of Equation 15.5
$pCO_2 = 38.3$ mmHg

15.2 Average blood velocity through the follow fiber: $v = 5.06$ cm s^{-1}
Oxygen concentration difference in mol l^{-1}:

$$(Cw - Cs) = 7.47 \times 10^{-4} \text{ mol l}^{-1}$$

Hemoglobin concentration:

$$C_{Hb} = \frac{(150 \times 40/42)}{68\,000} = 2.10 \times 10^{-3} \text{ mol l}^{-1}$$

Unreacted concentration of hemoglobin: 0.63×10^{-3} mol l^{-1}
From Equation 15.7

$$z+ = \frac{(7.47 \times 10^{-4} \times 1.76 \times 10^{-5} \times 13)}{(0.63 \times 10^{-3} \times 0.02^2 \times 5.06)}$$
$$= 0.134$$

By use of Equation 15.6, trial will give $\eta = 0.450$:
By use of Equations 15.8 and 15.9,

$$f = 0.636 \text{ and } Q/Q_0 = 0.364$$

Oxygen saturation at the exit

$$1 - 0.3 \times 0.364 = 0.891$$

89%

15.3 Kinematic viscosity is obtained from Figure 15.4b.

$$\Delta P = 1.88 \times 10^4 \text{ Pa} = 0.019 \text{ MPa} = 0.19 \text{ atm}$$

15.4 By use of Equation 15.27,
$\mathrm{Cl} = 160\ \mathrm{cm}^3\ \mathrm{min}^{-1}$

15.5 By use of Equations 15.31, 15.33, and 15.34,

$$E = \frac{(1 - \exp\ 0.9)}{(0.4 - \exp\ 0.9)} = 0.709$$

$$\mathrm{Dl} = Q_{\mathrm{B}} E = 142\ \mathrm{cm}^3\ \mathrm{min}^{-1}$$

Index

Biochemical Engineering: A Textbook for Engineers, Chemists and Biologists, Second Edition.
Shigeo Katoh, Jun-ichi Horiuchi, and Fumitake Yoshida.

Companion Website: www.wiley.com\go\katoh\biochem_eng_e2